



UNIL | Université de Lausanne

Unicentre
CH-1015 Lausanne
<http://serval.unil.ch>

Year: 2024

Vagal sensory afferents as regulators of mouse sleep

Cherrad Najma

Cherrad Najma, 2024, Vagal sensory afferents as regulators of mouse sleep

Originally published at : Thesis, University of Lausanne
Posted at the University of Lausanne Open Archive <http://serval.unil.ch>
Document URN : [urn:nbn:ch:serval-BIB_F938698C08EA7](http://nbn:ch:serval-BIB_F938698C08EA7)

Droits d'auteur

L'Université de Lausanne attire expressément l'attention des utilisateurs sur le fait que tous les documents publiés dans l'Archive SERVAL sont protégés par le droit d'auteur, conformément à la loi fédérale sur le droit d'auteur et les droits voisins (LDA). A ce titre, il est indispensable d'obtenir le consentement préalable de l'auteur et/ou de l'éditeur avant toute utilisation d'une oeuvre ou d'une partie d'une oeuvre ne relevant pas d'une utilisation à des fins personnelles au sens de la LDA (art. 19, al. 1 lettre a). A défaut, tout contrevenant s'expose aux sanctions prévues par cette loi. Nous déclinons toute responsabilité en la matière.

Copyright

The University of Lausanne expressly draws the attention of users to the fact that all documents published in the SERVAL Archive are protected by copyright in accordance with federal law on copyright and similar rights (LDA). Accordingly it is indispensable to obtain prior consent from the author and/or publisher before any use of a work or part of a work for purposes other than personal use within the meaning of LDA (art. 19, para. 1 letter a). Failure to do so will expose offenders to the sanctions laid down by this law. We accept no liability in this respect.



UNIL | Université de Lausanne

Faculté de biologie
et de médecine

Département des neurosciences fondamentales

Vagal sensory afferents as regulators of mouse sleep

Thèse de doctorat en Neurosciences

présentée à la

Faculté de biologie et de médecine
de l'Université de Lausanne

par

Najma CHERRAD

Master en bioinformatique et modélisation
de l'Université Libre de Bruxelles, Belgique

Jury

Prof. Mehdi Tafti, Président
Prof. Anita Lüthi, Directrice de thèse
PD Dr. Marzia De Lucia, Experte
Dr. Raphaëlle Winsky-Sommerer, Experte
PD Dr. Markus Schmidt, Expert

Thèse n° 410

Lausanne
2024

***Programme doctoral interuniversitaire en Neurosciences
des Universités de Lausanne et Genève***



**UNIVERSITÉ
DE GENÈVE**

Imprimatur

Vu le rapport présenté par le jury d'examen, composé de

Président·e	Monsieur	Prof.	Mehdi	Tafti
Directeur·trice de thèse	Madame	Prof.	Anita	Lüthi
Expert·e·s	Madame	Dre	Raphaëlle	Winsky-Sommerer
	Madame	Dre	Marzia	de Lucia
	Monsieur	Dr	Markus	Schmidt

le Conseil de Faculté autorise l'impression de la thèse de

Najma Cherrad

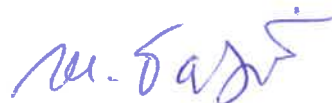
Titulaire d'un Master en Bioinformatique et Modélisation
de l'Université Libre de Bruxelles, Belgique

intitulée

**Vagal sensory afferents as regulators
of mouse sleep**

Lausanne, le 12 juillet 2024

pour Le Doyen
de la Faculté de Biologie et de Médecine



Contents

1	Acknowledgements	5
2	Abstract	7
2.1	Abstract	7
2.2	Résumé	8
3	Introduction	10
3.1	Prologue – Interoception, the internal sense of body awareness	10
3.2	Introductory remarks and major objectives of this introduction	13
3.3	Brain-body communication in sleep, a focus on autonomic coupling	15
3.3.1	Autonomic nervous system and sleep	15
3.3.2	Cardiovascular system during sleep	16
3.3.3	Respiratory system during sleep	17
3.3.4	Thermoregulation during sleep	18
3.3.5	Modulation or disruption of CNS-ANS coupling and effects on sleep	19
3.4	Body-brain communication, a focus on the vagus nerve	21
3.4.1	Basic anatomy - summary of afferent pathways	21
3.4.2	Genetic dissection of the vagus nerve	22
3.4.3	The sensory vagal-recipient brainstem regions : NTS, AP and Pa5	25
3.4.4	Overview over the reflexes	26
3.4.5	Vagal pathways targeting sleep-wake and thermoregulatory centers	28
3.4.6	Manipulation of the vagus nerve for clinical purposes	29
3.4.7	Open questions in the field, relation to the experimental part of the thesis	31
4	Results	33
4.1	Vagal sensory afferents regulate mouse sleep through brain-body cooling	33

4.2	Noradrenergic locus coeruleus activity functionally partitions NREM sleep to gatekeep the NREM-REM sleep cycle.	34
4.3	When the locus coeruleus speaks up in sleep: recent insights, emerging perspectives.	36
5	Discussion	38
5.1	Scientific contributions	38
5.1.1	Technical contributions	38
5.1.2	A chemogenetic approach to manipulate vagal sensory afferents <i>in vivo</i>	40
5.1.3	Transient brain-body cooling as a central mechanism underlying the effects of vagal sensory stimulation on sleep	41
5.1.4	Functional connectivity of L-JNG afferent fibers within NTS <i>in vitro</i>	44
5.2	Limitations and perspectives	46
5.2.1	Optogenetics <i>in vitro</i>	46
5.2.2	Optogenetics <i>in vivo</i>	46
5.2.3	Chemogenetics <i>in vivo</i>	47
5.2.4	Cortical temperature recordings	48
5.2.5	Body temperature measures	49
5.2.6	Ambient temperature control	49
5.2.7	Targeting subpopulation of vagal sensory afferents	50
5.2.8	LC-NA system	50
5.2.9	Sleep analysis	51
5.2.10	Concluding remarks	51
	Bibliography	I
	Appendices	XIX

1 Acknowledgements

First and foremost, I am deeply grateful to my thesis director, Anita Lüthi, for giving me the opportunity to work on this beautiful project with her over the past five years. She has always believed in my abilities and encouraged my strengths. She has not only allowed me to pursue my aspirations as a scientist but has also giving me the confidence and the support needed to accomplish this journey. I am truly thankful for her guidance and dedication throughout this unforgettable experience.

I extend my gratitude to Paul Franken for his support, expertise and insightful feedback on my project. I also wish to express my thanks to the members of my thesis committee, Raphaele Winsky-Sommerer, Marzia De Lucia, Markus Schmidt, and Mehdi Tafti, for the thoughtful discussions, valuable advice, and contributions to shaping my project.

My heartfelt appreciation goes to Laura Fernandez for her unconditional support, expertise in so many domains, and for bringing joy into my daily lab life. She is not only an amazing scientist but also a talented artist, an amazing mum, and a very good friend.

I am very grateful to Alejandro Osorio-Forero, the most passionate person I know. His energy in understanding the complexities of the sleeping brain and its story is truly inspiring. He has taught me to see the good in every person and I thank him for our endless conversations, laughter, and shared memories and for being such a wonderful friend.

Special thanks go to Romain Cardis, without whom I would not have started working in this lab. His supervision and guidance were precious in shaping my journey. He instilled in me the confidence and determination to pursue a PhD. I am thankful to Gil Vantomme for his teaching on patch-clamp techniques, enjoyable discussions, and shared laughter. I also extend my gratitude to the past members of the Lüthi lab, Elidie, Angelo, and Aurélie, with whom I shared knowledge and enjoyable moments. I am grateful to the master students I had the opportunity to supervise as they not only allowed me to guide them but also contributed to my growth as a supervisor.

My PhD experience would not have been the same without the other PhD candidates at the DNF. I particularly want to thank my beloved friend Andrea, my double trouble, my ride or die, for the beautiful memories we've shared and for the many more to come. I also want to

thank Nadia for being such a beautiful sun. I also want to thank Laura, Maxime, Arnau, Manon, Elena for the fun we had at organizing social events at the DNF.

I appreciate all the members of the DNF for the nice discussions during my PhD. Special thanks go to Christiane for her precious support. I also want to thank the dedicated animal caretakers. I express my gratitude to the administrative staff, especially Lise, Katharine, and Alexandra, for their helpfulness and for the nice interactions.

I would like to thank my biggest supporters since day 1, my mum, Catherine, and my dad, Khalid, for financially and emotionally supporting me throughout my studies. For always believing in me and for allowing me to grow into the person I am today. I want to thank my little brother, Sami, for his love and support. I admire his determination and strength in everything he accomplish.

I am truly grateful to my cousin Malika, for her unconditional support and for being a role model in my life as a strong, lovable and funny person.

I want to thank my family in Ville-La-Grand, Geneva, Casablanca and Bordeaux, and to my dear friends who have been with me through thick and thin.

I want to thank my lover, Chris, for his unwavering support, delicious meals during challenging times, and for bringing love and joy into my life. Our journey has only just begun, and I look forward to the adventures ahead.

This thesis is dedicated to my beautiful grandmothers, Mamour and Hajja, two strong women who have profoundly influenced me and still do. I also dedicate this thesis to my grandfather, Pierre, who passed away recently and whose memory I cherish dearly.

Finally, I dedicate this thesis to all oppressed people worldwide. May we strive for a world where everyone can enjoy the privilege of freedom and justice. Free Palestine. Free Congo. Free Sudan. Free Haïti. Free Kanaky. Freedom for all oppressed people.

Nobody is free until everyone is free.

2 Abstract

2.1 Abstract

When hungry, simple foods can seem delicious. When full, even the most tempting dishes lose their appeal. In brief, our perception of the sensory world depends on how we sense our body. Does such interoception also play a role when we are asleep? During sleep, sensory stimuli from the environment are poorly tracked, and arousal thresholds are high. Currently, very little is known about the diversity of interoceptive signaling during sleep, and we lack a neural fundament to decide whether interoception interacts with sleep's restorative and beneficial functions. My thesis is a contribution to the question of how interoceptive stimuli influence the regulation of mammalian sleep and its processing by the sleeping brain, focusing on a major body-brain connection, the vagus nerve.

The goal of this study was to characterize the physiological state of the sleeping mouse induced by vagal sensory stimulation in both its bodily and brain correlates and to identify some of its underlying mechanisms. Anatomical evidence indicates that stimulating sensory inputs from interoceptive systems would not only recruit autonomic feedback loops but also target central sites for the regulation of sleep-wake behavior. I demonstrate that this stimulation modulates sleep architecture and its spectral composition by inducing a non-rapid eye-movement (NREMS)-like state and preventing the occurrence of rapid-eye movement sleep (REMS) without affecting its regulatory mechanisms. Additionally, I find that vagal sensory stimulation induces a brain-body cooling, possibly due strengthened parasympathetic activity (vasodilation and heat loss) and/or activation of hypothalamic nuclei involved in temperature regulation. I provide evidence that a potential neuronal mechanism underlying this regulation could also be through the *locus coeruleus* (LC), receiving indirect innervation from the *nucleus tractus solitarius* (NTS) and known to suppress REMS when activated. These findings make me conclude that vagal sensory afferents powerfully regulate sleep by targeting several of its major physiological correlates in brain and body. Moreover, my findings further point out that the brain-body state induced by vagal sensory stimulation can be described as a novel sleep-like state where brain-body cooling is exacerbated while

LC activity strengthened. These observations reveal a major role for vagal afferent activity in body-brain physiology, which contributes to maintaining a balanced expression of NREMS and REMS through brain-body cooling. This highlights the importance of considering bodily processes when studying sleep regulation.

Together, my work shows that vagal sensory stimulation could help fine-tune temperature and neuromodulatory conditions during sleep, potentially improving sleep quality and enhancing cognitive functions. These findings also contribute to expanding our understanding of the clinical effects of vagus nerve stimulation (VNS), a widely used technique in humans for treating various neurological conditions.

2.2 Résumé

Lorsque nous avons faim, des aliments simples peuvent sembler délicieux. Lorsque nous sommes rassasiés, même les mets les plus alléchants perdent de leur attrait. En effet, notre perception du monde sensoriel dépend de ce que notre corps ressent. Mais est-ce que cette intéroception joue également un rôle quand on dort ? Pendant la phase de sommeil, les stimuli sensoriels de notre environnement sont moins bien détectés, et nos seuils d'éveil sont élevés. Actuellement, notre connaissance de la diversité des signaux intéroceptifs pendant le sommeil est limitée, et nous ignorons encore le support neurologique qui permettrait de comprendre comment l'intéroception pourrait influencer les fonctions réparatrices et bénéfiques du sommeil. Ma thèse vise à élargir nos connaissances sur l'impact des stimuli intéroceptifs sur la régulation du sommeil chez les mammifères, en se concentrant sur le nerf vague, une voie majeure de communication entre le corps et le cerveau.

Le but de cette étude était de caractériser l'état physiologique de la souris endormie à la suite d'une stimulation sensorielle vagale, en prenant en compte les effets sur le corps et sur le cerveau, et d'identifier certains mécanismes sous-jacents. Des preuves anatomiques indiquent que la stimulation des entrées sensorielles des systèmes intéroceptifs recruterait non seulement des boucles de rétroaction du système nerveux autonome mais ciblerait également des régions centrales pour la régulation du comportement éveil-sommeil. Mon travail démontre que cette

stimulation modifie l'architecture et la composition spectrale du sommeil, en créant un état similaire au sommeil lent et en diminuant le sommeil paradoxal, sans altérer ses mécanismes régulateurs. De plus, j'ai observé que la stimulation sensorielle vagale entraîne un refroidissement du cerveau et du corps, potentiellement lié à une activité parasympathique accrue (entraînant une vasodilatation et une perte de chaleur) et/ou à l'activation des noyaux hypothalamiques régulant la température. Ces résultats suggèrent qu'un mécanisme neuronal sous-tendant cette régulation pourrait également passer par le *locus coeruleus* (LC), qui reçoit une innervation indirecte du *nucleus tractus solitarius* (NTS) et est connu pour supprimer le sommeil paradoxal lorsqu'il est activé.

Cette découverte souligne l'impact significatif des afférences sensorielles vagales sur la régulation du sommeil en ciblant plusieurs de ses principaux corrélats physiologiques dans le cerveau et le corps. Mes résultats démontrent que cet état du corps et du cerveau induit par la stimulation sensorielle vagale crée un état similaire au sommeil lent dans lequel le refroidissement cérébral et corporel est exacerbé et l'activité du LC est augmentée. Ces observations mettent en évidence le rôle crucial de l'activité afférente vagale dans la physiologie de l'axe corps-cerveau, permettant de maintenir l'équilibre entre le sommeil lent et le sommeil paradoxal par le biais de ce mécanisme de refroidissement. Elles mettent également en lumière l'importance de considérer les processus corporels dans l'étude de la régulation du sommeil. Dans son ensemble, mon travail montre que la stimulation sensorielle vagale pourrait aider à affiner la température et les conditions neuromodulatrices pendant le sommeil, offrant des perspectives pour améliorer la qualité du sommeil et renforcer les fonctions cognitives. Enfin, ces résultats enrichissent notre compréhension des effets cliniques de la stimulation du nerf vague (VNS), une technique répandue dans le traitement de diverses conditions neurologiques chez l'humain.

3 Introduction

3.1 Prologue – Interoception, the internal sense of body awareness

Every living organism uses a variety of senses to navigate and apprehend its surroundings, collecting data and processing them to formulate an appropriate response. In humans, the traditional five senses—sight, hearing, taste, touch, and smell—are well-known. However, our understanding has evolved to include a broader spectrum of sensory experiences, such as proprioception (sense of body position) or vestibular sense (sense of balance and spatial orientation). In recent years, attention has been drawn to the sense of interoception that provides the brain with information about the internal state of the organism. These bodily states send signals that are relevant for basic behaviors, such as food intake, but they can also affect our emotional state [Critchley and Garfinkel, 2017]. Interestingly, we refer to interoceptive sensations as part of common jargon of our daily lives and that involve both elementary physical but also emotional sensations (Figure 3.1). For instance, “feeling our stomach growling” signifies our body is in need of food and nutrients. Contrary, when we say “I feel my stomach full”, it means our body has received signals of satiety after a meal. On another note, after an intense physical or mental activity, “feeling fatigued” is our body’s way of signaling us to slow down and recharge energy. Finally, whether we are “feeling cold or hot”, we refer to sensations coming from our skin’s thermoreceptors and sending messages to the brain to maintain optimal body temperature. Other types of commonly used expressions describe the way our emotions can trigger changes in our internal organs’ states. For example if “my heart is racing with nerves”, it is a way to describe the situation of excitement or stress that causes our heart to beat faster. Moreover, sensations from our stomach are not solely about digestion; consider the phrase “I have butterflies in my stomach” which captures the feeling of excitement or anxiety.

Interoception is crucial for maintaining overall health and well-being, as disruptions in interoceptive processing are associated with various psychiatric and neurological disorders. A person with interoceptive deficits may not be aware of

when they are hungry, thirsty, or need to go to the bathroom ¹. On a more dramatic note, a lack of interoceptive awareness can cause eating disorders [Bonaz et al., 2021] as well as a risk factor for self-harm and suicidal behaviors [Duffy et al., 2021]. Conversely, a heightened awareness of typical interoceptive signals can lead to anxiety and panic disorders amongst other psychiatric and neurological conditions [Khalsa et al., 2018; Bonaz et al., 2021]. There are a variety of tests available to measure interoceptive attention, such as heartbeat counting exercises. These techniques have been used recently to assist individuals on the autism spectrum who may have difficulty with interoceptive awareness, aiding them in strengthening this capacity [Khalsa et al., 2018].

While we commonly relate interoception to states of wakefulness and emotion, interoception is equally relevant for states of sleep. Thus, although sleep is accompanied by altered consciousness, the brain and the body keep interacting. During sleep, it is crucial for the organism to continue monitoring essential life functions, such as heart rate, breathing rate, oxygen levels or thermoregulation. Interoceptive signals contribute to the regulation of these physiological processes during sleep. They also contribute to the transitions between the different sleep stages and influence the perception of sleep quality. Moreover, sleep is a state of intense processing of wake-related information in both its factual and emotional dimensions, and this processing enables sleep to facilitate memory consolidation, emotional regulation, and cognitive functions essential for optimal brain function and overall well-being [Tallon-Baudry, 2023]. Interoception has a significant role in sleep, and major sleep disorders are accompanied by atypical interoception deficits (e.g. insomnia – abnormal feelings of heart rate and state of hyperarousal that also invades the body [Wei and Van Someren, 2020]).

Modern neuroscience provides the tools to identify the neural mechanisms underlying interoception. Indeed, it is increasingly clear that the brain interacts with the body through multiple interoceptive signaling pathways that have an identifiable neuronal substrate. This communication is made through the peripheral sensory receptors (chemoreceptors, mechanoreceptors, nociceptors, humoral receptors, etc...) which detect internal states such as changes in blood pressure, blood glucose levels,

¹<https://neurodivergentinsights.com/blog/poor-interoception>

visceral sensations (Figure 3.1). The sensory information is transmitted via afferent nerves of the autonomic nervous system (ANS) such as the vagus nerve (cranial nerve X) and the glossopharyngeal nerve (cranial nerve IX) and is relayed to the classical visceral recipients in the brainstem, the nucleus tractus solitarius (NTS) among others, but also to higher brain regions involved in interoceptive processing such as thalamus, hypothalamus, hippocampus, amygdala or insula (reviewed in [Azzalini et al., 2019; Berntson and Khalsa, 2021]). Investigating the integration of interoceptive signals in the brain and their influence on perceptual and cognitive processes will enhance our understanding of the complexities of brain-body interactions and their impact on human behavior and well-being, in particular during sleep.

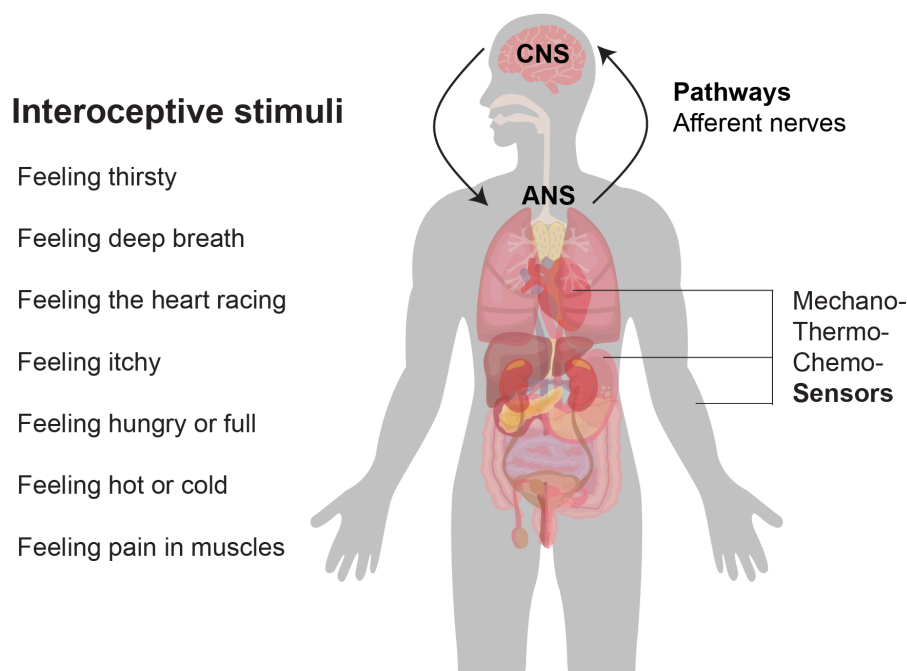


Figure 3.1: Scheme of interoceptive stimuli examples. Interoception is the internal sense of body awareness. Stimuli are detected by different sensors located in the peripheral nervous system and send signals to the central nervous system (CNS) via afferent nerves of the autonomic nervous system (ANS).

3.2 Introductory remarks and major objectives of this introduction

Wakefulness is linked to intense sensory-motor exchange with the external environment and with the internal body. In contrast, during sleep, the brain partially disengages from the external world, becoming less responsive to external stimuli. This sensory isolation is a defining feature of sleep that has dual, supposedly non-reconcilable, consequences for sleep. On the one hand, it isolates the sleeper from the environment, in principle putting it at risk to external dangers. On the other hand, this sensory isolation provides the opportunity for internal processing and restoration [Andrillon and Kouider, 2020]. Working at the interface between these two non-reconcilable aspects of sensory disconnection has been one of the most productive areas of investigation into sleep functions. For example, there are specific patterns of brain activity in non-rapid eye-movement sleep (NREMS), one of the two main phases of mammalian sleep [Brown et al., 2012], that have been associated with the suppression of external sensory inputs. These brain activities are the slow oscillations, function as a gate to prevent the cortex from processing sensory information; the k-complexes, a subset of slow oscillations, respond to external stimuli and potentially protect against sensory overload; and the sleep spindles, faster oscillations, are associated with memory consolidation and protect against external disturbances. In contrast, during rapid eye-movement sleep (REMS), the other phase present in mammalian sleep, the mechanisms associated with dreaming may inhibit the processing of external inputs [Andrillon and Kouider, 2020]. Sensory isolation serves as a protective mechanism for the brain, ensuring its restoration and plasticity in its synapses [Rasch and Born, 2013; Vyazovskiy, 2015; Brodt et al., 2023]. These and other examples show that the brain's natural mechanisms of sensory isolation during sleep are vital for various sleep functions, memory consolidation, dreaming, and overall cognitive processes. Disruptions in these mechanisms can contribute to sleep disorders such as insomnia or hypersomnia, and impact cognitive performance.

The main motivation of my thesis is that I postulate that a better understanding of the sleeping brain's interplay with bodily sensory signals will lead us forward in the understanding of sleep function. This argument is supported by several factors.

Firstly, the brain and the body must be coordinated in sleep to ensure a good control of internal bodily processes. Secondly, the original function of sleep has mostly been described as a resting state to preserve the body for energy conservation [Berger and Phillips, 1995]. Furthermore, animals without brains, such as jellyfish and hydras, do sleep [Arnold, 2017], challenging our conventional notions of sleep that would be solely driven by the brain. Moreover, it is a common experience that a full stomach affects the way we sleep; indeed, it is recommended not to eat too much or too close to bedtime to avoid sleep disruptions. The interactions between sleep and interoception are various and complex [Wei and Van Someren, 2020]. Interoceptive signals such as nociceptive stimuli can affect sleep initiation by increasing arousal [Bastuji et al., 2008]. Other signals can on the contrary induce sleepiness, such as gastrointestinal distention [Kukorelli and Juhasz, 1977; Orr and Chen, 2005]. Similarly, stimulating the carotid sinus has been found to produce brain activity resembling the slow waves seen during sleep [Azzalini et al., 2019; Silvani et al., 2015]. The interaction between sleep and thermoception also affects sleep initiation, as warming the skin induces sleepiness and increases the time spent in NREMS [Te Lindert and Van Someren, 2018; Harding et al., 2019]. Moreover, a rise in body temperature in the case of fever can lead to a suppression of REMS and a disruption of NREMS [Karacan et al., 1968; Imeri and Opp, 2009]. Hormonal changes in the menstruation cycle can also affect body temperature and thus sleep quality. It has been reported that body temperature and heart rate are higher in the luteal phase, leading to longer sleep initiation times, more frequent awakenings, and a tendency for less REMS [Driver et al., 2008]. This implies that sensory signals from the body might influence sleep, but we are uncertain whether they affect sleep architecture, spectral characteristics, and/or homeostatic regulatory mechanisms of sleep states. Therefore, it is important to investigate how these internal sensory stimuli affect mammalian sleep.

This thesis intends to make a contribution to the neural basis of body-brain communication during sleep, focusing on the impact of vagal sensory stimulation. This introduction will start by drawing attention to the coupling between the central nervous system and the autonomic nervous system as an integral part of sleep, for which some of the neural principles of coordination have been outlined. This part will be largely phenomenological, describing the bodily alterations accompanying

sleep states and highlighting, wherever possible, their roles. The introduction will then continue to outline some of the major pathways by which the body communicates to the brain, with a focus on the vagus nerve that will be the topic of the experimental study of this thesis. I will highlight the vagus nerve as part of the sensory motor reflexes that are important in the parasympathetic branch of the ANS. I will also highlight progress in the molecular dissection of vagal neuronal subtypes because these studies investigate the largely unexplored diversity of sensory stimuli arising from the body. I will continue on this diversity by presenting the brainstem areas that act as a hub to distribute afferent information. I will finally present the current state of knowledge of how vagus nerve stimulation (VNS), a widely approved technique, is used for clinical treatments and the possible alterations it may cause on sleep behavior. These two chapters will provide the basis to define the major objectives of this thesis and their relevance to provide the entry point into my experimental thesis work that has been centered around exploring how specific vagal sensory neuron activation affects states of sleep in mice.

3.3 Brain-body communication in sleep, a focus on autonomic coupling

3.3.1 Autonomic nervous system and sleep

The CNS is the central unit that processes the interoceptive and exteroceptive stimuli, and it is neurally connected to the different parts of the body through the peripheral nervous system. The peripheral nervous system is divided into two different systems, the somatic nervous system that controls voluntary actions, and the ANS that controls involuntary actions. The ANS is a control system that acts largely unconsciously and influences the function of internal organs. The ANS is composed of two systems, the sympathetic nervous system (SNS), that prepares the body for “fight or flight” responses, increasing cardiac output, accelerating respiratory rate, releasing stored energy, dilating pupils, inhibiting digestion and urination; and the parasympathetic nervous system (PNS), that restores the body to a calm state of “rest and digest”, slowing heart rate, decreasing respiratory rate, stimulating digestion, removing waste

and storing energy. Both systems are simultaneously tonically active and have opposite effects [McCorry, 2007]. Most of the peripheral systems change along the sleep-wake cycle, and depending on the specific vigilance state and the body's needs at that time, the balance between sympathetic and parasympathetic activity fluctuates. Sleep in particular is defined as a brain-bodily state during which ANS activity undergoes substantial variations in a manner aligned with brain states [De Zambotti et al., 2018]. The autonomic changes during NREMS and REMS are in large part the result of a central autonomic coordinator which will induce changes in the activity of sympathetic and parasympathetic preganglionic neurons in the spinal cord and the medulla respectively [Silvani and Dampney, 2013] (Figure 3.2). NREMS is a state of rest and recovery during which metabolic activity is reduced and relaxation is promoted. It is a state during which the parasympathetic activity becomes dominant whereas the sympathetic activity decreases compared to wakefulness. On the other hand, REMS shows a parasympathetic activity still active, although not as prominently as during NREMS, while an increase in sympathetic activity is observed. The central autonomic commands, regions of the CNS that regulate autonomic functions, play a critical role in the regulation of peripheral systems by maintaining the sympathetic-parasympathetic balance across the different sleep states. Among the bodily systems, sleep-wake cycles potently affect cardiovascular, breathing and thermoregulatory functions. The next chapters provide a brief insight into these changes, taking as examples heart rate, breathing rate and temperature control. The purpose is to provide quantitative information to provide an idea about the considerable strength of these changes, as well as a schematic conceptual model over the central autonomic commands related to sleep possibly arising from the cumulative activity of various central pattern generators (Figure 3.2).

3.3.2 Cardiovascular system during sleep

A major player in cardiovascular function is the activity of the heart, of which much of its physiology undergoes considerable changes during sleep, along with changes in blood pressure and cardiac output. During NREMS, blood pressure and heart rate decrease together with a decrease in skeletal muscle activity. In humans a normal heart rate is typically between 60 – 100 beats per minute (bpm), dropping to 40 – 50

bpm during sleep. In freely moving mice, heart rate ranges from 500 – 700 and drops to 350 – 400 during sleep, as observed in telemetric recordings [Mills et al., 2000; Silvani et al., 2008; Lecci et al., 2017]. In contrast, during REMS, these cardiovascular parameters increase back to levels comparable to wakefulness, while muscle tone decreases even more to a state of atonia [Chouchou and Desseilles, 2014; Silvani and Dampney, 2013]. Pioneer studies have described nighttime sleep as a state that provides increased protection against acute cardiovascular events compared to wakefulness [Muller et al., 1989]. An important role is played here by the resetting of the major regulator of blood pressure and heart rate, the baroreflex system, known for maintaining blood pressure at nearly constant levels [Silvani and Dampney, 2013] (Figure 3.2). Particularly during NREMS, the baroreflex system's sensitivity increases, and the threshold for triggering reflex responses is lower than during wakefulness. In other words the baroreceptors respond differently to alterations in blood pressure depending on the organism's vigilance states [Silvani and Dampney, 2013; Silvani et al., 2015]. The CNS modulates sympathetic and parasympathetic outflow to the heart and blood vessels, and together with the changes in baroreflex sensitivity, it will contribute to the overall cardiovascular deactivation. CNS makes the cardiovascular system adapt to the specific physiological changes and demands of each sleep state.

3.3.3 Respiratory system during sleep

The respiratory system, tightly linked to that of the cardiovascular system, also changes activity in a state-specific manner across the sleep-wake cycle [De Zambotti et al., 2018; Benarroch, 2018]. Breathing becomes more regular in NREMS, with a dominant parasympathetic activity decreasing respiratory rate and depth compared to wakefulness. Conversely, respiration during REMS presents irregularities resembling patterns observed during wakefulness, these are periods of rapid and shallow breathing, as well as occasional pauses known as apneas. The central respiratory generator located within the brainstem produces a respiratory drive (tonic activity) and respiratory rhythm (phasic activity) [Sowho et al., 2014] (Figure 3.2). Similar to the cardiovascular system, sleep provides a level of protection and modulation for respiratory functions. Tonic drive is reduced at sleep onset due to the airway resistance increasing by about 230% [Sowho et al., 2014]. The central

respiratory control centers adjust their activity, coordinating with other physiological systems to maintain adequate oxygenation and ventilation. The responsiveness of chemoreceptors to changes in blood oxygen and carbon dioxide levels also varies across sleep stages, contributing to the overall regulation of respiratory parameters.

3.3.4 Thermoregulation during sleep

The interactions between CNS and ANS also plays a crucial role in modulating the physiological process of thermoregulation so that core body temperature varies throughout the sleep-wake cycle. The ANS, particularly the sympathetic nervous system, is involved in thermoregulation by modulating blood flow to the skin and sweat gland activity, thus dissipating or conserving heat as needed [Szymusiak, 2018; De Zambotti et al., 2018] (Figure 3.2). At the onset of NREMS, core body temperature falls due to a reduction in sympathetic tone, leading to increased skin temperature, particularly at distal sites, and heat loss through peripheral vasodilation. Conversely, during REMS, core body temperature rises back towards wakefulness levels. This is attributed to sympathetic activation triggering peripheral vasoconstriction, which redirects blood flow away from the skin's surface, thus decreasing heat loss [Krauchi and Deboer, 2010; Harding et al., 2019]. During REMS, thermoregulation is absent, and ambient temperature has a greater impact on core body temperature compared to NREMS or wakefulness [Parmeggiani, 2003; Schmidt, 2014; Harding et al., 2019; Komagata et al., 2019]. The preoptic hypothalamus (POA), located in the anterior part of the hypothalamus, is a crucial region for the coordination between sleep and thermoregulation. The POA contains warm- and cold- sensitive neurons that are predominantly sleep- and wake- active, respectively [McGinty and Szymusiak, 2001; Harding et al., 2019]. These neural circuits contribute to the adjustments in thermoregulation during different sleep stages. Furthermore, the thermoregulatory system's adjustments during sleep are also influenced by the circadian clock located in the suprachiasmatic nucleus (SCN), a small region of the hypothalamus [Saper et al., 2005; Kräuchi, 2007]. The body's core temperature follows a circadian rhythm, with a natural decrease during the late evening and early night, reaching its lowest point during the night's midpoint before gradually rising towards morning [Kräuchi, 2007; Dibner et al., 2010].

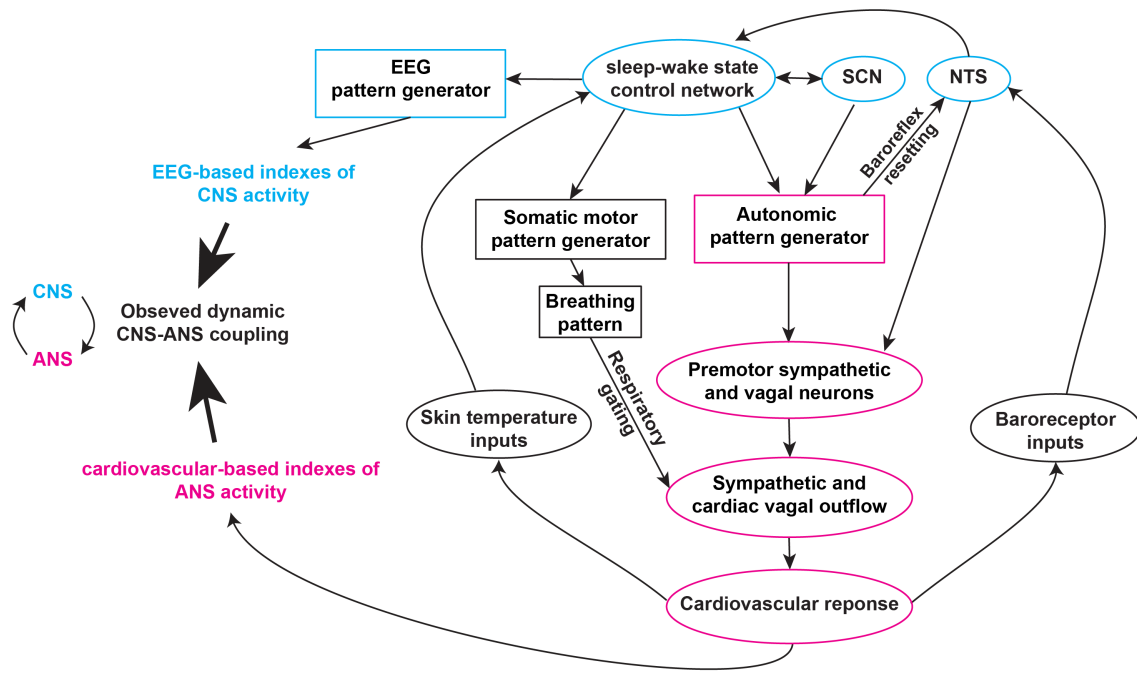


Figure 3.2: Schematic diagram of a conceptual model over the central autonomic commands related to sleep possibly arising from the cumulative activity of various central pattern generators. The cause of the bodily internal changes across the sleep-wake cycle is due to the changes in neuronal activity of the regions involved in sleep-wake control, that will induce changes in the activity of sympathetic and parasympathetic preganglionic neurons in the spinal cord and the medulla respectively [Silvani and Dampney, 2013]. This figure is adapted from [De Zambotti et al., 2018].

3.3.5 Modulation or disruption of CNS-ANS coupling and effects on sleep

Evaluating the CNS-ANS coupling during sleep involves various measures, such as assessing heart rate and heart rate variability (HRV) through electrocardiogram (ECG) signals. These measures offer valuable insights into ANS activity during sleep. HRV reflects the best dynamic interplay between the sympathetic and parasympathetic branches of the ANS by measuring the variation in time intervals between consecutive heartbeats. Analyzing HRV through looking at the different frequency components [Chouchou and Desseilles, 2014] provides a quantitative measure of the relative activity of the two branches, which is an index of cardiac health. High HRV generally indicates better autonomic flexibility and adaptability, whereas low HRV may suggest reduced autonomic and potential health risks [Vaughn et al., 1995; Cacioppo et al., 2007; Tobaldini et al., 2013; Chouchou and Desseilles, 2014; De Zambotti et al., 2018].

Disruptions of the CNS-ANS coupling contribute to a variety of neurologic

disorders and/or autonomic impairments. Autonomic dysfunction such as cardiovascular disorders (e.g. hypertension, arrhythmias), respiratory disorders (e.g. bronchial asthma) or thermoregulatory disorders (e.g. hyperthermia, hypothermia) can be associated with altered sleep patterns [Cortelli and Lombardi, 2005; Cheshire, 2016; Miglis, 2017; Tobaldini et al., 2017; Hashimoto and Yang, 2022].

As already mentioned in the introductory remarks, various research findings support that interoceptive stimuli can modify sleep by inducing sleepiness [Wei and Van Someren, 2020], including stimuli from the gastrointestinal system [Kukorelli and Juhasz, 1977; Orr and Chen, 2005] and the cardiovascular system [Azzalini et al., 2019; Silvani et al., 2015]. Moreover, a recent study has shown that artificially modulating the baroreflex in freely moving mice can affect the sleep-wake brain status. Indeed stimulation of the barosensitive neurons in the brainstem using optogenetics and chemogenetics techniques led to an increase in NREMS while decreasing wakefulness, together with a decrease in blood pressure and heart rate. Contrary to the effect of activation, inactivation of this pathway causes a decrease in NREMS with an increase in wakefulness [Yao et al., 2022]. Baroreflex physical activation, through devices or techniques, is now used as a therapy for resistant hypertension patients [Victor, 2015]. By studying the effects on sleep regulation, this study provides strong and direct evidence for the connection between heart and sleep control. Finally, a hypothesis has been made regarding the potential connection between internal sensory mechanisms and sleep homeostasis. For example, when deprived of sleep, individuals often experience elevated blood pressure and increased skin temperature in distal regions [Silvani et al., 2015]. Baroreceptors and thermoreceptors sensing these changes could then activate feedback loops that will contribute to the feeling of sleepiness. The relationship between internal bodily states and sleep neuronal circuitry is still not well understood, and there is a lack of a proper in-depth analysis of sleep architecture and spectral dynamics combined with modulation of internal organs physiology.

3.4 Body-brain communication, a focus on the vagus nerve

3.4.1 Basic anatomy - summary of afferent pathways

The connection between the CNS and ANS relies on efferent and afferent pathways [Saper, 2002], through which interoceptive information from internal tissues is transmitted to the CNS via a complex network involving the nervous system (electrical and chemical signals), endocrine system (hormones), and immune system (indirect signaling) [Critchley and Harrison, 2013]. A crucial pathway for transmitting information to and from the brain about internal organ function is the vagus nerve, the tenth pair and the longest of the cranial nerves and a critical component of the ANS, also known as “the wanderer nerve”. It innervates the majority of the organs (except the adrenal glands) and carries 75% of all parasympathetic fibers, comprising mixed sensory (afferents) and motor (efferents) fibers [Berthoud and Neuhuber, 2000], with over 80% transmitting afferent signals [Agostoni et al., 1957; Prechtel and Powley, 1990]. The cell bodies of the vagal sensory afferents are located into the vagal ganglion complex, including the jugular and nodose ganglia, less distinct in rodents [Nassenstein et al., 2010; Han and De Araujo, 2021]. The jugular-nodose ganglion (JNG) is a prominent enlargement of the vagus nerve located just before its entry into the cranial cavity. To enable a fast signal transmission and an efficient sensory integration, the sensory neurons of the JNG are pseudounipolar with one branch traveling towards the medulla oblongata, part of the brainstem, specifically to the main visceral recipients like NTS and *area postrema* (AP) from nodose ganglia, and paratrigeminal nucleus (Pa5) from jugular ganglia [McGovern et al., 2015; Han et al., 2018]. The other branch of the pseudounipolar JNG neurons innervates visceral organs and transmit sensory signals to maintain bodily homeostasis in the respiratory tract by controlling respiration rate and regulating airway tone (reviewed in [Mazzone and Udem, 2016]), in the gastrointestinal tract by controlling digestion and satiety (reviewed in [Waise et al., 2018]), or in the baroreflex system by controlling blood pressure and heart rate (reviewed in [Wehrwein and Joyner, 2013]).

3.4.2 Genetic dissection of the vagus nerve

To sense and respond to the diverse stimuli from various organs, the vagal sensory system contains a heterogeneous collection of specialized neuron types. Using single-cell RNA sequencing, a research team unveiled the transcriptional profile of neuron subtypes in the vagal sensory ganglia [Kupari et al., 2019]. The JNG complex contains mostly sensory neurons expressing the vesicular glutamate transporter 2 (Vglut2), a marker for peripheral sensory neurons (Figure 3.3). However, within this complex, the jugular and nodose ganglia present fundamental differences. Jugular Prdm12-expressing neurons are general somatosensory neurons similar to spinal neurons. They contain mechanosensors, nociceptors and cold- and mechano-heat nociceptors. In contrast, nodose Phox2b-expressing neurons are viscerosensory neurons with highly specialized types that regulate the physiological state of respiratory, gastrointestinal and cardiovascular systems. These nodose neurons contain mechano- and chemosensors, barosensors, stretch, tension and volume sensors [Kupari et al., 2019]. Classifying vagal afferent subtypes using genetic markers helps in understanding the neural control of autonomic physiology (reviewed in [Prescott and Liberles, 2022]). Bai et al. initially identified vagal sensory afferent projections onto the gastrointestinal tract by injecting a Cre-dependent virus in Vglut2-Cre mice. Then, they genetically mapped afferents from the gut by retrogradely tracing these different sites and performed RNA sequencing on the corresponding labeled neurons in the JNG complex. This investigation revealed that a specific subtype of neurons can innervate distinct visceral organs [Bai et al., 2019]. Different subsets of vagal sensory afferents trigger specific reflex responses due to their unique structures and functions. Some are specialized in chemical detection, while others are specialized in mechanical sensations [Berthoud et al., 2004; Brookes et al., 2013].

The laboratory of Stephen Liberles investigated a specific functional sub-population of neurons within the vagus nerve [Chang et al., 2015]. They began by identifying three genes expressed in vagal sensory neurons—Gpr65, P2ry1, and Npy2r—and generated corresponding Cre knock-in mice. These mice were then used for neural tracing experiments, where a Cre-dependent adeno-associated virus (AAV) was injected into the JNG complex. This allowed the researchers to map the

peripheral innervation of these three molecularly distinct sensory neuron subpopulations. Their findings revealed that P2ry1 and Npy2r neurons densely innervate the lungs, while Gpr65 neurons do not. Additionally, fibers from these two populations were also found in the stomach and heart, indicating a shared function for each neuron type across multiple organs, such as stretch detection [Ran et al., 2022]. To understand the potential impact of these neuron populations on breathing control, the researchers optogenetically stimulated them in freely breathing anesthetized mice that constitutively expressed channelrhodopsin (ChR2). This stimulation led to powerful and contrasting effects on breathing dynamics: stimulating P2ry1 neurons caused apnea, while stimulating Npy2r neurons induced rapid and shallow breathing [Chang et al., 2015]. Another study further highlighted the role of P2ry1 in monitoring airway defense reflexes [Prescott et al., 2020].

Another investigation, conducted by the Liberles group, focused on the gastrointestinal system [Williams et al., 2016]. Using the same genetic approach to map vagal sensory neuron anatomy, they identified two distinct subtypes of neurons innervating the gut, each playing a crucial role in gastrointestinal physiology control. Optogenetic activation of Glp1r-expressing neurons increased gastric pressure, responsive to stomach and intestinal distention. Conversely, stimulating Gpr65 neurons blocked the gastric contractions without affecting breathing or heart rate. Furthermore, these neurons were found to detect intestinal nutrients.

Following the observation of a decrease in blood pressure and heart rate upon activating Vglut2-Cre mice [Chang et al., 2015], they decided to focus on another group of vagal afferents involved in the cardiovascular system. They activated subsets of JNG sensory neurons expected to have a similar effect. Optogenetic stimulation of Piezo2 neurons in anesthetized mice also resulted in heart rate and blood pressure reduction, with projections from these specific vagal sensory neurons identified in the aortic arch, a part of the aorta. Piezo2 serves as a marker for all baroreceptor neurons; when these neurons were ablated, injection of phenylephrine, a vasoconstrictor commonly used to induce the baroreflex, failed to elicit a normal baroreceptor reflex [Min et al., 2019].

Other types of vagal afferents were investigated (Pirt, 5HT3, TRPV1 and Tac1) to determine the brain regions they innervated and identify their role in specific body regulation. Researchers used Cre-mice to map the projections of vagal afferent

populations in the brainstem. Results show that there is a preference for specific afferent subsets to innervate determined NTS areas [Kim et al., 2020].

The laboratory of De Araujo described the different types of vagal afferent especially the ones involved in monitoring and regulating digestion [Han et al., 2018]. Employing a combinatorial viral strategy, they targeted gut vagal sensory neurons in wild-type mice. Initially, the organs of interest, in this case, the gut, were transfected with a retrograde virus carrying a Cre construct, which would then be bilaterally transported to the JNGs. Then, a Cre-dependent virus expressing channelrhodopsin was injected into the right or left JNG. Optogenetic activation of the terminals in the NTS originating from the right JNG triggered the reward pathway, as confirmed by anatomical brain mapping (showing projections to substantia nigra exclusively on the right side). This demonstrates the gut's ability to influence neuropsychological functions.

These findings reveal the complexity and specificity of neural circuits within the vagus nerve and their crucial roles in regulating physiological responses across various organ systems. The heterogeneity among vagal sensory afferents enables the CNS to discern between various types of interoceptive stimuli. By dissecting the neural pathways originating from visceral sensory inputs, we gain insights into the individual mechanisms maintaining body homeostasis and how they are processed by the CNS. The parasympathetic system can provide detailed physiological control with each type of neuron possibly coordinating specific functions across multiple organs or regulating distinct aspects of autonomic physiology.

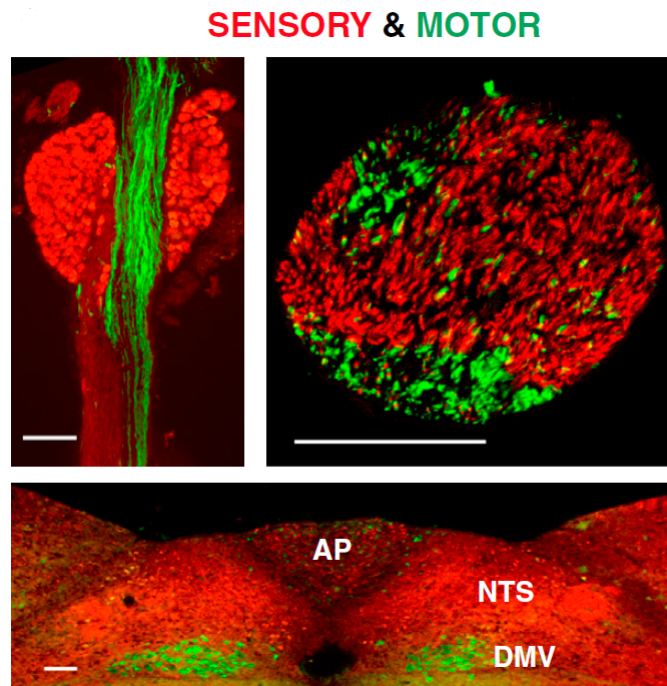


Figure 3.3: Markers for sensory and motor fibers of the vagus nerve. Fluorescence microscopy images of the JNG complex. JNG contains mostly sensory neurons Vglut2 (red) reaching visceral recipients in the brainstem, NTS and AP. The motor fibers of the vagus nerve (green) reach the DMV and the NA (not shown here). Figure from [Chang et al., 2015].

3.4.3 The sensory vagal-recipients brainstem regions : NTS, AP and Pa5

As previously discussed, neurons from the JNG project to the brainstem, where nodose neurons target NTS and AP, while jugular neurons target Pa5. The NTS can be divided into rostral, medial and caudal regions and serves as a crucial sensory gateway, relaying various visceral stimuli. These stimuli include mechano- and chemosensory information from the gastrointestinal tract, aorta, and lungs [Cutsforth-Gregory and Benarroch, 2017]. In the studies outlined in section 3.2, different genetic markers were used to investigate subtypes of vagal afferents representing various organs, revealing variations in the localisation of their brainstem projections (Figure 3.4).

Recently, the laboratory of Liberles discovered a more precise organization of internal organ representation within the NTS of mice [Ran et al., 2022]. They induced mechanical distension in different organs of the gut and upper airway using a surgically implanted balloon and observed the resulting responses in different parts of the NTS using two-photon calcium imaging technique. Within the NTS, discrete

neuronal populations predominantly encode sensory signals from distinct organs. This finding supports their previous study [Han et al., 2018], which suggests that the physical positions of organs in the body are reflected in the NTS representation (Figure 3.4).

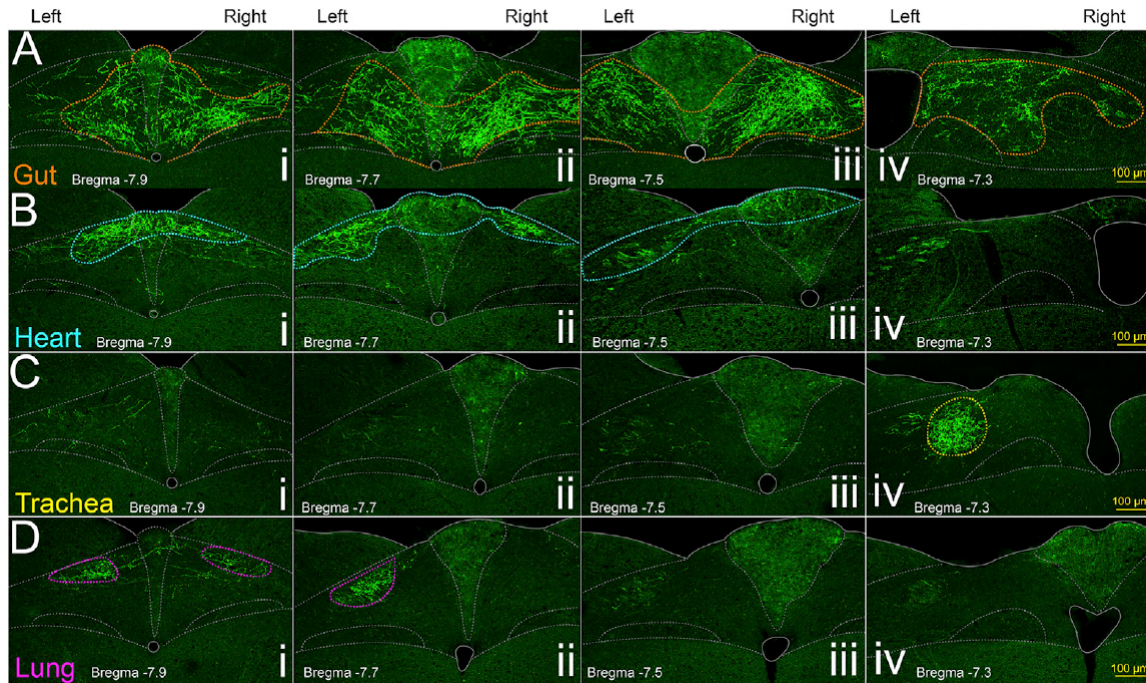


Figure 3.4: Vagal afferent projections in the NTS and AP The green fluorescent terminals come from different targeted organs injected with a retrograde virus Cre-carrying construct AAVrg-pmSyn1-EBFP-Cre. This was combined with the bilateral injection of a virus expressing ChR2 in the left and right JNGs. Gut (A) terminal fields occupied a distinctive area in ventromedial NTS from more caudal to more rostral levels (i-iv). Heart (B) terminal fields occupied a distinctive area in dorsomedial/dorsolateral NTS from more caudal to more rostral levels (i-iv). Trachea (C) terminal fields occupied a distinctive area in rostralateral NTS (i-iv). Lung (D) terminal fields occupied a distinctive area in caudodorsolateral NTS (i-iv). Figure from [Han et al., 2018].

3.4.4 Overview over the reflexes

Most sensory inputs of the vagus nerve into the CNS do not reach conscious levels of awareness. Instead, they influence reflex circuits important for organ function and body homeostasis, such as regulating cardiac function, respiration, gastrointestinal motility, and certain reflex actions (reviewed in [Prescott and Liberles, 2022]).

Vagal afferents innervate the heart, aorta, and other vessels below the diaphragm, influencing cardiovascular reflexes systems including baroreceptor reflex, Bainbridge reflex, hypoxic ventilatory response and Bezold-Jarisch reflex. Mechano- and chemosensory neurons are present in the heart and great arteries to monitor blood flow and its chemical composition. By modulating heart rate and blood pressure, the vagal afferent system can maintain cardiac and respiratory outputs

stable. One reflex of considerable importance is the baroreceptor reflex. For instance, an increase in blood pressure within the aorta activates baroreceptors that transmit signals on changes to the NTS. The NTS in turn, signals the dorsal motor nucleus of the vagus (DMV) and the *nucleus ambiguus* (Amb), which then transmit signals back to the heart. This results in a lowering of heart rate.

Regarding respiratory regulation, the vagus nerve is the main relay for sensory inputs originating from the lungs, trachea and larynx. These inputs influence essential respiratory parameters such as breathing rate, tidal volume and airway tone. Vagal sensory neurons detect airway threats and trigger protective reflexes such as coughing or swallowing. Furthermore, the vagus nerve is involved in the 'Hering-Breuer inspiratory reflex' [Berthoud and Neuhuber, 2000], which modulates breathing patterns by inhibiting inspiration during lung inflation, thus preventing overinflation and enhancing respiratory efficiency.

In the gut-brain axis, the vagus nerve is involved in a variety of behaviors. It serves as a conduit for conveying signals related to gut distension and nutrient availability to the brain. This feedback loop helps modulate feelings of satiety and hunger, thereby influencing food intake and contributing to the maintenance of a healthy body weight. Metabolically, vagal signaling influences processes such as glucose homeostasis, insulin secretion, and lipid metabolism.

Vagal sensory neurons also have the capacity to trigger immune responses, airway hyper-reactivity, sickness behaviors, and pain signals, such as those associated with a sore throat. By detecting pathogens and initiating immune defenses, the vagus nerve contributes to the body's defense mechanisms. The 'inflammatory reflex' is activated by the presence of pathogens or tissue damage, stimulating sensory fibers in the vagus nerve. This reflex is described as a localized and rapid response but can also trigger systemic anti-inflammatory effects by stimulating hormone release from the hypothalamus and pituitary gland [Tracey, 2002].

The role of the vagus nerve in the reflex systems described above reveal its importance in regulating physiological processes and in responding to internal and external stimuli.

3.4.5 Vagal pathways targeting sleep-wake and thermoregulatory centers

Neurons within the NTS establish connections with various brainstem and forebrain structures (Figure 3.5). There is a large amount projecting back to the NTS indicating the importance of reciprocal pathways. The vagal afferent system projects to brainstem areas, which then innervate emotional and memory-related regions such as the amygdala, hippocampus, and prefrontal cortex. Additionally, these projections reach sleep-related areas like the locus coeruleus (LC), and the hypothalamus, also involved in thermoregulation [Sawchenko, 1983; Han et al., 2018]. The preoptic/anterior hypothalamic regions are particularly crucial in regulating body temperature [Szymusiak, 2018]. They contain thermosensitive neurons, predominantly warm-sensitive, in the median preoptic nucleus and the medial preoptic area [Nakamura, 2011]. Activation of these warm-sensing neurons can promote sleep [McGinty and Szymusiak, 2001]. Moreover, projections to the Dorsal Raphe Nucleus (DR), a major serotonin-containing brainstem nucleus, play a significant role in sleep regulation. Serotonin, released from the DR, functions in promoting wakefulness and inhibiting REMS [Monti, 2010]. This interconnected network of neural pathways reveals the key role of the vagal afferent system in sleep regulation and the integration of thermoregulatory mechanisms with sleep-wake cycles (Figure 3.5).

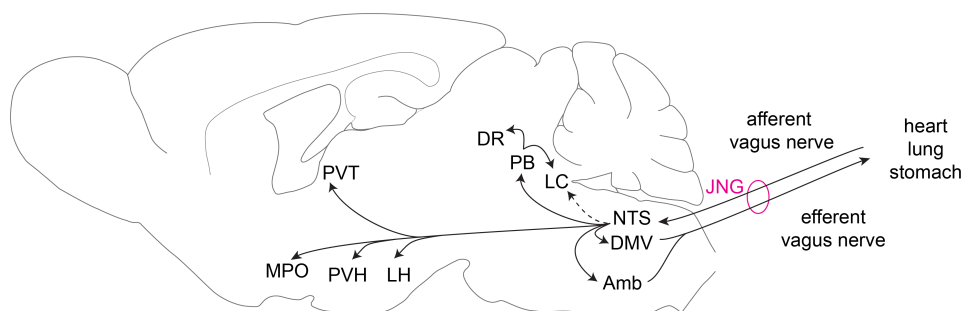


Figure 3.5: NTS-vagal afferent projections. Sagittal section of a mouse brain to show major projections from vagal afferents to principal brainstem nuclei and higher brain regions. Dotted line show an indirect connection between NTS and LC. Amb, *nucleus ambiguus*; DMV, dorsal motor nucleus of the vagus; DR, dorsal raphe; JNG, jugular-nodose ganglia; LC, *locus coeruleus*; LH, lateral hypothalamus; MPO, medial preoptic area; NTS, *nucleus tractus solitarius*; PB, parabrachial nucleus; PVH, paraventricular nucleus of the hypothalamus; PVT, paraventricular nucleus of the thalamus. Figure adapted from [Sawchenko, 1983]

3.4.6 Manipulation of the vagus nerve for clinical purposes

Due to its direct signaling pathway to the brain, researchers have been interested in stimulating the vagus nerve to influence brain activity instead of using invasive brain electrode implants. Initially, the effects of VNS on EEG activity were observed in cats in *encéphale isolé* preparation (with high cervical spinal section) [Chase and Nakamura, 1968]. As researchers found inhibitory effects on epileptic seizures [Zabara, 1992], VNS started to be used for the treatment of epilepsy when seizure drugs were not effective for the patients [George et al., 2000]. In 1997, VNS was approved by the Food and Drug Administration (FDA). Subsequent studies revealed mood improvements in epileptic patients regardless of the efficacy of seizures control, leading to its approval for treatment-resistant depression in 2005 [Rush et al., 2000; Austelle et al., 2022]. VNS typically involves the implantation of an electrode in the neck, which delivers electrical pulses directly to the left vagus nerve, similar to a cardiac pacemaker. The reason for using the left instead of the right vagus nerve is because it is thought to minimize potential cardiac side effects, such as bradycardia or asystole [Howland, 2014]. Over the last decade, a non-invasive method that does not necessitate surgery has been used to stimulate the vagus nerve, the transcutaneous VNS (tVNS or taVNS). This new technique only needs a portable device placed on the ear to target the auricular branch of the vagus nerve. The efficacy of tVNS has been validated with similar results to invasive VNS [Sharon et al., 2021].

The beneficial effects of VNS have expanded its use for other neuropsychiatric conditions such as anxiety disorders, cognitive impairments (Parkinson's, Alzheimer's) [Hays et al., 2013; Farrand et al., 2020; Broncel et al., 2020], disorders of consciousness [Vitello et al., 2023]. It has been shown to improve recovery after stroke [Hays et al., 2014; Khodaparast et al., 2014], favor brain plasticity [Clark et al., 1999; Childs et al., 2015; Sun et al., 2017; Jacobs et al., 2020], and influence decision making [Martin et al., 2004; Cao et al., 2016]. Not only can VNS improve brain-related disorders, but beneficial effects have also been seen in gastrointestinal disorders [Cirillo et al., 2022], obesity with VNS reducing food intake and body weight (due to release of anorexigenic hormones inducing a delay in gastric emptying) [Dai et al., 2020], and type 2 diabetes by reducing blood glucose (due to release of the peptide GLP-1) [Yin et al., 2019]. VNS is also viewed as a promising therapeutic approach in the treatment of inflammatory

disorders [Bonaz et al., 2017; Mastitskaya et al., 2021].

Information from the vagus nerve reaches the LC via the dorsal vagal complex [Han et al., 2018], as previously mentioned, and several studies have demonstrated the effects of VNS on monoaminergic systems. Indeed, VNS increases the cFos expression in LC neurons [Gieroba and Blessing, 1994], along with an increase in the discharge rate of LC neurons measured in LC unit activity [Groves et al., 2005; Dorr and Debonnel, 2006]. Recent *in vivo* Ca²⁺ imaging studies have also shown an increase in noradrenaline (NA) levels after VNS [Collins et al., 2021]. Furthermore, NA levels in the hippocampus and cortex, as well as dopamine in the prefrontal cortex and nucleus accumbens, increase following VNS [Roosevelt et al., 2006; Manta et al., 2013]. Additionally, a lesion of the LC in epileptic rats suppressed the anticonvulsant effects of VNS [Krahl et al., 1998]. VNS-induced pupil dilation [Bianca and Komisaruk, 2007; Jodoin et al., 2015; Sharon et al., 2021] is known to correlate with the firing of LC neurons. These findings reveal the significance of the LC in monitoring interoceptive stimuli from vagal sensory afferents.

Given our focus on visceral regions regulating sleep-wake cycle and the known impact of VNS on EEG activity, we were curious about how VNS affects sleep regulation. However, studies on the effects of VNS and tVNS on sleep lack clarity. The first studies in freely moving cats indicated that VNS promotes REMS and increases NREMS by affecting delta and sigma frequency bands [Fernández-Guardiola et al., 1999; Valdés-Cruz et al., 2002]. Contradictory results emerged from studies involving epileptic and depressive patients undergoing VNS treatment, showing enhanced daytime alertness, increased delta power in NREMS, and decreased REMS [Rizzo et al., 2003, 2004]. It is important to consider that human studies may involve patients on medications, which can influence sleep regulation, especially given the known effects of antiepileptic drugs. Additionally, the wide range of parameters used in VNS studies complicates direct comparisons among clinical findings. Investigating their individual contributions could offer insights into how VNS influences sleep regulation. Recent research has shown promising outcomes with tVNS, improving sleep quality in insomnia patients [Wu et al., 2022] and reducing daily sleepiness in narcoleptic patients [Winter et al., 2024]. These findings reveal a potential non-pharmacological approach for addressing sleep disorders, although the precise

mechanisms underlying these effects remain poorly understood (reviewed in [Romero-Osorio et al., 2018]).

Information from the vagus nerve reaches thermoregulatory centers, leading to the question: does VNS also affect thermoregulation? Studies in freely moving rats have shown that VNS decreased brain and core temperatures, resulting in tail heat loss due to vasodilation [Larsen et al., 2017]. Interestingly, rapid cycle VNS, known for its effects on hippocampal activity [Larsen et al., 2016], had a more pronounced impact on brain and core temperatures compared to standard cycle VNS, with similar parameters used in clinical treatments for epilepsy and depression. This highlights the variability in VNS effects depending on the parameters used. Further investigation by the same group revealed that the modulation of hippocampal activity was partially attributed to VNS-induced hypothermia, which could be prevented by external heating [Van Lysebettens et al., 2019]. In humans, although VNS increases energy expenditure by activating brown adipose tissue (BAT), no changes in overall body temperature were observed. The only change observed was a decrease in the distal skin temperature (feet and hands), indicating cutaneous vasoconstriction during VNS that would prevent heat loss [Vijgen et al., 2013]. This contradicts the notion of facilitated heat loss during VNS. This variation could be explained by the difference in the thermoregulatory specificity of different species, emphasizing the need for caution when translating VNS findings in rodents to humans. In conclusion, the manipulation of the vagus nerve provides a unique perspective on the complex dialogue between the body's internal systems and brain functions. However, the specific contributions of sensory and motor components of VNS remain to be fully elucidated.

3.4.7 Open questions in the field, relation to the experimental part of the thesis

Interoceptive pathways, particularly those involving the vagus nerve, remain a complex subject due to their potential implications for sleep regulation and physiological processes. Manipulating the vagus nerve through VNS leads to multiple beneficial effects on the brain, from plasticity to regulation of excitability to anti-inflammatory effects. All these are aspects of brain recovery that are also found

in sleep and we wonder whether vagal afferents could in fact boost some of sleep's beneficial functions. Yet to date it is not even known how vagal activity regulates basic sleep features, raising questions at different levels, related to sleep architecture, the multiple targets of vagal sensory afferents, the need to become more specific, but also the caution to make the difference between rodents and humans.

What are the underlying mechanisms by which vagal activity influences sleep architecture and quality? Does vagal activity primarily strengthen parasympathetic tone during sleep, or does it engage with other neural systems involved in sleep regulation, such as the LC?

How does vagal activity contribute to different states of sleep? Does vagal sensory input play a role in transitioning between these sleep states or in modulating the depth and quality of each state, potentially through its influence on thermoregulatory centers like the preoptic/anterior hypothalamic regions?

Given the organ-specific nature of vagal sensory pathways, how do signals from different organs influence sleep patterns? For instance, how might interoceptive signals related to gastrointestinal functions or cardiovascular activity affect sleep architecture and the spectral composition of sleep?

Considering the neuroplasticity and restorative functions associated with sleep, could vagal sensory afferents contribute to enhancing brain plasticity during sleep states?

The goal of my thesis is to manipulate vagal sensory afferents in freely moving mice in order to understand how interoceptive stimuli affect sleep regulation. My research aims to bridge the gap in our understanding of the specific roles of vagal activity in modulating sleep patterns and contribute to elucidating the mechanisms underlying the complex interplay between neural circuits, autonomic functions, and sleep states.

4 Results

4.1 Vagal sensory afferents regulate mouse sleep through brain-body cooling

Najma Cherrad, Alejandro Osorio-Forero, Yann Emmenegger, Laura MJ Fernandez, Paul Franken and Anita Lüthi

In preparation, BioRxiv by end of June 2024

Sensory isolation is a defining feature of sleep [Andrillon and Kouider, 2020], however much less is known about how internal bodily signals influence sleep-wake dynamics and the neural mechanisms underlying this interaction. Sleep and interoceptive signaling interact [Wei, 2019] and the autonomic activity changes across the vigilance states [Silvani and Dampney, 2013; De Zambotti et al., 2018]. The major pathway between the body and the brain is through the vagus nerve, part of the parasympathetic system [Berthoud and Neuhuber, 2000], which has been utilized as a clinical tool known as vagus nerve stimulation (VNS) to treat conditions such as epilepsy and depression [Broncel et al., 2020].

This study focus on the role of brain-body communication during sleep by selectively activating vagal sensory neurons using chemogenetics. *In vivo* chemogenetic stimulation of vagal sensory neurons resulted in elevated cFos activity in the NTS, accompanied by a reduction in heart rate and the induction of a unique NREMS-like state. Furthermore, the study revealed that this NREMS-like state led to a decrease in sleep spindle activity and an increase in low-frequency electroencephalographic power. This state, characterized by distinctive spectral patterns and temperature dynamics, not only suppressed REMS but also maintained a delicate equilibrium of sleep homeostasis. The NREMS-like state was associated with a cooling effect on both cortical and core body temperatures, which could be prevented by external warming, facilitating the restoration of normal sleep patterns. Vagal afferent activity has a crucial impact on body-brain physiology, specifically in maintaining a balance between NREMS and REMS through brain-body cooling. We suggest that bodily processes need to be included in the study of sleep regulation.

These findings not only deepen our knowledge of the neural mechanisms of sleep but also offer potential therapeutic avenues for targeting interoceptive pathways to optimize sleep outcomes and address sleep disorders.

This study is the principal work of my PhD thesis. I performed the *in vitro* experiments with the guidance and support of Prof. Anita Lüthi, Dr Gil Vantomme and Dr. Laura Fernandez. I carried out and designed the *in vivo* chemogenetics experiments. I did all the analysis, produced the figures and did the statistical analysis for the *in vitro* and *in vivo* experiments.

4.2 Noradrenergic locus coeruleus activity functionally partitions NREM sleep to gatekeep the NREM-REM sleep cycle.

Alejandro Osorio-Forero, Georgios Foustoukos, Romain Cardis, Najma Cherrad, Christiane Devenoges, Laura MJ Fernandez and Anita Lüthi
Nature Neuroscience, minor revisions 2024

Regulation of vigilant states has historically been studied by focusing on the overall activity of different brain systems [Aston-Jones and Cohen, 2005]. Under such framework, concepts such as REM-ON, REM-OFF, Wake-On, Wake-Off are commonly use [Brown et al., 2012]. Likewise, models such as flip-flops of state transitions [Saper et al., 2010] are based on reciprocate inhibition between these neuronal groups. More recent models of transition mechanisms propose a more heterogeneous relation between systems such as homeostatic drives [Park and Weber, 2020; Park et al., 2021] that further impact the architecture of NREM-REM ultradian cycles. Although these regulatory mechanisms might serve important roles in the control of vigilant states, other types of complex interactions across brain systems could be involved. In this work, we showed how the LC activity serves a permissive role for NREMS-to-REMS transitions. The study employed fiber photometry, a cutting-edge method that allows real-time monitoring of LC activity by measuring changes in fluorescence signals in

DBH-Cre mice. First, we found that NA signaling partitions NREMS, with high LC activity levels promoting an autonomic-subcortical arousal state that facilitates cortical microarousals, while low activity levels are essential for REMS entries. The fiber photometry technique was combined with closed-loop optogenetics to modulate LC activity at different moments in the NREMS-REMS cycle. Additionally, we used closed-loop automatic REMS restriction to study the role of the LC in moments of high REMS pressure. The findings demonstrate the role of LC in regulating the duration of NREMS and the total duration of the NREMS-REMS cycle.

Moreover, the research highlights the impact of external stimuli, such as stress-inducing wakefulness, on LC activity dynamics and subsequent sleep patterns. Stimulus-enriched wake experiences were found to disrupt the balance between high and low LC activity levels, leading to fragmented NREMS characterized by microarousals and delayed REMS onset. These findings point to the vulnerability of the NREMS-REMS cycle to external influences. This paper explores the role of noradrenergic LC activity in orchestrating the NREMS-REMS cycle and encourages future investigations into therapeutic interventions targeting LC function for sleep disorders.

This study is a collaboration between three former members of the lab. The story began with Romain Cardis, followed by Alejandro Osorio-Forero and Georgios Foustoukos. I contributed to the initial stages of this project at the beginning of my PhD under the supervision of Romain Cardis. As part of my training, I learned how to perform EEG/EMG implantations and analyze sleep data. This set of animals was REMS-deprived using motor vibration triggered by close-loop system designed by Romain Cardis. I analyzed the corresponding data and produced Figure 3b (“LC activity troughs rule REMS entries during REMS restriction (REMS-R)”) and Extended Data Figure 6 (“Validation of the efficiency and specificity of the REMS-R technique”).

4.3 When the locus coeruleus speaks up in sleep: recent insights, emerging perspectives.

Alejandro Osorio-Forero, Najma Cherrad, Lila Banterle, Laura MJ Fernandez and Anita Lüthi

International Journal of Molecular Sciences, 2022, doi.org/10.3390/ijms23095028

Commonly, noradrenergic activity has been historically associated almost exclusively to wakefulness [Aston-Jones and Cohen, 2005; Poe et al., 2020]. Pioneering work in the group of Prof. Aston-Jones already identified LC activity during NREM sleep [Aston-Jones and Bloom, 1981], these studies were further supported by more recent work in LC electrophysiology [Swift et al., 2018; Eschenko et al., 2012]. In this review we first focus on the historical aspects of LC noradrenergic activity during sleep. However, in the last years, the development of optogenetics and imaging techniques allow us to follow specific modulate and record neuronal activity and free levels of molecules in the brain at rates never seen before.

We thus review two studies [Kjaerby et al., 2022; Osorio-Forero et al., 2021] that describe an infraslow recurrent activity of the LC that releases noradrenaline in the thalamus and the prefrontal cortex. We further discuss the potential implications of this activity. The LC is the major NA brainstem nucleus that sends projections to many brain areas. By synthesizing recent research findings in animals and humans, this paper updates our understanding of the LC's functions during sleep. LC has traditionally been associated with a decrease of activity during sleep and a further reduction in REMS compared to NREMS. But recent findings from our lab reveal that noradrenergic signaling is also high during NREMS and fluctuates on an infraslow timescale [Lecci et al., 2017; Osorio-Forero et al., 2022]. This fluctuation contributes to the organization of brain oscillatory activity and seems to be important for sleep functions. The findings reviewed here have implications for understanding the intricate relationship between neuromodulation, brain activity, and sleep regulation.

One important feature of the noradrenergic system is its relation to autonomic activity [Wood and Valentino, 2017]. In this review I wrote the chapter on the relation between LC and the vagal afferent system. Many animal studies provide evidence

that the LC is an important target of vagal afferent nerve stimulation (reviewd in [Berger et al., 2021]) and vagus nerve stimulation (VNS) activates LC-NA system [Collins et al., 2021]. I discussed how sensory information from the vagus nerve reaches the LC via the dorsal vagal complex [Ruggiero et al., 1994; Lopes et al., 2016; Han et al., 2018], highlighting the importance of this pathway in autonomic feedback reflexes and control of physiological functions. The study sheds the light on the potential implications of vagal afferent signaling on LC function and its broader impact on sleep regulation and physiological processes.

5 Discussion

5.1 Scientific contributions

States of sleep are coordinated brain-bodily states. This coordination relies on reciprocal communication between the brain and the body and is central for sleep's beneficial actions on brain and bodily health. Neuroscientific approaches in sleep have traditionally focused on brain mechanisms relevant for sleep, asking how these mechanisms act to regulate bodily physiology. In my thesis, I have taken the reverse approach, asking how bodily sensory stimuli affect sleep. This question has required me to combine technical approaches from the brain-oriented neuroscience field with bodily manipulations. A critical step was the combination of viral transfection of vagal sensory neurons in combination with sleep and temperature recordings. Additionally, as also outlined in this discussion, I have driven this approach further to both brain and bodily viral transfection for fiber photometric and optogenetic manipulations. With the experiments conducted in the main project of this thesis, I provide detailed insights that vagal sensory stimulation of Vglut2-expressing neurons in the L-JNG induces a NREMS-like state and suppresses REMS. Furthermore, I have identified a brain-bodily cooling as a core mechanism for this effect, along with central mechanisms that likely also contribute. Together, my thesis has pioneered the technical challenges to study brain-body communication in sleep, and has made first steps to gain insight in the role of interoceptive signals in the regulation of sleep potentially through brain-body cooling and/or LC activity.

5.1.1 Technical contributions

The primary challenge of this thesis was to master the dissection of the JNG of the vagus nerve [Han and De Araujo, 2021] to transfect its sensory neurons with chemogenetic or optogenetic viruses. Accessing the JNG required a deep understanding of the anatomical arrangement of nerves and muscles to avoid unnecessary tissue or muscle damage. Furthermore, the proximity to the carotid and other veins necessitated extreme caution to prevent unwanted bleeding. I also had to create homemade retractors in addition to those purchased from the industry as they

were too large to manipulate muscles and nerves near the JNG. Through good practice and appropriate materials, I achieved a dissection where minimal tissue manipulation resulted in a 100% success rate of recovery. However, accessing the JNG was not the only challenging step; injecting the virus into the JNG posed another complication. I used glass pipettes with the smallest possible tip diameter, but not too small to avoid blockage. To confirm precise injection into the ganglion, I mixed the virus with a dye, turning the injection site blue as a visual indicator.

We integrated the manipulation of vagal sensory neuron activity with sleep recordings to examine their effects in freely behaving animals. I conducted EEG/EMG surgeries following established lab procedures and devised protocols to synchronize intraperitoneal injections of clozapine N-oxide (CNO) at the onset of the light phase with sleep recordings. In a later phase of my PhD, we collaborated with the laboratory of Paul Franken to measure cortical temperature. After initial data collection in their lab, we implemented the technique in ours, using a different type of thermistor. I developed protocols for thermistor calibration, involving immersion in water at two temperatures with constant current supply. I adapted the signal recording to integrate with the Intan system and created code for voltage-to-temperature conversion using established equations [Hoekstra et al., 2019].

To include body temperature recordings, I researched temperature literature and found that rectal temperature measurement in mice suited the temperature range, with prior habituation crucial to minimize stress [Meyer et al., 2017]. I also designed and tested heating experiments with various configurations to optimize the recovery of body and cortical temperature.

Furthermore, although not yet experimentally finalized, I have carried out pilot experiments to enable combined viral injections in both L-JNG and central brain areas. First, this involved combining fiber photometric measurements of NA level in the thalamus, virally injected with a GRAB sensor, with the viral injection of an excitatory Designer Receptor Exclusively Activated by Designer Drugs (DREADD) virus in the L-JNG. This approach will provide an initial assessment of LC activity during vagal sensory stimulation. Furthermore, we are also currently integrating vagal sensory stimulation with calcium imaging of the LC, virally injected with

jRCaMP calcium indicator, which will provide a more comprehensive view of LC activity by directly visualizing calcium dynamics, complementing the functional readout from the GRAB sensor.

I could also contribute to set up histological procedures for immunostaining of JNG tissue as well as cFos staining of brain sections after vagal sensory stimulation.

5.1.2 A chemogenetic approach to manipulate vagal sensory afferents *in vivo*

As outlined in the introduction of this thesis, the stimulation of the vagus nerve has been widely used for clinical treatment [Broncel et al., 2020]. Traditional VNS techniques typically stimulate both sensory and motor afferents simultaneously. Direct stimulation of motor efferents can lead to side effects through sympathetic stimulation of the cardiovascular, respiratory or digestive system. For example, VNS has been associated with inducing sleep apnoea [Romero-Osorio et al., 2018]. To avoid these effects, we specifically targeted the sensory neurons of the JNG. While I am aware that stimulation of these sensory neurons also recruits motor efferents, one expects this to happen in a more balanced manner in proportion to the number of activated sensory afferents. In contrast, a direct strong activation of motor afferents can be avoided.

Furthermore, chemogenetics allowed us to precisely target Vglut2-expressing neurons genetically, providing both specificity and the ability to acutely, reversibly, and dose-dependently activate these neurons. The vagal tone can then be enhanced by stimulating the parasympathetic system as it is naturally elevated during NREMS [Cerri and Amici, 2021; De Zambotti et al., 2018; Silvani and Dampney, 2013; Szymusiak, 2018]. This was confirmed by increased cFos activity in both the NTS and AP, together with a decrease in heart rate. Activation of the vagovagal reflex loop triggers efferent fibers, leading to direct downregulation of heart and blood flow. This mechanism likely importantly contributes to the observed drop in temperature given that vasodilation is an important consequence of parasympathetic activity [Harding et al., 2020; Szymusiak, 2018].

5.1.3 Transient brain-body cooling as a central mechanism underlying the effects of vagal sensory stimulation on sleep

5.1.3.1 General comments on temperature regulation and sleep

Sleep regulation and thermoregulation are tightly linked [Krauchi and Deboer, 2010]. The brain contains thermosensitive neurons in the preoptic anterior hypothalamus that will process cold and warm signals coming from the body. To maintain a stable core body temperature, these thermoregulatory regions trigger efferent responses such as shivering, sweating, vasodilation or vasoconstriction. The core body temperature and arousal states are regulated by the circadian clock located in the SCN, a small region of the hypothalamus [Saper et al., 2005; Kräuchi, 2007]. The core body temperature rhythm declines due to vasodilation in distal skin temperature (hands and feet in humans; tail in mice) and is strongly linked with NREMS onset [Kräuchi, 2007]. The relationship between these two systems has been challenged by disturbing one or the other. Changes in temperature can affect sleep regulation; heating the body by taking a bath before bedtime promotes faster sleep onset and increases NREMS [Horne and Shackell, 1987; Harding et al., 2019] by disrupting peripheral vasodilatory responses and triggering warm-sensitive neurons in the ventrolateral preoptic (VLPO). On the other hand, sleep deprivation disturbs the circadian temperature rhythm by increasing metabolic demand or inducing vasodilation [Krauchi and Deboer, 2010; Harding et al., 2019].

In our study, vagal sensory stimulation induced a polysomnographic state resembling NREMS, characterized by an increase in the low-frequency bands, a decrease in heart rate, and a reduction in brain and body temperatures. Additionally, the typical alternation between NREMS and REMS was disrupted as REMS was suppressed. However, the regulatory mechanisms of REMS were preserved; there was compensation for the REMS loss [Franken, 2002]. In light of the link between NREMS and thermoregulation, it will be important to determine whether these observations are a manifestation of this same link. For example, it is possible that the vagal sensory stimulation leads to a parasympathetic activity that is stronger than the one typically occurring in normal NREMS. This could have led to a stronger than normal brain-bodily cooling and an associated decline in EEG amplitude, while the overall

spectral profile remained reminiscent of NREMS. Monitoring the activity of the POA area in animals once in NREMS and once in the NREMS-like state would be helpful to clarify this. Additionally, measures of other central areas, such as the serotonergic raphe pallidus that regulated peripheral vasodilation, could be interesting. Additionally, I also find important to establish more multiparallel measures of brain-bodily activity during NREMS, to simultaneously measure cardiovascular parameters, breathing rates, and ideally, vagal activity directly. My findings strongly suggest that there could be a continuum between states of NREMS and the NREMS-like state in terms of more than just temperature.

5.1.3.2 REMS and temperature regulation

During REMS, there is a loss of temperature control [Parmeggiani, 2003; Cerri et al., 2017] with a suppression of thermoregulatory mechanisms such as shivering and non-shivering thermogenesis. Despite this, there is an increase in brain temperature due to vasoconstriction leading to more blood pumped toward the brain from the core body [Harding et al., 2019]. In our case, vagal sensory stimulation induced a decrease in brain and body temperature potentially due to vasodilation and heat loss through hypothalamic nuclei or autonomic feedback loops. During this period of brain-body cooling, REMS is absent and the extreme values we observed might not be ideal for a transition to a state very demanding in energy. However, when the CNO effect is dissipating and cortical temperature returns to normal values, it coincides with the reappearance of REMS. This highlights the intricate link between REMS and temperature. We wonder if the energy allocation hypothesis could go in the same direction as what we observed. Indeed, this hypothesis places REMS as a state in which all the energy is necessary in the brain to make it work properly in the sense that the energy resources are shifted away from the body to be allocated for the brain and especially for REMS [Schmidt, 2014]. However, in our study, while the temperature in the brain was decreasing, the temperature in the body as well. Here we induced a state where the whole brain-body system decreases its temperature. By actively inducing a warming of both cortical and body temperatures, we could partially recover the effects on sleep regulation with an earlier reappearance of REMS and a reduction in the time spent in NREMS-like state. Similarly, a study inducing

hypothermia in rats with VNS could recover several hippocampal electrophysiological parameters when the hypothermia was prevented with heating [Van Lysebettens et al., 2019].

5.1.3.3 Relationship to torpor

Vagal sensory stimulation resulted in a decrease in both cortical and body temperatures, leading to consideration of a potential induction of torpor even though the body temperature values did not reach the levels observed during torpor [Deboer and Tobler, 1995; Harding et al., 2019]. Additionally, the NREMS-like state is similar to the state of decreased overall brain activity [Deboer and Tobler, 1995] found in torpor, however, the mice remained easily arousable, as evidenced by the rise in cortical temperatures following rectal temperature measurements. After torpor, there is typically an increase in slow oscillation activity due to the loss of the restorative aspect of sleep [Palchykova et al., 2002]. However, in our case, delta activity is lowered after vagal sensory stimulation and only seems to recover after 24 h compared to the NaCl condition. Considering these points it is unlikely that we induced a state of torpor and we can say that we could induce a drop in body and brain temperature by stimulating bodily sensory signals with a stable ambient temperature and *ad libitum* food conditions.

5.1.3.4 Vagal sensory stimulation activates thermoregulatory centers

Preoptic hypothalamic neurons are known to be involved in thermoregulatory processes. Studies using chemogenetic stimulation of a subpopulation of these neurons located in the VLPO expressing galanin have shown REMS suppression together with a decrease in body temperature [Kroeger et al., 2018]. Another study found similar results when stimulating warm-sensitive glutamatergic/nitrergic neurons in the medial-median preoptic area [Harding et al., 2018]. These findings place the preoptic area of the hypothalamus as a possible candidate in mediating the hypothermic effect of vagal sensory stimulation through the NTS and the parabrachial nuclei, independently of LC activation.

5.1.3.5 Vagal sensory stimulation activates central sleep circuits

An important point I would like to clarify is the identification of the central neural mechanisms that underlie the alterations in sleep patterns. Numerous studies in both humans and animals have shown that VNS increases LC activity and noradrenergic signaling [Jodoin et al., 2015; Sharon et al., 2021; Berger et al., 2021]. Vagal afferents project to the LC via the dorsal vagal complex [Han et al., 2018]. In our laboratory, we successfully manipulated LC activity using optogenetic techniques and observed a suppression of REMS and attenuation of sigma fluctuation when the LC was stimulated [Osorio-Forero et al., 2024]. Combining vagal sensory stimulation with the measure of NA release in the thalamus via fiber photometry (GRAB sensor), we observed an increase in NA level, suggesting a high LC activity (Figure 5.1). These findings place the LC as a possible candidate to the observed effects on REMS.

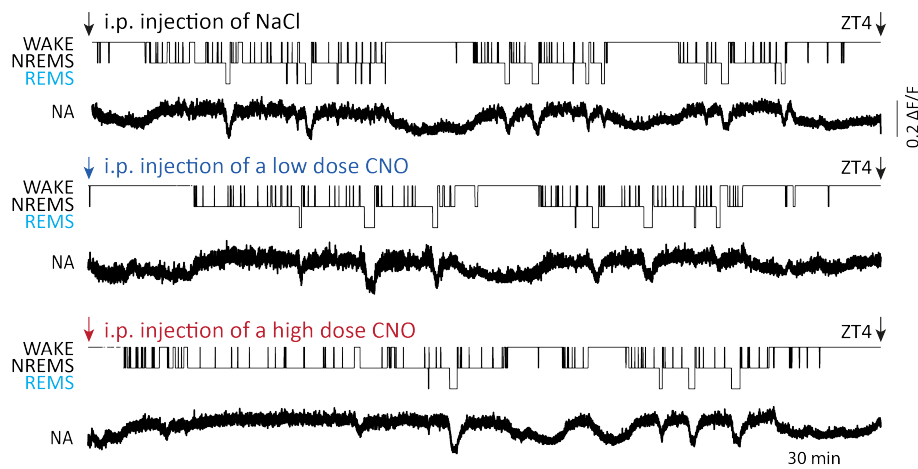


Figure 5.1: Hypnograms of a mouse injected with NaCl, CNO 1.5 mg/kg and CNO 2.5 mg/kg at light phase onset, with traces of noradrenaline (NA) level activity measured in the thalamus using fiber photometry. Note that NA level stays high in the CNO-effect period.

5.1.4 Functional connectivity of L-JNG afferent fibers within NTS *in vitro*

To functionally validate the vagal sensory afferent connectivity, we aimed to use patch-clamp recordings that provide the most direct read-outs of synaptic activity

and underlying ionic mechanisms. We were encouraged to do so based on ample prior studies that had used extracellular stimulation to activate the vagus nerve in acute slice preparations of the brainstem. However, as we sought to activate vagal sensory neurons specifically, we needed to combine optogenetic activation of these afferents with patch-clamp recordings. The challenge thus was to obtain sufficient ChR2 expression in vagal sensory neurons and to identify the sites of contact within the slice. To the best of my knowledge, ChR2-driven vagal sensory stimulation has never been used in combination with in vitro whole-cell patch-clamp recordings. In my experiments, I managed to obtain synaptic responses of NTS neurons through optogenetic activation of L-JNG neurons previously injected with a virus-expressing ChR2, with a number of similarities but also differences compared to pioneering work. These studies have focused on vagal fiber-evoked synaptic responses in the NTS [Miles, 1986; Andresen and Mendelowitz, 1996; Kline et al., 2002; Bailey et al., 2008]. In agreement with these studies, we also observed large synaptic currents, yet with much lower connectivity. We also were most successful once we identified a hotspot of connectivity in the NTS, particularly the caudal part. This could indicate that ChR2 expression did not work equally well in all sensory afferents, but occurred preferentially in a subgroup of afferents. Indeed, it is known that sensory afferents are not only functionally heterogeneous, but they also show different degrees of myelination, which could have affected the amount of ChR2 necessary to provide reliable stimulation. In agreement with earlier work, we also, where found that optogenetic stimulation elicits strong and stable EPSCs, yet that these were often composed of mono- and polysynaptic components [Bailey et al., 2008; Doyle and Andresen, 2001].

In a small series of experiments, we convinced ourselves that our sensory afferents formed monosynaptic contacts by using a well-established pharmacological paradigm. Initially, a bath of Tetrodotoxin (TTX) to block the sodium channels resulted in the suppression of light-evoked EPSCs. Subsequent application of a bath of 4-Aminopyridine (4AP), a potassium channel blocker, allowed us to recover the responses that were monosynaptic. Finally, applying a bath of 6,7-Dinitroquinoxaline-2,3-dione (DNQX), a AMPA receptor blocker, revealed the glutamatergic aspects of these synaptic connections by suppressing the evoked

responses. Our experiments clearly demonstrated a monosynaptic glutamatergic response (Figure 5.2), and this could not be done before with extracellular stimulation.

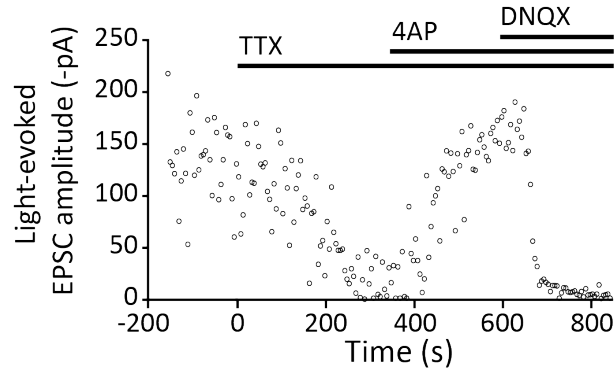


Figure 5.2: Monosynaptic nature of the vagal NTS synaptic connection. In vitro whole-cell patch clamp recordings from the NTS neurons with representative amplitude of light-elicited EPSCs in different pharmacological conditions (bath application of the drugs TTX, 4AP and DNQX). Note the reappearance of an evoked response when 4AP is applied.

5.2 Limitations and perspectives

5.2.1 Optogenetics *in vitro*

Limitations. Contrary to findings in the literature, our use of optogenetic stimulation to stimulate vagal sensory afferent led to a very low number of connected neurons. It appears that the transport of ChR2 from the JNG neurons to the brainstem NTS may not have been sufficient to consistently elicit responses. This was evidenced by the need to use long pulses (up to 5 ms) to trigger synaptic responses. Despite testing several serotypes of opsins, we did not achieve consistent success. However, we did notice that targeting the hotspot in the caudal NTS led to more reliable responses, suggesting that fibers expressing ChR2 were strongest in this area.

5.2.2 Optogenetics *in vivo*

Limitations. Our attempts to employ optogenetics in vivo were unsuccessful. Only a small amount of fibers appeared to express ChR2, in contrast to the broader transduction achieved with the chemogenetic DREADD virus.

Perspectives. To overcome these limits, we could try other viral vectors that may enhance the expression of ChR2 in vagal sensory fibers. Additionally, direct application of light on top of the JNG may improve the efficiency of optogenetic stimulation. But to my knowledge this has been done only in anesthetized animals, not in freely moving ones.

5.2.3 Chemogenetics *in vivo*

Limitations 1. Initially, we structured our experiments to alternate between different conditions on consecutive days, allowing for a 48-h interval in the case of high doses of CNO. However, at the beginning we encountered challenges in mastering the dissection of the JNG which made it difficult to consistently target the ganglion accurately. Although we achieved a 100% success rate in post-surgical recoveries, precise injection of virus in the JNG remained challenging. Consequently, our experimental paradigm was based on early observation of sleep effects, especially on the latency to the first consolidated REMS episode, with the low CNO dose (CNO 1.5 mg/kg) showing a duration about 1 hour and the high dose (CNO 2.5 mg/kg) showing effects for up to 4 hours. However, as surgeries improved over time, we observed effects with the low dose that could reach the 4 hours of the previous high dose.

Perspectives 1. Ideally, to avoid possible remaining effects between the sessions we should consider increasing the number of days between the different conditions or changing the dosage of CNO to have a more mild effect with the low dose.

Limitations 2. Our main study primarily focused on stimulating the sensory neurons of the left vagus nerve. This decision was influenced by VNS studies in humans, which typically target the left vagus nerve to minimize potential cardiac effects because vagal efferents target the cardiovascular system asymmetrically. However, the left and right JNGs innervate organs differently [Waise et al., 2018] and project to the brain in distinct regions [Han et al., 2018], even though some studies have not identified differences between left and right JNGs [Tan et al., 2020; Davis et al., 2020].

Perspectives 2. To expand our understanding of vagal sensory signaling and its impact on sleep, we should consider investigating the right JNG and perform the same experiments as for the left JNG.

Limitations 3. One limitation we encountered was the challenge of defining the transition from the NREMS-like state back to normal sleep. This transition is a gradual process and does not have a clear threshold. Initially, we looked at the time before the first consolidated REMS episode as an indicator, but we noted that neither sigma activity nor heart rate had fully recovered at this point.

Perspectives 3. To address this, we considered using heart rate as a marker for the return of NREMS and separating the data to establish a threshold that would characterize this transition more accurately. Heart rate serves as a strong correlate as it is very sensitive due to the baroreflex system. Our stimulation also triggers a feedback loop that directly regulates heart rate through the pathway, L-JNG, NTS, DMV, baroreceptors, leading to parasympathetic activation to slow down heart rate. Therefore, observing the heart rate returning to its normal value can serve as a good threshold for recovery from the NREMS-like state. Furthermore, to characterize even more this state, video recordings of sleeping behavior following vagal sensory stimulation, including positions and nesting habits, will provide valuable insights. Finally, performing a Loss of righting reflex (LORR) test to assess the animal's consciousness will confirm that the NREMS-like state is a reversible state.

5.2.4 Cortical temperature recordings

Limitations. During cortical temperature recordings, we used two types of thermistors. However, we encountered issues with one of the thermistors used in the main experiments because we found values lower than those reported in a previous study [Hoekstra et al., 2019], although the temperature dynamics appeared correct. This particular type of thermistor was only placed on the top of the brain surface and may have been intended for complete embedding in the brain tissue. Additionally, the calibration was performed with the thermistor fully immersed in the water, which may have affected the accuracy of cortical temperature measurements given its surface placement on the dura mater. We decided to present the relative difference in temperature rather than absolute values since the latter did not represent normal cortical temperature ranges in mice. Interestingly, the decrease in cortical temperature we observed after vagal sensory stimulation, was consistent across another set of data using a different type of thermistor that did not require

embedding and provide accurate values for mouse cortical temperature. Perspectives: Having an absolute temperature would allow us to give a more precise value of the temperature at the time REMS recover and perhaps find a permissive temperature intra-individual at which value REMS can reappear.

5.2.5 Body temperature measures

Limitations. Body temperature was measured at only two time points using a rectal probe to minimize disturbances to the animals' sleep. Rectal measurements are used as a proxy for core temperature [Meyer et al., 2017]. Since the primary focus of our project was on sleep and its characteristics, the methodology for temperature measurement was kept straightforward and minimally invasive.

Perspectives. To improve our understanding of temperature dynamics in relation to sleep patterns during vagal sensory stimulation, several approaches could be considered in future studies. We could use thermal cameras to visualize temperature fluctuations throughout the body, including areas such as the tail where heat loss is prominent. Additionally, using wearable body caps equipped with sensors to track body temperature changes continuously. Finally, installing thermosensors targeting different internal organs could provide detailed information on organ-specific variations.

5.2.6 Ambient temperature control

Limitations 1. Our method of heating involved placing heating pads inside and below the cage of the animals, and covered with aluminum to minimize noise during recordings. However, the temperature was maintained at a fixed value that was determined to recover body temperature to approximately normal levels, rather than being adapted to the body temperature of the animal. While this approach successfully reduced the drop in cortical and body temperature induced by vagal sensory stimulation, it did not account for individual variations or optimal temperature requirements for each animal. The worry also was to not heat too much the animal as a too elevated ambient temperature can prevent REMS appearance [Komagata et al., 2019] and will then confound with the effects we have with the vagal sensory stimulation.

Perspectives 1. A more precise heating control system is needed to adjust the temperature in real-time based on individual animal measurements. This approach would involve continuously monitoring the animals' temperature and dynamically adjusting the heating parameters to maintain their "normal" temperature levels. By doing so, we can investigate whether completely suppressing the observed effects on sleep is achievable by warming up the animals to their optimal temperature range.

Limitations 2. Additionally, exploring the impact of ambient temperature on sleep patterns is crucial, as ambient temperature significantly influences sleep regulation across different species. Indeed, REMS is very sensitive to ambient temperature and can be lost if the ambient temperature is higher or lower than the thermal neutral zone of the animal [Harding et al., 2020]. Our experiments were conducted at an ambient temperature of around 22°C, while the thermal neutral zone for mice ranges between 26°C and 34°C [Gaskill et al., 2009; Harding et al., 2020]. This discrepancy suggests that the mice were not housed at their preferred temperature during our experiments and certainly already triggered thermoregulatory processes to compensate.

Perspectives 2. In future studies, modifying only the ambient temperature could provide valuable insights into how sleep patterns and physiological responses are affected when mice are within their thermal neutral zones.

5.2.7 Targeting subpopulation of vagal sensory afferents

Perspectives. Researchers have managed to isolate only the sensory afferents coming from one organ in particular: the gut [Han et al., 2018], the airways [Williams et al., 2016] to explore the implications of organ-specific vagal afferent activity on sleep and its functions. For example, using Glp1r-Cre mice, target mechanical distention of the gut, can help investigate the impact of digestive system signals on sleep.

5.2.8 LC-NA system

Perspectives. Recent findings in the lab indicate that optogenetic inhibition of LC neurons increases the number of REM sleep episodes [Osorio-Forero et al., 2024]. Given the known influence of both LC activity and vagal sensory stimulation on sleep patterns, we aim to determine which system, LC or vagal tone, exerts a stronger effect

on REM sleep, or if there are alternative pathways involved in the effect of vagal sensory stimulation. To address this question, we propose a dual manipulation approach. Specifically, we plan to activate vagal sensory neurons using chemogenetic stimulation while simultaneously silencing LC neurons using optogenetic inhibition.

5.2.9 Sleep analysis

Limitations. One limitation encountered during spectral analysis of NREMS between NaCl and CNO conditions was the need to compare similar amounts of NREMS. This approach involved comparing NREMS periods that did not occur simultaneously during the light phase. As a result, variations in NREMS characteristics due to circadian rhythms at different phases of the light phase were not accounted for.

5.2.10 Concluding remarks

In this study, we could present the implication of bodily signaling in sleep regulation through vagal sensory stimulation. These findings could have significant implications for future investigations into the potential therapeutic benefits of VNS in humans. Specifically, the observed decrease in temperature resulting from VNS may play a role in neuroprotection and could contribute to the beneficial effects observed in clinical settings.

Bibliography

- Agostoni, E., Chinnock, J. E., Daly, M. D. B., and Murray, J. G. (1957). Functional and histological studies of the vagus nerve and its branches to the heart, lungs and abdominal viscera in the cat. *The Journal of Physiology*, 135(1):182–205.
- Andresen, M. C. and Mendelowitz, D. (1996). Sensory afferent neurotransmission in caudal nucleus tractus solitarius—common denominators. *Chem Senses*, 21(3):387–95.
- Andrillon, T. and Kouider, S. (2020). The vigilant sleeper: neural mechanisms of sensory (de)coupling during sleep. *Current Opinion in Physiology*, 15:47–59.
- Arnold, C. (2017). Jellyfish caught snoozing give clues to origin of sleep. *Nature*, page nature.2017.22654.
- Aston-Jones, G. and Bloom, F. E. (1981). Activity of norepinephrine-containing locus coeruleus neurons in behaving rats anticipates fluctuations in the sleep-walking cycle. *The Journal of Neuroscience*, 1(8):876–886.
- Aston-Jones, G. and Cohen, J. D. (2005). Adaptive gain and the role of the locus coeruleus–norepinephrine system in optimal performance. *Journal of Comparative Neurology*, 493(1):99–110.
- Austelle, C. W., O’Leary, G. H., Thompson, S., Gruber, E., Kahn, A., Manett, A. J., Short, B., and Badran, B. W. (2022). A comprehensive review of vagus nerve stimulation for depression. *Neuromodulation: Technology at the Neural Interface*, 25(3):309–315.
- Azzalini, D., Rebollo, I., and Tallon-Baudry, C. (2019). Visceral Signals Shape Brain Dynamics and Cognition. *Trends in Cognitive Sciences*, 23(6):488–509.
- Bai, L., Mesgarzadeh, S., Ramesh, K. S., Huey, E. L., Liu, Y., Gray, L. A., Aitken, T. J., Chen, Y., Beutler, L. R., Ahn, J. S., Madisen, L., Zeng, H., Krasnow, M. A., and Knight, Z. A. (2019). Genetic Identification of Vagal Sensory Neurons That Control Feeding. *Cell*, 179(5):1129–1143 e23.

- Bailey, T. W., Appleyard, S. M., Jin, Y. H., and Andresen, M. C. (2008). Organization and properties of GABAergic neurons in solitary tract nucleus (NTS). *J Neurophysiol*, 99(4):1712–22.
- Bastuji, H., Perchet, C., Legrain, V., Montes, C., and Garcia-Larrea, L. (2008). Laser evoked responses to painful stimulation persist during sleep and predict subsequent arousals. *Pain*, 137(3):589–599.
- Benarroch, E. E. (2018). Brainstem integration of arousal, sleep, cardiovascular, and respiratory control. *Neurology*, 91(21):958–966.
- Berger, A., Vespa, S., Dricot, L., Dumoulin, M., Iachim, E., Doguet, P., Vandewalle, G., and El Tahry, R. (2021). How Is the Norepinephrine System Involved in the Antiepileptic Effects of Vagus Nerve Stimulation? *Front Neurosci*, 15:790943.
- Berger, R. J. and Phillips, N. H. (1995). Energy conservation and sleep. *Behavioural Brain Research*, 69(1-2):65–73.
- Berntson, G. G. and Khalsa, S. S. (2021). Neural Circuits of Interoception. *Trends in Neurosciences*, 44(1):17–28.
- Berthoud, H. R., Blackshaw, L. A., Brookes, S. J. H., and Grundy, D. (2004). Neuroanatomy of extrinsic afferents supplying the gastrointestinal tract. *Neurogastroenterology & Motility*, 16(s1):28–33.
- Berthoud, H.-R. and Neuhuber, W. L. (2000). Functional and chemical anatomy of the afferent vagal system. *Autonomic Neuroscience*, 85(1-3):1–17.
- Bianca, R. and Komisaruk, B. R. (2007). Pupil dilatation in response to vagal afferent electrical stimulation is mediated by inhibition of parasympathetic outflow in the rat. *Brain Res.*, 1177:29–36.
- Bonaz, B., Lane, R. D., Oshinsky, M. L., Kenny, P. J., Sinha, R., Mayer, E. A., and Critchley, H. D. (2021). Diseases, Disorders, and Comorbidities of Interoception. *Trends in Neurosciences*, 44(1):39–51.
- Bonaz, B., Sinniger, V., and Pellissier, S. (2017). The Vagus Nerve in the Neuro-Immune Axis: Implications in the Pathology of the Gastrointestinal Tract. *Frontiers in Immunology*, 8(1452):1–14. Publisher: Frontiers.

- Brodt, S., Inostroza, M., Niethard, N., and Born, J. (2023). Sleep-A brain-state serving systems memory consolidation. *Neuron*, 111(7):1050–1075.
- Broncel, A., Bocian, R., Kłos-Wojtczak, P., Kulbat-Warycha, K., and Konopacki, J. (2020). Vagal nerve stimulation as a promising tool in the improvement of cognitive disorders. *Brain Res. Bull.*, 155:37–47.
- Brookes, S. J. H., Spencer, N. J., Costa, M., and Zagorodnyuk, V. P. (2013). Extrinsic primary afferent signalling in the gut. *Nature Reviews Gastroenterology & Hepatology*, 10(5):286–296.
- Brown, R. E., Basheer, R., McKenna, J. T., Strecker, R. E., and McCarley, R. W. (2012). Control of Sleep and Wakefulness. *Physiological Reviews*, 92(3):1087–1187.
- Cacioppo, J. T., Tassinari, L. G., and Berntson, G. (2007). *Handbook of Psychophysiology*. Cambridge University Press. Google-Books-ID: E7hRKwVBXb4C.
- Cao, B., Wang, J., Shahed, M., Jelfs, B., Chan, R. H. M., and Li, Y. (2016). Vagus Nerve Stimulation Alters Phase Synchrony of the Anterior Cingulate Cortex and Facilitates Decision Making in Rats. *Scientific Reports*, 6(35135):1–12. Publisher: Nature Publishing Group.
- Cerri, M. and Amici, R. (2021). Thermoregulation and Sleep: Functional Interaction and Central Nervous Control. *Compr Physiol*, 11(2):1591–1604.
- Cerri, M., Luppi, M., Tupone, D., Zamboni, G., and Amici, R. (2017). REM Sleep and Endothermy: Potential Sites and Mechanism of a Reciprocal Interference. *Front Physiol*, 8:624.
- Chang, R., Strohlic, D., Williams, E., Umans, B., and Liberles, S. (2015). Vagal Sensory Neuron Subtypes that Differentially Control Breathing. *Cell*, 161(3):622–633.
- Chase, M. H. and Nakamura, Y. (1968). Cortical and subcortical EEG patterns of response to afferent abdominal vagal stimulation: Neurographic correlates. *Physiology & Behavior*, 3(5):605–610.
- Cheshire, W. P. (2016). Thermoregulatory disorders and illness related to heat and cold stress. *Autonomic Neuroscience*, 196:91–104.

- Childs, J. E., Alvarez-Dieppa, A. C., McIntyre, C. K., and Kroener, S. (2015). Vagus nerve stimulation as a tool to induce plasticity in pathways relevant for extinction learning. *J. Vis. Exp.*, 102:e53032.
- Chouchou, F. and Desseilles, M. (2014). Heart rate variability: a tool to explore the sleeping brain? *Frontiers in Neuroscience*, 8(402):1–9.
- Cirillo, G., Negrete-Diaz, F., Yucuma, D., Virtuoso, A., Korai, S. A., De Luca, C., Kaniusas, E., Papa, M., and Panetsos, F. (2022). Vagus Nerve Stimulation: A Personalized Therapeutic Approach for Crohn’s and Other Inflammatory Bowel Diseases. *Cells*, 11(24):4103. Number: 24 Publisher: Multidisciplinary Digital Publishing Institute.
- Clark, K. B., Naritoku, D. K., Smith, D. C., Browning, R. A., and Jensen, R. A. (1999). Enhanced recognition memory following vagus nerve stimulation in human subjects. *Nature Neuroscience*, 2(1):94–98.
- Collins, L., Boddington, L., Steffan, P. J., and McCormick, D. (2021). Vagus nerve stimulation induces widespread cortical and behavioral activation. *Current Biology*, 31(10):2088–2098.e3.
- Cortelli, P. and Lombardi, C. (2005). Chapter 29 Sleep and autonomic nervous system dysfunction. In *Handbook of Clinical Neurophysiology*, volume 6, pages 343–353. Elsevier, Standford, USA.
- Critchley, H. and Harrison, N. (2013). Visceral Influences on Brain and Behavior. *Neuron*, 77(4):624–638.
- Critchley, H. D. and Garfinkel, S. N. (2017). Interoception and emotion. *Current Opinion in Psychology*, 17:7–14.
- Cutsforth-Gregory, J. K. and Benarroch, E. E. (2017). Nucleus of the solitary tract, medullary reflexes, and clinical implications. *Neurology*, 88(12):1187–1196.
- Dai, F., Yin, J., and Chen, J. D. Z. (2020). Effects and Mechanisms of Vagal Nerve Stimulation on Body Weight in Diet-Induced Obese Rats. *Obesity Surgery*, 30(3):948–956.

- Davis, E., Suarez, A., Liu, C., Cortella, A., de Lartigue, G., and Kanoski, S. (2020). Vagal afferent nerve ghrelin signaling influences energy balance and episodic memory. *The FASEB Journal*, 34(S1):1–1. _eprint: <https://onlinelibrary.wiley.com/doi/pdf/10.1096/fasebj.2020.34.s1.09882>.
- De Zambotti, M., Trinder, J., Silvani, A., Colrain, I. M., and Baker, F. C. (2018). Dynamic coupling between the central and autonomic nervous systems during sleep: A review. *Neuroscience & Biobehavioral Reviews*, 90:84–103.
- Deboer, T. and Tobler, I. (1995). Temperature dependence of EEG frequencies during natural hypothermia. *Brain Res*, 670(1):153–6.
- Dibner, C., Schibler, U., and Albrecht, U. (2010). The Mammalian Circadian Timing System: Organization and Coordination of Central and Peripheral Clocks. *Annual Review of Physiology*, 72(1):517–549.
- Dorr, A. E. and Debonnel, G. (2006). Effect of vagus nerve stimulation on serotonergic and noradrenergic transmission. *J. Pharmacol. Exp. Ther.*, 318(2):890–898.
- Doyle, M. W. and Andresen, M. C. (2001). Reliability of monosynaptic sensory transmission in brain stem neurons in vitro. *J Neurophysiol*, 85(5):2213–23.
- Driver, H. S., Werth, E., Dijk, D.-J., and Borbély, A. A. (2008). The Menstrual Cycle Effects on Sleep. *Sleep Medicine Clinics*, 3(1):1–11.
- Duffy, M. E., Smith, A. R., and Joiner, T. E. (2021). Interoceptive dysfunction indicates presence and severity of self-injurious behaviors in a clinically severe transdiagnostic sample. *Psychiatry Research*, 305(6):114210.
- Eschenko, O., Magri, C., Panzeri, S., and Sara, S. J. (2012). Noradrenergic Neurons of the Locus Coeruleus Are Phase Locked to Cortical Up-Down States during Sleep. *Cerebral Cortex*, 22(2):426–435.
- Farrand, A. Q., Verner, R. S., McGuire, R. M., Helke, K. L., Hinson, V. K., and Boger, H. A. (2020). Differential effects of vagus nerve stimulation paradigms guide clinical development for Parkinson’s disease. *Brain Stimulation*, 13(5):1323–1332.

- Fernández-Guardiola, A., Martínez, A., Valdés-Cruz, A., Magdaleno-Madriral, V., Martínez, D., and Fernández-Mas, R. (1999). Vagus nerve prolonged stimulation in cats: effects on epileptogenesis (amygdala electrical kindling): behavioral and electrographic changes. *Epilepsia*, 40(7):822–829.
- Franken, P. (2002). Long-term vs. short-term processes regulating REM sleep. *J Sleep Res*, 11(1):17–28.
- Gaskill, B. N., Rohr, S. A., Pajor, E. A., Lucas, J. R., and Garner, J. P. (2009). Some like it hot: Mouse temperature preferences in laboratory housing. *Applied Animal Behaviour Science*, 116(2-4):279–285.
- George, M. S., Sackeim, H. A., Rush, A., Marangell, L. B., Nahas, Z., Husain, M. M., Lisanby, S., Burt, T., Goldman, J., and Ballenger, J. C. (2000). Vagus nerve stimulation: a new tool for brain research and therapy. *Biological Psychiatry*, 47(4):287–295.
- Gieroba, Z. and Blessing, W. (1994). Fos-containing neurons in medulla and pons after unilateral stimulation of the afferent abdominal vagus in conscious rabbits. *Neuroscience*, 59(4):851–858.
- Groves, D. A., Bowman, E. M., and Brown, V. J. (2005). Recordings from the rat locus coeruleus during acute vagal nerve stimulation in the anaesthetised rat. *Neurosci. Lett.*, 379(3):174–179.
- Han, W. and De Araujo, I. E. (2021). Dissection and surgical approaches to the mouse jugular-nodose ganglia. *STAR Protocols*, 2(2):100474.
- Han, W., Tellez, L. A., Perkins, M. H., Perez, I. O., Qu, T., Ferreira, J., Ferreira, T. L., Quinn, D., Liu, Z.-W., Gao, X.-B., Kaelberer, M. M., Bohórquez, D. V., Shammah-Lagnado, S. J., De Lartigue, G., and De Araujo, I. E. (2018). A Neural Circuit for Gut-Induced Reward. *Cell*, 175(3):665–678.e23.
- Harding, E. C., Franks, N. P., and Wisden, W. (2019). The Temperature Dependence of Sleep. *Front Neurosci*, 13:336.
- Harding, E. C., Franks, N. P., and Wisden, W. (2020). Sleep and thermoregulation. *Curr Opin Physiol*, 15:7–13.

- Harding, E. C., Yu, X., Miao, A., Andrews, N., Ma, Y., Ye, Z., Lignos, L., Miracca, G., Ba, W., Yustos, R., Vyssotski, A. L., Wisden, W., and Franks, N. P. (2018). A Neuronal Hub Binding Sleep Initiation and Body Cooling in Response to a Warm External Stimulus. *Curr Biol*, 28(14):2263–2273 e4.
- Hashimoto, K. and Yang, C. (2022). Special issue on “Brain–body communication in health and diseases”. *Brain Research Bulletin*, 186:47–49.
- Hays, S. A., Khodaparast, N., Hulsey, D. R., Ruiz, A., Sloan, A. M., Rennaker, R. L., and Kilgard, M. P. (2014). Vagus Nerve Stimulation During Rehabilitative Training Improves Functional Recovery After Intracerebral Hemorrhage. *Stroke*, 45(10):3097–3100. Publisher: American Heart Association.
- Hays, S. A., Rennaker, R. L., and Kilgard, M. P. (2013). Targeting plasticity with vagus nerve stimulation to treat neurological disease. *Prog. Brain Res.*, 207:275–299.
- Hoekstra, M. M., Emmenegger, Y., Hubbard, J., and Franken, P. (2019). Cold-inducible RNA-binding protein (CIRBP) adjusts clock-gene expression and REM-sleep recovery following sleep deprivation. *Elife*, 8.
- Horne, J. A. and Shackell, B. S. (1987). Slow wave sleep elevations after body heating: proximity to sleep and effects of aspirin. *Sleep*, 10(4):383–392.
- Howland, R. H. (2014). Vagus Nerve Stimulation. *Current Behavioral Neuroscience Reports*, 1(2):64–73.
- Imeri, L. and Opp, M. R. (2009). How (and why) the immune system makes us sleep. *Nature Reviews Neuroscience*, 10(3):199–210.
- Jacobs, H. I., Priovoulos, N., Riphagen, J. M., Poser, B. A., Napadow, V., Uludag, K., Sclocco, R., Ivanov, D., and Verhey, F. R. (2020). Transcutaneous vagus nerve stimulation increases locus coeruleus function and memory performance in older individuals. *Alzheimer’s & Dementia*, 16(S6):e044766. _eprint: <https://onlinelibrary.wiley.com/doi/pdf/10.1002/alz.044766>.
- Jodoin, V. D., Lespérance, P., Nguyen, D. K., Fournier-Gosselin, M.-P., Richer, F., et al. (2015). Effects of vagus nerve stimulation on pupillary function. *Int. J. Psychophys.*, 98(3):455–459.

- Karacan, I., Wolff, S., Williams, R. L., Hirsch, C., and Webb, W. B. (1968). The Effects of Fever on Sleep and Dream Patterns. *Psychosomatics*, 9(6):331–339.
- Khalsa, S. S., Adolphs, R., Cameron, O. G., Critchley, H. D., Davenport, P. W., Feinstein, J. S., Feusner, J. D., Garfinkel, S. N., Lane, R. D., Mehling, W. E., Meuret, A. E., Nemeroff, C. B., Oppenheimer, S., Petzschner, F. H., Pollatos, O., Rhudy, J. L., Schramm, L. P., Simmons, W. K., Stein, M. B., and Zucker, N. (2018). Interoception and Mental Health: A Roadmap. *Biological Psychiatry: Cognitive Neuroscience and Neuroimaging*, 3(6):501–513.
- Khodaparast, N., Hays, S. A., Sloan, A. M., Fayyaz, T., Hulsey, D. R., Rennaker, R. L., and Kilgard, M. P. (2014). Vagus Nerve Stimulation Delivered During Motor Rehabilitation Improves Recovery in a Rat Model of Stroke. *Neurorehabilitation and Neural Repair*, 28(7):698–706.
- Kim, S.-H., Hadley, S. H., Maddison, M., Patil, M., Cha, B., Kollarik, M., and Taylor-Clark, T. E. (2020). Mapping of Sensory Nerve Subsets within the Vagal Ganglia and the Brainstem Using Reporter Mice for Pirt, TRPV1, 5-HT3, and Tac1 Expression. *eNeuro*, 7(2):1–24.
- Kjaerby, C., Andersen, M., Hauglund, N., Untiet, V., Dall, C., Sigurdsson, B., Ding, F., Feng, J., Li, Y., Weikop, P., Hirase, H., and Nedergaard, M. (2022). Memory-enhancing properties of sleep depend on the oscillatory amplitude of norepinephrine. *Nature Neuroscience*, 25(8):1059–1070.
- Kline, D. D., Takacs, K. N., Ficker, E., and Kunze, D. L. (2002). Dopamine modulates synaptic transmission in the nucleus of the solitary tract. *J Neurophysiol*, 88(5):2736–44.
- Komagata, N., Latifi, B., Rusterholz, T., Bassetti, C. L. A., Adamantidis, A., and Schmidt, M. H. (2019). Dynamic REM Sleep Modulation by Ambient Temperature and the Critical Role of the Melanin-Concentrating Hormone System. *Curr Biol*, 29(12):1976–1987 e4.
- Krahl, S. E., Clark, K. B., Smith, D. C., and Browning, R. A. (1998). Locus coeruleus lesions suppress the seizure-attenuating effects of vagus nerve stimulation. *Epilepsia*, 39(7):709–714.

- Krauchi, K. and Deboer, T. (2010). The interrelationship between sleep regulation and thermoregulation. *Front Biosci (Landmark Ed)*, 15(2):604–25.
- Kroeger, D., Absi, G., Gagliardi, C., Bandaru, S. S., Madara, J. C., Ferrari, L. L., Arrigoni, E., Munzberg, H., Scammell, T. E., Saper, C. B., and Vetrivelan, R. (2018). Galanin neurons in the ventrolateral preoptic area promote sleep and heat loss in mice. *Nat Commun*, 9(1):4129.
- Kräuchi, K. (2007). The human sleep–wake cycle reconsidered from a thermoregulatory point of view. *Physiology & Behavior*, 90(2-3):236–245.
- Kukorelli, T. and Juhasz, G. (1977). Sleep induced by intestinal stimulation in cats. *Physiology & Behavior*, 19(3):355–358.
- Kupari, J., Häring, M., Agirre, E., Castelo-Branco, G., and Ernfors, P. (2019). An Atlas of Vagal Sensory Neurons and Their Molecular Specialization. *Cell Reports*, 27(8):2508–2523.e4.
- Larsen, L. E., Lysebettens, W. V., Germonpre, C., Carrette, S., Daelemans, S., Sprengers, M., Thyron, L., Wadman, W. J., Carrette, E., Delbeke, J., Boon, P., Vonck, K., and Raedt, R. (2017). Clinical Vagus Nerve Stimulation Paradigms Induce Pronounced Brain and Body Hypothermia in Rats. *Int J Neural Syst*, 27(5):1750016.
- Larsen, L. E., Wadman, W. J., Marinazzo, D., van Mierlo, P., Delbeke, J., Daelemans, S., Sprengers, M., Thyron, L., Van Lysebettens, W., Carrette, E., Boon, P., Vonck, K., and Raedt, R. (2016). Vagus Nerve Stimulation Applied with a Rapid Cycle Has More Profound Influence on Hippocampal Electrophysiology Than a Standard Cycle. *Neurotherapeutics*, 13(3):592–602.
- Lecci, S., Fernandez, L. M. J., Weber, F. D., Cardis, R., Chatton, J.-Y., Born, J., and Lüthi, A. (2017). Coordinated infra-slow neural and cardiac oscillations mark fragility and offline periods in mammalian sleep. *Sci. Adv.*, 3(2):e1602026.
- Lopes, L. T., Patrone, L. G. A., Li, K. Y., Imber, A. N., Graham, C. D., Gargaglioni, L. H., and Putnam, R. W. (2016). Anatomical and functional connections between the locus coeruleus and the nucleus tractus solitarius in neonatal rats. *Neuroscience*, 2(324):446–468.

- Manta, S., El Mansari, M., Debonnel, G., and Blier, P. (2013). Electrophysiological and neurochemical effects of long-term vagus nerve stimulation on the rat monoaminergic systems. *Int. J. Neuropsychopharm.*, 16(2):459–470.
- Martin, C. O., Denburg, N. L., Tranel, D., Granner, M. A., and Bechara, A. (2004). The Effects of Vagus Nerve Stimulation on Decision-Making. *Cortex*, 40(4-5):605–612.
- Mastitskaya, S., Thompson, N., and Holder, D. (2021). Selective Vagus Nerve Stimulation as a Therapeutic Approach for the Treatment of ARDS: A Rationale for Neuro-Immunomodulation in COVID-19 Disease. *Frontiers in Neuroscience*, 15(667036):1–8. Publisher: Frontiers.
- Mazzone, S. B. and Udem, B. J. (2016). Vagal Afferent Innervation of the Airways in Health and Disease. *Physiological Reviews*, 96(3):975–1024.
- McCorry, L. K. (2007). Physiology of the Autonomic Nervous System. *American Journal of Pharmaceutical Education*, 71(4):1–11.
- McGinty, D. and Szymusiak, R. (2001). Brain structures and mechanisms involved in the generation of NREM sleep: focus on the preoptic hypothalamus. *Sleep Medicine Reviews*, 5(4):323–342.
- McGovern, A. E., Driessen, A. K., Simmons, D. G., Powell, J., Davis-Poynter, N., Farrell, M. J., and Mazzone, S. B. (2015). Distinct Brainstem and Forebrain Circuits Receiving Tracheal Sensory Neuron Inputs Revealed Using a Novel Conditional Anterograde Transsynaptic Viral Tracing System. *The Journal of Neuroscience*, 35(18):7041–7055.
- Meyer, C. W., Ootsuka, Y., and Romanovsky, A. A. (2017). Body Temperature Measurements for Metabolic Phenotyping in Mice. *Frontiers in Physiology*, 31(8):520.
- Miglis, M. G. (2017). Chapter 12 - Sleep and the Autonomic Nervous System. In *Sleep and Neurologic Disease*, pages 227–241. Elsevier, 1st edition.
- Miles, R. (1986). Frequency dependence of synaptic transmission in nucleus of the solitary tract in vitro. *J Neurophysiol*, 55(5):1076–90.

- Mills, P. A., Huettelman, D. A., Brockway, B. P., Zwiers, L. M., Gelsema, A. J. M., Schwartz, R. S., and Kramer, K. (2000). A new method for measurement of blood pressure, heart rate, and activity in the mouse by radiotelemetry. *Journal of Applied Physiology*, 88(5):1537–1544.
- Min, S., Chang, R. B., Prescott, S. L., Beeler, B., Joshi, N. R., Strohlic, D. E., and Liberles, S. D. (2019). Arterial Baroreceptors Sense Blood Pressure through Decorated Aortic Claws. *Cell Rep*, 29(8):2192–2201 e3.
- Monti, J. M. (2010). The role of dorsal raphe nucleus serotonergic and non-serotonergic neurons, and of their receptors, in regulating waking and rapid eye movement (REM) sleep. *Sleep Medicine Reviews*, 14(5):319–327.
- Muller, J. E., Tofler, G. H., and Stone, P. H. (1989). Circadian variation and triggers of onset of acute cardiovascular disease. *Circulation Progress Series*, 79(4):733–743.
- Nakamura, K. (2011). Central circuitries for body temperature regulation and fever. *American Journal of Physiology-Regulatory, Integrative and Comparative Physiology*, 301(5):R1207–R1228.
- Nassenstein, C., Taylor-Clark, T. E., Myers, A. C., Ru, F., Nandigama, R., Bettner, W., and Udem, B. J. (2010). Phenotypic distinctions between neural crest and placodal derived vagal C-fibres in mouse lungs. *The Journal of Physiology*, 588(23):4769–4783.
- Orr, W. C. and Chen, C. L. (2005). Sleep and the Gastrointestinal Tract. *Neurologic Clinics*, 23(4):1007–1024.
- Osorio-Forero, A., Cardis, R., Vantomme, G., Guillaume-Gentil, A., Katsioudi, G., Devenoges, C., Fernandez, L. M. J., and Luthi, A. (2021). Noradrenergic circuit control of non-REM sleep substates. *Curr Biol*, 31(22):5009–5023 e7.
- Osorio-Forero, A., Cherrad, N., Banterle, L., Fernandez, L. M. J., and Lüthi, A. (2022). When the Locus Coeruleus Speaks Up in Sleep: Recent Insights, Emerging Perspectives. *Int J Mol Sci*, 23(9):5028.
- Osorio-Forero, A., Foustoukos, G., Cardis, R., Cherrad, N., Devenoges, C., Fernandez, L. M. J., and Lüthi, A. (2024). Noradrenergic *locus coeruleus* activity functionally

- partitions NREM sleep to gatekeep the NREM-REM sleep cycle. *Biorxiv*, page 2023.05.20.541586.
- Palchykova, S., Deboer, T., and Tobler, I. (2002). Selective sleep deprivation after daily torpor in the Djungarian hamster. *Journal of Sleep Research*, 11(4):313–319. _eprint: <https://onlinelibrary.wiley.com/doi/pdf/10.1046/j.1365-2869.2002.00310.x>.
- Park, S.-H., Baik, J., Hong, J., Antila, H., Kurland, B., Chung, S., and Weber, F. (2021). A probabilistic model for the ultradian timing of REM sleep in mice. *PLOS Computational Biology*, 17(8):1–30.
- Park, S. H. and Weber, F. (2020). Neural and homeostatic regulation of REM sleep. *Front Psychol*, 11:1662.
- Parmeggiani, P. L. (2003). THERMOREGULATION AND SLEEP. *Frontiers in Bioscience*, 8:s557–567.
- Poe, G. R., Foote, S., Eschenko, O., Johansen, J. P., Bouret, S., Aston-Jones, G., Harley, C. W., Manahan-Vaughan, D., Weinschenker, D., Valentino, R., Berridge, C., Chandler, D. J., Waterhouse, B., and Sara, S. J. (2020). Locus coeruleus: a new look at the blue spot. *Nature Reviews Neuroscience*, 21(11):644–659.
- Prechtel, J. and Powley, T. (1990). The fiber composition of the abdominal vagus of the rat. *Anatomy and Embryology*, 181(2):101–115.
- Prescott, S. L. and Liberles, S. D. (2022). Internal senses of the vagus nerve. *Neuron*, 110(4):579–599.
- Prescott, S. L., Umans, B. D., Williams, E. K., Brust, R. D., and Liberles, S. D. (2020). An Airway Protection Program Revealed by Sweeping Genetic Control of Vagal Afferents. *Cell*, 181(3):574–589.e14.
- Ran, C., Boettcher, J. C., Kaye, J. A., Gallori, C. E., and Liberles, S. D. (2022). A brainstem map for visceral sensations. *Nature*, 609(7926):320–326.
- Rasch, B. and Born, J. (2013). About Sleep’s Role in Memory. *Physiological Reviews*, 93(2):681–766.

- Rizzo, P., Beelke, M., De Carli, F., Canovaro, P., Nobili, L., Robert, A., Fornaro, P., Tanganelli, P., Regesta, G., and Ferrillo, F. (2004). Modifications of sleep EEG induced by chronic vagus nerve stimulation in patients affected by refractory epilepsy. *Clin Neurophysiol*, 115(3):658–64.
- Rizzo, P., Beelke, M., De Carli, F., Canovaro, P., Nobili, L., Robert, A., Tanganelli, P., Regesta, G., and Ferrillo, F. (2003). Chronic vagus nerve stimulation improves alertness and reduces rapid eye movement sleep in patients affected by refractory epilepsy. *Sleep*, 26(5):607–11.
- Romero-Osorio, R., Gil-Tamayo, S., Nariño, D., and Rosselli, D. (2018). Changes in sleep patterns after vagus nerve stimulation, deep brain stimulation or epilepsy surgery: Systematic review of the literature. *Seizure*, 56:4–8.
- Roosevelt, R. W., Smith, D. C., Clough, R. W., Jensen, R. A., and Browning, R. A. (2006). Increased extracellular concentrations of norepinephrine in cortex and hippocampus following vagus nerve stimulation in the rat. *Brain Res.*, 1119(1):124–132.
- Ruggiero, D. A., Pickel, V. M., Milner, T. A., Anwar, M., Otake, K., Mtui, E. P., and Park, D. (1994). Viscerosensory Processing in Nucleus Tractus Solitarii: Structural and Neurochemical Substrates. In *Nucleus of the Solitary Tract*, pages 3–34. CRC Press, 1 edition. Num Pages: 32.
- Rush, A. J., George, M. S., Sackeim, H. A., Marangell, L. B., Husain, M. M., Giller, C., Nahas, Z., Haines, S., Simpson Jr, R. K., and Goodman, R. (2000). Vagus nerve stimulation (vns) for treatment-resistant depressions: a multicenter study. *Biol. Psych.*, 47(4):276–286.
- Saper, C. B. (2002). The Central Autonomic Nervous System: Conscious Visceral Perception and Autonomic Pattern Generation. *Annual Review of Neuroscience*, 25(1):433–469.
- Saper, C. B., Cano, G., and Scammell, T. E. (2005). Homeostatic, Circadian, and Emotional Regulation of Sleep. *Journal of Comparative Neurology*, 493(1):92–98.

- Saper, C. B., Fuller, P. M., Pedersen, N. P., Lu, J., and Scammell, T. E. (2010). Sleep State Switching. *Neuron Perspective*, 68(6):1023–1042.
- Sawchenko, P. (1983). Central connections of the sensory and motor nuclei of the vagus nerve. *Journal of the Autonomic Nervous System*, 9(1):13–26.
- Schmidt, M. H. (2014). The energy allocation function of sleep: a unifying theory of sleep, torpor, and continuous wakefulness. *Neurosci Biobehav Rev*, 47:122–53.
- Sharon, O., Fahoum, F., and Nir, Y. (2021). Transcutaneous Vagus Nerve Stimulation in Humans Induces Pupil Dilation and Attenuates Alpha Oscillations. *J Neurosci*, 41(2):320–330.
- Silvani, A., Calandra-Buonaura, G., Benarroch, E. E., Dampney, R. A., and Cortelli, P. (2015). Bidirectional interactions between the baroreceptor reflex and arousal: an update. *Sleep Medicine*, 16(2):210–216.
- Silvani, A. and Dampney, R. A. L. (2013). Central control of cardiovascular function during sleep. *American Journal of Physiology-Heart and Circulatory Physiology*, 305(12):H1683–H1692.
- Silvani, A., Grimaldi, D., Vandi, S., Barletta, G., Vetrugno, R., Provini, F., Pierangeli, G., Berteotti, C., Montagna, P., Zoccoli, G., and Cortelli, P. (2008). Sleep-dependent changes in the coupling between heart period and blood pressure in human subjects. *American Journal of Physiology-Regulatory, Integrative and Comparative Physiology*, 294(5):R1686–R1692.
- Sowho, M., Amatory, J., Kirkness, J. P., and Patil, S. P. (2014). Sleep and Respiratory Physiology in Adults. *Clinics in Chest Medicine*, 35(3):469–481.
- Sun, L., Peräkylä, J., Holm, K., Haapasalo, J., Lehtimäki, K., Ogawa, K. H., Peltola, J., and Hartikainen, K. M. (2017). Vagus nerve stimulation improves working memory performance. *Journal of Clinical and Experimental Neuropsychology*, 39(10):954–964. Publisher: Routledge _eprint: <https://doi.org/10.1080/13803395.2017.1285869>.
- Swift, K. M., Gross, B. A., Frazer, M. A., Bauer, D. S., Clark, K. J., Vazey, E. M., Aston-Jones, G., Li, Y., Pickering, A. E., Sara, S. J., and Poe, G. R. (2018). Abnormal

- Locus Coeruleus Sleep Activity Alters Sleep Signatures of Memory Consolidation and Impairs Place Cell Stability and Spatial Memory. *Current Biology*, 28(22):3599–3609.e4.
- Szymusiak, R. (2018). Body temperature and sleep. *Handb Clin Neurol*, 156:341–351.
- Tallon-Baudry, C. (2023). Interoception: Probing internal state is inherent to perception and cognition. *Neuron*, 111(12):1854–1857.
- Tan, H.-E., Sisti, A. C., Jin, H., Vignovich, M., Villavicencio, M., Tsang, K. S., Goffer, Y., and Zuker, C. S. (2020). The gut–brain axis mediates sugar preference. *Nature*, 580(7804):511–516.
- Te Lindert, B. H. and Van Someren, E. J. (2018). Chapter 21 - Skin temperature, sleep, and vigilance. In Romanovsky, A. A., editor, *Handbook of Clinical Neurology*, volume 156, pages 353–365. Elsevier.
- Tobaldini, E., Costantino, G., Solbiati, M., Cogliati, C., Kara, T., Nobili, L., and Montano, N. (2017). Sleep, sleep deprivation, autonomic nervous system and cardiovascular diseases. *Neuroscience & Biobehavioral Reviews*, 74:321–329.
- Tobaldini, E., Nobili, L., Strada, S., Casali, K. R., Braghiroli, A., and Montano, N. (2013). Heart rate variability in normal and pathological sleep. *Frontiers in Physiology*, 4(294):1–11.
- Tracey (2002). The inflammatory reflex. *Nature*, 420:853–859.
- Valdés-Cruz, A., Magdaleno-Madriral, V. M., Martínez-Vargas, D., Fernández-Mas, R., Almazán-Alvarado, S., Martínez, A., and Fernández-Guardiola, A. (2002). Chronic stimulation of the cat vagus nerve: effect on sleep and behavior. *Prog. Neuro-Psychopharm. Biol. Psych.*, 26(1):113–118.
- Van Lysebettens, W., Vonck, K., Larsen, L. E., Sprengers, M., Carrette, E., Bouckaert, C., Delbeke, J., Jan Wadman, W., Boon, P., and Raedt, R. (2019). Hypothermia Masks Most of the Effects of Rapid Cycling VNS on Rat Hippocampal Electrophysiology. *Int J Neural Syst*, 29(9):1950008.

- Vaughn, B. V., Quint, S. R., Messenheimer, J. A., and Robertson, K. R. (1995). Heart period variability in sleep. *Electroencephalography and Clinical Neurophysiology*, 94(3):155–162.
- Victor, R. G. (2015). Carotid baroreflex activation therapy for resistant hypertension. *Nature Reviews Cardiology*, 12(8):451–463.
- Vijgen, G. H. E. J., Bouvy, N. D., Leenen, L., Rijkers, K., Cornips, E., Majoie, M., Brans, B., and Lichtenbelt, W. D. v. M. (2013). Vagus Nerve Stimulation Increases Energy Expenditure: Relation to Brown Adipose Tissue Activity. *PLOS ONE*, 8(10):e77221. Publisher: Public Library of Science.
- Vitello, M. M., Briand, M.-M., Ledoux, D., Annen, J., El Tahry, R., Laureys, S., Martin, D., Gosseries, O., and Thibaut, A. (2023). Transcutaneous vagal nerve stimulation to treat disorders of consciousness: Protocol for a double-blind randomized controlled trial. *International journal of clinical and health psychology: IJCHP*, 23(100360):100360.
- Vyazovskiy, V. V. (2015). Sleep, recovery, and metaregulation: explaining the benefits of sleep. *Nat Sci Sleep*, 7:171–84.
- Waise, T. M. Z., Dranse, H. J., and Lam, T. K. T. (2018). The metabolic role of vagal afferent innervation. *Nature Reviews Gastroenterology & Hepatology*, 15(10):625–636.
- Wehrwein, E. A. and Joyner, M. J. (2013). Chapter 8 Regulation of blood pressure by the arterial baroreflex and autonomic nervous system. In *Handbook of Clinical Neurology*, volume 117, pages 89–102. Elsevier, 3 edition.
- Wei, Y. (2019). Interoception relates to sleep and sleep disorders. *Curr Opin Behav Sci*, 33:1–7.
- Wei, Y. and Van Someren, E. J. (2020). Interoception relates to sleep and sleep disorders. *Current Opinion in Behavioral Sciences*, 33:1–7.
- Williams, E., Chang, R., Strohlic, D., Umans, B., Lowell, B., and Liberles, S. (2016). Sensory Neurons that Detect Stretch and Nutrients in the Digestive System. *Cell*, 166(1):209–221.

- Winter, Y., Sandner, K., Bassetti, C. L. A., Glaser, M., Ciolac, D., Ziebart, A., Karakoyun, A., Saryyeva, A., Krauss, J. K., Ringel, F., and Groppa, S. (2024). Vagus nerve stimulation for the treatment of narcolepsy. *Brain Stimulation*, 17(1):83–88.
- Wood, S. K. and Valentino, R. J. (2017). The brain norepinephrine system, stress and cardiovascular vulnerability. *Neuroscience & Biobehavioral Reviews*, 74(Pt B):393–400.
- Wu, Y., Song, L., Wang, X., Li, N., Zhan, S., Rong, P., Wang, Y., and Liu, A. (2022). Transcutaneous Vagus Nerve Stimulation Could Improve the Effective Rate on the Quality of Sleep in the Treatment of Primary Insomnia: A Randomized Control Trial. *Brain Sciences*, 12(1296):1–10. Number: 10 Publisher: Multidisciplinary Digital Publishing Institute.
- Yao, Y., Barger, Z., Saffari Doost, M., Tso, C. F., Darmohray, D., Silverman, D., Liu, D., Ma, C., Cetin, A., Yao, S., Zeng, H., and Dan, Y. (2022). Cardiovascular baroreflex circuit moonlights in sleep control. *Neuron*, 110(23):3986–3999.e6.
- Yin, J., Ji, F., Gharibani, P., and Chen, J. D. (2019). Vagal Nerve Stimulation for Glycemic Control in a Rodent Model of Type 2 Diabetes. *Obesity Surgery*, 29(9):2869–2877.
- Zabara, J. (1992). Inhibition of Experimental Seizures in Canines by Repetitive Vagal Stimulation. *Epilepsia*, 33(6):1005–1012.

Appendices

Vagal sensory afferents regulate mouse sleep through brain-body cooling

Najma Cherrad¹, Alejandro Osorio-Forero^{1*}, Yann Emmenegger², Laura MJ Fernandez¹, Paul Franken², Anita Lüthi¹

¹Department of Fundamental Neurosciences, University of Lausanne, Rue du Bugnon 9, CH-1005 Lausanne, Switzerland

²Center for Integrative Genomics, University of Lausanne, Génopode, CH-1015 Lausanne, Switzerland

*Department of Sleep and Cognition, Netherlands Institute for Neuroscience, Meibergdreef 47, 1105 BA Amsterdam, The Netherlands

Article information:

Number of words in abstract: 240

Number of words in main text: 6,610

Number of figures: 6

Number of Supplemental Figures: 5

Number of references: 75

Acknowledgements: We are grateful to Myrtha Arnold (ETHZ) for first introducing us into vagal surgeries, and to Prof. Liberles (Harvard University) for further technical advice. We are indebted to the numerous colleagues who provided us with insightful comments and who shared knowledge on various aspects of this study, notably Prof. Henning Fenselau, Clément Menuet, Vladyslav Vyazovskiy, Patrick Fuller and Elda Arrigoni. We thank Dr. Patricia Molina for help with the cFos protocol and Marie Pertin for help with the immunostaining of ganglia. Dr. Gil Vantomme provided help with the first *in vitro* recordings, and Dr. Romain Cardis provided advice for Matlab coding and statistical analysis. The Master students David Gauthier and Nadine Eliasson are acknowledged for their contributions to unpublished portions of this work.

Author contributions: NC carried out all experiments and analyses, with the help of YE for temperature recordings and of AOF and LF for analysis and figure preparations. AL and PF conceived the original project, NC and AL wrote the first draft of the manuscript and received input from all authors.

33

34 **Abstract**

35 **Sensory information flow from the external world is attenuated during sleep, yet we still know little**
36 **about the processing of sensory stimuli originating from within the body. Cardiovascular,**
37 **gastrointestinal and airway sensory signals are sent via the vagus nerve to the brainstem vagal**
38 **complex which can relay this information to brainstem and hypothalamic sleep-wake centers and**
39 **trigger parasympathetic feedback to the body. We combined chemogenetic stimulation of vagal**
40 **sensory neurons in the jugular-nodose ganglion of Vglut2-Cre mice with sleep-wake recordings,**
41 **heart rate and brain-body temperature measures to probe the actions of vagal sensory neuronal**
42 **activity on sleep. *In vitro* whole-cell patch-clamp recordings from the *nucleus tractus solitarius* (NTS)**
43 **neurons, combined with optogenetics, revealed vagal-NTS glutamatergic synaptic contacts. *In vivo***
44 **chemogenetic vagal sensory neuron stimulation elevated cFos activity in NTS, reduced heart rate,**
45 **and induced a transient non-rapid-eye-movement (NREMS)-like state, characterized by higher**
46 **relative low-frequency (0.5 – 4 Hz) electroencephalographic power and decreased sleep spindle (10**
47 **– 15 Hz) activity. The presence of this NREMS-like state precluded REMS but preserved its**
48 **homeostatic regulation. The NREMS-like state was accompanied by a cortical and core body cooling**
49 **that, when countered by external warming, accelerated the recovery to normal sleep. Furthermore,**
50 **REMS re-appeared at a largely dose-independent threshold of cortical temperature. We conclude**
51 **that a primary mechanism by which vagal sensory activity regulates sleep is through brain-body**
52 **cooling. This could promote the restorative effects of NREMS and hence boost the therapeutic**
53 **effects of vagus nerve stimulation.**

54

55

56

57

58

59

60

61

62

63

64

65

66 **Introduction**

67 A decreased reactivity to external sensory stimuli is a defining behavioral feature of sleep.
68 Studies on the brain mechanisms that underlie this decreased reactivity showed that sleep modifies
69 the way signals from the sensory periphery propagate within thalamocortical sensory pathways (for
70 review, see (Andrillon & Kouider, 2020; Fernandez & Lüthi, 2020; McCormick & Bal, 1997; Nir & de
71 Lecea, 2023)). These studies also helped establish the relevance of sensory isolation for sleep's
72 functions in brain restoration and plasticity (Brodt et al., 2023; Vyazovskiy, 2015). In contrast, much
73 less is known about how sensory afferents from within the bodily organs interact with the sleeping
74 brain. Sleep plays a vital role for cardiovascular (Silvani & Dampney, 2013) and gastrointestinal (Orr et
75 al., 2020) health. Conversely, discomfort within these and other bodily sensory systems adversely
76 affects sleep, which can lead to a cycle of worsening conditions (de Zambotti et al., 2018; Kourbanova
77 et al., 2022; Orr et al., 2020; Wei, 2019). Therefore, uncovering the neural basis of brain-body
78 interactions during sleep is relevant for mechanistic insights into sleep's benefits for brain and body.

79 Common experience tells us that sleep and bodily sensations interact (Wei, 2019). Some of these
80 interactions are sleep-disruptive, such as nociceptive stimuli (Bastuji et al., 2008). Others may improve
81 sleep. For example, gastrointestinal distention to activate mechanoreceptors innervating the stomach
82 musculature can promote low-frequency brain activity typical for sleep (for review, see (Orr & Chen,
83 2005)). Medical interventions producing a stretching of the carotid sinus mechanoreceptors, involved
84 in the blood pressure-stabilizing baroreceptor reflex, can increase or decrease arousal levels
85 depending on the intensity of stimulation (for review, see (Silvani et al., 2015)). Bodily sensory afferents
86 hence provide a rich source of signals that could modify sleep. To date, however, we know little about
87 whether such modifications primarily concern specific spectral signatures of the sleep encephalogram
88 or impact sleep's architecture and regulation more extensively.

89 Novel opportunities in analyzing body-brain crosstalk during sleep arise with the increased
90 genetic accessibility of the neuronal pathways interfacing between bodily organs and the brain. Here
91 stands out the Xth cranial nerve known as vagus nerve that is a mixed sensory-motor nerve composed
92 of chemo-, mechano-, osmo- and temperature-sensitive fibers arising from cardiovascular,
93 gastrointestinal and respiratory systems. The vagus nerve is formed by pseudo-unipolar neurons
94 located in the bilateral jugular-nodose ganglia (JNG) that are part of a larger ganglionic complex
95 containing also spinal and other cranial neurons (Prescott & Liberles, 2022). Major brainstem targets
96 of vagal sensory afferents are the medullar *nucleus tractus solitarius* (NTS) and the *area postrema* (AP).
97 From there, reflex connections are formed to the dorsal motor nucleus of the vagus and the *nucleus*

98 *ambiguus*, the parasympathetic motor output divisions (Neuhuber & Berthoud, 2021). Additionally,
99 NTS neurons project broadly to brainstem, midbrain and hypothalamic circuits involved in sleep-wake
100 control, including the monoaminergic *locus coeruleus* (LC) and dorsal raphe nuclei, as well as preoptic
101 hypothalamic areas (for review, see (Holt, 2022)). Vagal sensory activity could thus modulate sleep in
102 diverse ways, including through its actions on the autonomic nervous system and on central areas.

103 That vagal activity may affect sleep has been brought up in the context of vagus nerve
104 stimulation (VNS), which traditionally targets both sensory and motor branches of the nerve and is
105 well-known as adjunct therapy for epilepsy, depression or obesity (Karemaker, 2022). Some of these
106 actions of VNS have been linked to an activation of the central neuromodulatory systems including
107 noradrenaline (Berger et al., 2021; Mridha et al., 2021; Sharon et al., 2021). VNS has been further
108 reported to modify sleep architecture and spectral properties in humans (Hallbook et al., 2005; Rizzo
109 et al., 2004; Rizzo et al., 2003; Zanchetti et al., 1952) including in insomnia (Krone et al., 2023; Yoon,
110 2019). However, there are also reports on sleep-disruptive effects caused by reduced cardiac and/or
111 respiration rates when motor fibers are excessively stimulated (for review, see (Romero-Osorio et al.,
112 2018)). In rodents, aside stimulation of central neuromodulation (Mridha et al., 2021), VNS was also
113 found to induce bodily hypothermia, which has been ascribed to peripheral vasodilation (Larsen et al.,
114 2017) or to reduced brown adipose tissue activation (Madden et al., 2017). These studies indicate that
115 VNS likely modulates sleep, yet they leave open how the sensory and the motor-related nerve activity
116 contributes.

117 Using specific chemogenetic stimulation of vagal sensory afferents in freely sleeping mouse, we
118 noted a pronounced, dose-dependent expression of a non-rapid-eye-movement sleep (NREMS)-like
119 state with properties clearly distinct from physiological NREMS in terms of amplitudes and dynamic
120 variations. REMS did not express during this state yet showed a post-recovery rebound. The sleep
121 alterations, notably the delay to REMS re-appearance correlated with the amplitude of a brain-body
122 hypothermia that could be shortened when reducing hypothermia through bodily warming. We
123 conclude that brain-body cooling is an important effector when vagal sensory neurons are specifically
124 activated in rodents and plays a dominant role in sleep regulation.

125

126 **Results**

127 **Histological and functional verification of Vglut2-expressing vagal sensory afferent stimulation on** 128 **vagal-recipient brainstem areas**

129 The majority of vagal sensory neurons express the vesicular glutamate transporter type 2
130 (Vglut2), which distinguishes them from cholinergic vagal motor neurons (Chang et al., 2015; Raab &

131 Neuhuber, 2007). In whole-mounts of extracted left JNG (L-JNG) ganglia immunostained for VGLUT2
132 protein, we observed multiple fluorescently labeled cellular somata located within the ganglion and
133 lining its borders, while sparing the sites of passage of motor fibers (**Figure 1a** (Chang et al., 2015)).
134 We injected *Vglut2-Cre* mice with a conditional mCherry-expressing viral construct into the left JNG (L-
135 JNG) (*ssAAV8/2-hSyn1-dlox-mCherry(rev)-dlox-WPRE-hGHp(A)*) to specifically target vagal sensory
136 neurons and to examine their sites of projection (**Figure 1b**). After at least 3 weeks post-injection, we
137 observed clusters of red fibers entering the ipsilateral left NTS from its lateral and ventrolateral sides.
138 Fibers were apparent as clusters principally within the central portion across the antero-posterior
139 extent (from Br -7.76 mm to Br -6.7 mm, n = 3 mice, **Figure 1c**), demonstrating that transfected L-JNG
140 neurons projected to a major component of the dorsal vagal complex.

141 We tested the functional connectivity of L-JNG afferent fibers within NTS neurons through
142 studying vagally evoked synaptic responses in NTS neurons. Acute brainstem slices were prepared from
143 *Vglut2-Cre* mice previously transfected for conditional expression of the excitatory opsin Chr2 in L-JNG
144 (*AAV1.EF1a.DIO.hChr2(H134R)-eYFP.WPRE.hGH*), and cell bodies within the NTS patched with
145 neurobiotin-containing patch pipettes (**Figure 1d1**). Patched neurons were recovered *post hoc*
146 together with microscopic fluorescent visualization of sensory afferent fibers surrounding the cell body
147 (**Figure 1d2**). In the whole-cell recording mode, somatic current injections were used to characterize
148 action potential discharge patterns, and whole-field optogenetic blue light pulses (470 nm, 1 – 5 ms
149 duration, 3.8 mW) were applied to evoke synaptic responses (**Figure 1d3**). We found postsynaptic
150 currents in ~17% (18/107) of the neurons patched and could localize 13 connected neurons within the
151 caudal and intermediate NTS (Br -7.9 mm to Br -7.1 mm), of which 7 were clustered in the dorsal region
152 of the NTS adjacent to the AP (**Figure 1d4**). Patched cells had a resting membrane potential of $-61.8 \pm$
153 4.8 mV and responded with action potentials reaching peak amplitudes of 61.6 ± 9.6 mV upon
154 depolarizing current injection (**Figure 1e1**, n = 13). Mean membrane time constants, derived from
155 monoexponential fitting to hyperpolarizing current responses, were typically > 50 ms (83.6 ± 42.3 ms).
156 Together with the low membrane capacitance (32.2 ± 12.6 pF, see e.g. (Fernandez et al., 2018)), this
157 suggests that the patched NTS neurons are part of an electrotonically compact neuronal cell type,
158 which could relate to earlier reports on high membrane resistances for these neurons (Kline et al.,
159 2002) (**Figure 1e1**), to which their extended dendrites could contribute (**Figure 1d2, 1f1**). When
160 somatically injected with suprathreshold depolarizing current (3 – 80 pA), neurons showed tonic firing
161 patterns that increased with current amplitude and that reached values ranging between 1 – 14 Hz
162 (**Figure 1e2**). Evoked postsynaptic currents (EPSCs), measured in voltage-clamp at holding potential of
163 -60 to -70 mV, presented as multicomponent inward currents with variable latencies, suggesting
164 combined mono- and polysynaptic afferents (Doyle & Andresen, 2001). In 13/18 cells, we found a fixed

165 latency with a jitter < 0.5 ms (range 0.09 – 0.49 ms) for all evoked responses, suggesting a
166 monosynaptic connection. However, in 10 of these 13 recordings, responses with larger delay and a
167 jitter > 1 ms were also evoked, indicating that polysynaptic circuits were recruited (**Figure 1e3**).
168 Putative monosynaptic responses showed a mean peak amplitude of -68.5 ± 62.8 pA and mean
169 latencies of 6.7 ± 2.5 ms (**Figure 1e4**). These values are longer than typical monosynaptic latencies, as
170 also remarked in previous studies (Bailey et al., 2008; Miles, 1986). In four recordings with a putative
171 monosynaptic connection, we found that bath application of DNQX (10 μ M), an antagonist of
172 glutamatergic α -amino-3-hydroxy-5-methyl-4-isoxazolepropionic acid (AMPA) receptors, suppressed
173 evoked EPSPs to $\sim 9\%$ of the original response (**Figure 1f1 - f3**, n = 4). Therefore, virally targeted L-JNG
174 sensory neurons activate NTS neurons through glutamatergic synapses involving both putative mono-
175 and, in a majority of connections, also polysynaptic pathways.

176

177 **Chemogenetic stimulation of vagal sensory afferents dose-dependently induces a NREMS-like state** 178 **with different spectral characteristics**

179 We next asked whether vagal sensory activity modified sleep-wake behavior in freely moving
180 mice (**Figure 2a,b**). We aimed to elevate vagal sensory neuron activity in a persistent manner to mimic
181 an elevation in parasympathetic tone, as is typical for NREMS (de Zambotti et al., 2018). Based on a
182 previous study (Fernandez et al., 2018), we chose chemogenetic manipulation, which works dose-
183 dependently and persists over hours, both elements suitable for sleep studies. We focused on the L-
184 JNG that has been most extensively documented to contain vagal sensory neurons from the
185 gastrointestinal system (Han et al., 2018; Williams et al., 2016), the airways (Chang et al., 2015) and
186 the cardiovascular system (Min et al., 2019). Animals transfected with an excitatory DREADD- and
187 mCherry-expressing viral vector (ssAAV8/2-hSyn1-dlox-hM3D(Gq)_mCherry-dlox-WPRE-hGH(pA))
188 were injected 3 – 4 weeks later with NaCl or with CNO at a low dose (1.5 mg/kg, (Fernandez et al.,
189 2018)) that alone does not affect basic sleep-wake behaviors (Traut et al., 2023). We sacrificed animals
190 60 – 90 min later for cFos immunohistochemistry in the brainstem (n = 3, **Figure 2c + Suppl Figure**
191 **1a1,a2,b**). CNO but not NaCl injection led to elevated cFos expression levels within areas of the NTS
192 (For NaCl: 0.25 % (n = 1) and for CNO 1.5 mg/kg: 9 % (n = 2) of cFos+ / DAPI cells), within which DREADD-
193 expressing vagal afferent fibers were also predominantly labeled. Strong cFos expression and fiber
194 labeling were also observed within the AP (For NaCl: 0.1% (n = 1) and for CNO 1.5 mg/kg: 42.1 % (n =
195 2) of cFos+ / DAPI cells), a brain area involved in regulating food intake (Borgmann et al., 2021) and
196 nausea behaviors (Zhang et al., 2021). This supports that chemogenetic activation of Vglut2-expressing
197 vagal fibers robustly stimulated vagal-recipient brainstem areas.

198 We next combined viral transfection of the L-JNG with EEG/EMG surgical implantations (n = 11
199 animals) for sleep-wake monitoring. Once ready for experimentation, animals were injected
200 intraperitoneally with NaCl or CNO within 30 min after light onset (Zeitgeber Time ZT = 0), which
201 corresponds to the start of their preferred resting phase. Recordings were obtained in consecutive
202 recording sessions that lasted 5 h and were followed by 1 – 2 days of recovery. The CNO doses (1.5
203 mg/kg or 2.5 mg/kg, referred to as CNO 1.5 and CNO 2.5 in the remainder of this text) were chosen
204 low enough to not interfere directly with sleep (Traut et al., 2023). **Figure 2d1** shows an example
205 recording from a NaCl-injected mouse, with the hypnogram revealing the typical alternation between
206 wakefulness, NREMS and REMS. The transition from wakefulness to NREMS was accompanied by
207 increases in EEG power in the low-frequency delta (δ) (1.5 – 4 Hz) and the sleep spindle-containing
208 sigma (σ) band (10 – 15 Hz), while the ratio of the theta (θ , 6 – 8 Hz) over δ (1.5 – 4 Hz) power (θ/δ
209 ratio) marked transitions to REMS. Compared to NaCl, CNO at 1.5 mg/kg produced clear alterations in
210 the spectral composition of EEG states (**Figure 2d2**). From the initial wakefulness after injection, the
211 mouse entered a state in which relative EEG δ power appeared large while σ power diminished
212 compared to natural NREMS. Furthermore, a fluctuating activity of σ power described for NREMS
213 (Lecci et al., 2017) that is driven by noradrenergic signals (Osorio-Forero et al., 2021) was no longer
214 visually recognizable. We also no longer observed increases in the θ/δ ratio, signaling a suppression of
215 REMS-related brain activity. The animal thus persisted in a state with spectral properties reminiscent
216 of, yet clearly distinct from, NREMS. This state was accompanied by occasional brief periods of
217 wakefulness, but no signatures of REMS (see also **Figure 3**). In this example recording, CNO-induced
218 spectral alterations gradually recovered within 74 min when REMS reappeared, as evident by increases
219 in the θ/δ ratio (**Figure 2d1-3**). These spectral changes became even more pronounced when CNO was
220 injected at 2.5 mg/kg (**Figure 2d3**), and the time for recovery lasted 174 min.

221 In a first step, we characterized the spectral composition of the EEG state induced by CNO, we
222 constructed normalized power spectra for the time until the first consolidated REMS bout and
223 compared these to the spectra obtained from NaCl conditions. For this comparison, we calculated NaCl
224 spectra for times spent in NREMS that were equally long as the time spent in the CNO-induced states
225 (n = 11). This comparison confirmed that CNO produced a brain state enriched in relative power for
226 the low-frequency bands typical for NREMS, including power for slow oscillations (SO, 0.75 – 1.5 Hz)
227 and for the δ band (1.5 – 4 Hz), while σ power (10 – 15 Hz) was suppressed (**Figure 2e**, n = 11, for SO:
228 NaCl vs CNO 1.5; 4.0 ± 0.7 % and 4.5 ± 0.9 %, $p = 8.5 \times 10^{-3}$; CNO 1.5 vs CNO 2.5; 4.0 ± 0.7 % and 4.6 ± 0.7 %,
229 $p = 3.2 \times 10^{-3}$; for δ : NaCl vs CNO 1.5; 2.9 ± 0.2 % and 3.2 ± 0.2 %, $p = 1.3 \times 10^{-3}$; CNO 1.5 vs CNO 2.5; 2.9 ± 0.2
230 % and 3.2 ± 0.2 %, $p = 2.3 \times 10^{-3}$; for σ : NaCl vs CNO 1.5; 0.6 ± 0.1 % and 0.5 ± 0.05 %, $p = 8.2 \times 10^{-4}$; CNO 1.5
231 vs CNO 2.5; 0.6 ± 0.1 % and 0.5 ± 0.1 %, $p = 6.0 \times 10^{-5}$).

232 In a second step, we quantified how these alterations evolved over time in comparison to the
233 NaCl condition. For this purpose, we calculated absolute power in the δ - and the σ -bands with respect
234 to NaCl. We chose for this comparison the last two time bins of a 5-h interval after CNO injection,
235 during which much of the CNO effects recovered. Interestingly, CNO lowered power in both these
236 bands compared to NaCl in a dose-dependent manner (**Figure 2f1, 2f2, Suppl. Figure 1c1,c2**, for the
237 two first bins; for δ : NaCl vs CNO 1.5; 139 ± 13 % and 128 ± 23 %, $p = 0.17$; CNO 1.5 vs CNO 2.5; 128 ± 23
238 % and 103 ± 31 %, $p = 6.8\times 10^{-3}$; for σ : NaCl vs CNO 1.5; 98.8 ± 12 % and 70 ± 23 %, $p = 1.4\times 10^{-3}$, CNO 1.5
239 vs CNO 2.5; 70 ± 23 % and 51 ± 21 %, $p = 1.3\times 10^{-3}$), with a gradual recovery towards NaCl values over the
240 5 h (**Suppl. Figure 1c2,c2**, for the two last bins; for δ : NaCl vs CNO 1.5; 100 ± 12 % and 99 ± 13 %, $p =$
241 0.69 ; CNO 1.5 vs CNO 2.5 99 ± 13 % and 80 ± 19 %, $p = 4.0\times 10^{-3}$; for σ : NaCl vs CNO 1.5; 100 ± 7 % and
242 97 ± 11 %, $p = 0.28$; CNO 1.5 vs CNO 2.5; 97 ± 11 % and 90 ± 9 %, $p = 0.17$). Compared to NREMS, the EEG
243 state induced by chemogenetic vagal sensory stimulation showed an enriched presence of low-
244 frequency EEG oscillatory activities, while dynamic variations of sleep spindles were absent. Moreover,
245 the CNO-induced EEG signatures showed a reduced absolute power. These alterations remained
246 prominent until the first consolidated REM sleep bout, after which a recovery of spectral dynamics
247 typical for normal NREMS re-appeared. The CNO-induced brain state thus presents itself as a NREMS-
248 like state that slowly recovers to normal NREMS in terms of the size and the composition of its spectral
249 characteristics. We refer to the combination of the CNO-induced state and its gradual recovery to
250 NREMS as NREMS*. We preferred this nomenclature to describe the time course of variables from the
251 onset of CNO injection to its recovery rather than setting sharp thresholds to distinguish between the
252 CNO-induced state and normal NREMS.

253 Third, we asked whether CNO induced a change in the animal's sleep-wake behavior during the
254 period of CNO exposure. There was a decrease in the latency to onset of NREMS* (**Figure 3a**, $n = 11$,
255 NaCl vs CNO 1.5; 32.8 ± 7 min and 16.3 ± 8 min, $p = 3.2\times 10^{-4}$; CNO 1.5 vs CNO 2.5; 16.3 ± 8 min and 12.9 ± 5
256 min, $p = 0.12$). Animals injected with a non-DREADD-related viral construct (ssAAV8/2-hSyn1-dlox-
257 mCherry(rev)-dlox-WPRE-hGHp(A)) showed no change in NREMS onset latency compared to NaCl
258 (**Suppl. Figure 2a**, $n = 6$, NaCl vs CNO 1.5; 30.8 ± 13 min and 27.5 ± 6 min, $p > 0.016$; CNO 1.5 vs CNO 2.5;
259 27.5 ± 6 min and 27.6 ± 6 min, $p > 0.016$). Over 5 h after CNO injection, the time spent in NREMS* was
260 dose-dependently enhanced at the expense of times spent in wakefulness and in REMS (**Figure 3b**, n
261 $= 11$; for wake: NaCl vs CNO 1.5; 38.9 ± 4 min and 26.8 ± 5 min, $p = 9.8\times 10^{-4}$; CNO 1.5 vs CNO 2.5; 26.8 ± 5
262 min and 22.5 ± 6 min, $p = 9.8\times 10^{-4}$; for NREMS*: NaCl vs CNO 1.5; 53.4 ± 3 min and 66.1 ± 6 min, $p = 9.8\times 10^{-4}$;
263 4 ; CNO 1.5 vs CNO 2.5; 66.1 ± 6 min and 73.9 ± 7 min, $p = 9.8\times 10^{-4}$; for REMS: NaCl vs CNO 1.5; 7.6 ± 1 min
264 and 7.0 ± 1 min, $p = 0.28$; CNO 1.5 vs CNO 2.5; 7.0 ± 1 min and 3.6 ± 2 min, $p = 9.8\times 10^{-4}$). Compared to
265 NaCl, NREMS* showed no increase in the density of microarousals, defined as brief periods of

266 wakefulness lasting 4 – 12 s (**Figure 3c1**, for 0 h to 0.5 h of NREMS*: NaCl: $48.4 \pm 11 \text{ h}^{-1}$, CNO 1.5: 44.2 ± 11
267 h^{-1} , CNO 2.5: $55.8 \pm 14 \text{ h}^{-1}$, $p > 0.016$ for all; for 0.5 h to 1 h of NREMS*: NaCl: $42.1 \pm 5 \text{ h}^{-1}$, CNO 1.5:
268 $37.0 \pm 11 \text{ h}^{-1}$ and CNO 2.5: $41.3 \pm 11 \text{ h}^{-1}$, $p > 0.016$ for all) and mean bout lengths remained unaltered for
269 both CNO doses (**Figure 3c2**, for 0 h to 0.5 h of NREMS*: NaCl: $1.0 \pm 0.2 \text{ min}$, CNO 1.5: $1.0 \pm 0.4 \text{ min}$ and
270 CNO 2.5: $0.9 \pm 0.2 \text{ min}$, $p > 0.016$ for all; for 0.5 h to 1 h of NREMS*: NaCl: $1.0 \pm 0.1 \text{ min}$, CNO 1.5: 1.3 ± 0.5
271 min and CNO 2.5: $1.1 \pm 0.3 \text{ min}$, $p > 0.016$ for all). Together, CNO accelerates entry into and lengthens
272 times spent in NREMS* at the expense of wake and REMS. Nevertheless, NREMS* remains interrupted
273 by brief microarousals that are well-known for NREMS (Osorio-Forero et al., 2024). This defines
274 NREMS* as a state of rapid reversibility in similarity to physiological NREMS.

275 Both NREMS and REMS are regulated homeostatically, such that a decreased time spent in any
276 of these states leads to a later compensatory modification in times and/or intensity of that state,
277 measured in relative δ power for NREMS (Franken & Dijk, 2024; Park & Weber, 2020). We addressed
278 whether the time spent in NREMS* affected NREMS over 48 h after CNO injection. We carried out this
279 analysis for the recordings with the high CNO dose (2.5 mg/kg), because the induced effects were more
280 pronounced and thus better suited to reveal homeostatic compensatory effects. The cumulative times
281 spent in NREMS* did not recover to baseline NREMS times for up to 48 h after i.p. injection (**Figure 4a**,
282 **Suppl. Figure 3a**, $n = 9$, NaCl vs CNO 2.5; for the 1st light phase: NaCl vs CNO 2.5; $-4.1 \pm 17 \text{ min}$ and
283 $51.8 \pm 27 \text{ min}$, $p = 3.0 \times 10^{-4}$; for the 1st dark phase: NaCl vs CNO 2.5; $-13.0 \pm 30 \text{ min}$ and $-75.0 \pm 54 \text{ min}$, p
284 $= 2.9 \times 10^{-3}$; for the 2nd light phase: NaCl vs CNO 2.5; $-15.2 \pm 54 \text{ min}$ and $71.4 \pm 66 \text{ min}$, $p = 3.2 \times 10^{-3}$; for
285 the 2nd dark phase: NaCl vs CNO 2.5; $-15.2 \pm 75 \text{ min}$ and $77.7 \pm 82 \text{ min}$, $p = 2.8 \times 10^{-3}$). However, the relative
286 δ power remained below control levels in the first dark phase after CNO injection (**Figure 4b**, **Suppl.**
287 **Figure 3b1, b2**, for the 1st dark phase: NaCl vs CNO 2.5; $122.8 \pm 6 \%$ and $113.2 \pm 6 \%$, $p = 9.1 \times 10^{-4}$) and
288 did not recover until the second light-dark cycle (ZT24 – 48). In contrast, σ power recovered fully within
289 the first light phase. This suggests that the expression of NREMS* decreased subsequent NREMS
290 intensity although CNO is no longer systemically active. To test this further, we quantified alterations
291 in heart rate that we derived from the R-peaks detectable in the EMG signal in a subgroup of 9 animals
292 (see (Lecci et al., 2017)) (**Figure 4c**). NREMS* showed a strong decrease in heart rate compared to NaCl
293 comparable to previous studies in anesthetized mouse (Chang et al., 2015). This decrease recovered
294 during the first light phase for both NREMS* and REMS (**Figure 4d1,d2**, **Suppl. Figure 3c1,c2**, $n = 9$, for
295 NREMS* for the 1st light phase: NaCl vs CNO 2.5 ; $473 \pm 26 \text{ bpm}$ and $389 \pm 46 \text{ bpm}$, $p = 1.4 \times 10^{-3}$; for REMS
296 for the 1st light phase: NaCl vs CNO 2.5 ; $503 \pm 26 \text{ bpm}$ and $444 \pm 30 \text{ bpm}$, $p = 1.4 \times 10^{-4}$). This recovery is
297 a further indication for a recovery from systemic CNO effects within 12 h.

298 We next quantified the latency to the first consolidated REMS bout and found it to be dose-
299 dependently delayed (**Figure 4e**, $n = 11$, NaCl vs CNO 1.5; $16.7 \pm 6 \text{ min}$ and $79.2 \pm 68 \text{ min}$, $p = 2.9 \times 10^{-3}$;

300 CNO 1.5 vs CNO 2.5; 79.2 ± 68 min and 177.6 ± 118 min, $p = 9.8 \times 10^{-4}$), with the effect absent in control
301 animals expressing a non-DREADD-related viral construct (**Suppl. Figure 3d**, $n = 6$, NaCl vs CNO 1.5;
302 17.1 ± 6 min and 19.9 ± 13 min, $p > 0.016$; CNO 1.5 vs CNO 2.5; 19.9 ± 13 min and 26.6 ± 14 min, $p > 0.016$).
303 The loss of REMS induced by CNO was fully compensated within the first light-dark cycle (**Figure 4f**,
304 **Suppl. Figure 3e**, $n = 9$, NaCl vs CNO 2.5; for the 1st light phase: NaCl vs CNO 2.5; -0.8 ± 4 min and -
305 10.2 ± 8 min, $p = 6.6 \times 10^{-3}$; for the 1st dark phase: NaCl vs CNO 2.5; -0.2 ± 6 min and -5.1 ± 6 min, $p = 0.02$;
306 for the 2nd light phase: NaCl vs CNO 2.5; 0.2 ± 7 min and -1.9 ± 6 min, $p = 0.1$; for the 2nd dark phase: NaCl
307 vs CNO 2.5; 1.6 ± 10 min and -0.4 ± 9 min, $p = 0.1$).

308 REMS homeostasis thus remained functional during the vagal sensory stimulation and produced
309 a REMS rebound to compensate for lost REMS. In contrast, the extra time spent in NREMS* was not
310 recovered, while NREMS showed reduced intensity for up to 24 h after vagal sensory stimulation. The
311 presence of NREMS* thus modifies NREMS properties in a more prolonged manner. This could point
312 to a homeostatic downregulation of its intensity, while also involving differences in the
313 pharmacokinetics of CNO in central brain areas.

314

315 **Vagal sensory afferent stimulation produces a transient brain-body cooling**

316 The dual and parallel effects of CNO on both the NREMS* EEG signal and on the expression of
317 REMS strongly suggested a shared underlying cause. A drop in body temperature, as found during
318 spontaneous torpor (Krauchi & Deboer, 2010) or induced by chemogenetically stimulating
319 hypothalamic thermoregulatory centers (Harding et al., 2020), is a likely cause for EEG amplitude
320 suppression. REMS is also reduced by ambient (Amici et al., 2008; Komagata et al., 2019) or bodily
321 cooling (Harding et al., 2018; Kroeger et al., 2018). We implanted a separate group of Vglut2-Cre
322 animals expressing excitatory chemogenetic receptors with an epoxy-based thermistor over the cortex
323 contralateral to the EEG electrodes and measured cortical temperature during NaCl and CNO injections
324 ($n = 7$; **Figure 5a**). Cortical temperature varied with vigilance states as described (Hoekstra et al., 2019),
325 declining during NREMS and transiently increasing with every REMS bout (**Figure 5b-c**, $n = 7$, wake vs
326 NREMS, with values in z-score; 0.38 ± 0.07 and -0.55 ± 0.14 , $p = 0.02$; NREMS vs REMS; -0.55 ± 0.14 and -
327 0.24 ± 0.21 , $p > 0.025$). Vagal sensory stimulation instead produced a progressive decline in cortical
328 temperature (**Figure 5d**) that began with the onset of NREMS* and that induced a larger temperature
329 drop (**Figure 5e**) compared to NaCl injection ($n = 7$, NaCl vs CNO 1.5; -0.4 ± 0.2 °C and -1.9 ± 0.8 °C, $p =$
330 0.02 ; CNO 1.5 vs CNO 2.5; -1.9 ± 0.8 °C and -2.0 ± 0.8 °C, $p = 0.38$). During these cortical temperature
331 recordings, REMS onset latency was delayed, but REMS reappeared when the temperature drop had
332 partially recovered. REMS expression is limited to a narrow range of core body temperature, with a
333 sharp threshold below which REMS disappears (Harding et al., 2020). We found that the cortical

334 temperature drop and the delay to REMS onset were negatively correlated across CNO doses (**Figure**
335 **5f1**, $n = 7$, Pearson's R , $R^2 = 0.96$, slope = -0.5 °C/100 min, $p = 6.7 \times 10^{-9}$). Thus, the stronger the brain-
336 body cooling, the longer it took for REMS to re-appear. Furthermore, the temperature value at the
337 moment of the first consolidated REMS bout (> 12 s) fell within a narrow window that was only weakly
338 dependent on the REMS onset latency, as evident by a shallow slope (**Figure 5f2**, $n = 7$, Pearson's R , R^2
339 = 0.58 , slope = -0.1 °C/100 min, $p = 1.7 \times 10^{-3}$), consistent with a threshold temperature value at which
340 REMS could be expressed. In a separate set of recordings using a thermistor with a glass-embedded
341 sensor (**Suppl. Figure 4a,b1,b2**), we found the same correlation between drop in temperature and
342 REMS onset latency raw traces (**Suppl. Figure 4c**, $n = 9$, Pearson's R , $R^2 = 0.89$, slope = -1.7 °C/100 min,
343 $p = 4.8 \times 10^{-14}$), albeit temperature variations were larger for this kind of sensor. Based on these parallel
344 results with two different sensory types, we concluded that REMS suppression induced by vagal
345 sensory stimulation was likely causally related to the cortical temperature drop.

346 Brain and core body temperature levels are tightly linked during NREMS (Krauchi & Deboer,
347 2010; Obal et al., 1985). We also found that rectally measured core body temperature values fell during
348 NREMS*, obtained at 45 min and 2 h after the CNO injection in separate sessions (**Figure 5g1**). The
349 procedure of rectal probe insertion briefly woke up the animals and mildly and transiently affected
350 cortical temperature but did not otherwise interfere with the cortical temperature drop observed after
351 CNO injections (**Figure 5g2**, for 45 min after i.p. injection: NaCl vs CNO 1.5; 37.6 ± 0.2 °C and 33.9 ± 2.2
352 °C, $p = 1.6 \times 10^{-3}$; for 2 h after i.p. injection: NaCl vs CNO 1.5; 37.3 ± 0.5 °C and 33.9 ± 2.3 °C, $p = 1.6 \times 10^{-3}$).
353 These data indicate that vagal sensory stimulation leads to a brain-body cooling that strongly
354 correlates with sleep architectural alterations.

355 We aimed to counteract on brain-body cooling to test whether we could antagonize the effects
356 of vagal sensory stimulation through CNO injection. This was done by ambient warming through
357 heating pads positioned within and below the cages for the first hour after i.p. injection (**Figure 6a**). As
358 a result, temperature decline was reduced for both the body (see Methods) and for the cortical surface
359 (**Figure 6b, c**, NaCl vs CNO 1.5; -0.5 ± 0.1 °C and -2.4 ± 0.6 °C, $p = 7.8 \times 10^{-3}$; CNO 1.5 vs CNO 1.5 + heating;
360 -2.4 ± 0.6 °C and -1.9 ± 0.5 °C, $p = 7.8 \times 10^{-3}$). Antagonizing cortical temperature decline led to the recovery
361 of major alterations in sleep observed previously with vagal sensory stimulation. There was a shorter
362 latency to REMS onset (**Figure 6d**, NaCl vs CNO 1.5 ; 17 ± 4 min and 357 ± 145 min, $p = 7.8 \times 10^{-3}$; CNO 1.5
363 vs CNO 1.5 + heating; 357 ± 145 min and 267 ± 97 min, $p = 0.02$) and a restoration of the natural spectral
364 dynamics of NREMS, as evident by inspecting the time course of δ and σ power (**Figure 6e**, **Suppl.**
365 **Figure 5a1**, for δ ; for the two first bins: NaCl vs CNO 1.5; 163 ± 18 % and 102 ± 19 %, $p = 3.3 \times 10^{-5}$; CNO
366 1.5 vs CNO 1.5 + heating; 102 ± 19 % and 142 ± 32 %, $p = 3.2 \times 10^{-4}$; for the two last bins: NaCl: 100 ± 11 %,
367 CNO 1.5: 99 ± 17 % and CNO 1.5 + heating: 110 ± 13 %, $p > 0.05$ for all; **Suppl. Figure 5a2**, for σ ; for the

368 two first bins: NaCl vs CNO 1.5; 84 ± 13 % and 24 ± 7 %, $p = 1.9 \times 10^{-5}$; CNO 1.5 vs CNO 1.5 + heating; 24 ± 7
369 % and 32 ± 7 %, $p = 7.8 \times 10^{-5}$; for the two last bins: NaCl: 100 ± 9 %, CNO 1.5: 88 ± 13 % and CNO 1.5 +
370 heating: 103 ± 13 %, $p > 0.05$ for all). The heating manipulation had a similar negative correlation
371 between cortical temperature drop and REMS onset latency as for the undisturbed conditions (**Figure**
372 **6f**, $n = 8$, Pearson's R , $R^2 = 0.88$, slope = -0.5 °C/100 min, $p = 7.7 \times 10^{-8}$). In contrast, the temperature at
373 which REMS re-appeared remained independent of REMS latency (**Figure 6g**, $n = 8$, Pearson's R , $R^2 =$
374 0.20 , slope = -0.1 °C/100 min, $p > 0.05$).

375

376 Discussion

377 States of sleep are accompanied by bidirectional brain-body interactions that remain poorly
378 understood in terms of their mechanisms (Silvani et al., 2015; Wei, 2019) and in their roles for bodily
379 restoration and health (de Zambotti et al., 2018; Orr et al., 2020). Here, we found that vagal sensory
380 stimulation induced a NREMS-like state and suppressed REMS, with both effects largely due to an
381 associated cooling of brain and bodily temperatures. In natural sleep, brain and body temperature
382 decrease at sleep onset in humans (Landolt et al., 1995), rats (Franken et al., 1992; Obal et al., 1985)
383 and mice (Hoekstra et al., 2019). These decreases are caused by a net decline in heat production due
384 to combined effects of decreased behavioral activity, lowered metabolism and altered autonomic
385 activity that causes peripheral vasodilation (Szymusiak, 2018). Temperature declines can also be
386 triggered by ambient warming (Harding et al., 2020; Szymusiak, 2018) or in result to fasting-induced
387 states of energy conservation, such as torpor (Harding et al., 2019; Huang et al., 2021). Our study adds
388 to the diversity of biological origins for hypothermia by showing that bodily sensory signals can cause
389 brain-bodily cooling while ambient temperature remained stable and food was amply available. Still,
390 as also discussed below, it is likely that the effects of vagal sensory activity share some common
391 mechanisms of cooling that accompany sleep onset, which renders them relevant for insights into the
392 molecular and neural processes that benefit from temperature fluctuations associated with sleep.

393 We used chemogenetic stimulation for two methodological reasons. First, we aimed to
394 specifically stimulate sensory vagal neurons while sparing direct motor fiber stimulation to reduce
395 possible unwanted side effects, as reported for VNS (Romero-Osorio et al., 2018). The genetic targeting
396 of Vglut2-expressing neurons by chemogenetic tools offered this specificity together with the
397 possibility to activate these neurons acutely, reversibly and in a dose-dependent manner. Furthermore,
398 chemogenetic effects lasted for hours, which provided sufficient data for an in-depth analysis of
399 polysomnographic signals so far not available for vagal sensory stimulation. Second, we found that
400 optogenetic transduction of nodose ganglia led to only a small amount of light-sensitive synaptic

401 connections in the NTS, which indicated that optogenetic stimulation *in vivo* would likely be less
402 efficient in modulating sleep.

403 The chemogenetic stimulation induced a dominant influence of the parasympathetic branch of
404 the autonomic nervous system, which is also characteristic for natural NREMS (Cerri & Amici, 2021; de
405 Zambotti et al., 2018; Silvani & Dampney, 2013; Szymusiak, 2018). The increase in NTS cFos activity
406 and the strong decrease in heart rate during both NREMS and REMS indicate that vagal sensory
407 stimulation increases parasympathetic output that could cause brain-bodily cooling through
408 depressing cardiovascular activity and associated blood flow, and through vasodilation (Harding et al.,
409 2020; Szymusiak, 2018). However, we also found cFos expression of AP neurons that relay satiety- and
410 vomiting-stimulating signals (Borgmann et al., 2021), and the broad cFos expression in NTS indicates
411 activation of airway pathways that will impact on breathing rates and volumes (Chang et al., 2015),
412 which could also impact on temperature regulation. While the temperature decline we observe are
413 thus likely to arise from a global and steady stimulation of vagal reflex circuits, it is noteworthy that a
414 recent study focusing on baroreflex-sensitive NTS neurons only also reports a suppression of REMS,
415 while the power spectrum of NREMS appeared to be also shifted to lower frequencies (Yao et al.,
416 2022). Therefore, it is possible that a strengthening parasympathetic tone and hypothermia could also
417 be relevant, at least in part, for the activity of subgroups of vagal sensory fibers.

418 We used *in vitro* whole-cell patch-clamp recordings to ensure that the viral manipulation of L-
419 JNG neurons targeted brainstem-projecting glutamatergic vagal sensory neurons. Pioneering studies
420 have previously used extracellular stimulation of the solitary tract that contains vagal sensory fibers to
421 demonstrate evoked glutamatergic responses in NTS neurons (Bailey et al., 2008; Kline et al., 2002;
422 Miles, 1986). In contrast to these studies, the percentage of connected neurons using optogenetic
423 stimulation of vagal sensory afferents was low (< 20 % vs 80-100 %). The expression of
424 channelrhodopsin at the distal portion of the terminals, being remote from the cell bodies for several
425 millimeters, could have been insufficient to evoke robust responses consistently. This possibility is
426 supported that relatively long optogenetic pulses (up to 5 ms) were required for detectable synaptic
427 response, indicating a prolonged activation of depolarizing axonal currents to reach action potential
428 threshold. Also, we carried out recordings at room temperature, in contrast to previous work done
429 mostly between 32 – 37 °C. Still, we corroborate available findings of a high synaptic interconnectivity
430 at the level of the NTS, because we found that almost every afferent stimulation was followed by
431 polysynaptic components (Bailey et al., 2008; Doyle & Andresen, 2001). We also observed that even
432 long-latency responses showed relatively small jitter, suggesting that we might have occasionally
433 activated both fast-conducting A- and slow-conducting C-type fibers (see e.g. (Miles, 1986)).

434 Vagal sensory stimulation at the onset of the light phase induced a polysomnographic state with
435 signatures reminiscent of physiological NREMS, including notably an increase in low-frequency power,
436 a decreased heart rate and brain-bodily cooling. When scoring the CNO-induced state, we noted that
437 it transits back to normal NREMS in a manner that was graded in all these physiological correlates.
438 Moreover, the NREMS-like state continued to show a similar propensity to briefly revert to wakefulness
439 as normal NREMS. This profile prompted us to describe this state as NREMS-like because it exacerbates
440 features of NREMS while retaining similar levels of spontaneous arousability. However, three
441 important aspects were different from physiological sleep. First, the increase in sleep spindle activity
442 was reduced and the associated infraslow fluctuations were absent. Second, there were overall
443 decreased power levels relative to the NaCl-condition for both the δ and the σ bands, suggesting a
444 state of decreased overall brain activity (Deboer & Tobler, 1995). Third, as a most striking indication
445 that the CNO-induced NREMS-like state was distinct, it did not interchange with REMS. We propose
446 that future studies investigating vagus sensory neurons in the context of sleep include the
447 polysomnographic analyses presented in this study to distinguish between physiological NREMS or a
448 NREMS-like state with distinct spectral dynamics and consequences for brain-bodily physiology.

449 We identified brain-body cooling as a major mechanism for the effects of vagal sensory
450 stimulation on sleep. Hypothermia developed over the same time scales as the sleep alterations, with
451 the onset of hypothermia largely coinciding with the onset of the sleep-like state. Furthermore, REMS
452 re-appeared sharply once cortical temperature recovered, which is consistent with a steep
453 dependence of REMS on body temperature (Harding et al., 2019). Attenuating cortical and bodily
454 hypothermia by ambient heating partially restored some of the physiological characteristics of normal
455 NREMS, including the expression of REMS. Vagal sensory stimulation's temperature drop thus
456 dominates effects on sleep in mice, in a manner reminiscent of the EEG/EMG signatures of daily torpor
457 in mice (Huang et al., 2021). For the moment, several points argue against the CNO-induced state being
458 a torpor-like state. The bodily temperature drop was less pronounced than for torpor (Deboer & Tobler,
459 1995; Harding et al., 2019) and arousability remained unchanged. Furthermore, the CNO-induced
460 NREMS-like state did not provoke a detectable increase in times spent in NREMS, for which there is
461 evidence in torpor of hamsters (Deboer & Tobler, 2000; Vyazovskiy et al., 2017). A possible explanation
462 is that, compared to torpor, the CNO-induced hypothermia may be weak enough so that restorative
463 actions associated with natural hypothermia can be preserved. However, it will be important to further
464 test where the CNO-induced state ranges in the continuum of states associated with lowered brain-
465 bodily temperature (Harding et al., 2019). For example, is the CNO-induced state an 'too cold' NREMS
466 and can torpor be induced through further increases vagal sensory nerve stimulation? Answering these
467 questions could shed further light on the purpose of brain cooling for sleep functions. Advances in

468 methodologies to fine-tune brain temperature in sleep could be clinically relevant, which becomes
469 increasingly relevant given that sleep, thermoregulation, and molecular players in neurodegeneration
470 interact (Guisle et al., 2020). Critical for this will be to elucidate the thermoregulatory mechanisms
471 underlying the CNO-induced hypothermia, and to further probe vagal sensory stimulation over a
472 greater range of chemogenetic activation and through other technical means.

473 Aside brain-bodily cooling, central circuits activated by vagal sensory afferents also remain to be
474 considered. There is strong evidence for increased noradrenergic signaling in response to vagus nerve
475 stimulation (Berger et al., 2021; Mridha et al., 2021; Sharon et al., 2021). REMS is suppressed by even
476 small elevations of LC activity (Osorio-Forero et al., 2024). Noradrenergic signaling pathways can also
477 target hypothermia-producing hypothalamic preoptic areas (Yu et al., 2018) or contribute to heat
478 retention through sympathetic thermoeffector mechanisms (Blessing et al., 2016). The vagally driven
479 activation of LC could thus be directly involved in hypothermia. Alternatively, it could represent a
480 mechanism possibly compensating for heat loss. For example, the LC has a relatively weak intrinsic
481 temperature sensitivity (Corrodi et al., 1967). LC can also be activated as a result of systemic stress, for
482 example during loss of blood pressure (Anselmo-Franci et al., 1998). Whether the interplay between
483 hypothermia and LC could be relevant for vagal sensory stimulation, and for the link between NREMS
484 and thermoregulation more generally, remains to be addressed.

485 A strong suppression of REMS paired with hypothermia has also been described for
486 chemogenetic stimulation of subpopulations of preoptic hypothalamic neurons expressing the
487 neuropeptide galanin within portions of the ventrolateral preoptic nucleus (Kroeger et al., 2018).
488 Homeostatic regulation of REMS was further preserved (Kroeger et al., 2018), in remarkable similarity
489 to our observation with vagal sensory stimulation. A suppression of REMS, together with a low-
490 frequency power NREMS-like state associated with hypothermia was also described for a population
491 of warm-sensitive glutamatergic/nitregic neurons in the medial-median preoptic area (Harding et al.,
492 2018). The phenomenological similarities to our data position these hypothalamic neuronal
493 populations as candidate areas that could be involved in mediating the actions of vagal sensory
494 stimulation, possibly through pathways involving the NTS and the parabrachial nuclei, independently
495 of LC activation.

496 This study presents a detailed analysis of the sleep states induced by vagal sensory stimulation,
497 highlighting a major role of brain-body cooling in the induction of a NREMS-like state that is
498 incompatible with REMS. We further present evidence that this state shows features of a NREMS-like
499 state with possibly conserved restorative effects, which makes it relevant in future investigations on
500 the molecular and cellular consequences of hypothermia (Hoekstra et al., 2019). Of particular interest

501 will also be whether vagal sensory afferents' hypothermic effects can be relevant for human, for which
502 there is evidence for LC activation during VNS, yet cortical temperature has not yet been measured.
503 Clarifying this could further broaden the scope of VNS, for example in the context of medical
504 technologies for clinical conditions in which mild hypothermia is desirable (Cerri, 2024).

505

506 References

- 507 Amici, R., Cerri, M., Ocampo-Garces, A., Baracchi, F., Dentico, D., Jones, C. A., Luppi, M., Perez, E.,
508 Parmeggiani, P. L., & Zamboni, G. (2008). Cold exposure and sleep in the rat: REM sleep
509 homeostasis and body size. *Sleep*, 31(5), 708-715. <https://doi.org/10.1093/sleep/31.5.708>
- 510 Andrillon, T., & Kouider, S. (2020). The vigilant sleeper: neural mechanisms of sensory (de)coupling
511 during sleep. *Curr Opin Physiol*, 15, 47-59. <https://doi.org/10.1016/j.cophys.2019.12.002>
- 512 Anselmo-Franci, J. A., Peres-Polon, V. L., da Rocha-Barros, V. M., Moreira, E. R., Franci, C. R., & Rocha,
513 M. J. (1998). C-fos expression and electrolytic lesions studies reveal activation of the posterior
514 region of locus coeruleus during hemorrhage induced hypotension. *Brain Res*, 799(2), 278-
515 284. [https://doi.org/10.1016/s0006-8993\(98\)00468-5](https://doi.org/10.1016/s0006-8993(98)00468-5)
- 516 Bailey, T. W., Appleyard, S. M., Jin, Y. H., & Andresen, M. C. (2008). Organization and properties of
517 GABAergic neurons in solitary tract nucleus (NTS). *J Neurophysiol*, 99(4), 1712-1722.
518 <https://doi.org/10.1152/jn.00038.2008>
- 519 Bastuji, H., Perchet, C., Legrain, V., Montes, C., & Garcia-Larrea, L. (2008). Laser evoked responses to
520 painful stimulation persist during sleep and predict subsequent arousals. *Pain*, 137(3), 589-
521 599. <https://doi.org/10.1016/j.pain.2007.10.027>
- 522 Berger, A., Vespa, S., Dricot, L., Dumoulin, M., Iachim, E., Doguet, P., Vandewalle, G., & El Tahry, R.
523 (2021). How Is the Norepinephrine System Involved in the Antiepileptic Effects of Vagus Nerve
524 Stimulation? *Front Neurosci*, 15, 790943. <https://doi.org/10.3389/fnins.2021.790943>
- 525 Blessing, W., McAllen, R., & McKinley, M. (2016). Control of the Cutaneous Circulation by the Central
526 Nervous System. *Compr Physiol*, 6(3), 1161-1197. <https://doi.org/10.1002/cphy.c150034>
- 527 Borgmann, D., Ciglieri, E., Biglari, N., Brandt, C., Cremer, A. L., Backes, H., Tittgemeyer, M., Wunderlich,
528 F. T., Bruning, J. C., & Fenselau, H. (2021). Gut-brain communication by distinct sensory
529 neurons differently controls feeding and glucose metabolism. *Cell Metab*, 33(7), 1466-1482
530 e1467. <https://doi.org/10.1016/j.cmet.2021.05.002>
- 531 Brodt, S., Inostroza, M., Niethard, N., & Born, J. (2023). Sleep-A brain-state serving systems memory
532 consolidation. *Neuron*, 111(7), 1050-1075. <https://doi.org/10.1016/j.neuron.2023.03.005>
- 533 Cardis, R., Lecci, S., Fernandez, L. M., Osorio-Forero, A., Chu Sin Chung, P., Fulda, S., Decosterd, I., &
534 Luthi, A. (2021). Cortico-autonomic local arousals and heightened somatosensory arousability
535 during NREMS of mice in neuropathic pain. *Elife*, 10. <https://doi.org/10.7554/eLife.65835>
- 536 Cerri, M. (2024). Torpor: A whole-brain view of the underlying neural network. *Curr Biol*, 34(1), R33-
537 R35. <https://doi.org/10.1016/j.cub.2023.11.053>
- 538 Cerri, M., & Amici, R. (2021). Thermoregulation and Sleep: Functional Interaction and Central Nervous
539 Control. *Compr Physiol*, 11(2), 1591-1604. <https://doi.org/10.1002/cphy.c140012>
- 540 Chang, R. B., Strohlic, D. E., Williams, E. K., Umans, B. D., & Liberles, S. D. (2015). Vagal Sensory Neuron
541 Subtypes that Differentially Control Breathing. *Cell*, 161(3), 622-633.
542 <https://doi.org/10.1016/j.cell.2015.03.022>
- 543 Corrodi, H., Fuxe, K., & Hokfelt, T. (1967). A possible role played by central monoamine neurones in
544 thermo-regulation. *Acta Physiol Scand*, 71(2), 224-232. [https://doi.org/10.1111/j.1748-
545 1716.1967.tb03728.x](https://doi.org/10.1111/j.1748-1716.1967.tb03728.x)

546 de Zambotti, M., Trinder, J., Silvani, A., Colrain, I. M., & Baker, F. C. (2018). Dynamic coupling between
547 the central and autonomic nervous systems during sleep: A review. *Neurosci Biobehav Rev*, *90*,
548 84-103. <https://doi.org/10.1016/j.neubiorev.2018.03.027>

549 Deboer, T., & Tobler, I. (1995). Temperature dependence of EEG frequencies during natural
550 hypothermia. *Brain Res*, *670*(1), 153-156. [https://doi.org/10.1016/0006-8993\(94\)01299-w](https://doi.org/10.1016/0006-8993(94)01299-w)

551 Deboer, T., & Tobler, I. (2000). Slow waves in the sleep electroencephalogram after daily torpor are
552 homeostatically regulated. *Neuroreport*, *11*(4), 881-885. [https://doi.org/10.1097/00001756-
553 200003200-00044](https://doi.org/10.1097/00001756-200003200-00044)

554 Doyle, M. W., & Andresen, M. C. (2001). Reliability of monosynaptic sensory transmission in brain stem
555 neurons in vitro. *J Neurophysiol*, *85*(5), 2213-2223. <https://doi.org/10.1152/jn.2001.85.5.2213>

556 Fernandez, L. M., Vantomme, G., Osorio-Forero, A., Cardis, R., Beard, E., & Luthi, A. (2018). Thalamic
557 reticular control of local sleep in mouse sensory cortex. *Elife*, *7*.
558 <https://doi.org/10.7554/eLife.39111>

559 Fernandez, L. M. J., & Lüthi, A. (2020). Sleep spindles: mechanisms and functions. *Physiol Rev*, *100*(2),
560 805-868. <https://doi.org/10.1152/physrev.00042.2018>

561 Franken, P., & Dijk, D. J. (2024). Sleep and circadian rhythmicity as entangled processes serving
562 homeostasis. *Nat Rev Neurosci*, *25*(1), 43-59. <https://doi.org/10.1038/s41583-023-00764-z>

563 Franken, P., Tobler, I., & Borbely, A. A. (1992). Sleep and waking have a major effect on the 24-hr rhythm
564 of cortical temperature in the rat. *J Biol Rhythms*, *7*(4), 341-352.
565 <https://doi.org/10.1177/074873049200700407>

566 Guisle, I., Gratuze, M., Petry, S., Morin, F., Keraudren, R., Whittington, R. A., Hebert, S. S., Mongrain, V.,
567 & Planel, E. (2020). Circadian and sleep/wake-dependent variations in tau phosphorylation are
568 driven by temperature. *Sleep*, *43*(4). <https://doi.org/10.1093/sleep/zsz266>

569 Hallbook, T., Lundgren, J., Kohler, S., Blennow, G., Stromblad, L. G., & Rosen, I. (2005). Beneficial effects
570 on sleep of vagus nerve stimulation in children with therapy resistant epilepsy. *Eur J Paediatr*
571 *Neurol*, *9*(6), 399-407. <https://doi.org/10.1016/j.ejpn.2005.08.004>

572 Han, W., Tellez, L. A., Perkins, M. H., Perez, I. O., Qu, T., Ferreira, J., Ferreira, T. L., Quinn, D., Liu, Z. W.,
573 Gao, X. B., Kaelberer, M. M., Bohorquez, D. V., Shammah-Lagnado, S. J., de Lartigue, G., & de
574 Araujo, I. E. (2018). A Neural Circuit for Gut-Induced Reward. *Cell*, *175*(3), 887-888.
575 <https://doi.org/10.1016/j.cell.2018.10.018>

576 Harding, E. C., Franks, N. P., & Wisden, W. (2019). The Temperature Dependence of Sleep. *Front*
577 *Neurosci*, *13*, 336. <https://doi.org/10.3389/fnins.2019.00336>

578 Harding, E. C., Franks, N. P., & Wisden, W. (2020). Sleep and thermoregulation. *Curr Opin Physiol*, *15*,
579 7-13. <https://doi.org/10.1016/j.cophys.2019.11.008>

580 Harding, E. C., Yu, X., Miao, A., Andrews, N., Ma, Y., Ye, Z., Lignos, L., Miracca, G., Ba, W., Yustos, R.,
581 Vyssotski, A. L., Wisden, W., & Franks, N. P. (2018). A Neuronal Hub Binding Sleep Initiation
582 and Body Cooling in Response to a Warm External Stimulus. *Curr Biol*, *28*(14), 2263-2273
583 e2264. <https://doi.org/10.1016/j.cub.2018.05.054>

584 Hoekstra, M. M., Emmenegger, Y., Hubbard, J., & Franken, P. (2019). Cold-inducible RNA-binding
585 protein (CIRBP) adjusts clock-gene expression and REM-sleep recovery following sleep
586 deprivation. *Elife*, *8*. <https://doi.org/10.7554/eLife.43400>

587 Holt, M. K. (2022). The ins and outs of the caudal nucleus of the solitary tract: An overview of cellular
588 populations and anatomical connections. *J Neuroendocrinol*, *34*(6), e13132.
589 <https://doi.org/10.1111/jne.13132>

590 Huang, Y. G., Flaherty, S. J., Pothecary, C. A., Foster, R. G., Peirson, S. N., & Vyazovskiy, V. V. (2021). The
591 relationship between fasting-induced torpor, sleep, and wakefulness in laboratory mice. *Sleep*,
592 *44*(9). <https://doi.org/10.1093/sleep/zsab093>

593 Karemaker, J. M. (2022). The multibranching nerve: vagal function beyond heart rate variability. *Biol*
594 *Psychol*, *172*, 108378. <https://doi.org/10.1016/j.biopsycho.2022.108378>

595 Kline, D. D., Takacs, K. N., Ficker, E., & Kunze, D. L. (2002). Dopamine modulates synaptic transmission
596 in the nucleus of the solitary tract. *J Neurophysiol*, 88(5), 2736-2744.
597 <https://doi.org/10.1152/jn.00224.2002>

598 Komagata, N., Latifi, B., Rusterholz, T., Bassetti, C. L. A., Adamantidis, A., & Schmidt, M. H. (2019).
599 Dynamic REM Sleep Modulation by Ambient Temperature and the Critical Role of the Melanin-
600 Concentrating Hormone System. *Curr Biol*, 29(12), 1976-1987 e1974.
601 <https://doi.org/10.1016/j.cub.2019.05.009>

602 Kourbanova, K., Alexandre, C., & Latremoliere, A. (2022). Effect of sleep loss on pain-New conceptual
603 and mechanistic avenues. *Front Neurosci*, 16, 1009902.
604 <https://doi.org/10.3389/fnins.2022.1009902>

605 Krauchi, K., & Deboer, T. (2010). The interrelationship between sleep regulation and thermoregulation.
606 *Front Biosci (Landmark Ed)*, 15(2), 604-625. <https://doi.org/10.2741/3636>

607 Kroeger, D., Absi, G., Gagliardi, C., Bandaru, S. S., Madara, J. C., Ferrari, L. L., Arrigoni, E., Munzberg, H.,
608 Scammell, T. E., Saper, C. B., & Vetrivelan, R. (2018). Galanin neurons in the ventrolateral
609 preoptic area promote sleep and heat loss in mice. *Nat Commun*, 9(1), 4129.
610 <https://doi.org/10.1038/s41467-018-06590-7>

611 Krone, L. B., Feher, K. D., Rivero, T., & Omlin, X. (2023). Brain stimulation techniques as novel treatment
612 options for insomnia: A systematic review. *J Sleep Res*, 32(6), e13927.
613 <https://doi.org/10.1111/jsr.13927>

614 Landolt, H. P., Moser, S., Wieser, H. G., Borbely, A. A., & Dijk, D. J. (1995). Intracranial temperature
615 across 24-hour sleep-wake cycles in humans. *Neuroreport*, 6(6), 913-917.
616 <https://doi.org/10.1097/00001756-199504190-00022>

617 Larsen, L. E., Lysebettens, W. V., Germonpre, C., Carrette, S., Daelemans, S., Sprengers, M., Thyron, L.,
618 Wadman, W. J., Carrette, E., Delbeke, J., Boon, P., Vonck, K., & Raedt, R. (2017). Clinical Vagus
619 Nerve Stimulation Paradigms Induce Pronounced Brain and Body Hypothermia in Rats. *Int J*
620 *Neural Syst*, 27(5), 1750016. <https://doi.org/10.1142/S0129065717500162>

621 Lecci, S., Fernandez, L. M. J., Weber, F. D., Cardis, R., Chatton, J.-Y., Born, J., & Lüthi, A. (2017).
622 Coordinated infra-slow neural and cardiac oscillations mark fragility and offline periods in
623 mammalian sleep. *Sci. Adv.*, 3(2), e1602026. <https://doi.org/10.1126/sciadv.1602026>

624 Madden, C. J., Santos da Conceicao, E. P., & Morrison, S. F. (2017). Vagal afferent activation decreases
625 brown adipose tissue (BAT) sympathetic nerve activity and BAT thermogenesis. *Temperature*
626 *(Austin)*, 4(1), 89-96. <https://doi.org/10.1080/23328940.2016.1257407>

627 McCarthy, A., Wafford, K., Shanks, E., Ligocki, M., Edgar, D. M., & Dijk, D. J. (2016). REM sleep
628 homeostasis in the absence of REM sleep: Effects of antidepressants. *Neuropharmacology*,
629 108, 415-425. <https://doi.org/10.1016/j.neuropharm.2016.04.047>

630 McCormick, D. A., & Bal, T. (1997). Sleep and arousal: thalamocortical mechanisms. *Annu Rev Neurosci*,
631 20, 185-215. <https://doi.org/10.1146/annurev.neuro.20.1.185>

632 Miles, R. (1986). Frequency dependence of synaptic transmission in nucleus of the solitary tract in
633 vitro. *J Neurophysiol*, 55(5), 1076-1090. <https://doi.org/10.1152/jn.1986.55.5.1076>

634 Min, S., Chang, R. B., Prescott, S. L., Beeler, B., Joshi, N. R., Strohlic, D. E., & Liberles, S. D. (2019).
635 Arterial Baroreceptors Sense Blood Pressure through Decorated Aortic Claws. *Cell Rep*, 29(8),
636 2192-2201 e2193. <https://doi.org/10.1016/j.celrep.2019.10.040>

637 Mridha, Z., de Gee, J. W., Shi, Y., Alkashgari, R., Williams, J., Suminski, A., Ward, M. P., Zhang, W., &
638 McGinley, M. J. (2021). Graded recruitment of pupil-linked neuromodulation by parametric
639 stimulation of the vagus nerve. *Nat Commun*, 12(1), 1539. <https://doi.org/10.1038/s41467-021-21730-2>

640

641 Neuhuber, W. L., & Berthoud, H. R. (2021). Functional anatomy of the vagus system - Emphasis on the
642 somato-visceral interface. *Auton Neurosci*, 236, 102887.
643 <https://doi.org/10.1016/j.autneu.2021.102887>

644 Nir, Y., & de Lecea, L. (2023). Sleep and vigilance states: Embracing spatiotemporal dynamics. *Neuron*,
645 111(13), 1998-2011. <https://doi.org/10.1016/j.neuron.2023.04.012>

646 Obal, F., Rubicsek, G., Alfoldi, P., Sary, G., & Obal, F. (1985). Changes in the brain and core
647 temperatures in relation to the various arousal states in rats in the light and dark periods of
648 the day. *Pflugers Arch*, 404(1), 73-79. <https://doi.org/10.1007/BF00581494>
649 Orr, W. C., & Chen, C. L. (2005). Sleep and the gastrointestinal tract. *Neurol Clin*, 23(4), 1007-1024.
650 <https://doi.org/10.1016/j.ncl.2005.05.004>
651 Orr, W. C., Fass, R., Sundaram, S. S., & Scheimann, A. O. (2020). The effect of sleep on gastrointestinal
652 functioning in common digestive diseases. *Lancet Gastroenterol Hepatol*, 5(6), 616-624.
653 [https://doi.org/10.1016/S2468-1253\(19\)30412-1](https://doi.org/10.1016/S2468-1253(19)30412-1)
654 Osorio-Forero, A., Cardis, R., Vantomme, G., Guillaume-Gentil, A., Katsioudi, G., Devenoges, C.,
655 Fernandez, L. M. J., & Luthi, A. (2021). Noradrenergic circuit control of non-REM sleep
656 substates. *Curr Biol*, 31(22), 5009-5023 e5007. <https://doi.org/10.1016/j.cub.2021.09.041>
657 Osorio-Forero, A., Foustoukos, G., Cardis, R., Cherrad, N., Devenoges, C., Fernandez, L. M. J., & Lüthi,
658 A. (2024). Noradrenergic locus coeruleus activity functionally partitions NREM sleep to
659 gatekeep the NREM-REM sleep cycle. *Biorxiv*, 2023.2005.2020.541586.
660 <https://doi.org/10.1101/2023.05.20.541586>
661 Park, S. H., & Weber, F. (2020). Neural and homeostatic regulation of REM sleep. *Front Psychol*, 11,
662 1662. <https://doi.org/10.3389/fpsyg.2020.01662>
663 Prescott, S. L., & Liberles, S. D. (2022). Internal senses of the vagus nerve. *Neuron*, 110(4), 579-599.
664 <https://doi.org/10.1016/j.neuron.2021.12.020>
665 Raab, M., & Neuhuber, W. L. (2007). Glutamatergic functions of primary afferent neurons with special
666 emphasis on vagal afferents. *Int Rev Cytol*, 256, 223-275. [https://doi.org/10.1016/S0074-
667 7696\(07\)56007-9](https://doi.org/10.1016/S0074-7696(07)56007-9)
668 Rizzo, P., Beelke, M., De Carli, F., Canovaro, P., Nobili, L., Robert, A., Fornaro, P., Tanganelli, P., Regesta,
669 G., & Ferrillo, F. (2004). Modifications of sleep EEG induced by chronic vagus nerve stimulation
670 in patients affected by refractory epilepsy. *Clin Neurophysiol*, 115(3), 658-664.
671 <https://doi.org/10.1016/j.clinph.2003.10.026>
672 Rizzo, P., Beelke, M., De Carli, F., Canovaro, P., Nobili, L., Robert, A., Tanganelli, P., Regesta, G., & Ferrillo,
673 F. (2003). Chronic vagus nerve stimulation improves alertness and reduces rapid eye
674 movement sleep in patients affected by refractory epilepsy. *Sleep*, 26(5), 607-611.
675 <https://doi.org/10.1093/sleep/26.5.607>
676 Romero-Osorio, R., Gil-Tamayo, S., Nariño, D., & Rosselli, D. (2018). Changes in sleep patterns after
677 vagus nerve stimulation, deep brain stimulation or epilepsy surgery: Systematic review of the
678 literature. *Seizure*, 56, 4-8.
679 Sharon, O., Fahoum, F., & Nir, Y. (2021). Transcutaneous Vagus Nerve Stimulation in Humans Induces
680 Pupil Dilation and Attenuates Alpha Oscillations. *J Neurosci*, 41(2), 320-330.
681 <https://doi.org/10.1523/JNEUROSCI.1361-20.2020>
682 Silvani, A., Calandra-Buonaura, G., Benarroch, E. E., Dampney, R. A., & Cortelli, P. (2015). Bidirectional
683 interactions between the baroreceptor reflex and arousal: an update. *Sleep Med*, 16(2), 210-
684 216. <https://doi.org/10.1016/j.sleep.2014.10.011>
685 Silvani, A., & Dampney, R. A. (2013). Central control of cardiovascular function during sleep. *Am J*
686 *Physiol Heart Circ Physiol*, 305(12), H1683-1692.
687 <https://doi.org/10.1152/ajpheart.00554.2013>
688 Szymusiak, R. (2018). Body temperature and sleep. *Handb Clin Neurol*, 156, 341-351.
689 <https://doi.org/10.1016/B978-0-444-63912-7.00020-5>
690 Traut, J., Mengual, J. P., Meijer, E. J., McKillop, L. E., Alfonsa, H., Hoerder-Suabedissen, A., Song, S. H.,
691 Feher, K. D., Riemann, D., Molnar, Z., Akerman, C. J., Vyazovskiy, V. V., & Krone, L. B. (2023).
692 Effects of clozapine-N-oxide and compound 21 on sleep in laboratory mice. *Elife*, 12.
693 <https://doi.org/10.7554/eLife.84740>
694 Vantomme, G., Rovo, Z., Cardis, R., Beard, E., Katsioudi, G., Guadagno, A., Perrenoud, V., Fernandez, L.
695 M. J., & Luthi, A. (2020). A Thalamic Reticular Circuit for Head Direction Cell Tuning and Spatial
696 Navigation. *Cell Rep*, 31(10), 107747. <https://doi.org/10.1016/j.celrep.2020.107747>

- 697 Vyazovskiy, V. V. (2015). Sleep, recovery, and metaregulation: explaining the benefits of sleep. *Nat Sci*
698 *Sleep*, 7, 171-184. <https://doi.org/10.2147/NSS.S54036>
- 699 Vyazovskiy, V. V., Palchykova, S., Achermann, P., Tobler, I., & Deboer, T. (2017). Different Effects of Sleep
700 Deprivation and Torpor on EEG Slow-Wave Characteristics in Djungarian Hamsters. *Cereb*
701 *Cortex*, 27(2), 950-961. <https://doi.org/10.1093/cercor/bhx020>
- 702 Wei, Y., Van Someren, E.J.W. (2019). Interoception relates to sleep and sleep disorders. *Curr Opin Behav*
703 *Sci*, 33, 1-7.
- 704 Williams, E. K., Chang, R. B., Strohlic, D. E., Umans, B. D., Lowell, B. B., & Liberles, S. D. (2016). Sensory
705 Neurons that Detect Stretch and Nutrients in the Digestive System. *Cell*, 166(1), 209-221.
706 <https://doi.org/10.1016/j.cell.2016.05.011>
- 707 Yao, Y., Barger, Z., Saffari Doost, M., Tso, C. F., Darmohray, D., Silverman, D., Liu, D., Ma, C., Cetin, A.,
708 Yao, S., Zeng, H., & Dan, Y. (2022). Cardiovascular baroreflex circuit moonlights in sleep control.
709 *Neuron*, 110(23), 3986-3999 e3986. <https://doi.org/10.1016/j.neuron.2022.08.027>
- 710 Yoon, H.-K. (2019). Therapeutic Application of Transcutaneous Auricular Vagus Nerve Stimulation in
711 Primary Insomnia. *Chronobiol Med*, 1, 51-54.
- 712 Yu, X., Franks, N. P., & Wisden, W. (2018). Sleep and Sedative States Induced by Targeting the Histamine
713 and Noradrenergic Systems. *Front Neural Circuits*, 12, 4.
714 <https://doi.org/10.3389/fncir.2018.00004>
- 715 Zanchetti, A., Wang, S. C., & Moruzzi, G. (1952). [Effect of afferent vagal stimulation on the
716 electroencephalogram of the cat in cerebral isolation]. *Boll Soc Ital Biol Sper*, 28(4), 627-628.
717 <https://www.ncbi.nlm.nih.gov/pubmed/13018424> (Reazione elettrencefalografica di risveglio
718 ottenuta nel gatto encefalo isolato mediante stimolazione di fibre afferenti vagali.)
- 719 Zhang, C., Kaye, J. A., Cai, Z., Wang, Y., Prescott, S. L., & Liberles, S. D. (2021). Area Postrema Cell Types
720 that Mediate Nausea-Associated Behaviors. *Neuron*, 109(3), 461-472 e465.
721 <https://doi.org/10.1016/j.neuron.2020.11.010>

722

723 **Material and Methods**

724

725 **Animal husbandry**

726 Mice from the Slc17a6^{tm2(cre)Lowl}/J (JAX Stock#016963), commonly referred to as Vglut2-Cre
727 line, were bred on a C57BL/6J background (breeders were kindly provided by Alan Carleton,
728 UNIGE). The mice were bred in a humidity- and temperature-controlled animal facility with a
729 12 h / 12 h light-dark cycle. For viral injections, 4 – 8 week-old animals were transferred into
730 a ventilated cabinet in the P2 safety level facility with similar conditions on the day prior to
731 injection. They remained in the P2 facility for 72 h after the viral injection. For *in vitro*
732 experiments, animals were transferred into a housing room with a 12 h / 12 h light-dark cycle
733 (lights onset at 9:00 am, corresponding to ZT0) where they remained for at least 3 weeks until
734 *in vitro* electrophysiology. For *in vivo* experiments, animals remained there for at least 2
735 weeks before surgery for sleep recordings. Once animals had received surgical implants for
736 sleep recordings, they were single-housed in cages equipped with tall Plexiglas walls (~30 cm)
737 without roof. Animals were kept in their home cage in the sleep recording room for at least

738 one week prior to habituation and recording. Through all experimental procedures, food and
739 water were given *ad libitum*. All experimental procedures were carried out according to the
740 Swiss National Guidelines on Animal experimentation and subject to a license approved by
741 the Cantonal Veterinary Office for Animal Experimentation.

742

743

744 **Surgery for viral injections in JNG**

745 Mice were given analgesic (carprofen, 5mg/kg s.c.), anesthetized by isoflurane inhalation (5 %
746 in oxygen), and placed on a warming surface for maintenance of body temperature at 37 °C.
747 Anesthesia was maintained via a nose cone through which isoflurane was provided (1.5 – 2.5
748 % in oxygen), while the mouse was placed on its back. The skin was shaved and local
749 anesthetics (lidocaine (6 mg/kg) + bupivacaine (2.5 mg/kg, 20 µl) injected subcutaneously at
750 the location of the future incision. An incision was made on the ventral surface of the neck via
751 fine scissors (incision of 3 – 4 mm), the salivary glands were exposed and separated. A
752 magnetic fixator retraction system (FST, retractors with 1-mm tip diameter) was used to gently
753 displace the different muscles lying on top of the JNG. To expose the L-JNG, one retractor each
754 were placed on the left salivary gland and on the left sternomastoid muscle. A third retractor
755 was used to displace the left sternohyoid and the omohyoid muscles to the right. Finally, a
756 fourth retractor was placed on the left digastric muscle. The left hypoglossal nerve was gently
757 separated from the vagus nerve through slightly lifting with a fifth retractor (0.5 mm tip
758 diameter), which exposed the L-JNG. A manual manipulator was used to insert a thin glass
759 pipette (5-000-1001-X, 649 Drummond Scientific) pulled on a vertical puller (Narishige PP-
760 830), initially filled with mineral oil, and backfilled with the virus just prior to injection, into
761 the L-JNG. The injected volume of virus ranged between 250 – 350 nL. The following viral
762 constructs were used for:

- 763 - expression of ChR2 in L-JNG sensory neurons: 11 animals were transfected with a Cre-
764 dependent virus AAV1.EF1a.DIO.hChR2(H134R)-eYFP.WPRE.hGH (titer 1.9×10^{13} GC/ml) and
765 1 animal with AAV1-CamKIIa.hChR2(H134R)-eYFP.WPRE.hGH (titer 1.1×10^{13} GC/ml)
- 766 - expression of excitatory chemogenetic DREADD receptors in L-JNG sensory neurons: 21
767 animals were transfected with a virus encoding Cre-dependent excitatory DREADD
768 ssAAV8/2-hSyn1-dlox-hM3D(Gq)_mCherry-dlox-WPRE-hGH(pA) (titer 3×10^{12} GC/ml)

769 - expression of control virus for fluorescent labelling vagal sensory fibers and for the
770 chemogenetic stimulation in L-JNG sensory neurons: 1 animal with AAV1-
771 CamKIIa.hChR2(H134R)-eYFP.WPRE.hGH (titer 1.1×10^{13} GC/ml), 1 animal with AAV8-hSyn-
772 FLEX-Jaws-KGC-GFP-ER2 (titer 3.2×10^{12} GC/ml), and 4 animals with ssAAV8/2-hSyn1-dlox-
773 mCherry(rev)-dlox-WPRE-hGHp(A) (titer 9×10^{12} GC/ml)

774

775 ***In vitro* electrophysiological recordings**

776 Brain slice preparation.

777 Coronal brainstem slices containing the NTS and AP were prepared from Vglut2-Cre mice
778 previously injected with a ChR2-expressing viral vector as described above. 4 – 7 weeks after
779 viral injection, mice aged 8 – 12 weeks were subjected to isoflurane anaesthesia (4% in O₂)
780 after which they were decapitated, brains extracted and quickly immersed in ice-cold
781 oxygenated solution with partial substitution of NaCl containing (in mM): NaCl 66, KCl 2.5,
782 NaH₂PO₄ 1.25, NaHCO₃ 26, D-saccharose 105, D-glucose 27, L(+)-ascorbic acid 1.7, CaCl₂ 0.5
783 and MgCl₂ 7), using a sliding vibratome (Histocom). Brains were cut at the level of bregma in
784 the coronal plane and the posterior portion containing the brainstem was glued with the
785 trimmed surface on an ice-cold metal blade, with the ventral side apposed to a supporting
786 agar block. Acute 300- μ m-thick coronal brainstem slices were prepared in the same ice-cold
787 oxygenated sucrose solution, transferred to a storage chamber and kept for 30 min in a
788 recovery solution at 35°C (in mM: NaCl 131, KCl 2.5, NaH₂PO₄ 1.25, NaHCO₃ 26, D-glucose 20,
789 L(+)-ascorbic acid 1.7, CaCl₂ 2, MgCl₂ 1.2, *myo*-inositol 3, pyruvate 2) after which they were
790 kept at room temperature for at least 1 h. All recordings were done at room temperature.

791 Patch-clamp recording techniques.

792 Recording glass pipettes were pulled from borosilicate glass (TW150F-4) (WPI) with a DMZ
793 horizontal puller (Zeitz Instr.) to a final resistance of 4.6 – 6.1 M Ω . Pipettes were filled with a
794 K⁺-based intracellular solution that contained in mM: KGluconate 140, HEPES 10, KCl 10, EGTA
795 0.1, phosphocreatine 10, Mg-ATP 4, Na-GTP 0.4, supplemented with neurobiotin (2mg/mL),
796 pH 7.3, 290–305 mOsm. Slices were placed in the recording chamber of an upright microscope
797 (Olympus BX50WI) and continuously superfused with oxygenated ACSF containing in mM:
798 NaCl 131, KCl 2.5, NaH₂PO₄ 1.25, NaHCO₃ 26, D-glucose 20, L(+)-ascorbic acid 1.7, CaCl₂ 2 and
799 MgCl₂ 1.2.

800 The area containing the left NTS and AP was identified through a 10X immersion objective in
801 transillumination microscopy after which cells bodies were visualized through a 40X
802 immersion objective in differential interference contrast optics. Prior to recording, pipette
803 offset was zeroed, and cells patched in the whole-cell recording configuration. Patched
804 neurons were immediately tested for connectivity once whole-cell access was obtained. The
805 preferred area for successful patching of cells responding to light stimulation was identified
806 within the medial portion of the NTS adjacent to the AP (Bregma -7.64 to -7.32 mm). In this
807 area, immunoenhancement of EYFP also revealed a high density of green fibers, indicating
808 that the ChR2_EYFP protein was expressed up to the terminals of the sensory axons (**Figure**
809 **1d2, f1**). Expression quality of this protein was thus better than the one observed with the
810 reporter virus alone, in which clearly labelled fibers could be seen up to central portions of
811 the NTS (see **Figure 1c**).

812 Signals were amplified using a Multiclamp 700B amplifier, digitized via a Digidata1322A and
813 sampled at 10 kHz with Clampex10.2 (Molecular Devices). Immediately after gaining whole-
814 cell access, passive cellular properties and action potential discharge frequencies were
815 measured using direct somatic current injections in the voltage- or the current-clamp
816 recordings configuration. Cells included for analysis had access resistances between 21 and
817 48 M Ω , which was not compensated for. A liquid junction potential of \sim -10 mV was also not
818 compensated for.

819 Recording protocols.

820 After gaining whole-cell access, cells were first held in voltage-clamp at -60 mV and
821 hyperpolarized in brief steps (10 mV, 100 ms) after which whole-field blue LED (Cairn Res)
822 light pulses (470 nm, duration: 1 – 5 ms, maximal light intensity 3.8 mW, 0.75 mW/mm²) were
823 given to check for a synaptic response. Light pulses were given maximally once every 5 – 10 s
824 for 5 – 10 sweeps. Once synaptic connectivity was established, cellular action potential
825 discharge properties were tested in current-clamp mode using somatic current injections
826 from -50 to 80 pA in square current steps lasting 0.5 – 2 s. Evoked responses were then again
827 measured in voltage-clamp at a frequency of 0.1 – 0.2 Hz. The effects of DNQX (10 μ M) were
828 tested on evoked postsynaptic potentials (EPSPs) in current-clamp mode with cells held at the
829 membrane potential of -68 to -60 mV and EPSPs evoked at 0.1 – 0.2 Hz. Per slice only one
830 synaptically connected cell was studied. At the end of the recording, sections were fixed in
831 PFA 4% in PBS for *post hoc* recovery of the neurobiotin-filled cells (Vector Labs).

832 Analysis of cellular physiology data.

833 Passive cellular properties including membrane time constant (τ_m), cellular capacitance (C_m)
834 and resting membrane potential (RMP) were analyzed according to standard procedures
835 (Vantomme et al., 2020). The membrane resistance was not directly calculated from the
836 steady-state current response due to poorly characterized, presumably active, current
837 components apparent with small hyperpolarizations from a holding potential of -60 mV
838 (Miles, 1986), and due to very high levels of spontaneous synaptic currents. However,
839 estimations from τ_m and C_m indicate that these resistances were high ($> 600 \text{ M}\Omega$), as also
840 reported previously (Kline et al., 2002). Action potential discharge was quantified by
841 measuring action potential amplitude from the inflection point to the peak and by measuring
842 the mean frequency of discharge in suprathreshold current injections lasting 2 s and
843 quantified as a function of current amplitude. All neurons showed tonic action potential
844 discharge with minor adaptation. EPSCs were quantified in terms of latency to test for the
845 presence of putative mono- or polysynaptic responses (Doyle & Andresen, 2001). The latency
846 was characterized in terms of its jitter that was calculated as the standard deviation of six
847 sequentially evoked responses. In most cases, EPSCs were composed of multipeak events,
848 accordingly only the amplitude of the first peak response was measured. DNQX was applied
849 after a stable baseline of 12 consecutive evoked EPSPs at inter-stimulus intervals of 5 s. The
850 possible presence of inhibitory synaptic currents was not tested. The *in vitro* data were
851 manually analyzed using Clampfit v10.2 cursor measurements and monoexponential fitting
852 procedures.

853

854 **Histology**

855 **Immunohistochemical staining of extracted ganglia**

856 The access to the JNG was done following the surgical description explained above. The JNG
857 was extracted by cutting the vagus nerve above and below it with fine forceps, placed in PFA
858 (4 %) for 60 – 90 min, and then washed in buffer PB (0.1 M) before incubation in sucrose (30
859 % in PB) overnight. The JNG was put in Tissue-Tek® and frozen at -80 °C to be cut on a cryostat
860 at a thickness of 12 μm . Immunofluorescence was done on the JNG sections using the first
861 antibody anti-VGLUT2 raised in mouse (Merck Millipore, MAB5504) and the second antibody
862 Cy3 goat anti-mouse (Jackson, 115-165-003).

863

864 **Immunohistochemical staining and fluorescent microscopy of vagal sensory fibers and**
865 **brainstem neurons**

866 Recovery of cellular morphology of patch-clamped neurons. The PFA-fixed 300 µm-thick brain
867 sections were first washed in PBS for 30 min, then washed in PBS-containing Triton 1% for 30
868 min. After being incubated in blocking solution (PBS-containing Triton 1 % and normal goat
869 serum 2 %) for 30 min, slices were incubated for 5 days with the primary antibody (rabbit anti-
870 eYFP, 1:3200, Lucerna Chem, STJ97104) at 4 °C. The sections were washed in PBS and
871 incubated in the secondary antibody (goat anti-rabbit ALEXA 488, 1:500, Jackson
872 ImmunoResearch, 111-545-003) and in Streptavidin-coupled ALEXA594 (1:8000, Lucerna
873 Chem, STJ16100613) diluted in PBS-containing Triton 0.3 % and normal goat serum 2 %, for 1
874 day at 4°C. Before mounting, the sections were washed in PBS for 45 min.

875 cFos staining after chemogenetic stimulation of vagal sensory afferents: At the end of the
876 experiments, the animals were i.p. injected with NaCl or CNO 1.5 mg/kg around ZT0 and
877 placed in a quiet space for 60 – 90 min. After perfusion of extracted brain with 4% PFA for 1
878 day, brains were cryoprotected by transferring them to a 30% sucrose-containing PB before
879 being cut in a cryotome at 50-µm thickness. Sections were first washed in PBS during 30 min
880 and then in PBS-containing Triton 0.3 % for 30 min to finally being incubated in a blocking
881 solution of PBS-containing Triton 0.3 % and normal goat serum 2 % for 1h. After overnight
882 incubation in the primary antibody (rabbit anti-cFos, 1:1000, BioConcept, 2250S) at 4 °C, the
883 sections were washed in PBS-containing Triton 0.3 % for 30 min and then incubated in the
884 secondary antibody (goat anti-rabbit ALEXA 488, 1:300, Jackson ImmunoResearch, 111-545-
885 003) for 90 min. Then, they were washed in PBS for 20 min, incubated in PBS-containing
886 Hoechst 1 % for 10 min for DAPI staining of neurons, then washed again for 10 min and
887 mounted. A confocal microscope (Leica Stellaris 8) equipped with a 63x oil objective (HC PL
888 APO 63x/1.40 oil CS2) was used to acquire the images through red, green, and blue emission
889 channels. Detection and counting of the fraction of cFos-expressing neurons over DAPI
890 detected neurons was done using a machine learning-based approach in QuPath (version
891 0.5.1). The random forest classifier was trained on images from NaCl injection and CNO 1.5
892 mg/kg injection.

893

894 **Thermistor calibration**

895 Thermistors were connected to a constant current source of 100 μ A and immersed into a
896 water bath held at either 25 $^{\circ}$ C or 37 $^{\circ}$ C. Once the thermistor was inserted in the water and
897 the temperature was stable, the heating of the water bath was turned off to avoid vibrations
898 and voltage measures were then taken immediately for 20 s. Current sources were tested
899 before for stability over a time period of 12 h. Voltages across the thermistor were measured
900 for the two different temperatures and the corresponding resistances calculated using Ohm's
901 law. For every thermistor, a material constant was calculated according to the equation with
902 temperature values T in $^{\circ}$ Kelvin ($^{\circ}$ C + 273.15), following the procedure by (Hoekstra et al.,
903 2019):

$$904 \quad \beta = \frac{T_{25} * T_{37}}{T_{25} - T_{37}} * \ln \frac{R_{37^{\circ}C}}{R_{25^{\circ}C}}$$

905

906 The cortical temperature (t) in $^{\circ}$ C could then be calculated according to the equation:

$$907 \quad t(^{\circ}C) = \left[\frac{1}{\beta} * \log \left[\frac{R_t}{R_{25^{\circ}C}} \right] + \frac{1}{T_{25^{\circ}C}} \right]^{-1} - 273.15$$

908

909 **EEG/EMG Surgeries combined with thermistor implantation**

910 Surgeries for EEG/EMG recordings.

911 The surgeries for implantation of EEG/EMG electrodes were done at least 2 weeks after the
912 viral injection in the L-JNG. After pre-treatment with Carprofen (5 mg/kg s.c.) and induction
913 of isoflurane anesthesia (5 % in oxygen), animal were fixed on a stereotaxic apparatus (Kopf).
914 Anesthesia was maintained at 1.5 – 2 % of isoflurane in a mixture of O₂ and N₂O. An incision
915 was made to expose the skull and the bone was scratched with a scalpel blade for a good
916 adhesion of the head implant. After small craniotomies (0.3 – 0.5 mm) over the left frontal
917 and parietal regions, two gold-coated copper-wire electrodes were placed on top of the *dura*
918 *mater* that serves as EEG electrodes. A silver wire (Harvard Apparatus) was inserted into the
919 occipital bone over the cerebellum for neutral reference (without touching the *dura mater*)
920 and for EMG recordings two gold wires were inserted into muscles of the neck. All electrodes
921 were glued (Loctite Schnellkleber 401) and soldered to a multisite connector (Barrettes
922 Connectors 1.27 mm, male connectors, Conrad).

923

924 Surgeries for cortical temperature recordings.

925 We combined EEG/EMG surgery with implantation of miniature thermistors of two different
926 types. A first series was done using Digikey thermistors (P25BA102J, 1 k Ω , sensor bead in glass
927 probe). These were no longer available for a second series of recordings for which then
928 Digikey thermistors (SC30F103W, 10 k Ω , epoxy sensor in polyimide sleeve) were purchased.
929 Data from the second recording series are presented with absolute temperatures, while the
930 first series used relative values and z-scores due to variable absolute temperatures.
931 Thermistors were placed on the cortical surface via a craniotomy drilled at coordinates
932 (relative to Bregma in mm): AP -2.5, L -2.5 on the left hemisphere. To minimally damage the
933 tissue, the thermistor was inserted by maximally 1 mm, leaving 5 mm outside. The thermistor
934 was then glued to the skull and embedded in dental cement together with the EEG and EMG
935 electrodes, letting the two wires protrude for later direct connection to the current generator.

936

937 **Timeline of the combined chemogenetics and sleep recordings experiment**

938 Once ready for recording, mice were first recorded for 48 h baseline recordings without any
939 injections. After habituation, mice were then injected in groups of 4 by either NaCl, CNO (1.5
940 mg/kg) or CNO (2.5 mg/kg) in alternating recording sessions, with the experimenter blinded
941 to the injection solution. Every recording started at ZT0 with injections taking place within the
942 first 45 min. The mice were then left undisturbed in their home cage and recorded for at least
943 5 up to 47 h depending on the experimental series. Per CNO dose, at least 1 – 3 recordings
944 were done per mouse, NaCl injections were carried out 2 – 4 times interspersed between the
945 CNO conditions. All animals were euthanized at the end of the experiment and brains
946 perfused for histological examination of fiber expression.

947

948 **EEG/EMG and cortical temperature recordings**

949 After a recovery period of 1 week, animals were habituated to the cabling and to the i.p.
950 injections for 5 – 7 days, followed by 48 h-baseline recordings. All the signals (EEG frontal and
951 parietal, left and right EMG, S1 LFP) were acquired at 1 kHz using an Intan digital RHD2132
952 amplifier board and a RHD2000 USB Interface board connected with SPI cables (all Intan
953 Technologies) via a custom-made support system (Homemade adapters containing an
954 Omnetics A79022-001 connector linked to a female Conrad Barrettes Connector). The data
955 were acquired with MATLAB (RHD2000 MATLAB toolbox and a customized software). When
956 we combined sleep recordings with cortical temperature measures, animals were connected

957 to the same current source used before for thermistor calibration and 100 μ A-currents were
958 injected from the onset of the recordings, while recording the voltage signal at 1 kHz through
959 an analog digital input of the Intan RHD2132 amplifier board.

960

961 **Rectal body temperature measure**

962 We measure body temperature during combined sleep and cortical temperature recordings
963 using a fine rectal probe (Physitemp RET-3 rectal probe for mice). Animals were previously
964 habituated to the procedure for at least 5 days. To measure body temperature, the animal
965 body was gently lifted by its tail and placed on its 4 paws. The tail was bent above the body
966 to make the rectum accessible. The probe was previously covered with Vaseline© and gently
967 inserted into the rectum to a fixed depth (typically, up to 2 cm). Stable temperature
968 recordings were obtained within \sim 10 s after insertion. The probe was disinfected after every
969 use. During recordings, rectal temperature was measured at two time points, 45 min and 2 h
970 after the i.p. injection of either NaCl or CNO.

971

972 **External body warming procedure**

973 To prevent the hypothermia induced by vagal sensory stimulation, we used heating pads
974 placed inside and below the cage that we turned on at the time of the i.p. injection for 1 h.
975 The heating pad was previously tested such that it prevented the decline in rectal
976 temperature by \sim 75 % (without heating pad the body temperature drop was -3.6 °C whereas
977 it was -0.9 °C with the heating pad, $n = 2$). For this effect, the heating pads had to be heated
978 to $37 - 39$ °C.

979

980 ***In vivo* data analysis**

981 Scoring of vigilance states.

982 Sleep scoring was done according to established procedures in the lab (Cardis et al., 2021;
983 Lecci et al., 2017; Osorio-Forero et al., 2021) in a manner blinded to the treatment, using a
984 custom-made software developed in MATLAB (MathWorks) available on GitHub
985 (<https://github.com/luthilab/IntanLuthiLab>). The three major vigilance states were scored in
986 4-s epochs according to the following criteria. Wakefulness was identified based on combined
987 high EMG activity and a low voltage differential EEG activity exhibiting fast oscillatory
988 patterns. NREMS was defined based on the appearance of high-amplitude, low-frequency

989 components in the slow oscillation (SO, 0.75- 1.5 Hz), δ (1.5 – 4 Hz) or σ (10 – 15 Hz) range.
990 REMS was recognized based on muscle atonia in combination with the appearance of theta
991 frequency (6 – 8 Hz) in the EEG. Microarousals were scored as maximally 3 consecutive wake
992 episodes preceded and followed by NREMS. The onset of REMS was set as the first epoch with
993 a clearly distinguishable θ peak and the absence of low-frequency activity in the EEG. In case
994 of unipolar recordings, REMS was scored only once low frequencies in the frontal EEG
995 disappeared even when the parietal EEG already showed θ activity. This intermediate sleep-
996 like state was considered as part of NREMS. During CNO injections, NREMS was scored
997 because of a clearly elevated low-frequency component in the EEG together with a visually
998 notable absence of sleep spindle activity and a low-amplitude EMG.

999

1000 Sleep architecture and spectral analysis.

1001 Based on the visual inspection of the raw traces, we defined a state of NREMS* for
1002 experiments involving injection of CNO. NREMS* was scored based on criteria for NREMS,
1003 notably the appearance of low-frequency activity and the reduction of muscle tone. NREMS*
1004 was also defined to contain the epochs of gradual recovery to NREMS. No threshold was set
1005 to define the full return of physiological NREMS.

1006 Architectural analyses. We determined NREMS or NREMS* onset latency by calculating the
1007 time from the i.p. injection point to the first NREMS or NREMS* epoch (**Figure 3a**). Whenever
1008 we compared NaCl or CNO conditions, we refer to NREMS^(*) in the legends. We calculated
1009 REMS onset latency as the time difference between the first NREMS or NREMS* epoch and
1010 the first sequence of 3 consecutive epochs of REMS (= 12 s) (**Figure 4e**). To compare the
1011 amounts of time spent in the different vigilance states per condition, we calculated the
1012 number of epochs per vigilance states as percentage of time within the first 5 h after i.p.
1013 injection of NaCl or CNO (**Figure 3b**). Microarousals, defined as maximally 12 s of wakefulness
1014 during NREMS or NREMS*, were quantified as events per h of NREMS or NREMS*. The density
1015 of microarousals was calculated taking equal time of NREMS for NaCl or of NREMS* for CNO
1016 conditions (bin = 30 min) during which microarousals were detected (**Figure 3c1**). The same
1017 binning was done for the calculation of lengths of NREMS or NREMS* bouts (**Figure 3c2**). To
1018 assess the full dynamics of times spent in NREMS* and REMS during the chemogenetic
1019 stimulation and in the recovery period, we calculated accumulated times spent in either state
1020 for 48 h after i.p. injection. The calculation of accumulated times was done in reference to the

1021 previous 48h-baseline recordings (without any injection) in bins of 60 min. Subsequent bins
1022 gather the accumulated difference from baseline: $\text{Accumulated_state_NaCl/CNO (h)} =$
1023 $\text{state_NaCl/CNO (h)} - \text{state_baseline (h)} + \text{Accumulated_state_NaCl/CNO (h-1)}$ (McCarthy et
1024 al., 2016). In this plot, data lying on negative slopes indicate a loss of sleep time compared to
1025 the baseline, whereas data lying on positive slopes indicate a recovery of sleep times (**Figure**
1026 **4a,f**). For statistical analyses, we calculated means across light and dark phases (**Suppl. Figure**
1027 **3a,e**).

1028 Spectral analysis. Power spectral analysis of vigilance states was done to identify spectral
1029 changes induced by NaCl or CNO exposure according to procedures established in the lab
1030 (Fernandez et al., 2018; Lecci et al., 2017). Power spectra were normalized by the summed
1031 power values from 0.75 to 35 Hz. We took the first consolidated REMS episode as the
1032 timepoint until which we calculated the power spectra starting from the i.p. injection. For
1033 comparison, a power spectrum after NaCl injection was calculated for every mouse for similar
1034 times spent in NREMS, and this separately for both the low and high doses of CNO (**Figure 2d,**
1035 **right panels**). For display, time-frequency plots and dynamics of the characteristic spectral
1036 power bands were calculated using wavelet transform as described (Osorio-Forero et al.,
1037 2021). Mean power levels in power bands characteristic for NREMS were calculated by
1038 summing power values within the frequency ranges corresponding to that band (**Figure 2e**).
1039 The dynamics of spectral bands of NREMS (δ and σ) were calculated for equal numbers of
1040 time-bins of NREMS or NREMS* for the NaCl and CNO conditions. The number of bins was
1041 chosen based on the length of the recordings and is given in the legends. We then normalized
1042 power in the δ - and the σ -bands with respect to the corresponding NaCl power bands for the
1043 last two time bins of the recording (**Figure 2f1,f2, 4b, 6e**). For all these parameters,
1044 calculations were done for every recording session first and then means calculated per
1045 condition and finally across animals. For statistical analysis of dynamic variations in spectral
1046 power we calculated means for the first and the last two time-bins (**Suppl. Figure 1c1,c2,**
1047 **5a1,a2**) or across light and dark phases (**Suppl. Figure 3b1,b2**).

1048 Heart rate analysis.

1049 Heart rate (HR) was calculated from the R-R intervals detected in the EMG in a subgroup of
1050 animals (Lecci et al., 2017) in bins of 60 min. First 2 hours were not taken for HR during REMS
1051 because not all animals have REMS happening at hour 1 and 2 after i.p. injection (**Figure**

1052 **4d1,d2**). For statistical analyses, we calculated means across light and dark phases (**Suppl.**
1053 **Figure 3c1,c2**).

1054 Cortical temperature analysis

1055 Temperature was extracted from the voltage measure of the thermistor as indicated above.
1056 We calculated all points histograms of temperature values for wake, NREMS and REMS in
1057 baseline condition to ensure ourselves that the thermistor properly captured the dynamic
1058 variation in spontaneous sleep-wake behaviors (Hoekstra 2019). As the thermistor only
1059 partially was in contact with the brain tissue, absolute temperature varied between 28 – 29.5
1060 °C in 24h-baseline recordings and was thus lower compared to values found in the literature
1061 that are between 34 – 37 °C (Hoekstra et al., 2019). Therefore, only relative temperature
1062 changes relative to baseline values just before NaCl or CNO injection were analyzed. We
1063 measure the drop of cortical temperature from the i.p. injection point to the first consolidated
1064 REMS period (**Figure 5e,f1**). The recovery temperature is measured as the difference between
1065 the temperature at i.p. injection point and temperature at the time of the first consolidated
1066 REMS episode (**Figure 5f2**).

1067 Statistical analysis.

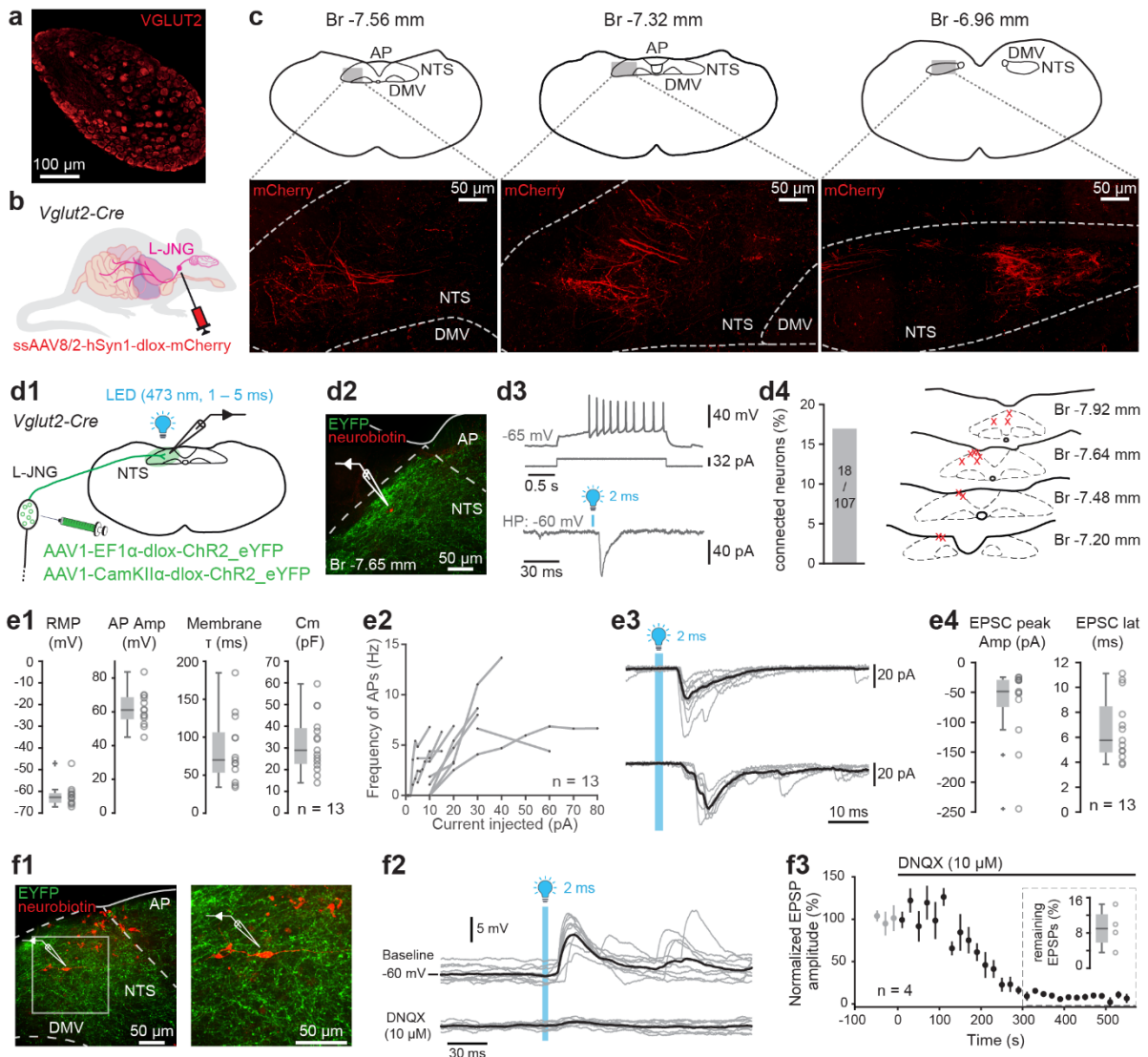
1068 The statistical tests were done using MATLAB (Mathworks). The normality of the datasets was
1069 tested using the Shapiro-Wilk test, as well as the variance using the Bartlett test. For the
1070 comparison of two datasets, we used a paired Student's t test for parametric datasets, or we
1071 used the corresponding Wilcoxon signed rank test for non-parametric datasets. For the
1072 comparisons of three datasets (e.g. in the case of analysis with the three conditions NaCl, CNO
1073 1.5 mg/kg and CNO 2.5 mg/kg), we performed a one-way repeated-measures ANOVA for
1074 parametric datasets followed by post hoc Student's t-tests in case of significance, or a one-
1075 way repeated measures Friedman tests for non-parametric datasets followed by post hoc
1076 Wilcoxon signed-rank tests in case of significance. For the correlation analysis we used a linear
1077 regression model (fitlm in Matlab).

1078

1079

1080

1081



1083

1084 **Figure 1. Anatomical and functional verification of vagal sensory afferent transduction**

1085 a. Fluorescence microscopy image of a L-JNG immunostained for VGLUT2 protein. Labelled cell
 1086 bodies are found throughout the ganglion, with the exception of the area through which the
 1087 motor fibers pass (top left area).

1088 b. Schematic of the experimental approach. Neurons in the left jugular-nodose ganglion (L-
 1089 JNG) of *Vglut2-Cre* mice were virally transfected with a mCherry-reporter gene (*ssAAV8/2-*
 1090 *hSyn1-dlox-mCherry*).

1091 c. Fluorescence microscopy images of the vagal-recipient areas in the brainstem, taken from
 1092 animals transfected in the L-JNG with the mCherry reporter gene indicated in a. Images from
 1093 three different anteroposterior levels are shown, with their anatomical location indicated in
 1094 the schematic coronal sections shown on top. NTS, *nucleus tractus solitarius*, AP, *area*
 1095 *postrema*, DMV, dorsal motor nucleus of the vagus.

1096 d1. Schematic of experimental preparation for *in vitro* patch-clamp recordings, carried out in
 1097 acute brain slices from *Vglut2-Cre* animals virally transfected for ChR2 (*AAV1-EF1 α -dlox-*
 1098 *ChR2_eYFP* or *AAV1-CaMKII α -dlox-ChR2_eYFP*). Neurons were patched within the NTS and

1099 synaptic connectivity studied by applying light pulses (parameters indicated in blue text)
1100 through the objective on the slice.

1101 d2. Micrograph of a patched NTS cell soma (red) surrounded by ChR2_EYFP-expressing vagal
1102 sensory fibers (green). The cell was filled with neurobiotin during the recording and recovered
1103 *post hoc*.

1104 d3. Representative action potential firing pattern of a NTS cell in response to a depolarizing
1105 somatic current pulse (top two traces) and example optogenetically evoked synaptic response
1106 in the same cell held in voltage-clamp at -60 mV.

1107 d4. Percentage of synaptically connected NTS neurons shown as bargraph, together with the
1108 localization of the 13 neurons from which recordings were completed. All cell bodies were
1109 located within the NTS at different anteroposterior levels.

1110 e1. Box-and-whisker plot of the intrinsic electrophysiological properties of 13 synaptically
1111 connected NTS neurons, including resting membrane potential (RMP), action potential
1112 amplitude (AP amp), membrane time constant (membrane τ), membrane capacitance (C_m).

1113 e2. Current-frequency response curves of all optogenetically responsive NTS cells. The
1114 discharge frequency corresponds to the mean action potential rate per current response.

1115 e3. Optogenetically evoked excitatory postsynaptic currents from 2 different NTS neurons.
1116 Individual responses are shown in grey, the mean response in black. Recordings from 2
1117 different cells are shown. The top example shows a case of fixed response latency, the bottom
1118 one a case with variable response latency.

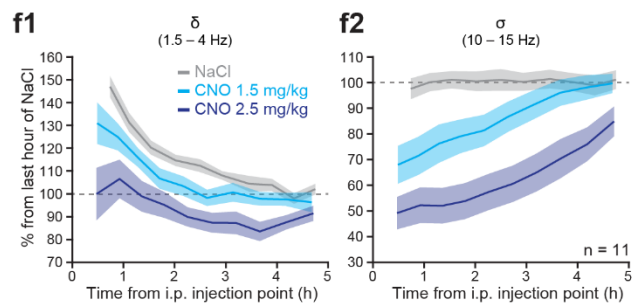
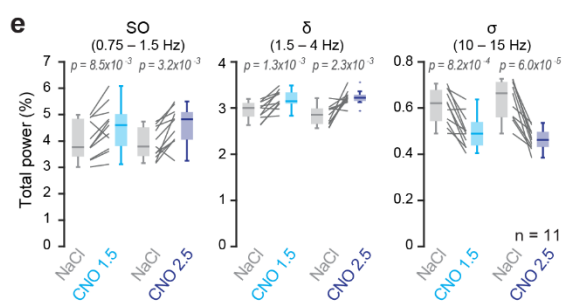
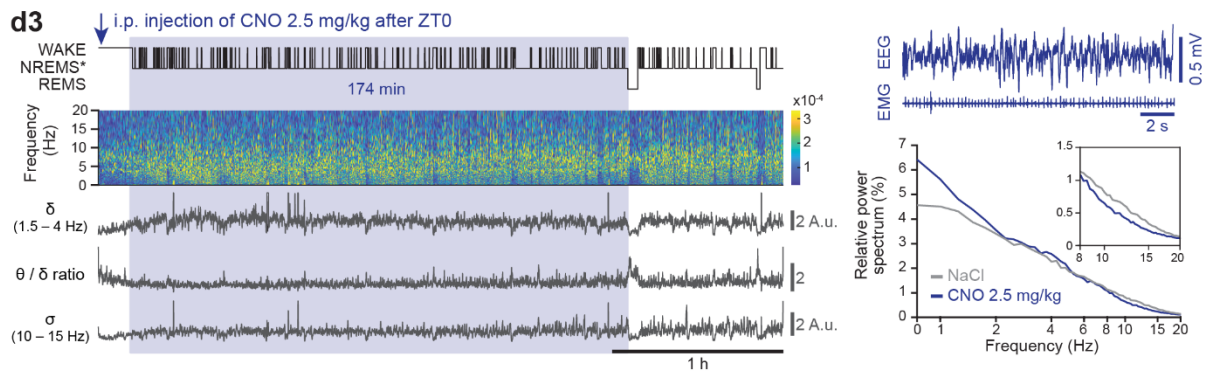
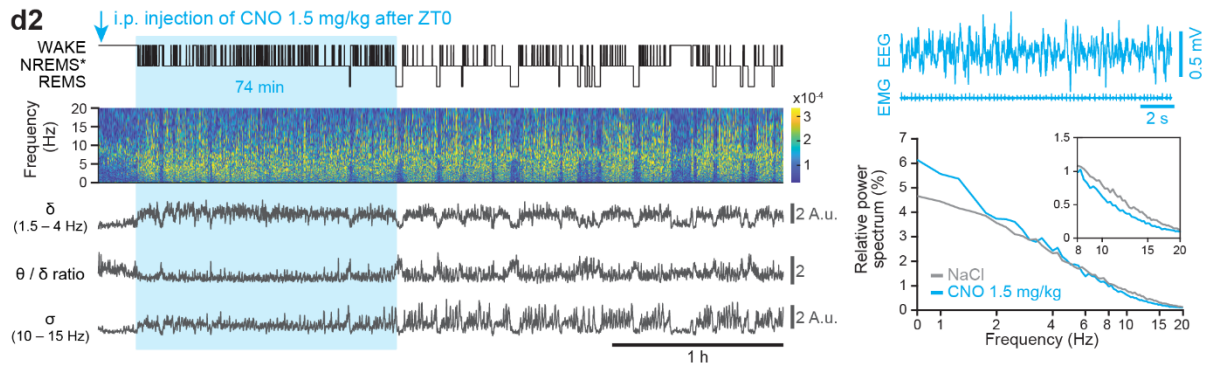
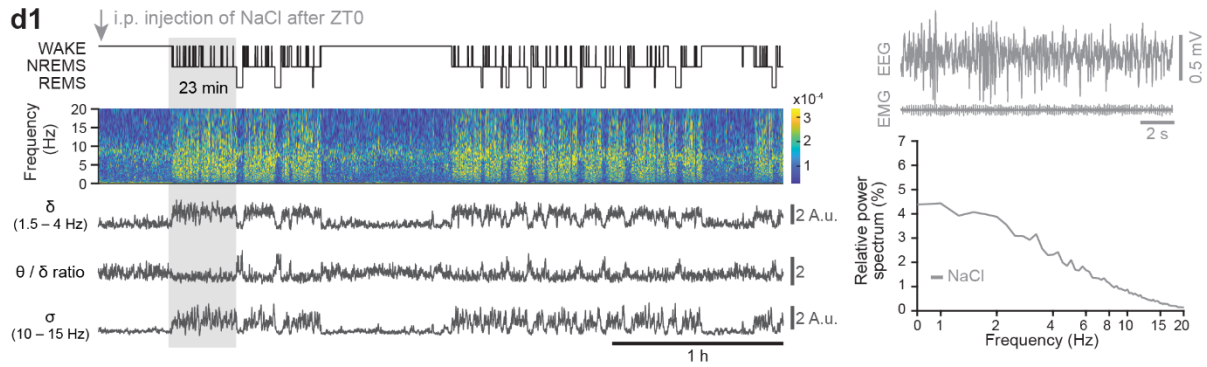
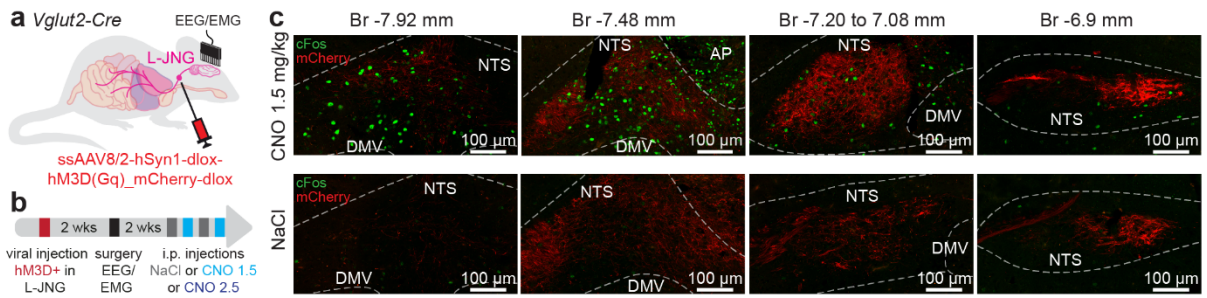
1119 e4. Box-and-whisker plot of EPSC response properties for $n = 13$ synaptically connected NTS
1120 neurons. Left graph shows the peak amplitude, calculated for the first peak in single- and
1121 multicomponent responses. Latencies were calculated from the onset of the light pulse and
1122 are plotted for responses with < 0.5 ms jitter.

1123 f1. Micrographs of a recorded NTS cell shown at two magnifications to illustrate one of the
1124 extended dendritic arbors typically observed. EYFP immunostaining was applied to enhance
1125 the visibility of the fibers.

1126 f2. Representative opto-EPSPs (grey), with mean response shown in black. Top responses are
1127 shown for baseline conditions, bottom responses after bath application of the AMPA-type
1128 glutamatergic receptor antagonist DNQX ($10 \mu\text{M}$).

1129 f3. Time course of DNQX actions on normalized EPSPs for $n = 4$ recordings. Inset shows the
1130 remaining response in the presence of DNQX, calculated as the mean EPSP after 300 s,
1131 expressed in percent of the baseline EPSP.

1132



1133

1134

1135 **Figure 2. Chemogenetic activation of vagal sensory afferents induces a NREMS-like state**

1136 a. Schematic of the viral transfection surgeries. Mice from the Vglut2-Cre line were virally
1137 transfected in the L-JNG to express the excitatory chemogenetic receptor hM3D(Gq), after
1138 which they were implanted for EEG/EMG recordings.

1139 b. Schematic of the experimental design. After viral injection and EEG/EMG surgical
1140 implantations, repeated recording sessions were carried out starting at ZT0, at which animals
1141 were injected i.p. with either NaCl or the chemogenetic ligand CNO at either 1.5 mg/kg or 2.5
1142 mg/kg. There was a 2 weeks-interval between the two surgeries and the start of the recording.
1143 NaCl or CNO injections were carried out repeatedly and interleaved as described in the
1144 Methods.

1145 c. Fluorescent microscopic verification of cFos expression in the NTS and AP in response to
1146 chemogenetic activation of vagal sensory neurons or after saline injections. Animals were
1147 sacrificed at 60 – 90 min after i.p. injections and processed for immunohistochemistry (see
1148 Methods).

1149 d. Example recordings from one mouse, injected with NaCl (d1) or CNO at the two different
1150 doses in repeated recording sessions (d2, d3). For the three recordings, the first 4 h are shown
1151 starting at ZT0, with on top the hypnogram, the time-frequency plot between 0 – 20 Hz, and
1152 the power dynamics of two spectral bands characteristics for NREMS, the δ band (1.5 – 4 Hz)
1153 and the σ band (10 – 15 Hz). Additionally, the θ/δ ratio is shown that characterizes NREMS-
1154 to-REMS transitions. Colored rectangles indicate the data used to quantify the power spectra
1155 shown on the right, together with raw EEG/EMG traces. Power spectra were calculated for
1156 the time until the first consolidated REMS period and for the same times spent in NREMS as
1157 the ones used for the CNO-associated power spectra. Light blue, low dose of CNO (1.5 mg/kg),
1158 dark blue, high dose of CNO (2.5 mg/kg). For comparison, the power spectrum for NaCl
1159 injections is plotted in d2 and d3 for equal times spent in NREMS. In d2, d3, insets zoom-in to
1160 highlight relative power levels for the σ band (10 – 15 Hz).

1161 e. Quantification of relative power in three major spectral bands typical for NREMS, the slow
1162 oscillation (SO) band (0.75 – 1.5 Hz), the δ band (1.5 – 4 Hz), and the σ band (10 – 15 Hz).
1163 Boxplots are presented for NaCl (grey), CNO 1.5 mg/kg (light blue), CNO 2.5 mg/kg (dark blue)
1164 for the three bands, with connecting grey lines showing data from individual animals (n = 11).
1165 Paired two-tailed t-tests were carried out for all paired datasets, with p values indicated.

1166 f. Time course of δ (f1) and σ (f2) power, normalized to the corresponding power levels for
1167 the NaCl condition for the time bins between hours 4 – 5. Note that, compared to NaCl, both
1168 δ and σ power levels were suppressed but recover over a time course of \sim 5 h (see also **Figure**
1169 **4b**). See **Suppl. Figure 1c1,c2** for statistical analysis of the two first and two last time bins.

1170

1171

1172

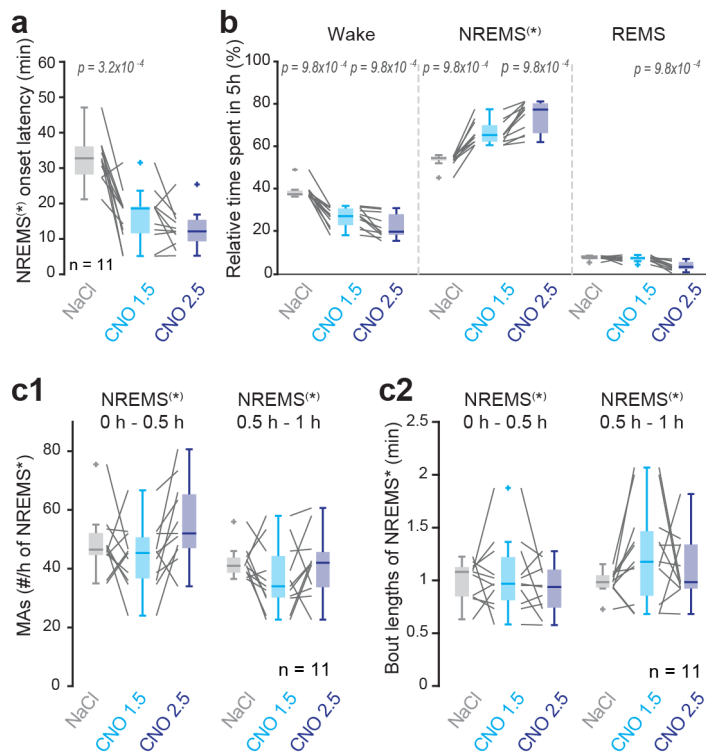
1173

1174

1175

1176

1177



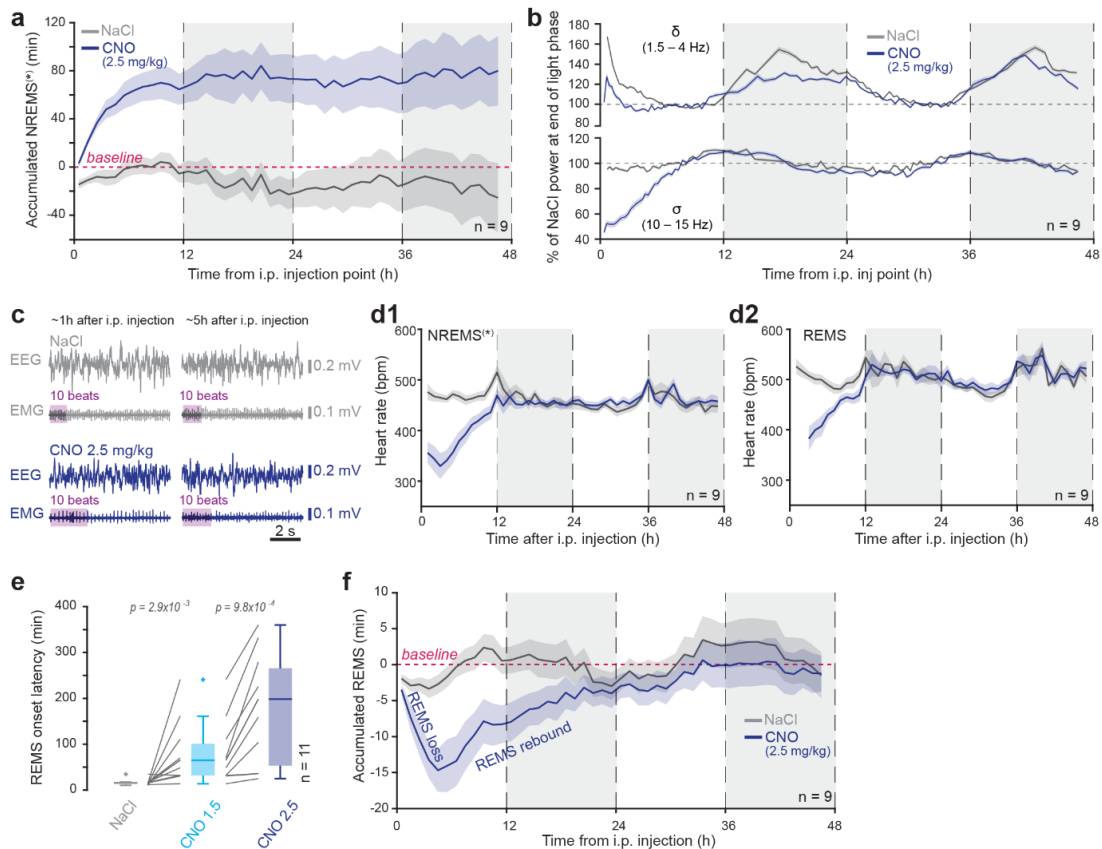
1178 **Figure 3. Chemogenetic activation of vagal sensory afferents alters the architecture of sleep**

1179 a. Box-and-whisker plot of latencies to enter NREMS* (defined as the CNO-induced state and
 1180 its gradual recovery to NREMS) for animals expressing the excitatory chemogenetic receptor
 1181 hM3D(Gq) in the L-JNG. For control animals expressing a non-chemogenetic viral construct,
 1182 see **Suppl Figure 2a**. Boxplots are presented for NaCl (grey), CNO 1.5 mg/kg (light blue), CNO
 1183 2.5 mg/kg (dark blue), with connecting grey lines symbolizing data from individual animals. A
 1184 one-way repeated-measures ANOVA with post hoc t-tests, with p values indicated. Bonferroni
 1185 corrected $p = 0.025$.

1186 b. As a, for times spent in Wake, NREMS* and REMS during 5 h of recordings from the time
 1187 of i.p. injections. One-way repeated-measures Friedman tests with post hoc Wilcoxon signed-
 1188 rank tests. Bonferroni corrected $p = 0.025$.

1189 c. As a, for microarousal (MA) density (c1) and bout lengths (c2). One-way repeated-measures
 1190 Friedman tests with post hoc Wilcoxon signed-rank tests, or one-way repeated-measures
 1191 ANOVA with post hoc t-tests. Bonferroni corrected $p = 0.025$.

1192



1193

1194 **Figure 4. Chemogenetic activation of vagal sensory afferents preserves homeostatic**
 1195 **regulation of NREMS and REMS**

1196 a. Cumulative times spent in NREMS* compared to baseline NREMS (without any injection)
 1197 over 48 h. An increase in values indicates a greater time spent in NREMS*. Data were obtained
 1198 for CNO injections at 2.5 mg/kg to induce stronger responses that help emphasize the
 1199 recovery process. See **Suppl. Figure 3a** for statistical analysis over 12-h periods.

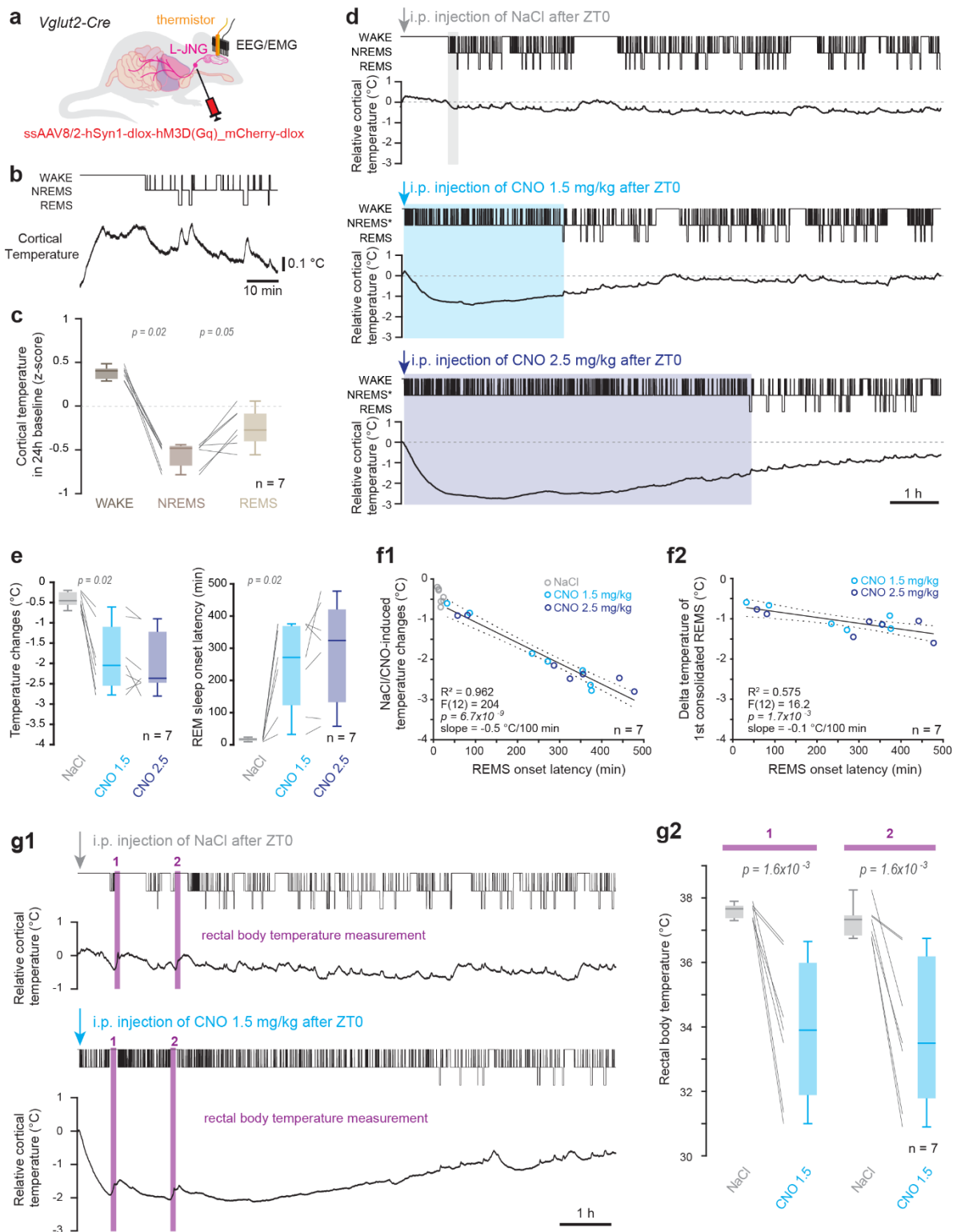
1200 b. Dynamics of δ and σ power over the same period as a, calculated for 30-min bins of times
 1201 spent in NREMS* and graphed in percentage of power values for NaCl injections for the time
 1202 bins between hours 11 – 12 (end of the light phase). Note the decrease in power in the first
 1203 dark phase that recovers in the second 24 h-cycle. See **Suppl. Figure 3b1,b2** for statistical
 1204 analysis over 12-h periods.

1205 c. Representative recordings of EEG/EMG with the heart beats visible in the EMG traces, for
 1206 2 time points after i.p. injections. Colored rectangles highlight 10 heart beats.

1207 d1, d2. Time course of heart rate changes for NREMS* (d1) and REMS (d2). Note the full
 1208 recovery of heart rate at the end of the first light phase. See **Suppl. Figure 3c1,c2** for statistical
 1209 analysis over 12-h periods.

1210 e. Box-and-whisker plots for REMS onset latencies, calculated from the onset of NREMS for
 1211 NaCl injections, and of NREMS* for CNO injections. One-way repeated-measures Friedman
 1212 tests with post hoc Wilcoxon signed-rank tests. Bonferroni corrected $p = 0.025$.

1213 f. Cumulative differences in times spent in REMS compared to a baseline (without any
 1214 injection) EEG/EMG recording. This analysis is plotted for the data obtained with NaCl and 2.5
 1215 mg/kg CNO-injections to emphasize the REMS recovery process. A small loss of REMS at the
 1216 beginning of the resting phase for NaCl was due to the arousing effect of the injection. See
 1217 **Suppl. Figure 3e** for statistical analysis over 12-h periods.



1219

1220 **Figure 5. Vagal sensory nerve stimulation produces a transient brain-body cooling.**1221 a. Schematic of the surgeries for combined vagal sensory stimulation, EEG/EMG recordings
1222 plus cortical temperature measures in *Vglut2-Cre* animals.

1223 b. Representative recording of cortical temperature during spontaneous sleep-wake

1224 transitions.

1225 c. Quantification of temperature measures in freely sleeping mice in baseline (no i.p.
1226 injections), showing box-and-whisker plots for mean values (One-way repeated-measures
1227 Friedman tests with post hoc Wilcoxon signed-rank tests. Bonferroni corrected $p = 0.025$).

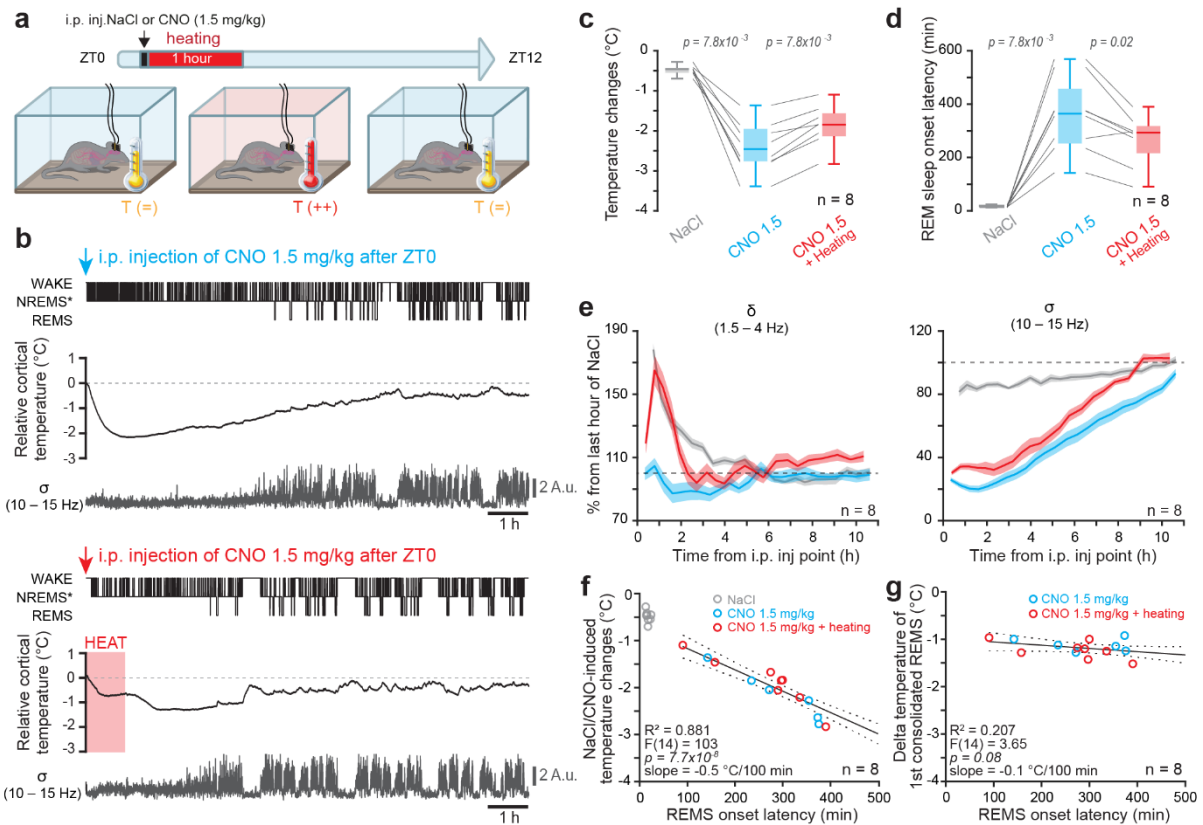
1228 d. Representative recordings from one mouse injected with either NaCl or CNO at 1.5 mg/kg
1229 or at 2.5 mg/kg. Hypnogram on top, relative cortical temperature below for the three
1230 conditions. Colored rectangles show time to onset of the first consolidated REMS period.
1231 Insets to the right zoom-in on the onset of the first NREMS* period.

1232 e. Box-and-whisker plots of temperature drops (left), measured as the difference between
1233 the minimum temperature with respect to NREMS* onset until the first consolidated REMS
1234 period; and the REMS onset latencies (right), measured as in **Figure 4e**. One-way repeated-
1235 measures Friedman tests with post hoc Wilcoxon signed-rank tests. Bonferroni corrected $p =$
1236 0.025 .

1237 f. Linear regression between REMS onset latency and temperature drops (f1), showing a
1238 strong negative correlation (slope $-0.5\text{ }^{\circ}\text{C}/100\text{ min}$; $R^2 = 0.962$). Linear regression between
1239 REMS onset latency and temperature at which REMS re-appears (f2), showing a weak
1240 negative correlation (slope $-0.1\text{ }^{\circ}\text{C}/100\text{ min}$; $R^2 = 0.575$).

1241 g. Representative recordings as in d, combined with rectal temperature measures at time
1242 points indicated by vertical-colored bars (g1). Every rectal measure produced a transient
1243 increase in cortical temperature that recovered before the CNO-induced temperature drop
1244 dissipated. Box-and-whisker plots for corresponding mean values (g2). One-way repeated-
1245 measures Friedman tests with post hoc Wilcoxon signed-rank tests.

1246
1247
1248
1249
1250



1251

1252 **Figure 6. Prevention of vagal sensory stimulation-induced hypothermia by ambient**
 1253 **warming restores REMS.**

1254 a. Schematic of experimental set-up to provide ambient heating to the animals while
 1255 stimulating vagal sensory afferents together with EEG/EMG and cortical temperature
 1256 recordings.

1257 b. Representative recordings from one mouse injected with CNO (1.5 mg/kg) in the absence
 1258 (top) or presence (bottom) of external warming (red shaded rectangle). From top to bottom,
 1259 hypnogram, cortical temperature and the dynamics of σ (10 – 15 Hz) power are shown.

1260 c. Box-and-whisker plot of temperature drops recorded during NaCl or CNO (1.5 mg/kg)
 1261 injections alone, and with CNO injections combined with ambient warming. One-way
 1262 repeated-measures Friedman tests with post hoc Wilcoxon signed-rank tests.

1263 d. Box-and-whisker plots for REMS onset latencies for the three conditions specified in panel
 1264 c, measured as in **Figure 4e**. One-way repeated-measures Friedman tests with post hoc
 1265 Wilcoxon signed-rank tests.

1266 e. Spectral dynamics during the three conditions, calculated as in **Figure 2f1,f2**. See **Suppl.**
 1267 **Figure 5a1,a2** for statistical analysis of the 2 first bins and 2 last bins.

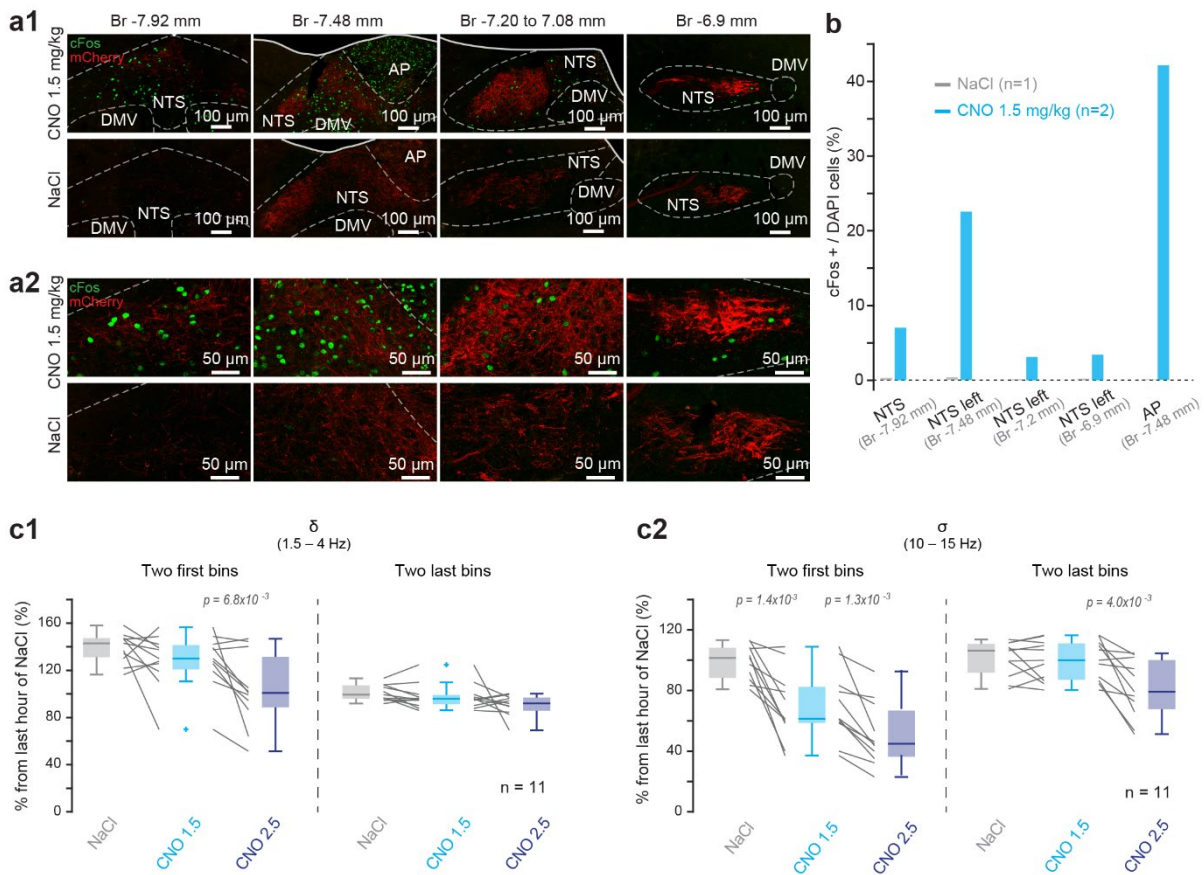
1268 f. Linear regression between REMS onset latency and temperature drop for data obtained
 1269 from NaCl, CNO (1.5 mg/kg), and CNO (1.5 mg/kg) combined with ambient warming (slope -
 1270 0.5 °C/ 100 min; $R^2 = 0.881$).

1271 g. Same as f for the relation between REMS onset latency and the temperature at which REMS
 1272 reappears (slope -0.1 °C/ 100 min; $R^2 = 0.207$).

1273

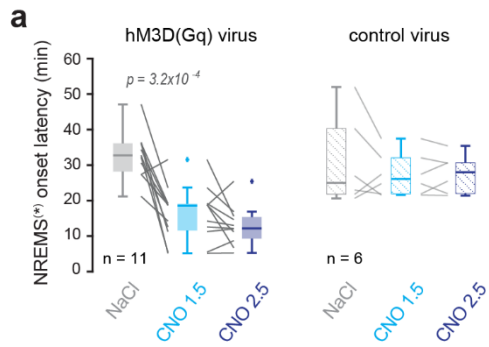
1274

1275 **Supplementary Figures and Legends**



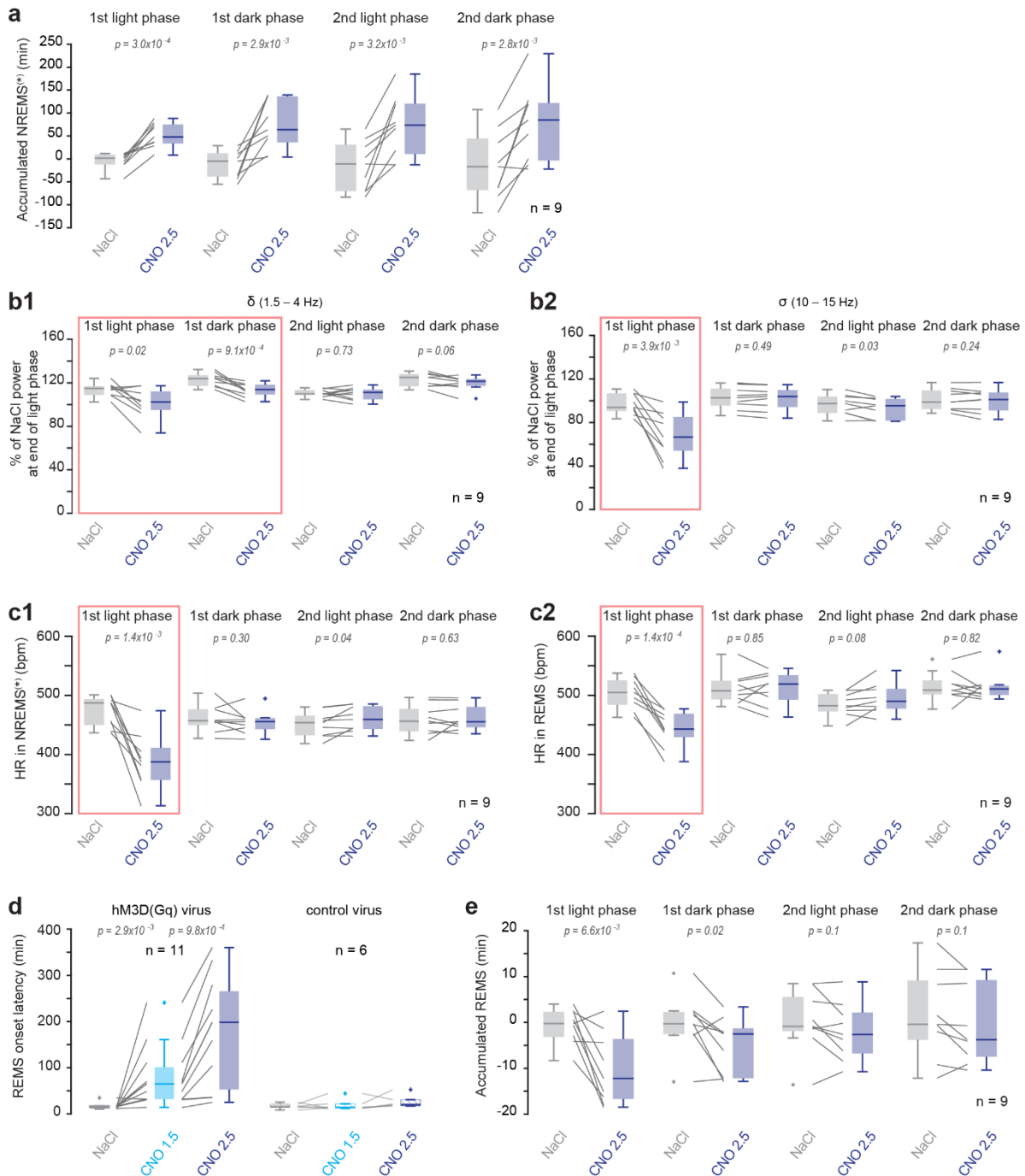
1276
 1277 **Supplementary Figure 1. Quantification of cFos expression in vagal-recipient areas of the**
 1278 **dorsal vagal complex and of absolute power dynamics in response to vagal sensory**
 1279 **stimulation.**

1280 a1, a2. Zoom-out (a1) and Zoom-in (a2) of fluorescent micrographs shown in **Figure 2c** for
 1281 CNO (1.5 mg/kg) and NaCl injections.
 1282 b. Quantification of % cFos expressing-somata relative to nuclear staining using DAPI (see
 1283 Methods) for both NaCl and CNO injections, carried out for four anteroposterior Bregma
 1284 levels for NTS and for one level for AP.
 1285 c1, c2. Quantification and statistical analysis for data presented in **Figures 2f1,f2**, with mean
 1286 absolute power levels shown for the first two and the last two time bins for δ (c1) and σ (c2)
 1287 power. One-way repeated-measures Friedman tests with post hoc Wilcoxon signed-rank
 1288 tests, or one-way repeated-measures ANOVA with post hoc t-tests.
 1289



1290 **Supplementary Figure 2. Quantification of NREMS* dynamics and associated controls.**

1291 a. Box-and-whisker plots of NREMS* onset latency for hM3D(Gq)-expressing and control
 1292 virus-expressing animals (AAV1-CamKIIa.hChr2(H134R)-eYFP.WPRE.hGH, AAV8-hSyn-FLEX-
 1293 Jaws-KGC-GFP-ER2, ssAAV8/2-hSyn1-dlox-mCherry(rev)-dlox-WPRE-hGHP(A)). One-way
 1294 repeated-measures Friedman tests with post hoc Wilcoxon signed-rank tests, or one-way
 1295 repeated-measures ANOVA with post hoc t-tests.



1296

1297

Supplementary Figure 3. Quantification of dynamics of the recovery process across spectral parameters and heart rate, and of REMS onset latencies.

1298

1299 a. Box-and-whisker plots of accumulated NREMS* across the light and dark phases shown in
 1300 **Figure 4a** for NaCl and CNO (2.5 mg/kg) injections. Student paired t-tests.

1301 b1, b2. Box-and-whisker plots of mean relative δ (b1) and σ (b2) power values across the light
 1302 and dark phases shown in **Figure 4b** for NaCl and CNO (2.5 mg/kg) injections. Wilcoxon signed-
 1303 rank tests or Student paired t-tests. Red rectangles highlight the data that survive statistical
 1304 testing with Bonferroni correction for multiple comparison ($p = 0.0125$).
 1305

c1, c2. Box-and-whisker plots of mean heart rates across the light and dark phases shown in

1306 **Figure 4d1,d2** for NaCl and CNO (2.5 mg/kg) injections for NREMS* (c1) and REMS (c2).
1307 Wilcoxon signed-rank tests or paired t-tests.

1308 d. Box-and-whisker plots of REMS onset latencies for hM3D(Gq)-expressing and control virus-
1309 expressing animals. One-way repeated-measures Friedman tests with post hoc Wilcoxon
1310 signed-rank tests, or one-way repeated-measures ANOVA with post hoc t-tests.

1311 e. Box-and-whisker plots of accumulated REMS across the light and dark phases shown in
1312 **Figure 4f** for NaCl and CNO (2.5 mg/kg) injections. Student paired t-tests.

1313

1314

1315

1316

1317

1318

1319

1320

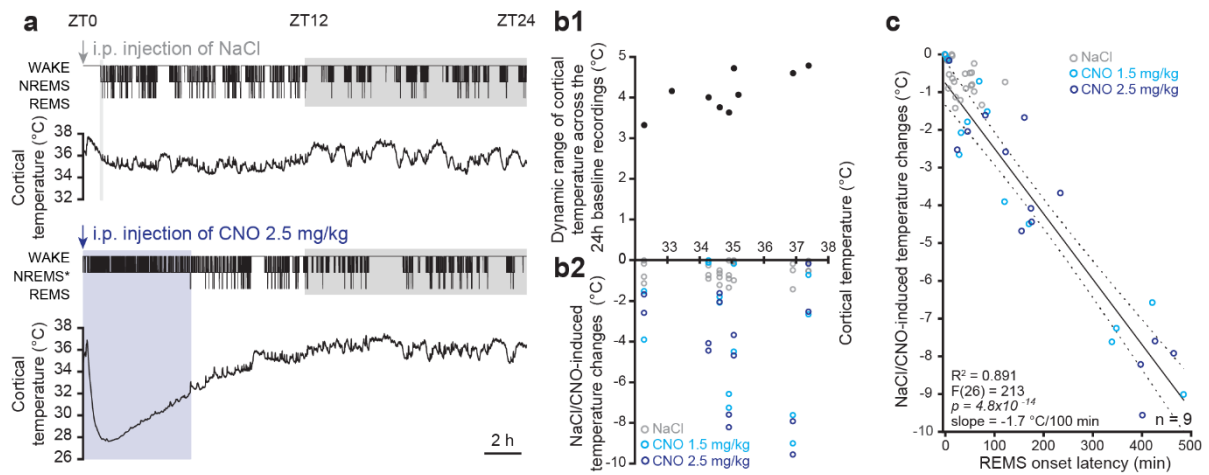
1321

1322

1323

1324

1325



1326

1327 **Supplementary Figure 4.**

1328 a. Representative recordings from one mouse injected with either NaCl or CNO at 2.5 mg/kg
 1329 with thermistor using glass-embedded sensors.

1330 b1,b2. Mean and dynamic range of cortical temperature for all animals (b1). Filled points
 1331 represent single animals. Note that animals have similar dynamic ranges in spite of different
 1332 absolute values due to sensors. NaCl/CNO-induced temperature changes (b2). One datapoint
 1333 per 24-h session measured from ZT0 until REMS onset.

1334 c. Linear regression between REMS onset latency and temperature drops, showing a strong
 1335 negative correlation (slope $-1.7^\circ\text{C}/100\text{ min}$; $R^2 = 0.89$).

1336

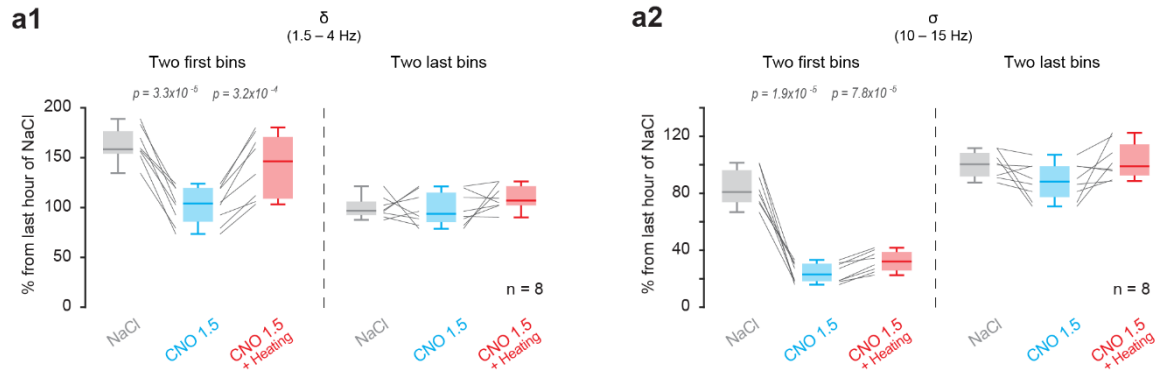
1337

1338

1339

1340

1341



1342

1343 **Supplementary Figure 5. Quantification of dynamics of the recovery process across spectral**
 1344 **parameters.**

1345 a1, a2. Quantification and statistical analysis for data presented in **Figure 6e**, with mean
 1346 absolute power levels shown for the first two and the last two time bins for δ (a1) and σ (a2)
 1347 power. One-way repeated-measures Friedman tests with post hoc Wilcoxon signed-rank
 1348 tests, or one-way repeated-measures ANOVA with post hoc t-tests.

1349

1 **Noradrenergic *locus coeruleus* activity**
2 **functionally partitions NREM sleep to**
3 **gatekeep the NREM-REM sleep cycle**

4 **Alejandro Osorio-Forero^{1,2}, Georgios Foustoukos¹, Romain Cardis¹, Najma Cherrad,**
5 **Christiane Devenoges, Laura M.J. Fernandez and Anita Lüthi**

6 Department of Fundamental Neurosciences, University of Lausanne, Rue du Bugnon 9, CH-1005
7 Lausanne, Switzerland

8 ¹Equal contribution

9 ² Department of Sleep and Cognition, Netherlands Institute for Neuroscience, Meibergdreef 47, 1105
10 BA Amsterdam, The Netherlands

11 **Number of Figures: 7, Words in Abstract: 150, Words in Main Text: 4,580; Number of references:**
12 **53+3 for methods**

13 **Correspondence:** anita.luthi@unil.ch

14 **Author contributions:** AOF, RC, NC, LF and AL originally started this project. GF developed all LC fiber
15 photometry experimentation and corresponding analyses. RC developed the REMS restriction
16 procedure. AOF and GF developed analysis scripts, and all authors contributed to data analysis. LF
17 made the final figure versions and schemes. AL wrote the manuscript, with input from all authors.

18 **Acknowledgements:** The authors acknowledge fruitful discussions with Paul Franken, Stephany Fulda,
19 Caroline Lustenberger, Markus Schmidt, Francesca Siclari, Aurélie Stephan, Mehdi Tafti and Eus van
20 Someren. We thank Dr. Simone Astori and Olivia Zanoletti from the Carmen Sandi lab (EPFL, Lausanne)
21 for carrying out the corticosterone measurements and Aurélie Guillaume-Gentil for assistance with
22 viral injections. We recognize Dr. Sandro Lecci for providing the first datasets relevant for this study.
23 Many thanks to Drs. Feng and Li for generously providing us with the first aliquots of the GRAB_{NE} sensor.
24 The constructive comments of Dr. Julie Buron, Lila Banterle and Paola Milanese on the manuscript are
25 very appreciated. We are grateful to the animal caretakers, especially Michelle Blom and Titouan
26 Tromme, and to Dr. Laure Sériot for expert veterinary advice. This work was supported by the Swiss
27 National Science Foundation (Grant no. 184759 to AL), a FBM UNIL Doctoral Fellowship to AOF, and
28 Etat de Vaud.

29 **Conflict of interest.** The authors declare no conflict of interest.

30 **Abstract**

31 The noradrenergic *locus coeruleus* (LC) is vital for brain states underlying wakefulness, whereas its
32 roles for sleep remain uncertain. Combining mouse sleep-wake monitoring, behavioral
33 manipulations, LC fiber photometry and closed-loop optogenetics, we found that LC neuronal
34 activity partitioned non-rapid-eye-movement sleep (NREMS) into alternating brain and autonomic
35 states that rule the NREMS-REMS cycle in ~50-s intervals. High LC activity induced a subcortical-
36 autonomic arousal state that facilitated cortical microarousals, while low activity was obligatory for
37 NREMS-to-REMS transitions. This functional alternation set the duration of the NREMS-REMS cycle
38 by ruling REMS entries during undisturbed sleep, while limiting these over ~50-s intervals during
39 REMS restriction. A stimulus-enriched, stress-promoting wakefulness increased high LC activity
40 levels at the expense of low ones in subsequent NREMS, fragmenting NREMS through microarousals
41 and delaying REMS onset. We conclude that LC activity fluctuations gatekeep the NREMS-REMS cycle
42 over recurrent infraslow intervals yet also convey sleep's vulnerability to adverse wake experiences.

43
44 **Key words:** ultradian sleep cycle || arousability || sleep homeostasis || REMS restriction ||
45 automated REMS deprivation || microarousal || noradrenaline || norepinephrine || infra-slow ||
46 ultradian || optogenetics || K-complex || sleep disorders

47

48

49

50

51

52

53

54

55

56

57

58

59

60

61

62 Introduction

63 The pontine brainstem *locus coeruleus* (LC) is a wake-promoting brain area that constitutes the
64 principal source of noradrenaline (NA) for forebrain circuits and arousal-modulating nuclei¹⁻⁴. LC
65 neuronal activity levels grade with the level of wakefulness⁴ and with physiological signatures of
66 cortical^{2,3} and autonomic arousal^{3,5}. Elevated LC activity is implicated in the cognitive and autonomic
67 manifestations of states of hyperarousal during stress- and anxiety-provoking experiences^{1,6}.
68 Conversely, clinically important sedatives act on NA signaling⁷. Together, this illustrates LC's broad
69 implication in regulating arousal levels in states of wakefulness.

70 Many noradrenergic LC neurons remain active in sleep⁵ and increase arousability^{8,9}. During non-
71 rapid-eye-movement sleep (NREMS) in mouse, activity levels of LC neuron populations fluctuate on an
72 infraslow time scale of ~50 s (corresponding to ~0.02 Hz), generating varying levels of free NA in the
73 forebrain¹⁰⁻¹². In thalamus, infraslow NA fluctuations depolarize neuronal membrane potentials, which
74 suppresses the capability of thalamic circuits to generate sleep spindles, known as NREMS EEG
75 hallmarks in the 10 – 15 Hz frequency range¹⁰ that shield NREMS from sensory stimuli¹³⁻¹⁵. Spontaneous
76 microarousals (MAs) that are typical for mammalian NREMS coincide preferentially with high LC
77 activity, thus low spindle density^{11,14}. To date, whether LC activity fluctuations have a broader
78 relevance for the dynamics of sleep and its function remains to be determined. For example, for sleep
79 to take its natural progression across NREMS and REMS, it is necessary that global brain states be
80 driven across transitory, less stable periods. In human sleep, signatures of sleep 'instability' and
81 elevated arousability have been described¹⁶, yet a possible implication of arousal mechanisms and the
82 associated brain states are unknown.

83 LC activity in sleep has also been associated with REMS control and is part of theoretical models
84 for the mammalian NREMS-REMS cycle as a REM-off area^{17,18}. Supporting experimental evidence
85 involves optogenetic activation of LC neurons, which increases the time spent in NREMS at the expense
86 of REMS, whereas inhibition can have opposite effects^{8,10-12}. In humans, widely used sedatives that
87 interfere with NA signaling modify REMS⁵. Furthermore, the level of LC activity in wakefulness
88 negatively associates with human REMS quality¹⁹. Therefore, a balanced assessment of LC's role for
89 REMS-regulatory and potential REMS-disruptive actions is desirable and is indeed pressing as its
90 relevance for the processing of emotional experience in human sleep becomes increasingly
91 recognized²⁰.

92 Here, we show that LC rules the time scales over which the NREMS-REMS cycle evolves, setting
93 the moments when transitions between NREMS and REMS are allowed, and when not. This ruling
94 involves the alternation between high and low LC activity levels that associate with distinct arousal

95 signatures at the autonomic, subcortical and cortical arousal levels. This alternation creates a
96 previously unrecognized architectural unit of ~50 s, over which the NREMS-REMS cycle evolves.

97 **Results**

98 **LC activity surges during NREMS coordinate brain and autonomic states to regulate arousability**

99 To monitor the activity of LC neurons during undisturbed sleep, we conditionally expressed the
100 genetically encoded Ca²⁺ sensor jGCaMP8s in dopamine-β-hydroxylase-(DBH)-Cre mice, which drives
101 the expression of viral constructs in NA-synthesizing neurons with a high degree of specificity (~80
102 %^{10,21}, **Extended Data Figure 1a, 5**). We then implanted animals with EEG/EMG electrodes together
103 with an optic fiber stub over the LC for combined sleep and fiber photometric recordings of LC neuronal
104 activity (**Figure 1a,b**). Local field potential (LFP) electrodes were positioned within the primary
105 somatosensory S1 cortex and the hippocampal CA1 area. The EEG signals served to score the major
106 vigilance states Wake, NREMS and REMS and the MAs based on standard polysomnography^{10,14,15,22}.
107 The S1 LFP recordings were used to monitor local power dynamics in frequency bands characteristic
108 for NREMS and the CA1 LFP recordings to define the onset of REMS (see Methods).

109 Across the 12-h light phase (Zeitgeber time (ZT)0- ZT12), the major resting phase of mice, the
110 photometrically recorded Ca²⁺ activity of noradrenergic LC populations ('LC activity') varied
111 characteristically with states of wake, NREMS and REMS (**Figure 1c**)^{11,12}. LC activity was elevated during
112 wakefulness, but it decayed to a lower baseline in NREMS, on top of which a fluctuating pattern
113 appeared. In 10 animals with a dynamic range of relative fluorescence changes ranging within 16.3 –
114 95.3 % (mean 41.6 ± 9.3 %) in the first 2 h of the light phase (ZT0-ZT2) and a histologically confirmed
115 fiber positioning (**Figure 1b**), LC fluctuations were present throughout NREMS bouts but were absent
116 during REMS (**Figure 1c**). Mean LC activity levels in ZT0-ZT2 were progressively lower from wakefulness
117 to NREMS and REMS (**Figure 1d**) (for detailed information about statistical tests and results for all
118 datasets presented in the figures, see **Supplemental Table 1**). However, activity levels in NREMS varied
119 widely and overlapped with wakefulness (by 56.5 ± 11.4 %, calculated up to the mean - 2 standard
120 deviations of wake levels; **Figure 1d, Extended Data Figure 1b**). In mouse NREMS, the collective
121 neuronal activity levels of the noradrenergic LC could thus increase as strongly as in some periods of
122 wakefulness.

123 LC activity elevates arousability from NREMS⁹, but the underlying brain states have not been
124 examined. The LC projects cortically and subcortically, including to autonomic output centers^{1,5},
125 suggesting that LC coordinates brain-bodily arousal levels in NREMS. We first confirmed that
126 fluctuating LC activity in NREMS led to functional output. Dual fiber photometric measures based on
127 jGCaMP8s fluorescence in LC and on NA biosensor (GRAB_{NE1h}²³) measures in thalamus confirmed

128 phase-locked variations in both signals (cross-correlation coefficient > 0.5 , $n = 2$) (**Extended Data Figure**
129 **1c, d**). Furthermore, LC generated multiple-peak ‘activity surges’ that coincided with power decreases
130 in the sleep spindle-containing σ (10 – 15 Hz) power band, whereas σ power rose whenever LC activity
131 was low (**Extended Data Figure 1e1**)¹⁰⁻¹³, evident as a negative correlation between LC activity and σ
132 power (**Extended Data Figure 1e2**). Therefore, LC activity surges generated robust NA release that
133 activated thalamus through suppressing-spindle activity.

134 We next isolated LC activity surges and studied the associated brain states together with heart
135 rate as a measure of autonomic activation (**Figure 1e-i, Extended Data Figure 2, 3**). We noted that 30.0
136 % of LC activity surges were accompanied by a MA (**Figure 1e, f**, $n = 10$), recognizable by an EEG
137 desynchronization and a concomitant EMG activity lasting ≤ 12 s¹⁴. LC activity surges with a MA were
138 greater and longer than without a MA (**Figure 1g**, $n = 10$). Non-MA-associated surges were further
139 accompanied by a decrease in σ (10 – 15 Hz) power and an increased heart rate, reflecting a
140 coordinated thalamic and cardiac activation. MA-associated surges similarly altered σ power and heart
141 rate, yet with larger effect size (**Figure 1h, i**, $n = 10$). However, the two types of surges coupled
142 oppositely to low-frequency power changes. Power in the δ range (1.5 – 4 Hz) showed an increase for
143 non-MA-associated surges ($p = 0.035$, paired t -test, effect size $D = -1.02$), which indicates a period of
144 cortical deactivation or recurrent ‘downstates’. The MA-associated surges were instead accompanied
145 by a pronounced decrease in δ power, indicating cortical activation. Opposite dynamics were also
146 obtained for the γ band (60 – 80 Hz), a cortical activation signature. Similar spectral dynamics were
147 observed in the S1 LFP recordings, supporting an involvement of local thalamocortical circuits
148 (**Extended Data Figure 3a-c**). MA-associated surges showed γ power increases that coincided with
149 EMG activity, a MA-defining feature (**Extended Data Figure 3d**). Point-by-point statistical analyses
150 suggested that all EEG and LFP spectral power changes and the heart rate accelerations were induced
151 by LC activity within 50 s before the peak rather than by divergent EEG or LFP dynamics starting earlier
152 (> 50 s before the peak). These analyses demonstrate that LC activity surges during NREMS coordinate
153 a previously undescribed brain-bodily state, characterized by a combined cardiac and thalamic
154 activation that appeared dissociated from established signatures of cortical activation. During this
155 state, MAs appeared preferentially and activated cortex.

156 **Low LC activity levels were required for transitions to REMS**

157 Low LC activity levels have been previously associated with NREMS-to-REMS transitions (‘REMS
158 entries’), but the causal role of the natural LC activity troughs for REMS entries has not been tested
159 directly. During the natural LC activity fluctuations, REMS entries coincided with troughs ($n = 9$) (**Figure**
160 **2a, Extended Data Figure 4a**). We next optogenetically prevented or induced activity declines in DBH-

161 Cre animals expressing the excitatory opsin channelrhodopsin-2 (ChR2) or the inhibitory opsin Jaws in
162 LC neurons¹⁰. We tracked LC fluctuations on-line through monitoring the σ power dynamics in the S1
163 LFP. Previous tests demonstrated that such monitoring allows to reliably distinguish between LC
164 activity surges and troughs¹⁰.

165 We optogenetically activated LC in ChR2-expressing animals¹⁰ at moments of rising σ power
166 (corresponding to LC troughs, see also **Extended Data Figure 1e1**) in the first 20 min of every h during
167 ZT1-ZT9, with corresponding sham stimulations (LEDs turned-off) in separate sessions (**Figure 2b**)¹⁰.
168 This reduced the time spent in REMS and the frequency of REMS entries but did not alter the density
169 of MAs (0.58 ± 0.08 / min vs 0.62 ± 0.14 /min, Wilcoxon's signed rank test; $p = 0.3$; $n = 9$) and wake
170 time, supporting a specific action on REMS. Conversely, we expressed the orange light-activated
171 chloride pump 'Jaws' in DBH-Cre animals and inhibited LC at moments when it was naturally high,
172 evident by a decrease in σ power, which specifically increased REMS time and the frequency of REMS
173 entries (**Figure 2c**, $n = 10$). We confirmed the efficacy of this inhibition in 2 DBH-Cre animals expressing
174 Jaws in the LC and GRAB_{NE1h} in the thalamus (**Figure 2d**) and through confirming high cellular
175 transfection rates ($n = 4$; **Extended Data Figure 5**). Therefore, an optogenetically imposed decrease in
176 natural LC activity, mimicking natural troughs, was permissive for REMS entries, while preventing these
177 troughs suppressed REMS entries.

178 The propensity to enter REMS increases linearly with the time spent in NREMS, which reflects
179 its homeostatic regulation²⁴. We found that mean LC activity levels across NREMS bouts remained
180 stable until just before REMS onset, arguing against homeostatic regulation of LC activity (**Figure 2e,f**;
181 $n = 10$). These experiments establish that LC activity troughs, whether naturally occurring or
182 optogenetically promoted, generated windows of opportunity for REMS entries throughout the major
183 time spent in NREMS.

184 **LC activity fluctuations ruled the timing of REMS entries during REMS restriction**

185 The infraslow alternation between high and low LC activity levels suggests that the time it takes for LC
186 activity to decay from surge to trough could determine the NREMS time prior to a REMS entry. If this
187 was the case, a sequential infraslow time interval not previously considered in conceptual work on the
188 NREMS-REMS cycle would be identified²⁵. To test this, we sought to increase the frequency of REMS
189 entries while monitoring their timing relative to on-going LC activity. We developed a REMS restriction
190 (REMS-R) method in mice to reduce time spent in REMS while preserving NREMS time. We taped
191 vibrating motors to the animals' headstage to interrupt REMS through brief vibrations (2 s) in closed-
192 loop feedback (**Figure 3a**)¹⁴. When interrupting every detected REMS entry over a 6-h period from ZT0-
193 ZT6, attempts to enter REMS became frequent (**Figure 3b**, $n = 9$) while they remained stable in baseline

194 or control recordings (n = 9). The REMS-R further preserved homeostatic regulation of NREMS and
195 induced a REMS rebound (**Extended Data Figure 6**)²⁴.

196 We examined the timing of REMS entries with respect to LC activity fluctuations during REMS-R
197 in a next group of 8 animals. Every attempted REMS entry remained invariably preceded by a decay of
198 LC activity (**Figure 3c**). Furthermore, although REMS-R shortened the time between consecutive REMS
199 entries, these remained locked to moments of low LC activity levels (**Figure 3d, Extended Data Figure**
200 **4b**). Starting from the 4th h of the REMS-R, the mean interval between successive attempts remained
201 stable and settled at 48.2 ± 6.3 s at ZT6 (**Figure 3e1**, n = 8). To examine how strictly low LC activity
202 levels were required even during high REMS pressure, we calculated activity values for the last 5 s
203 before every REMS entry. We found these levels to remain stably low and constant during the entire
204 6 h of REMS-R (**Figure 3e2**, n = 8), showing that they had to fall below a lower bound for REMS to
205 initiate, even during high homeostatic pressure. To directly test whether LC activity could suppress
206 REMS entries under these conditions, we combined optogenetic LC stimulation in Chr2-expressing
207 DBH-Cre animals with REMS-R (**Figure 3f**, n = 6). We successfully suppressed REMS entries during the
208 entirety of the REMS-R, with sham (LED-off) conditions showing no effect, demonstrating that LC
209 activity overrode REMS pressure. Together, these experiments identify the infraslow natural
210 alternation between LC surges and troughs as a previously unrecognized architectural unit that
211 gatekeeps the duration of the NREMS-REMS cycle over successive ~50 s-intervals.

212 **LC activity fluctuations stabilized the natural NREMS-REMS cycle duration**

213 The mechanisms regulating natural cycle length remain poorly understood²⁵. Here, we asked
214 whether infraslow LC activity fluctuations were relevant for natural cycle length in undisturbed mouse
215 sleep²⁶. In mouse, times spent in NREMS vary in length from < 1 min to > 30 min before a next REMS
216 entry²⁶. To probe whether LC inhibition can modify cycle length, we aimed to choose cycles with
217 relatively little variability in duration. Following previous investigations on the interrelationship
218 between NREMS and REMS duration in mouse sleep^{26,27}, we analyzed how the time spent in NREMS
219 depended on prior REMS time in the light phase (n = 17). This showed that long REMS bouts (> 120 s)
220 were most consistently followed by long NREMS bouts, whereas shorter (< 100 s) REMS bouts were
221 followed by more variable NREMS times (**Figure 4a, b**). In undisturbedly sleeping Jaws-expressing DBH-
222 Cre mice (n = 7), we measured the duration of each REMS bout in real-time, and, once it lasted ≥ 120
223 s, we triggered optogenetic inhibition of LC. In a double closed-loop experimental design, the onset of
224 this inhibition was set 'early' (within 50-100 s after NREMS onset) or 'late' (after NREMS time lasting
225 twice the duration of the preceding REMS bouts ± 10 s) to probe LC's role at different moments in the
226 NREMS-REMS cycle. When LC inhibition started early in NREMS, we observed no significant change in

227 the frequency of REMS entries or in times spent in REMS, yet time spent in wakefulness was increased
228 (**Figure 4c**, $n = 7$). In contrast, when LC inhibition started late, repeated REMS entries took place almost
229 twice as frequently compared to Sham stimulation, while wake time remained preserved (**Figure 4d**, n
230 $= 7$). We confirmed the efficiency and specificity of LC inhibition by histological examination (**Extended**
231 **Data Figure 7a**), by correlating effects on REMS entries with sleep spindle densities (**Extended Data**
232 **Figure 7b**)¹⁰, and by testing mCherry-only-expressing controls ($n = 7$) (**Extended Data Figure 7c**).
233 Natural LC activity fluctuations may thus play diverse roles at different moments in the normal NREMS-
234 REMS-cycle, including a specific prevention of REMS entries late in the cycle. This prolonged the time
235 spent in NREMS and the total duration of the NREMS-REMS cycle.

236 **A stimulus-enriched wake experience increased LC activity fluctuations in NREMS, disrupting the** 237 **NREMS-REMS cycle**

238 Given the implication of LC activity fluctuations for the NREMS-REMS cycle, modifications in the
239 strength of these fluctuations could powerfully disrupt sleep. A recent study found that acute stress
240 during wakefulness can perturb LC activity in subsequent NREMS¹², but effects of wake time *per se* and
241 of the type of wake experience remain to be dissociated. Here, we subjected jGCaMP8s-expressing
242 DBH-Cre mice ($n = 9$) to two different 4 h-long sleep deprivation (SD) procedures from ZT0-ZT4. One
243 SD was achieved by the ‘gentle handling’ technique that prevents animals from falling asleep while
244 minimally disturbing their spontaneous activity patterns in the cage (**Figure 5a**)⁴⁵. The stimulus-
245 enriched SD (SSD) was instead paired with auditory and somatosensory stimuli, to which the animals
246 were not previously habituated and exposed to in an unpredictable manner, thus promoting LC
247 activation (**Figure 5b**)^{1,3}. Blood sampling immediately after the SSD in a separate group of animals ($n =$
248 8) revealed increases in corticosterone levels compared to baseline (**Extended Data Figure 8**),
249 indicating elevation of stress levels in addition to the sensory exposure, which strongly implicates LC^{1,4}.
250 The SD produced by gentle handling instead does not increase corticosterone levels²⁸.

251 As evident from the two representative recordings of sleep-wake behavior immediately after SD
252 or SSD of the same animal (**Figure 5a-c**), LC continued fluctuating between surges and troughs during
253 NREMS, yet with the former ones distinctly strengthened (see **Figure 5f**). Both SD and SSD resulted in
254 comparable increases in low-frequency power of the EEG δ (1.5 – 4 Hz) band, indicating that the
255 homeostatic pressure to sleep had become elevated similarly in response to the 4-h wake time (**Figure**
256 **5d**, $n = 9$). Remarkably, the density of MAs changed in opposite directions for SSD compared to SD. SD
257 decreased MA frequency in subsequent NREMS, indicating NREMS consolidation after a period of
258 wakefulness²². The SSD instead resulted in a marked increase in MA density and hence fragmented
259 NREMS (**Figure 5e**, $n = 9$). Furthermore, LC activity, measured in peak frequency (see Methods), was
260 higher in the first h of SSD compared to SD (**Figure 5f**, measured in $n = 7$ animals with stable dynamic

261 range > 15% across SD and SSD). Finally, the latency to REMS onset was increased in SSD compared to
262 SD and the number of REMS entries decreased within ZT4-ZT5 (**Figure 5g**, $n = 9$). In comparison to an
263 extended period of wakefulness, a stimulus-enriched wake experience combined with stress
264 transiently increased LC activity, disrupted sleep architecture for a post-SD/-SSD period of 1-2 h, and
265 antagonized the homeostatic effects of sleep consolidation.

266 **Inhibiting LC activity antagonized sleep disruptions induced by a stimulus-enriched wake experience**

267 We examined the role of LC activity fluctuations in the SSD-induced sleep disruptions. First, we
268 determined the spectral profiles associated with non-MA and MA-associated LC activity peaks, as done
269 for baseline recordings (see **Figure 1h, i**). There were no longer any increases in δ (1.5 – 4 Hz) power
270 for non-MA associated events (**Figure 6a**) in comparison to the SD condition ($n = 7$, paired t -test, $p =$
271 0.038 , effect size $D = -1.42$), while REMS entries remained invariably associated with LC activity troughs
272 ($n = 7$, **Figure 6b**). Second, to causally test the consequences of elevated LC activity, we subjected 9
273 Jaws-expressing DBH-Cre animals to two SSDs spaced at least 10 days apart, of which one was followed
274 by 1 or 2 h of Jaws-mediated bilateral inhibition of LC, the other one by LED-off (sham) exposure, in a
275 counterbalanced manner. LC inhibition attenuated the fragmentation of NREMS and shortened REMS
276 onset latency (**Figure 6c**). The exact pattern of LC's activity in NREMS thus depended on the type of
277 wake experience. Once modified in favor of higher LC activity levels, spontaneous arousability
278 increased and REMS became delayed. These data suggest that abnormal LC activity fluctuations can
279 be causally involved in two important hallmarks of deteriorated sleep quality that are NREMS
280 fragmentation and delayed REMS onset.

281 **Discussion**

282 We identify the noradrenergic LC as a gatekeeper for the organization of mammalian sleep into
283 NREMS-REMS cycles. The underlying principle of action is LC's partitioning of NREMS into two distinct
284 brain and autonomic states, of which one is arousal-promoting, the other one permissive for REMS
285 (**Figure 7**). To date, we know much about the neural circuits underlying either NREMS or REMS, and
286 both play important roles for sleep's restorative and memory-promoting functions²⁹. In comparison,
287 the circuit mechanisms that rule the alternation between NREMS and REMS have remained open,
288 despite pioneering modeling and experimental work^{17,25,30}. The identification of the LC as a gatekeeper
289 for the NREMS-REMS cycle is conceptually novel because it points to an upstream mechanism that sets
290 the time windows for the operation of NREM- or REMS-regulating circuits.

291 The LC was included as a REMS-off (that is, REMS-suppressing) brain area in the first theoretical
292 models for the NREMS-REMS cycle^{17,18}. Here, we found that LC plays dual roles in this cycle. High LC
293 activity suppressed while low activity permitted REMS. Important in this duality is that we found these

294 two roles to be segregated in time over infraslow intervals due to the slow interchange of LC activity
295 between high and low levels. Even after a 6 h-long REMS restriction, every attempt to enter REMS
296 remained strictly timed to the moments when LC activity levels fell below a lower bound. Furthermore,
297 LC activity at a low rate of 1 Hz suppressed REMS powerfully even during REMS-R. This robust
298 segregation of LC's dual roles imposes an infraslow architectural unit to NREMS over which permissive
299 moments for REMS are gated. We propose that a more dynamic understanding of how the brain-wide
300 network of REMS-promoting circuits, extending from prefrontal cortex³¹ to amygdala³², hypothalamus,
301 midbrain and brainstem (for review, see ref²⁵) dynamically interacts will profit from probing their
302 interaction with the LC's gatekeeping role.

303 Our study further challenges the widely held notion that LC promotes arousal through
304 desynchronizing EEG activity and suppressing low-frequency EEG waves^{1,3}. While we find that LC
305 activity surges acted in an arousal-promoting manner for the autonomic nervous system (through
306 accelerating heart rate) and for thalamic sleep spindle-generating circuits (through suppressing sleep
307 spindles)¹⁰ we additionally identify a simultaneous cortical 'sleep-like' EEG or LFP activity. LC surges
308 during NREMS thus did not typically generate a cortical activation while subcortical and autonomic
309 arousals occurred consistently. Interestingly, a functional imaging study in anesthetized rats indicated
310 that thalamic regions continuously and faithfully responded to LC activity across a range of
311 optogenetically evoked discharge frequencies, while cortical responses were more multifaceted³³. It is
312 further remarkable that arousals during human NREMS are heterogeneous in cortical activation but
313 more stereotyped in thalamus³⁴. Our insights provide mechanistic support for such observations and
314 will be relevant in on-going efforts to dissect the temporal sequences of arousal processes³⁵ and their
315 possible dysfunctions in disorders of arousals³⁶.

316 Although generalizing insights from rodent sleep must be done cautiously, we think that our
317 findings could be valuable for revisiting arousal signatures in the human sleep EEG. There are
318 established arousal scoring guidelines for human sleep, nevertheless, how some EEG signatures relate
319 to arousal remains debated^{16,37}. One example is a singular, large low-frequency EEG wave that is
320 prominent in human NREMS stage 2, referred to as 'K-complex'³⁸ that has been variably described as
321 sleep-protecting or arousal-related EEG hallmarks³⁸. Our data from mouse indicate that increases in
322 low-frequency activity in the EEG can be a forebrain manifestation of activated brainstem arousal
323 circuits, which supports mechanistic propositions for the K-complex in human sleep^{39,40}.

324 Possible neural mechanisms by which LC activity activates the thalamus while promoting low-
325 frequency activity in the cortex can be derived from available knowledge on NA's actions within
326 thalamocortical circuits. Single LC unit recordings from rats in NREMS showed that individual spikes

327 are phase-locked to cortical slow (low-frequency) waves⁴¹. Therefore, the NA release generated by
328 neuronal discharge during NREMS could be insufficient to disrupt the bistability of cortical up and
329 down states. Once LC activity surges are larger, as is for example the case after SSD, cortical bistability
330 may be overcome and the increase in low-frequency power may disappear. A better understanding of
331 the mechanisms underlying sleep-wake transitions will undoubtedly be contingent on an analysis of
332 how LC activity reconfigures thalamocortical circuits but also how it interplays with other arousal
333 systems.

334 Further dissection of LC's functional heterogeneity will be indispensable in understanding LC's
335 powerful ruling of when REMS entries are permitted. Direct optogenetic suppression of NA release in
336 target areas of REMS control could determine whether this ruling is dominated by LC or whether it is
337 a consequence of a larger set of time-limiting processes in NREMS. Evidence in support of this latter
338 possibility is provided by our finding that LC activity may play distinct roles in the NREMS-REMS cycle
339 at early compared to later moments. Recent studies further show that REMS is heterogeneous in space
340 and time, showing asynchronous onset⁴² and heterogeneous spectral properties⁴³ across cortical
341 areas. It will be very interesting to determine to what extent the heterogeneity of LC projections^{33,44},
342 combined with variable NA release, could underlie these variations.

343 Non-reducible time intervals of a duration similar to the one reported here were previously
344 observed in REMS-restriction protocols^{45,24,46}. Here, we provide a first mechanistic basis for this
345 observation that involves LC's neural activity dynamics as its temporal determinant. As infraslow
346 activity patterns in NREMS are preserved in brainstem and hypothalamic areas^{12,47,48}, it is unlikely that
347 LC acts alone. Still, we note that the noradrenergic LC is implied in neuronal and glial activity regulation
348 and it might also support vasomotor activity in the brain during NREMS^{5,49}. These diverse functions
349 could need some time to complete and be dependent on LC in interplay with other infraslow processes.
350 It is also noteworthy that reptile sleep shows alternations between NREM- and REMS-like states on an
351 infraslow time scale^{50,51}. We think that the infraslow time scale could be an evolutionarily conserved
352 architectural unit for the NREMS-REMS cycle over which a gatekeeping mechanism evolved later to
353 adapt the NREMS-REMS cycle to a variety of physiological needs.

354 Recent studies identified the LC to be involved in sleep disruptions preceded by acute stressful
355 experiences^{12,52}, illustrating the growing recognition of neural circuits involving monoamine release as
356 a source for sleep disturbances. Furthermore, abnormal NA activity in sleep can compromise the
357 adaptive processing of emotional experiences, which poses risk for mental health²⁰. We found that a
358 comparatively mild aversive wake experience was sufficient to shift the balance of LC activity
359 fluctuations towards more sustained surges of activity. Remarkably, this shift overrode the effects of

360 homeostatic NREMS pressure and lead to more MAs instead of fewer ones²². Shifts in LC activity can
361 thus disrupt sleep even in a 'sleepy' brain. This suggests that the LC makes sleep vulnerable to recent,
362 even transient, and moderately adverse wake experiences.

363 **Limitations**

364 We focused on the global population activity of noradrenergic LC neurons and studied
365 optogenetic effects without distinguishing neurons based on projection patterns or unitary discharge
366 patterns. A challenge for the future will be to identify LC neuronal subpopulations anatomically and
367 functionally to determine how the dual functionality in sleep described here arises. The LC is further
368 part of an extended brainstem-hypothalamic circuit with widespread infraslow activity patterns, which
369 asks for caution in causally relating effects on sleep-wake patterns to LC activity alone. This is
370 particularly relevant for the case of MAs to which activity in diverse brainstem and hypothalamic areas
371 contributes. To resolve the time windows over which the natural NREMS-REMS cycle is specifically
372 dependent on LC activity fluctuations, more extensively time-controlled and rapid optogenetic
373 interference tools will be needed. Here, the identification of the LC neuronal subgroups interacting
374 with REMS-regulatory areas is an important next step. Such advances are also required to determine
375 whether the 50-s time interval is solely contingent on LC activity decline, or whether this decline is a
376 consequence of other time-sensitive biological functions of NREMS.

377 **Conclusions**

378 The study offers a neural mechanism relevant for the alternation of mammalian sleep between
379 states of NREMS and REMS. Beyond this fundamental insight, our work will strengthen the connection
380 between rodent and human sleep because we propose testable biomarkers for LC activity in human
381 sleep that are based on the identification of a novel brain-autonomic state of arousal. Furthermore,
382 elucidating the origins of LC's gatekeeping role could shine light on certain NREMS functions that
383 inevitably require time or coordination to complete before a transition to REMS can be made. The
384 susceptibility of sleep-active LC to the preceding wake experience further brings novel opportunities
385 to dissect the mechanisms underlying an interdependence between sleep and daily experience.

386

387 **References**

- 388 1 Poe, G. R. *et al.* Locus coeruleus: a new look at the blue spot. *Nat Rev Neurosci* **21**, 644-659,
389 doi:10.1038/s41583-020-0360-9 (2020).
- 390 2 Berridge, C. W. Noradrenergic modulation of arousal. *Brain Res Rev* **58**, 1-17,
391 doi:10.1016/j.brainresrev.2007.10.013 (2008).
- 392 3 Sara, S. J. & Bouret, S. Orienting and reorienting: the locus coeruleus mediates cognition
393 through arousal. *Neuron* **76**, 130-141, doi:10.1016/j.neuron.2012.09.011 (2012).

394 4 Aston-Jones, G. & Cohen, J. D. An integrative theory of locus coeruleus-norepinephrine
395 function: adaptive gain and optimal performance. *Annu Rev Neurosci* **28**, 403-450,
396 doi:10.1146/annurev.neuro.28.061604.135709 (2005).

397 5 Osorio-Forero, A., Cherrad, N., Banterle, L., Fernandez, L. M. J. & Lüthi, A. When the locus
398 coeruleus speaks up in sleep: recent insights, emerging perspectives. *Int J Mol Sci* **23**,
399 doi:10.3390/ijms23095028 (2022).

400 6 Morris, L. S., McCall, J. G., Charney, D. S. & Murrugh, J. W. The role of the locus coeruleus in
401 the generation of pathological anxiety. *Brain Neurosci Adv* **4**, 2398212820930321,
402 doi:10.1177/2398212820930321 (2020).

403 7 Yu, X., Franks, N. P. & Wisden, W. Sleep and sedative states induced by targeting the histamine
404 and noradrenergic Systems. *Front Neural Circuits* **12**, 4, doi:10.3389/fncir.2018.00004 (2018).

405 8 Carter, M. E. *et al.* Tuning arousal with optogenetic modulation of locus coeruleus neurons.
406 *Nat Neurosci* **13**, 1526-1533, doi:10.1038/nn.2682 (2010).

407 9 Hayat, H. *et al.* Locus coeruleus norepinephrine activity mediates sensory-evoked awakenings
408 from sleep. *Sci Adv* **6**, eaaz4232, doi:10.1126/sciadv.aaz4232 (2020).

409 10 Osorio-Forero, A. *et al.* Noradrenergic circuit control of non-REM sleep substates. *Curr Biol* **31**,
410 5009-5023 e5007, doi:10.1016/j.cub.2021.09.041 (2021).

411 11 Kjaerby, C. *et al.* Memory-enhancing properties of sleep depend on the oscillatory amplitude
412 of norepinephrine. *Nat Neurosci* **25**, 1059-1070, doi:10.1038/s41593-022-01102-9 (2022).

413 12 Antila, H. *et al.* A noradrenergic-hypothalamic neural substrate for stress-induced sleep
414 disturbances. *Proc Natl Acad Sci U S A* **119**, e2123528119, doi:10.1073/pnas.2123528119
415 (2022).

416 13 Fernandez, L. M. J. & Lüthi, A. Sleep spindles: mechanisms and functions. *Physiol Rev* **100**, 805-
417 868, doi:10.1152/physrev.00042.2018 (2020).

418 14 Cardis, R. *et al.* Local cortical arousals and heightened (somato)sensory arousability during
419 non-REM sleep of mice in chronic pain. *Elife* **10**, e65835, doi:10.7554/eLife.65835 (2021).

420 15 Lecci, S. *et al.* Coordinated infra-slow neural and cardiac oscillations mark fragility and offline
421 periods in mammalian sleep. *Sci. Adv.* **3**, e1602026, doi:10.1126/sciadv.1602026 (2017).

422 16 Halasz, P., Terzano, M., Parrino, L. & Bodizs, R. The nature of arousal in sleep. *J Sleep Res* **13**,
423 1-23, doi:10.1111/j.1365-2869.2004.00388.x (2004).

424 17 McCarley, R. W. & Hobson, J. A. Neuronal excitability modulation over the sleep cycle: a
425 structural and mathematical model. *Science* **189**, 58-60, doi:10.1126/science.1135627 (1975).

426 18 Brown, R. E., Basheer, R., McKenna, J. T., Strecker, R. E. & McCarley, R. W. Control of sleep and
427 wakefulness. *Physiol Rev* **92**, 1087-1187, doi:10.1152/physrev.00032.2011 (2012).

428 19 Koshmanova, E. *et al.* *In vivo* locus coeruleus activity while awake is associated with REM sleep
429 quality in healthy older individuals. *bioRxiv*, doi:10.1101/2023.02.10.527974 (2023).

430 20 Cabrera, Y. *et al.* Overnight neuronal plasticity and adaptation to emotional distress. *Nat Rev*
431 *Neurosci* **25**, 253-271, doi:10.1038/s41583-024-00799-w (2024).

432 21 Zhang, Y. *et al.* Fast and sensitive GCaMP calcium indicators for imaging neural populations.
433 *Nature*, doi:10.1038/s41586-023-05828-9 (2023).

434 22 Franken, P., Malafosse, A. & Tafti, M. Genetic determinants of sleep regulation in inbred mice.
435 *Sleep* **22**, 155-169 (1999).

436 23 Feng, J. *et al.* A genetically encoded fluorescent sensor for rapid and specific *in vivo* detection
437 of norepinephrine. *Neuron* **102**, 745-761 e748, doi:10.1016/j.neuron.2019.02.037 (2019).

438 24 Franken, P. Long-term vs. short-term processes regulating REM sleep. *J Sleep Res* **11**, 17-28
439 (2002).

440 25 Park, S. H. & Weber, F. Neural and homeostatic regulation of REM sleep. *Front Psychol* **11**,
441 1662, doi:10.3389/fpsyg.2020.01662 (2020).

442 26 Park, S. H. *et al.* A probabilistic model for the ultradian timing of REM sleep in mice. *PLoS*
443 *Comput Biol* **17**, e1009316, doi:10.1371/journal.pcbi.1009316 (2021).

444 27 Benington, J. H. & Heller, H. C. REM-sleep timing is controlled homeostatically by accumulation
445 of REM-sleep propensity in non-REM sleep. *Am J Physiol* **266**, R1992-2000,
446 doi:10.1152/ajpregu.1994.266.6.R1992 (1994).

447 28 Kopp, C., Longordo, F., Nicholson, J. R. & Lüthi, A. Insufficient sleep reversibly alters
448 bidirectional synaptic plasticity and NMDA receptor function. *J Neurosci* **26**, 12456-12465,
449 doi:10.1523/JNEUROSCI.2702-06.2006 (2006).

450 29 Brodt, S., Inostroza, M., Niethard, N. & Born, J. Sleep-A brain-state serving systems memory
451 consolidation. *Neuron* **111**, 1050-1075, doi:10.1016/j.neuron.2023.03.005 (2023).

452 30 Hobson, J. A., McCarley, R. W. & Wyzinski, P. W. Sleep cycle oscillation: reciprocal discharge by
453 two brainstem neuronal groups. *Science* **189**, 55-58, doi:10.1126/science.1094539 (1975).

454 31 Weber, F., Hong, J., Lozano, D., Beier, K. & Chung, S. Prefrontal Cortical Regulation of REM
455 Sleep. *Res Sq*, doi:10.21203/rs.3.rs-1417511/v1 (2023).

456 32 Hasegawa, E. *et al.* Rapid eye movement sleep is initiated by basolateral amygdala dopamine
457 signaling in mice. *Science* **375**, 994-1000, doi:10.1126/science.abl6618 (2022).

458 33 Grimm, C. *et al.* Locus Coeruleus firing patterns selectively modulate brain activity and
459 dynamics. *Nature Neuroscience*, in press, doi:10.1101/2022.08.29.505672 (2024).

460 34 Peter-Derex, L., Magnin, M. & Bastuji, H. Heterogeneity of arousals in human sleep: A stereo-
461 electroencephalographic study. *Neuroimage* **123**, 229-244,
462 doi:10.1016/j.neuroimage.2015.07.057 (2015).

463 35 Setzer, B. *et al.* A temporal sequence of thalamic activity unfolds at transitions in behavioral
464 arousal state. *Nat Commun* **13**, 5442, doi:10.1038/s41467-022-33010-8 (2022).

465 36 Castelnovo, A., Lopez, R., Proserpio, P., Nobili, L. & Dauvilliers, Y. NREM sleep parasomnias as
466 disorders of sleep-state dissociation. *Nat Rev Neurol* **14**, 470-481, doi:10.1038/s41582-018-
467 0030-y (2018).

468 37 Lüthi, A., Franken, P., Fulda, S., Siclari, F., Van Someren E.J.W. Do all noradrenaline surges
469 disrupt sleep? *Nat Neurosci* **26**, 955-956, doi:10.1038/s41593-023-01313-8 (2023).

470 38 Halász, P. The K-complex as a special reactive sleep slow wave - a theoretical update. *Sleep*
471 *Med Rev* **29**, 34-40 (2016).

472 39 Siclari, F. *et al.* Two distinct synchronization processes in the transition to sleep: a high-density
473 electroencephalographic study. *Sleep* **37**, 1621-1637, doi:10.5665/sleep.4070 (2014).

474 40 Carro-Dominguez, M., Huwiler, S., Oberlin, S., Oesch T.L., Badii, G., Lüthi, A., Wenderoth, N.,
475 Meissner, S.N., Lustenberger C. Pupil size reveals arousal level dynamics in human sleep.
476 *Biorxiv* (2023).

477 41 Eschenko, O., Magri, C., Panzeri, S. & Sara, S. J. Noradrenergic neurons of the locus coeruleus
478 are phase locked to cortical up-down states during sleep. *Cereb Cortex* **22**, 426-435,
479 doi:10.1093/cercor/bhr121 (2012).

480 42 Peter-Derex, L. *et al.* Regional variability in intracerebral properties of NREM to REM sleep
481 transitions in humans. *Proc Natl Acad Sci U S A* **120**, e2300387120,
482 doi:10.1073/pnas.2300387120 (2023).

483 43 Funk, C. M., Honjoh, S., Rodriguez, A. V., Cirelli, C. & Tononi, G. Local Slow Waves in Superficial
484 Layers of Primary Cortical Areas during REM Sleep. *Curr Biol* **26**, 396-403,
485 doi:10.1016/j.cub.2015.11.062 (2016).

486 44 Schwarz, L. A. *et al.* Viral-genetic tracing of the input-output organization of a central
487 noradrenaline circuit. *Nature* **524**, 88-92, doi:10.1038/nature14600 (2015).

488 45 Benington, J. H., Woudenberg, M. C. & Heller, H. C. REM-sleep propensity accumulates during
489 2-h REM-sleep deprivation in the rest period in rats. *Neurosci Lett* **180**, 76-80,
490 doi:10.1016/0304-3940(94)90917-2 (1994).

491 46 Endo, T., Schwierin, B., Borbély, A. A. & Tobler, I. Selective and total sleep deprivation: effect
492 on the sleep EEG in the rat. *Psychiatry Res* **66**, 97-110, doi:10.1016/s0165-1781(96)03029-6
493 (1997).

494 47 Stucynski, J. A., Schott, A. L., Baik, J., Chung, S. & Weber, F. Regulation of REM sleep by
495 inhibitory neurons in the dorsomedial medulla. *Curr Biol* **32**, 37-50 e36,
496 doi:10.1016/j.cub.2021.10.030 (2022).

- 497 48 Kato, T. *et al.* Oscillatory population-level activity of dorsal raphe serotonergic neurons is
498 inscribed in sleep structure. *J Neurosci* **42**, 7244-7255, doi:10.1523/JNEUROSCI.2288-21.2022
499 (2022).
- 500 49 Nedergaard, M. & Goldman, S. A. Glymphatic failure as a final common pathway to dementia.
501 *Science* **370**, 50-56, doi:10.1126/science.abb8739 (2020).
- 502 50 Shein-Idelson, M., Ondracek, J. M., Liaw, H. P., Reiter, S. & Laurent, G. Slow waves, sharp
503 waves, ripples, and REM in sleeping dragons. *Science* **352**, 590-595,
504 doi:10.1126/science.aaf3621 (2016).
- 505 51 Yamazaki, R. *et al.* Evolutionary origin of distinct NREM and REM sleep. *Front Psychol* **11**,
506 567618, doi:10.3389/fpsyg.2020.567618 (2020).
- 507 52 Lo, Y., Yi, P. L., Hsiao, Y. T. & Chang, F. C. Hypocretin in locus coeruleus and dorsal raphe nucleus
508 mediates inescapable footshock stimulation (IFS)-induced REM sleep alteration. *Sleep* **45**,
509 doi:10.1093/sleep/zsab301 (2022).
- 510 53 Fernandez, L. M. *et al.* Thalamic reticular control of local sleep in sensory cortex. *Elife* **7**,
511 e39111, doi:10.7554/eLife.39111 (2018).
- 512 54 Owen, S. F. & Kreitzer, A. C. An open-source control system for in vivo fluorescence
513 measurements from deep-brain structures. *J Neurosci Methods* **311**, 170-177,
514 doi:10.1016/j.jneumeth.2018.10.022 (2019).
- 515 55 Sherathiya, V. N., Schaid, M. D., Seiler, J. L., Lopez, G. C. & Lerner, T. N. GuPPy, a Python toolbox
516 for the analysis of fiber photometry data. *Sci Rep* **11**, 24212, doi:10.1038/s41598-021-03626-
517 9 (2021).
- 518 56 Yüzgec, O., Prsa, M., Zimmermann, R. & Huber, D. Pupil Size Coupling to Cortical States Protects
519 the Stability of Deep Sleep via Parasympathetic Modulation. *Curr Biol* **28**, 392-400 e393,
520 doi:10.1016/j.cub.2017.12.049 (2018).

521

522 **Materials and Methods**

523 **ANIMALS AND HUSBANDRY**

524 The study used two mouse lines - the C57BL/6J line and the B6.FVB(Cg)-Tg(Dbh-
525 cre)KH212Gsat/Mmucd (MMRRC Stock#036778-UCD) line, referred to here as DBH-Cre line, that was
526 originally provided to us by David McCormick and Paul Steffan, University of Oregon. Mice were bred
527 on a C57BL/6J background and housed in a humidity- and temperature-controlled animal house with
528 a 12 h / 12 h light-dark cycle (lights on at 9 am, corresponding to ZT0). Food and water were available
529 *ad libitum* throughout all experiments. For viral injections, 3- to 10-week-old mice of either sex were
530 transferred to a housing cabinet in a P2 safety level room, where they stayed from 1 day before to 3
531 days after the viral injection. They were then transferred to the sleep-wake recording room and left to

532 recover for ≥ 1 week before undergoing the implantation surgery, after which they were single-housed
533 in standard-sized cages. The grids on top of the cage were removed and replaced by 30 cm-high
534 Plexiglass walls. Fresh food was regularly placed on the litter and the water bottle inserted through a
535 hole in the cage wall. Objects (tissues, paper rolls, table tennis balls) were given for enrichment.
536 In total, 10 DBH-Cre mice were used for two 12-h baseline sleep recordings in the light phase in
537 combination with fiber photometry under undisturbed conditions (**Figures 1, 2a, e, f, Extended Data**
538 **Figures 1b, e, 4**). Nine of these animals were used for analysis of LFP signals (**Extended Data Figure 3**).
539 Two of these DBH-Cre animals were also used for combined fiber photometric monitoring of LC activity
540 and NA levels (**Extended Data Figure 1c, d**). For combined LC optogenetic inhibition with fiber
541 photometric monitoring of NA release, 2 DBH-Cre animals were used (**Figure 2d**). Of the 10 DBH-Cre
542 animals included for fiber photometric monitoring of LC activity, 8 were also used for 1-2 sessions of
543 REMS-R in combination with fiber photometric monitoring of LC activity (**Figure 3c-e**), and 9 underwent
544 1-2 sessions of SD and one session of SSD in combination with fiber photometric monitoring of LC
545 activity (**Figures 5d-g, 6a, b**). Animals in which the dynamic range of fluorescence fell below 15% during
546 repeated fiber photometric sessions of SD and SSD, were no longer included in the analysis of LC
547 activity. 9 + 10 DBH-Cre mice were used for optogenetic manipulation during different phases of the
548 infraslow fluctuation in σ power (**Figure 2b, c**). These animals were already used in an earlier study and
549 re-analyzed here¹⁰. Seven DBH-Cre mice were used for optogenetic inhibition early or late in the
550 NREMS-REMS cycle, and an additional 7 were used for control viral injections (**Figure 4c, d, Extended**
551 **Data Figures 5, 7b, c**). For the analysis of the statistics of the NREMS-REMS cycle, baseline or sham
552 sleep recordings from these 14 animals, plus additionally 3 animals otherwise not used in the present
553 study, were included (**Figure 4a, b**). For the validation of the REMS-R procedure, 9 C57BL/6J animals
554 were used (**Figure 3a, b, Extended Data Figure 6**). For REMS-R in combination with optogenetic
555 stimulation, 6 DBH-Cre animals were used (**Figure 3f**). 9 animals were used for SSD in combination with
556 optogenetic LC inhibition (**Figure 6c**). A separate group of 8 animals were used for quantification of
557 corticosterone levels at ZT4 in baseline and after SSD (**Extended Data Figure 8**). All experiments were
558 conducted in accordance with the Swiss National Institutional Guidelines on Animal Experimentation
559 and were approved by the Swiss Cantonal Veterinary Office Committee for Animal Experimentation.

560

561 VIRAL VECTORS AND INJECTIONS

562 General and local anesthesia, analgesia, temperature control, stereotaxic fixation and drilling of
563 craniotomies for injections of viral vectors were as described¹⁰. All viral vectors were obtained from
564 the Viral Vector Facility of the University of Zürich. For fiber photometric monitoring, DBH-Cre mice
565 were unilaterally injected over the right LC (Coordinates relative to Bregma in mm throughout the
566 Methods section: Lateral (L) 1.05; Antero-posterior (AP) -5.4; dorsal-ventral (DV) -3.2) with AAV5-

567 hSyn1-dlox-jGCaMP8s-dlox-WPRE-SV40p(A) (titer 5.8×10^{12} vg/ml, 300nL) at an injection rate of 50-100
568 nL/min using a thin glass pipette (5-000-1001-X, Drummond Scientific) pulled on a vertical puller
569 (Narishige PP-830), initially filled with mineral oil, and backfilled with the virus-containing solution just
570 prior to injection. For transfection of the LC for optogenetics, viral vectors were ssAAV5/2-hEF1 α -dlox-
571 hChR2(H134R)_mCherry(rev)-dlox-WPRE-hGHp(A) (9.1×10^{12} vg/ml, 0.8 – 1 μ L, unilateral) or ssAAV-5/2-
572 hSyn1-dlox-Jaws_KGC_EGFP_ERES(rev)-dlox-WPRE-bGHp(A)-SV40p(A) (6.4×10^{12} vg/ml, 300 nL
573 bilateral). Control experiments for optogenetic excitation were described previously¹⁰, the control
574 virus for optogenetic inhibition experiments was ssAAV-5/2-EF1 α -dlox-mCherry(rev)-dlox-WPRE-
575 bGHp(A) (7.3×10^{12} vg/ml, 300 nL bilateral). For monitoring of free NA levels, ssAAV9/2-hSyn1-
576 GRAB_NE1h-WPRE-hGHp(A) (7.2×10^{12} vg/ml, 500 nL) was injected unilaterally in primary
577 somatosensory thalamus (L 2.0; AP -1.6; DV -3.0), to express the NA biosensor GRAB_{NE1h}, as described
578 before¹⁰. Two animals each were dually injected for combined ipsilateral expression of jGCaMP8s and
579 GRAB_{NE1h} or for combined expression of Jaws (bilateral) and GRAB_{NE1h} (unilateral). After the injections,
580 the incision was sutured and disinfected, and the animals were supervised and given paracetamol at 2
581 mg/ml for the next 4 days.

582

583 **SURGERIES**

584 **Surgeries for sleep-wake recordings.** Surgeries were done > 1 week following the viral injection.
585 Anesthesia was induced and maintained by isoflurane 5% and 1.5 – 2.5%, respectively, in a mixture of
586 O₂ and N₂O and analgesics applied i.p. (Carprofen 5mg/kg). Animals were fixed in a Kopf stereotax and
587 injected into the scalp with a mix of lidocaine (6 mg/kg)/bupivacaine (2.5 mg/kg), and eye ointment
588 applied. To expose the skull, the skin was incised, and the bone scratched with a fresh scalpel blade to
589 improve adhesion of the head implant. Then, we drilled small craniotomies (0.3 – 0.5 mm) over left
590 frontal and parietal bones and positioned two conventional gold-coated copper-wire electrodes in
591 contact with the dura mater for EEG recordings. LFP electrodes were implanted ipsi-, EEG electrodes
592 contralaterally. High-impedance tungsten LFP microelectrodes (10–12 M Ω , 75- μ m shaft diameter,
593 FHC) were implanted in the primary somatosensory cortex (L +3.0; AP -0.7; DV -0.85) and the
594 hippocampus (L +2.0; AP -2.46; DV -1.2 to -1.3). Additionally, as a neutral reference, a silver wire
595 (Harvard Apparatus) was inserted into the occipital bone over the cerebellum and two gold pellets
596 were inserted into the neck muscles for EMG recordings. All electrodes were fixed using Loctite
597 Schnellkleber 401 glue and soldered to a multisite connector (Barrettes Connectors 1.27 mm, male
598 connectors, Conrad). Animals were single-housed after surgeries.

599 **Surgeries for fiber photometry recordings.** Optic fiber implantation occurred together with the
600 surgical implantations for sleep-wake recordings. Shortly, an optic fiber stub coupled to a cannula
601 (Doric Lenses, MFC_400/430-0.66_3.5mm_ZF1.25(G)_FLT) was implanted over the right LC (L +0.9; AP

602 -5.4; DV -2.7) at an insertion speed of 1 mm/min using a Kopf stereotaxic holder, for 1 animal the fiber
603 was implanted with an angle of 20 degrees leading to a different set of coordinates (L +1.84; AP -5.4;
604 DV -2.9). For dual fiber photometry, this procedure was repeated over the primary somatosensory
605 thalamus (L +1.8; AP -1.7; DV -2.5), over which the fiber stub was vertically inserted. Fibers were glued
606 to the skull and were part of the dental cement structure holding the entire implant into place.

607 **Surgeries for optogenetics.** For optogenetic stimulation of noradrenergic LC neurons, 4 mm-long optic
608 fibers were purchased pre-prepared (MFC_200/250-0.66_4mm_ZF1.25(G)_FLT) or fabricated from a
609 multimode fiber (225 μm outer diameter, Thorlabs, BFL37-2000/FT200EMT) using the custom-made
610 procedure described in ref¹⁰. For optogenetic inhibition, 5 mm-long optic fibers attached to an optic
611 canula were used (CFMLC12L05, Thorlabs). The implantation coordinates for stimulation were (L +0.9;
612 AP -5.4; DV -2.5 unilaterally in the right LC), while for inhibition two fibers were implanted bilaterally
613 using a 20° angle from the vertical (L +/-1.84; AP -5.4; DV -2.5). The emitted light intensity at the fiber
614 tip was evaluated prior to implantation for every fiber.

615

616 **RECORDING PROCEDURES AND PROTOCOLS**

617 **Sleep recordings.** Sleep-wake recordings took place within the animals' home cage. Once recovered
618 from surgery for > 1 week, animals were habituated to cabling to an ultrathin Intan SPI cable and
619 adaptor board via a custom-made support system (Homemade adapters containing an Omnetics
620 A79022-001 connector linked to a female Barrettes Connector from Conrad). These served as
621 intermediate between the head implant of the animal and the headstage (RHD2132 amplifier board)
622 that was connected to the Intan USB interface Acquisition Board (RHD2000). All signals (EEG frontal
623 and parietal, left and right EMG, S1 and CA1 LFPs) were acquired in unipolar mode at 1 kHz.

624 All recordings were done in the 12-h light phase (ZT0-ZT12). The two fiber photometry recording
625 sessions were kept separate for at least 1 day. For closed-loop optogenetic stimulation and inhibition
626 sessions timed to the infraslow σ power fluctuations in NREMS, 2 sessions were done per condition
627 (Rising or declining σ power, Sham (LED-off) or Light stimulation)¹⁰, spaced by one day and data
628 averaged between sessions. For optogenetic inhibition timed to the early or the late phase of the
629 NREM-REMS cycle, 10 to 20 sessions per animal were recorded over 3 weeks' time. For the two REMS-
630 R sessions per animal, at least 2 interleaved days were given. REMS-R and yoked recording sessions
631 were interleaved by at least 2 days in a random manner. Per animal, there were 1-2 SSDs that were kept
632 at least 7 days apart. The SSD was spaced apart from the SD sessions by at least 7 days, and 10 days
633 were given for two SSDs combined with LC optogenetic inhibition or sham (LED-off) exposure. For
634 details of the light exposure, see *Optogenetic protocols*.

635 **Fiber photometry recordings.** Two signal generators modulated the blue (465 nm) and the violet (405
636 nm) LED of the Doric Fluorescence MiniCube LEDs (ilFMC4-G2_IE(400-410)_E(460-490)_F(500-550)_S)

637 using sinusoidal signals at 319 and 211 Hz, respectively. The combined modulated light was then
638 transmitted through a 400- μ m-thick fiberoptic patchcord (MFP_400/430/1100-0.57_1m_FMC-
639 ZF1.25_LAF, Doric Lenses) to the implanted optic canula on the head of the animal. A photodetector
640 integrated into the MiniCube turned the emitted light from the fluorescent sensors into a current
641 signal that was fed into an analog signal of the Intan RHD2132 amplifier board as described
642 previously¹⁰. The measured power at the tip of the optic fiber was, for both wavelengths, 20 – 30 μ W
643 ensuring minimal bleaching throughout the 12 h of recordings.

644 **Optogenetic protocols.** For optogenetic interference at different phases of the infraslow σ power
645 fluctuations, protocols were applied as described¹⁰. The optogenetic manipulations took place every
646 first 20 min for every h from ZT1-ZT9 (8 h). Stimulation sessions (with LED on) took place in exchange
647 with sham session (LED off). For both session types, 1 - 3 recordings were carried out on separate days.
648 During the 40-min intervening period, initial transient alterations in sleep architecture were observed
649 for minutes 0-10 min, which fully recovered before the next period of light exposure. Entries into
650 NREMS were detected online through setting a threshold for the low-frequency (1 – 4 Hz) over θ (6 –
651 10 Hz) ratio for the differential frontal-parietal EEG signal and the decrease in the absolute EMG
652 amplitude. Occasional brief interruptions in LED stimulation during NREMS are due to a trespassing of
653 that ratio, either caused by muscle twitches or spectral fluctuations. Once in NREMS, σ power
654 fluctuations were monitored online and increasing or decreasing slopes detected through a machine-
655 learning procedure¹⁰. For LC stimulation, we used 1 Hz pulses of 10 ms applied to a PlexBright Plexon
656 BlueLED unit emitting 465 nm blue light at 2.8-3.2 mW intensity. For LC inhibition, we used continuous
657 stimulation of an orange LED module (620 nm, 1.55 – 1.7 mW at the tip). Control experiments for light
658 exposure were carried out for both optogenetic stimulation, including an assessment for heating
659 effects (see ref¹⁰), and for optogenetic inhibition (**Extended Data Figure 7c**).

660 For optogenetic interference at different time points in the NREMS-REMS cycle, we used a closed-loop
661 algorithm to identify REMS and NREMS based on the low-frequency (1 – 4 Hz) over θ (6 – 10 Hz) ratio
662 for the differential frontal-parietal EEG signal and the EMG activity based on 4-s windows with a 3 s
663 overlap (i.e. updated every s), as previously described¹⁴. Upon online identification of long REMS bouts
664 (>120 s), 20-min continuous optogenetic inhibition started randomly after 50 – 100 s of NREMS (*early*
665 *inhibition*), or after twice the time of the identified REMS bout (at least 240 s or 2 times the duration
666 of the preceding REMS bout) with a random 10-s jitter (*late inhibition*). The time points chosen to start
667 the early or the late inhibition were based on a previous study analyzing the probabilities for REMS
668 entries after a long REMS bout²⁶. Several sessions were recorded so that we collected data from a total
669 of 87 long REMS bouts for early and of 106 long REMS bouts for late inhibition.

670 For optogenetic inhibition after SSD (see below for procedure), LC was continuously inhibited for 1 or
671 2 h after the end of the SSD using continuous illumination. The stimulation started once a 10-s-long

672 NREMS duration was automatically detected, using a closed-loop algorithm based on the low-
673 frequency (1 – 4 Hz) over θ (6 – 10 Hz) ratio for the differential frontal-parietal EEG signal and the EMG
674 activity. This resulted in a mean of 36.3 ± 5.1 min and 34.5 ± 4.5 min of sleep/h of light stimulation
675 for sham and test conditions, respectively ($n = 9$). One additional animal was *post hoc* excluded from
676 analysis because it slept only ~ 5 min during the 2-h post SSD light exposure, which provided insufficient
677 data for analysis. Per animal, one SSD followed by LC inhibition and one SSD followed by Sham
678 inhibition was carried out in a counterbalanced design.

679

680 **BEHAVIORAL MANIPULATIONS**

681 **REMS restriction (REMS-R).** We used small vibrating motors (DC 3–4.2 V Button Type Vibration Motor,
682 diameter 11 mm, thickness 3 mm) that we fixed using double-sided tape to the end of the recording
683 cables, close to the animals' heads. The motors were driven to vibrate through a closed-loop system
684 using a Raspberry Pi¹⁴. Once the θ (6 – 10 Hz) / δ (1 – 4 Hz) ratio of the CA1 LFP signal passed a threshold
685 of 1.5 for > 2 s, and EMG activity fell below a threshold of 0.35 (calculated based on a normalization of
686 the logarithm of the absolute EMG), the motors vibrated for 2 s and woke up the animal, as monitored
687 by polysomnography. A control session for protocol standardization was included, in which the motor
688 of an animal was activated based on the closed-loop of the neighbor animal (yoked controls). The
689 animals included only for the validation for the REMS-R procedure were separate from the ones in
690 which LC activity was monitored during the REMS-R. In these latter 8 recordings, the mean duration of
691 REMS bouts during the REMS-R before vibration was 8.9 ± 2.4 s. The REMS-R was carried out from ZT0-
692 ZT6 for all experiments except when REMS-R was combined with LC optogenetic stimulation, for which
693 it lasted from ZT1-ZT9 (see *Optogenetic protocols*).

694 **Gentle sleep deprivation (SD).** Animals were kept awake from ZT0-ZT4 while in their home cage and
695 tethered to the recording apparatus. One person supervised two animals at the time and added
696 nesting materials (pieces of Kleenex tissue) or gently interfered with the animals' spontaneous
697 behavior once it started adopting a sleeping posture²⁸. For this, we used a ~ 30 cm-long stick scotched
698 to a ball of Kleenex tissue to gently displace the litter around the nest or to wipe the wall of the cage.
699 The animal was never touched throughout the entire procedure.

700 **Stimulus-enriched sleep deprivation (SSD).** The animals were placed in a novel cage and subjected to
701 several manipulations every 20-30 min to touching (1-2 min), gentle cage shaking (5 min) or auditory
702 stimulation (knocking at the cage, 5 min) from ZT0-ZT4. Two animals were supervised per person.
703 These manipulations were paired one each for touching and cage shaking and auditory stimulation and
704 cage shaking, and once done the three together. At the end, animals were transferred back to their
705 home cage and left undisturbed. In animals used for fiber photometric recording of LC fluorescence,
706 one SSD was carried out. In animals in which LC was inhibited after SSD, two SSDs per animal were

707 carried out (one for sham LED-off inhibition, one for light inhibition). Corticosterone measures were
708 carried out at ZT4 for baseline (undisturbed) and SSD conditions per animal by drawing tail vein blood
709 samples. Samples were kept on ice in heparin-coated tubes and centrifuged at 4° for 4 min 9,400xg.
710 Plasma was extracted and corticosterone levels measured with the Enzo Life Sciences kit (Catalog No.
711 ADI-901-097).

712

713 HISTOLOGY

714 At the end of all the recording sessions, animals were injected i.p. with a lethal dose of pentobarbital.
715 The position of each LFP electrode was subsequently marked using electro-coagulations (50 μ A, 8 – 10
716 s). Afterwards, ~40 mL paraformaldehyde (4 %) were perfused transcardially at a rate of ~3 mL min⁻¹.
717 The brains were then extracted, post-fixed for 24 h in 4 % PFA at 4°C, cryoprotected in 30% sucrose for
718 1-2 days if needed, and the tissue was sliced in 50- μ m-thick (for brainstem) or 100- μ m-thick (for
719 thalamus or cortex) sections using either a vibratome (Microtome Leica VT1000 S; speed: 0.25 – 0.5
720 mm/s) or a manually guided freezing microtome (Microm). Sections were either immediately mounted
721 (using Mowiol as a mounting medium) or stored in 0.1 M PB. The anatomical location of optic fibers,
722 LFP electrodes and the expression of the fluorescent proteins was verified with a Nikon SMZ25
723 Stereomicroscope equipped with a Nikon DS-Ri2 (16 Mpx) color camera. For higher magnification
724 images, an Axiovision Imager Z1 (Zeiss) microscope was used (objectives used EC-Plan Neofluar
725 2.5x/0.075 ∞ /0.17, 5x/0.16 ∞ /0.17, 10x/0.3 ∞ /- or 20x/0.5 ∞ /0.17).

726 For assessing the colocalization of jGCaMP8s with tyrosine hydroxylase (TH) in the LC neurons,
727 coronal brain sections 50 μ m-thick (~-5.3 mm from bregma), were first washed 3 x in 0.3% Triton in
728 PBS, incubated in blocking solution (PBS, 0.3 % Triton, 2 % normal goat serum) for 1 h and then
729 overnight with the primary antibody (mouse anti-TH antibody, dilution 1:2000, Immunostar, 22941) at
730 4 °C while on a shaker. After incubation for at least 12 h, sections were washed 3 x with PBS containing
731 0.3 % Triton. The secondary antibody was added (1:100 donkey anti-mouse antibody coupled to Alexa
732 Fluor 594, Invitrogen, A21203, in PBS containing 0.3 % Triton) and sections were incubated for 1-1.5 h
733 at room temperature on a shaking platform. Sections were then rinsed with 0.1 M PB and mounted
734 using Mowiol. The images were acquired through red and green emission channels using a confocal
735 microscope (Leica Stellaris 8). For the quantification of transfection rates (see **Extended Data Figure**
736 **5**), we stained sections for TH as described above and acquired confocal images with a 20 x air objective
737 (HC PL APO 20x/0.75 CS2). The QuPath software (<https://qupath.readthedocs.io/en/0.5/>) was used to
738 detect TH-positive cells (using a thresholding method) from the red channel, each of which was then
739 classified as EGFP-positive using the information in the green channel. We quantified a single confocal
740 LC image for each of the 4 animals.

741

742 ANALYSIS PROCEDURES

743 Sleep analysis.

744 **Sleep scoring.** We scored sleep stages in 4-s epochs using the EEG/EMG signals according to standard
745 procedures using a custom-made semiautomated Matlab routine available on our Github Repository
746 (<https://github.com/Romain2-5/IntanLuthiLab>). Wakefulness was scored when high-frequency EEG
747 activity coincided with strong EMG activity; NREMS was scored when high-amplitude low-frequency
748 components, such as slow oscillations (0.5 – 1.5 Hz) and δ activity (1.5 – 4 Hz), and recurrent sleep
749 spindles (10 – 15 Hz) appeared in combination with low muscle tone; REMS was scored whenever a θ
750 peak (6 – 10 Hz) appeared and muscle atonia developed. For determining the exact onset of REMS, a
751 thresholding of θ/δ power was used for the CA1 LFP signal (see ‘Spectral dynamics’). For epochs at
752 transitions, the vigilance state that covered > 2 s was scored. Microarousals were scored when
753 maximally 3 wake epochs (≤ 12 s) showing both EEG desynchronization (predominance of faster, low-
754 amplitude, over slower high-amplitude activity) and EMG activity appeared and were preceded and
755 followed by NREMS. An epoch was also scored as (part of a) MA when wake activity (in both EEG and
756 EMG) lasted < 2 s. For analysis of intervals between successive REMS episodes during REMS-R, the
757 motor vibration signal was used. The interval between two successive REMS episodes was quantified
758 as the time spent in NREMS (in seconds) between two successive motor onsets (for this analysis, MAs
759 were considered as part of NREMS).

760 **Spectral dynamics.** The dynamics of spectral bands were calculated from the S1 and CA1 LFPs using
761 wavelet transforms with Gabor-Morlet Kernels with 4 cycles of standard deviation for the Gaussian
762 envelope at 0.1 Hz resolution. For spectral analysis involving S1 LFP signals or EEG, frequency bands
763 analyzed were δ (1.5 – 4 Hz), θ (6 – 10 Hz), σ (10 – 15 Hz), β (16 – 25 Hz), γ (60 – 80 Hz). The hippocampal
764 LFP was used for calculation of the ratio of a θ (6 – 10 Hz) over δ (1 – 4 Hz) ratio (θ/δ) in the CA1 LFP
765 electrode, in which the δ band was started at 1 Hz for convenience. For band-defined dynamic changes,
766 the S1 or EEG signals were first down-sampled from 1 kHz to 200 Hz, the Wavelet transform calculated
767 within the desired frequency bands and summed over all frequencies within that band. The derived
768 signals were down-sampled at 10 Hz and low-pass-filtered at a cut-off frequency of 0.1 Hz. The
769 detection of individual spindles was calculated as previously described^{10,53}. For the CA1 signal, a similar
770 procedure was applied to obtain the ratio for θ/δ and a threshold of 1.5 was chosen to define REMS
771 onset around the previously defined manual transition. The dynamics of the EMG were calculated as
772 absolute values from the 0.1 Hz-filtered trace.

773 **Heart rate quantification.** Heart rate was quantified as described before using the R-R peaks recorded
774 by the EMG, using the square of its derivative and the Matlab FindPeaks function^{10,14}.

775 Fiber photometric analysis.

776 **Extraction of $\Delta F/F_0$ signals and baseline correction.** A functional signal (from the blue excitation LED),
777 carrying the Ca^{2+} -dependent activity, and an isosbestic, Ca^{2+} -independent one (from the violet
778 excitation LED) were used for signal demodulation utilizing the workflow and the MATLAB codes
779 available as open source⁵⁴. The $\Delta F/F_0$ signal was then computed using as F_0 the fitted isosbestic signal,
780 following the procedure explained in ref⁵⁵.

781 For all analysis, fiber photometric signals were included in the analysis only if the dynamic range,
782 calculated between the minimum and the maximum of the signal within the first 2 h of the recording,
783 was > 15%. In the next paragraphs describing specific analyses, this extracted signal is referred to as
784 the 'LC signal'.

785 **All-points histograms.** We constructed all-points histograms from z-scored LC signals obtained from
786 all 10 animals for the first 2 h of the light phase. Overlap between NREMS and Wake periods was
787 calculated as the number of data points in NREMS that are greater than the mean - 2 standard
788 deviations of the levels in wakefulness.

789 **Analysis of LC peaks and LC activity surges.** The definitions of the LC peaks and activity surges are
790 visually illustrated in **Extended Data Figure 2** and are briefly summarized here in a semi-quantitative
791 description. First, the LC signal was low-pass-filtered at 0.5 Hz (FIR filter of order 100) and rectified by
792 the lower envelope (96-s sliding window) of the signal low-pass-filtered at 0.1 Hz. Second, we detected
793 the peaks in the rectified signal using the FindPeaks function of Matlab[®] that reached a prominence
794 threshold as quantitatively explained in the Figure. Third, the LC activity surges in NREMS were
795 identified as multiple peak-events with a rapid onset. To extract such events, LC peaks within
796 consolidated NREMS (>96 s of NREMS, excluding the time period of LC signal decay after wakefulness)
797 were examined for maxima in 20 s-long sliding windows. To define the start and the end of the surges,
798 we used the z-score of the 100 s window around each such maximal peak. The start was defined by
799 the first peak using the derivative of the signals, while the end of the transient was the moment when
800 the signal reached 15% of the maximal value of the 100-s window. The start and the onset of each
801 activity surge were used for quantification as presented in **Figure 1e-g**. All codes for this analysis are
802 available on (<https://github.com/Romain2-5/IntanLuthiLab>). For the analysis of LC peaks after SD and
803 SSD, mean peak frequency values were calculated for equal times spent in NREMS (12 bins for baseline
804 conditions, 8 for the SD and SSD conditions).

805 **Cross-correlations between LC activity, NA levels, σ power.** Cross-correlations were calculated
806 analogously to the previous one done for NA fluctuations and σ power¹⁰ using z-scored σ power and
807 LC signals, or the NA and LC signals, at 0.1-s resolution, for all NREMS bouts > 96 s, including MAs, from
808 ZT0-ZT12. A mean cross-correlation per animal was calculated and presented for the time interval
809 between -200 s to 200 s. For the cross-correlation between NA and LC signals (**Extended Data Figure**
810 **1d**), the two animals with dually recorded fiber photometry were used. In the case of the cross-

811 correlations between LC activity and σ power, the position of side peaks could be extracted in 6 out of
812 10 cases (based on the dynamic range of the LC signal, see **Extended Data Figure 1e2**). Cross-
813 correlations were then averaged across animals. A positive time lag indicates that the LC signal
814 increases preceded σ power decreases or NA increases. 'LC activity surges' correspond to the high LC
815 activity levels that anticorrelate with the σ power and that appear on infraslow time intervals (30 – 50
816 s).

817 **Spectral analysis around LC activity peaks.** Local maxima of the LC signals were defined using a 20-s
818 sliding window on the LC $\Delta F/F_0$ signal, as described above. We derived the z-scored spectral dynamics
819 for different frequency bands using the wavelet approach previously described (See *Spectral*
820 *dynamics*) around these maxima from – 150 s to + 50 s. In a second step, these peaks were classified
821 according to whether or not they were associated with a MA (defined by EEG/EMG activity as described
822 in *Sleep Scoring*) within 5 s around the peak. Additionally, we calculated the absolute EMG activity and
823 the z-scored heart rate within these windows and repeated this analysis for both for the S1 LFP and
824 the EEG during NREMS bouts for all times. Mean amplitudes for the LC signal and for heart rate were
825 calculated as the difference from the peak time to the minimum value before the peak (-10 s to 0 s).
826 Mean amplitudes for spectral power bands were calculated from times 0 s to 1 s.

827 **Spectral analysis at REMS onset.** The exact timing of REMS onset was defined using a thresholding for
828 θ/δ at 1.5 using the CA1 LFP electrode. Using the parietal EEG electrode provided similar results. The
829 dynamics for preceding NREMS were then obtained for the S1 LFP σ band and for the low-pass filtered
830 absolute EMG signal.

831 **Sleep architecture analysis during LC optogenetic stimulation and inhibition.** For LC stimulation or
832 inhibition according to the phase of the σ power fluctuation, times spent in Wake, NREMS and REMS
833 were calculated for the test or sham stimulation 20-min sessions and expressed in % of total time.
834 Transitions were calculated as the number of REMS-epochs followed by NREMS and calculated as
835 REMS entries per minute of time spent in NREMS. For LC inhibition at different moments in the NREMS-
836 REMS cycle, a similar procedure was applied.

837 **Mean LC activity in NREMS bouts.** The LC fluorescent signal was extracted between REMS bouts lasting
838 ≥ 12 s, z-scored for all NREMS including MAs, and plotted over normalized NREM time between the
839 consecutive REM bouts. The derived signals were averaged based on the length of the preceding REM
840 bout as previously done for similar purposes²⁶.

841 **Quantification of rebound REMS after REMS-R.** To demonstrate the efficiency of the REMS-R, we
842 quantified rebound REMS by calculating cumulative times spent in REMS during REMS-R and the 6 h –
843 post REMS-R period.

844 **LC signal analysis during REMS-R.** To determine the relative level of LC activity prior to REMS entry
845 during the REMS-R, we extracted bouts where a transition to REMS was present and preceded by at

846 least 12 s of NREMS. The $\Delta F/F_0$ LC activity was then z-scored for each bout and we reported the mean
847 $\Delta F/F_0$ value during the last 5 s before the transition to REMS.

848 **LC stimulation during REMS-R.** For each 20 min stimulation block (first 20 min of every h from ZT1–
849 ZT9) during the REMS-R, we normalized the time in equal amounts of NREMS for the periods before,
850 during and after stimulation (10 bins per block) and calculated the number of REM entries per min of
851 NREMS. A similar approach was done to the analogous periods during sham stimulation, *ceteris*
852 *paribus*, with the LEDs turned off.

853 **STATISTICS**

854 The statistics were done using Python, Matlab R2021a or R statistical language version 4.0.1. The
855 normality of data distributions was assessed using the Shapiro–Wilk and Levene tests. In cases of
856 normality violations, non-parametric Kruskal-Wallis and Wilcoxon tests were used. Datasets were
857 collected in experimental designs allowing preferentially repeated measures and/or paired statistical
858 analysis. Post-hoc analyses were done only when the one-way factor or the interaction between
859 factors was significant ($p < 0.05$). Bonferroni’s correction for multiple comparisons was applied
860 routinely, and the corrected α thresholds are given in the figure legends. Differences in the dynamics
861 of power bands and heart rate were calculated using *t*-tests and correcting for multiple comparisons
862 using False Discovery Rates (FDR) where the significant values satisfy $P(k) < 0.05 * k/2000$, where *P* is
863 the vector of the ranked *p* values of the point-to-point *t*-test within the window (-150 s to 50 s at 10
864 Hz). In all figure legends, the statistical tests used are mentioned, while sample numbers and *p* values
865 are indicated directly in the figure panels. Details of all statistical tests and effect sizes are summarized
866 in **Supplementary Table 1**. Further essential sleep information for all experiments is provided in
867 **Supplementary Table 2**.

868

869

870

871

872

873

874

875

876

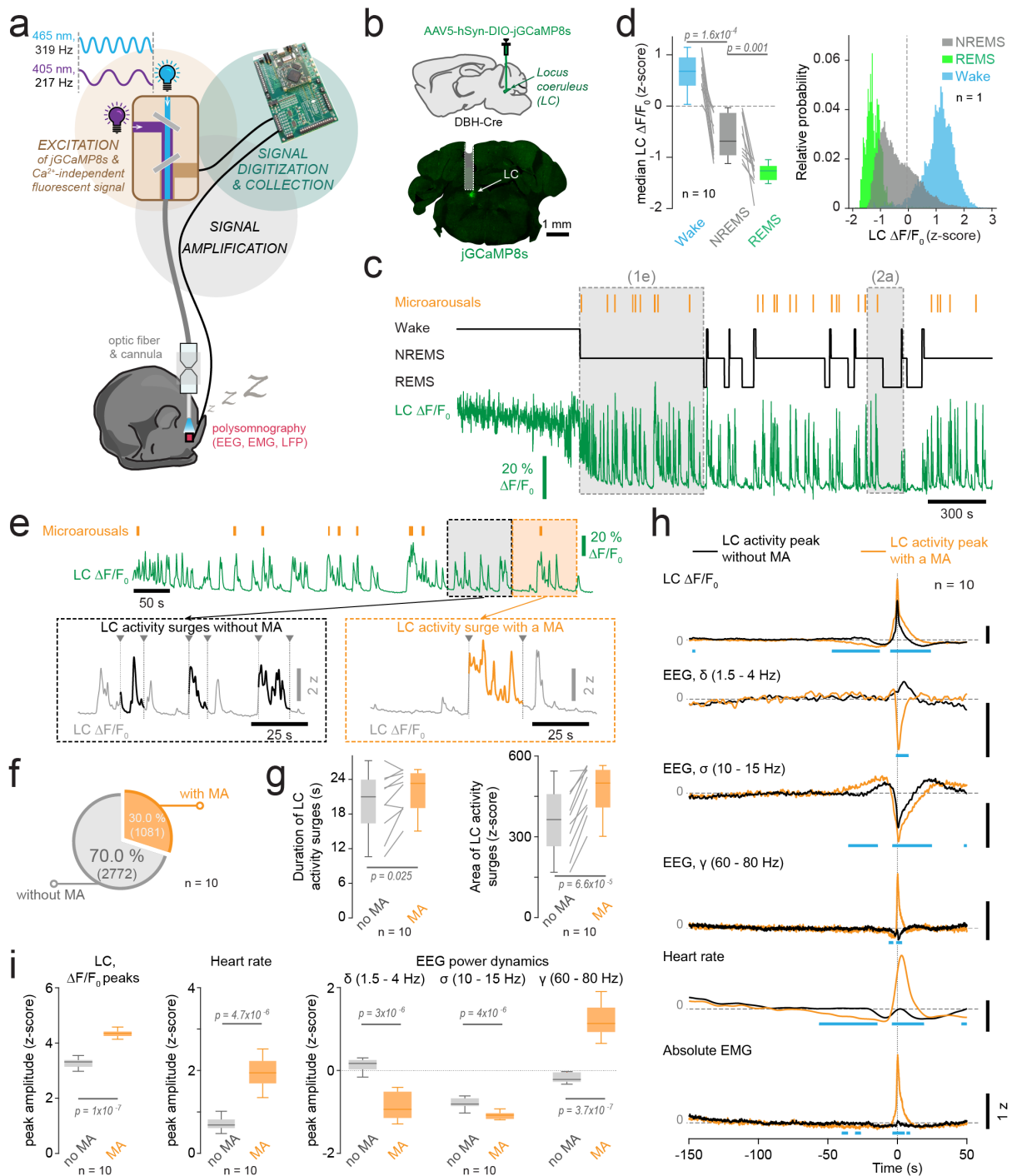
877

878

879

880

881 **Main figures and legends**



882

883

884 **Figure 1. Locus coeruleus (LC) activity surges during NREMS and associated brain and autonomic**

885 **arousal correlates**

886 a) Experimental scheme for sleep recordings in combination with fiber photometry of Ca²⁺

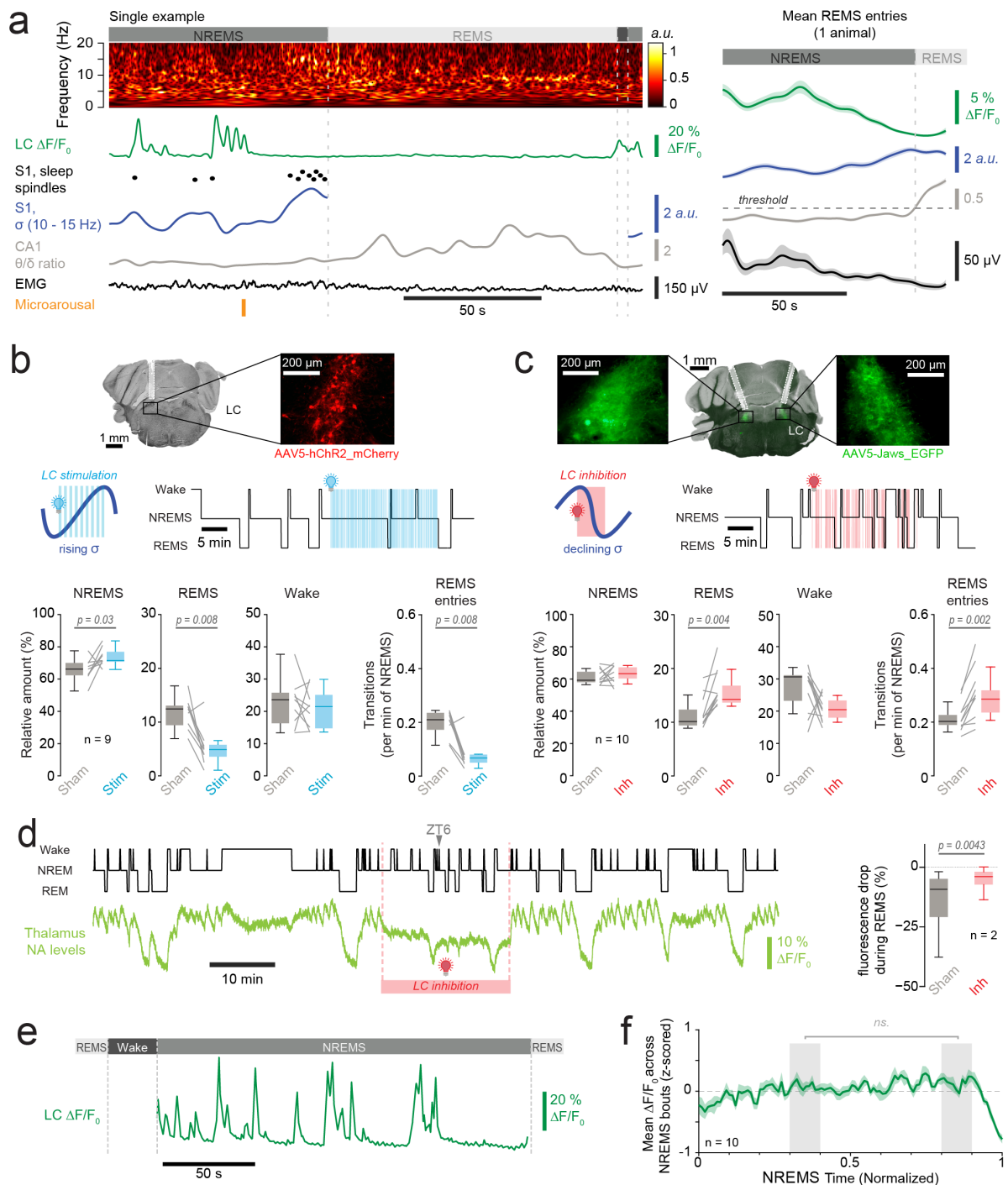
887 activity in the LC.

888 b) Schematic of viral injection into a dopamine- β -hydroxylase (DBH)-Cre mouse and example *post*

889 *hoc* histological verification of jGCaMP8s expression and optic fiber location.

- 890 c) Example sleep hypnogram (black) and jGCaMP8s fluorescent signal (green) recorded from LC
891 (in $\Delta F/F_0$). Orange vertical lines: microarousals (MAs). Grey rectangles: trace portions that are
892 expanded in other figure panels (as indicated).
- 893 d) Left, Box-and-whisker plot of mean LC fluorescence levels for wake, NREMS and REMS for
894 Zeitgeber times (ZT) ZT0-ZT2 for $n = 10$ animals, with grey lines connecting values for individual
895 animals; one-way repeated-measures ANOVA with *post hoc t*-tests, resulting p values are given
896 in the plot. Bonferroni-corrected $p = 0.025$. Right, all-points-histogram for z-scored
897 fluorescence across wake, NREMS and REMS for a representative animal. For further
898 information, see Extended Data Figure 1b.
- 899 e) Example trace expanded from panel c. Colored dotted rectangles indicate two trace portions
900 expanded below. For these expanded portions, thick traces show LC activity surges without
901 MAs (left) and with a MA (right). The on- and offset of these surges is marked with arrowheads
902 connected to vertical lines, as obtained from the analysis in Extended Data Figure 2.
- 903 f) Pie chart for proportion of LC activity surges without and with MA for $n = 10$ animals for ZT0-
904 ZT2. Numbers in parentheses are total counts.
- 905 g) Box-and-whisker plots for duration (left) and area (right) of LC activity surges identified as
906 illustrated in panel e for $n = 10$ animals. Grey lines connect mean values from individual
907 animals. Paired *t*-tests, with p values given in plot. Bonferroni-corrected $p = 0.025$.
- 908 h) Spectral analysis of EEG signals corresponding to LC activity peaks that were classified based
909 on whether they occurred without a MA (black) or with a MA (orange). Corresponding power
910 dynamics for the delta (δ), sigma (σ) and gamma (γ) frequency bands are aligned vertically, on
911 top of heart rate and absolute EMG. Traces are means across $n = 10$ animals. Blue bars denote
912 significant p values as calculated via false discovery rates (see Methods).
- 913 i) Quantification of mean peak values from traces shown in h in the time interval 0-1 s ($n = 10$).
914 Paired *t*-tests, with Bonferroni-corrected $p = 0.017$ for spectral power analyses.

915 See **Supplementary Table 1** for detailed statistical information.



916

917

918 **Figure 2. LC activity troughs during NREMS permit REMS entries.**

919 a) Left, Example recording of LC fluorescence during a NREMS-to-REMS transition ('REMS entry',
 920 from Figure 1c), together with S1 sleep spindles, and σ power, CA1 θ/δ ratio and absolute EMG.
 921 Right, Mean dynamics of these signals for the same animal. 3 more examples are shown in
 922 Extended Data Figure 4a.

923 b) Optogenetic stimulation of LC. Top, Histological verification of fiber positioning and viral
 924 transfection (red fluorescence). Middle, Schematic of the light stimulation protocol based on

925 closed-loop feedback analysis of σ power (left). Blue vertical lines show timing of optogenetic
926 stimulation (Stim), superimposed on example portion of hypnogram (right). Bottom, Box-and-
927 whisker-plot quantifications, calculated for the 20-min light vs sham (LED-off) stimulation
928 periods for $n = 9$ animals. Grey lines, paired datasets per animal. Wilcoxon signed-rank tests.

929 c) As b), for optogenetic inhibition (Inh) of LC ($n = 10$).

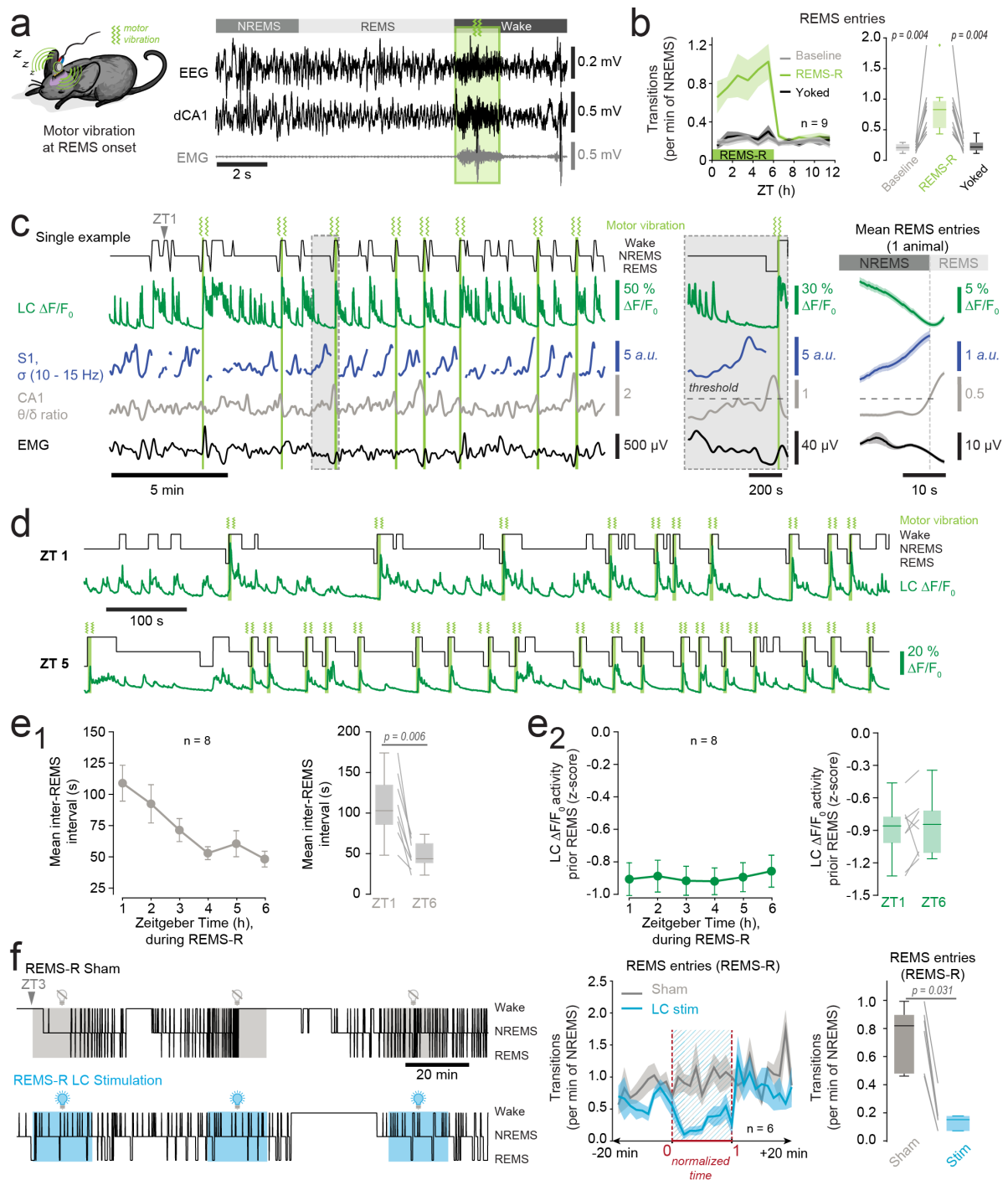
930 d) Example recording from an animal that expressed Jaws in LC and GRAB_{NE1h} in somatosensory
931 thalamus. Portion underlain with orange square indicates period of LC inhibition.
932 Quantification was done in $n = 2$ animals for 45 REMS bouts each in control and in light
933 illumination. REMS bouts in both conditions were selected for equal durations before
934 comparing GRAB_{NE1h} fluorescence decreases.

935 e) Example trace for LC fluorescence during a NREMS bout.

936 f) Mean LC fluorescence activity across time-normalized NREMS bouts ($n = 10$). Shaded areas,
937 data used for statistical analysis. Paired t -test.

938 See **Supplementary Table 1** for detailed statistical information.

939



940

941

942 **Figure 3. LC activity troughs rule REMS entries during REMS restriction (REMS-R).**

943 a) Schematic of REMS-R implementation and representative recording showing an interrupted
 944 REMS bout (green rectangle with motor vibration symbol).

945 b) Frequency of REMS entries for $n = 9$ animals subjected (in repeated sessions) to REMS-R from
 946 ZT0-ZT6, to yoked conditions (animals given vibrations timed to REMS from their neighbors)
 947 and to undisturbed conditions (baseline), followed by 6 h of recovery. To the right, box-and-

948 whisker plot quantifications, with grey lines showing paired data for individual animals (n = 9).
949 Wilcoxon signed-rank test.

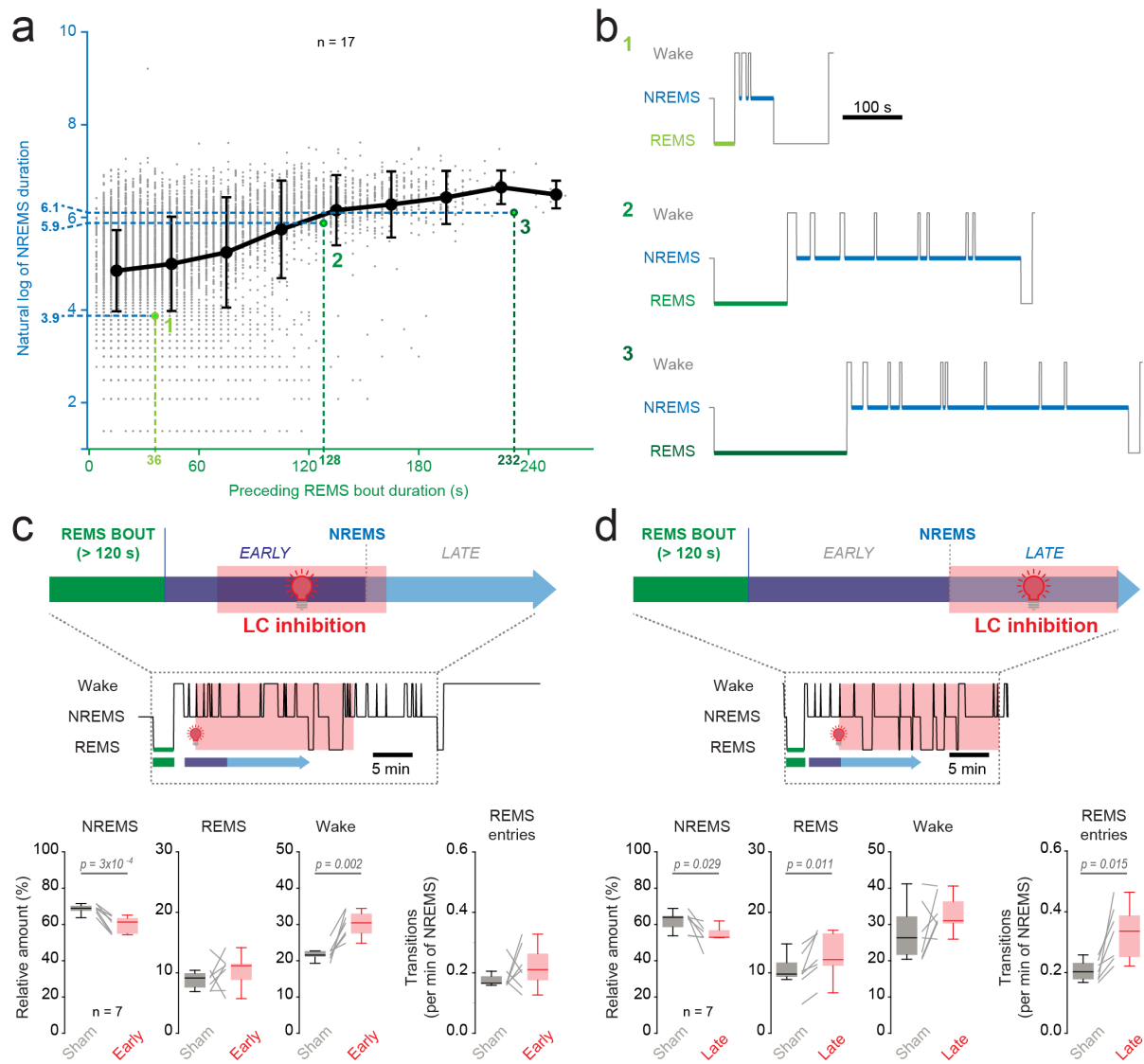
950 c) Example recording during REMS-R, with grey rectangle indicating portion expanded on the
951 right together with mean transitional dynamics calculated as in Figure 2a. More example
952 NREMS-REMS transitions are shown in Extended Data Figure 4b.

953 d) Example recording at ZT1 and at ZT5, corresponding to early and late moments during the
954 REMS-R.

955 e) e1) Quantification of hourly mean (inter-REMS) intervals across a 6 h-REMS-R, with boxplot for
956 ZT1 and ZT6 values shown on the right; e2) Same for LC activity levels in the 5 s before REMS
957 entries. Grey lines connect paired data per animal. Paired *t*-tests for e1 and e2 (n = 8 for both).

958 f) Example recording for a REMS-R combined with Sham (LED-off) or optogenetic stimulation of
959 LC at 1 Hz. Quantification of REMS entries across the stimulation period. Note the higher REMS
960 transition frequency before optogenetic stimulation compared to baseline sleep (Figure 2 b,
961 c). Box-and-whisker quantification of mean data for the entire REMS-R (n = 6). Wilcoxon
962 signed-rank test.

963 See **Supplementary Table 1** for detailed statistical information.

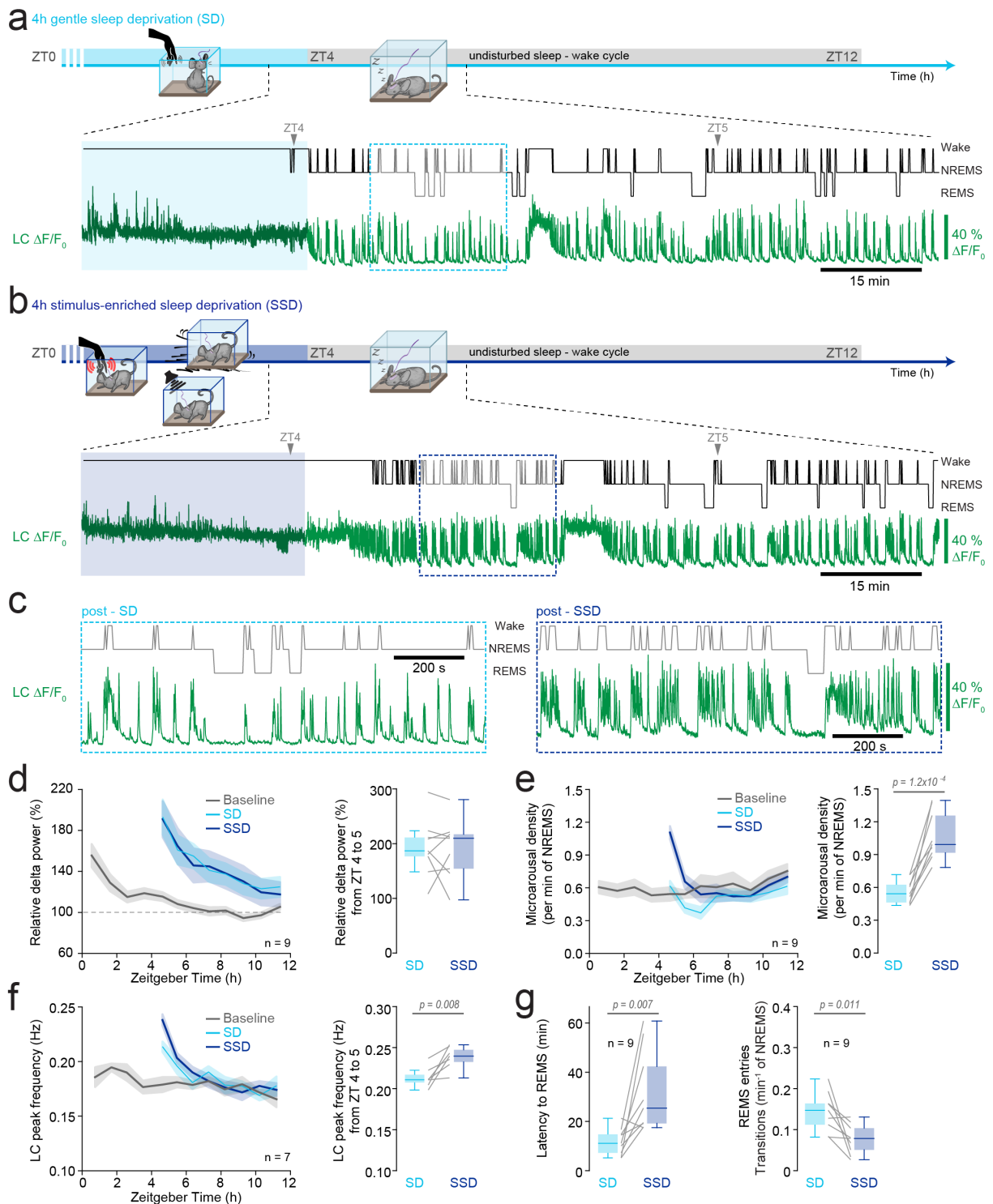


964
965
966
967
968
969
970
971
972
973
974
975
976
977

Figure 4. LC activity fluctuations were necessary for REMS entries late but not early in the natural NREMS-REMS cycle.

- a) Scatter plot of NREMS times (blue, in units of natural logarithm) vs preceding REMS bout durations (green) for undisturbed sleep of $n = 17$ animals in the light phase, as done in ref²⁶. Numbered datapoints mark examples shown in panel b.
- b) Representative examples for datapoints highlighted with numbers in panel a.
- c) Top, schematic of the LC optogenetic inhibition protocol starting early in the NREMS bout, once a REMS episode lasting > 120 s occurred. Example hypnogram is presented below. Box-and-whisker plots quantify times spent in wake, NREMS and REMS, and the frequency of REMS entries for early light inhibition ($n = 7$). Wilcoxon signed-rank or paired t -test.
- d) As c, for LC inhibition starting late in the NREMS bout ($n = 7$). Wilcoxon signed-rank or paired t -tests.

See **Supplementary Table 1** for detailed statistical information.



978

979

980 **Figure 5. A stimulus-enriched but not a gentle sleep deprivation disrupted subsequent sleep and**
 981 **enhanced LC activity**

982 a) Schematic of experimental timeline for gentle sleep deprivation (SD), with example
 983 hypnograms and corresponding LC activity from the end of the SD to 4 h in post-SD. Dotted
 984 rectangle indicates portion expanded in c.

- 985 b) As a, for the stimulus-enriched sleep deprivation (SSD). Dotted rectangle indicates portion
986 expanded in c.
- 987 c) Expanded portions of traces in a, b.
- 988 d) Mean dynamics of EEG δ (1.5 – 4 Hz) power for $n = 9$ animals subjected to baseline recordings,
989 SD and SSD. Box-and-whisker quantification for data from ZT4-ZT5, corresponding to the first
990 h after SD or SSD, with grey lines showing paired data per animal. Paired t -test.
- 991 e) As c, for the density of MAs ($n = 9$). Paired t -test.
- 992 f) As c, for LC peak frequency ($n = 7$). Paired t -test.
- 993 g) Box-and-whisker quantification for REMS onset latency, quantified from the time of NREMS
994 onset, and the frequency of REMS entries, for the first h after SD or SSD (ZT4-ZT5, $n = 9$). Paired
995 t -tests.

996 See **Supplementary Table 1** for detailed statistical information.

997

998

999

1000

1001

1002

1003

1004

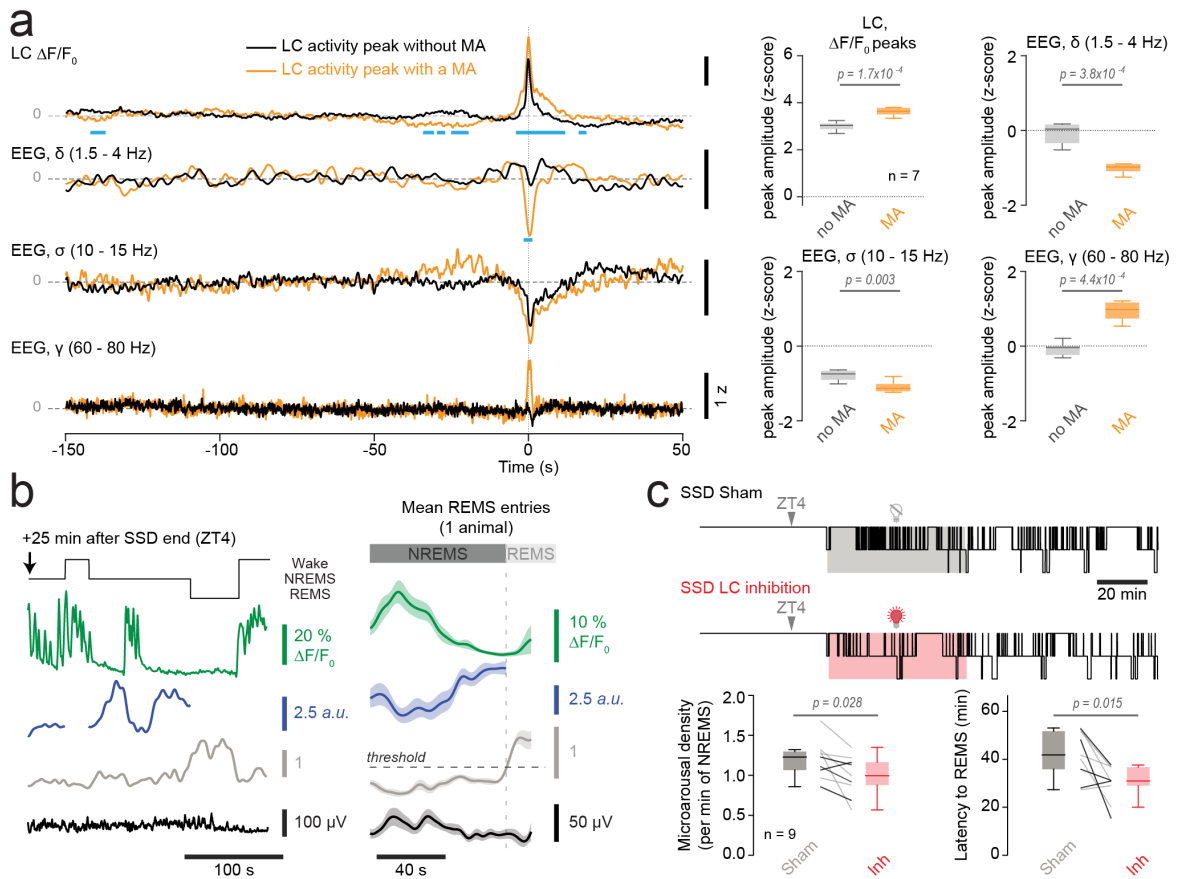


Figure 6. Acute LC inhibition suppressed sleep-disruptive effects of a stimulus-enriched wakefulness

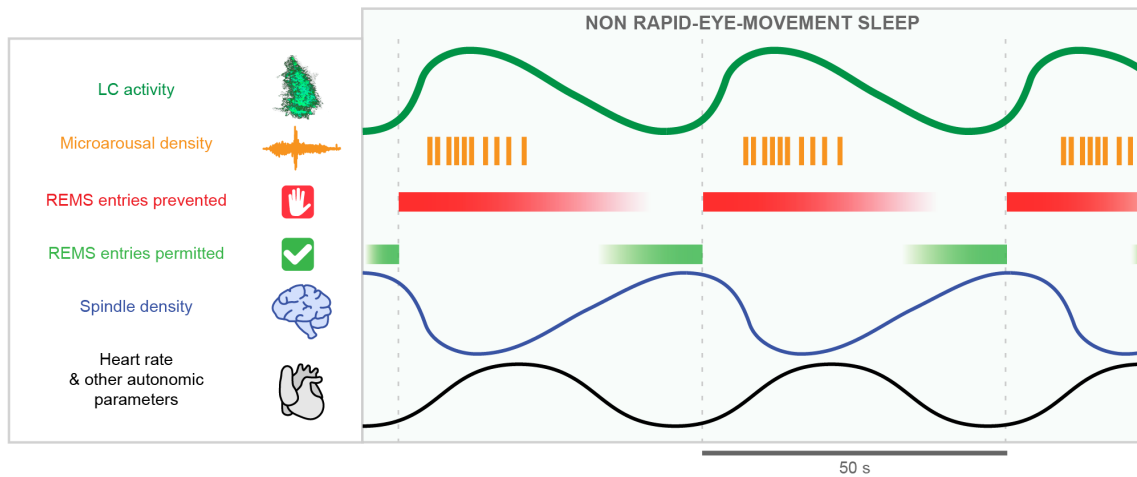
a) Spectral analysis of EEG signals corresponding to LC activity peaks, as done in Figure 1 h, for the first 2 h after the end of the SSD. LC activity peaks were classified based on whether they occurred without a MA (black) or with a MA (orange). Traces are means across $n = 7$ animals. Blue bars denote significant p values as calculated by false discovery rates. Quantification of mean peak values as in Figure 1i Paired t -tests, with Bonferroni-corrected $p = 0.017$ for spectral power analyses.

b) Example recording of a REMS entry after SSD. Mean transitional dynamics calculated as in Figure 2a.

c) Example hypnograms from one mouse after SSD with or without Jaws-mediated optogenetic inhibition of LC.

Box-and-whisker quantification of MA density and REMS onset latency after SSD with sham (LED-off) or light stimulation ($n = 9$). Grey and black lines connect data from animals exposed to 1-h or 2-h light-induced LC inhibition post-SSD. Paired t -test.

See **Supplementary Table 1** for detailed statistical information.



1022

1023 **Figure 7. Scheme summarizing the functional partitioning of NREMS and its relevance for the**
 1024 **NREMS-REMS cycle**

1025 From top to bottom, the time course of physiological parameters relevant for the partitioning of
 1026 NREMS into arousability-promoting/REMS-suppressing and REMS-promoting periods. Two full cycles
 1027 and one half cycle of this functional partitioning are shown-(vertical dashed lines). Red and Green Stop
 1028 and Go signals: REMS-suppressing and REMS-permissive periods. Other autonomic parameters include
 1029 pupil size fluctuations as demonstrated in ref⁵⁶.

1030

1031

1032

1033

1034

1035

1036

1037

1038

1039

1040

Noradrenergic *locus coeruleus* activity

functionally partitions NREM sleep to

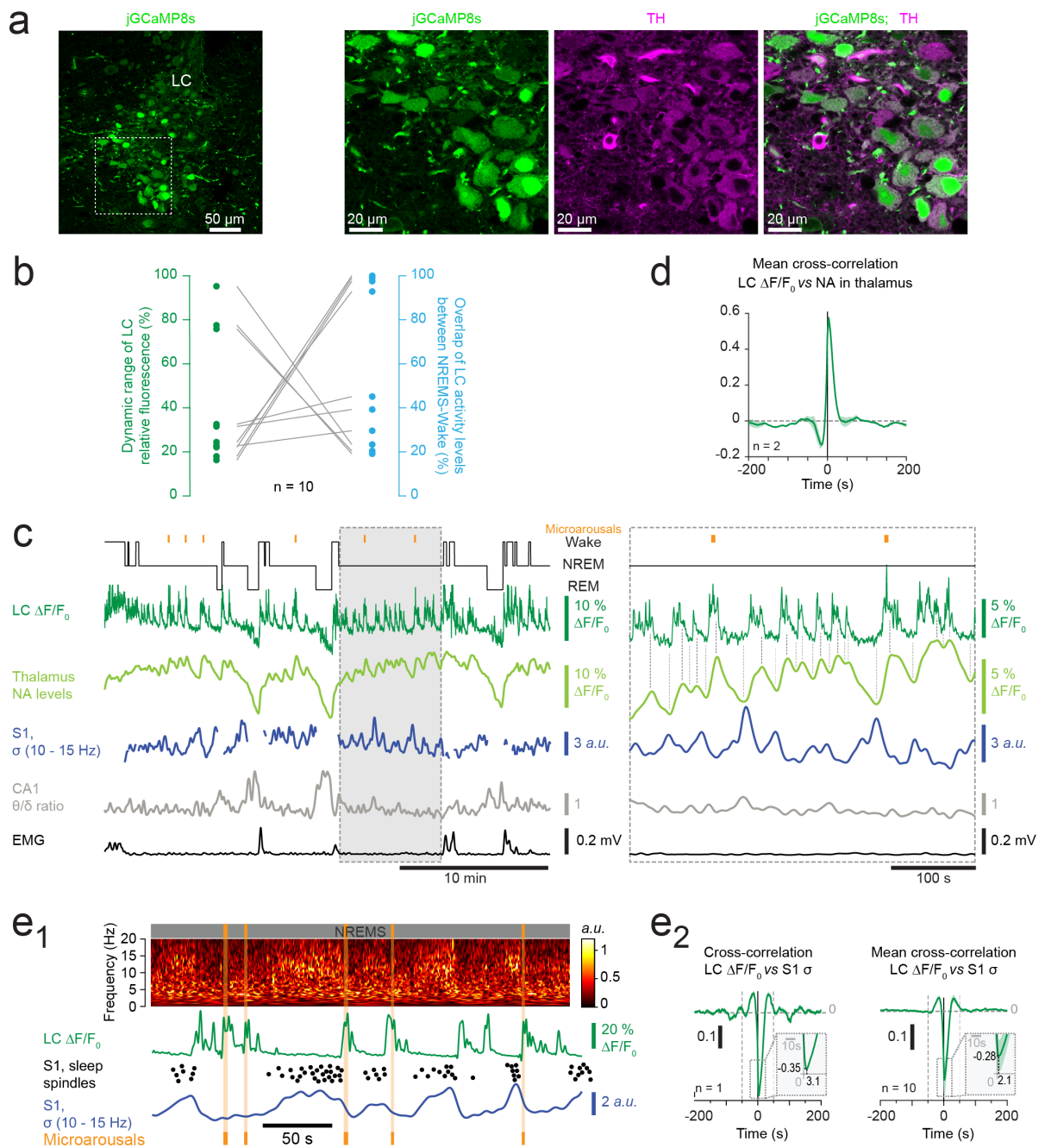
gatekeep the NREM-REM sleep cycle

Alejandro Osorio-Forero^{1,2}, Georgios Foustoukos¹, Romain Cardis¹, Najma Cherrad,
Christiane Devenoges, Laura M.J. Fernandez and Anita Lüthi

Extended Data Figures 1-8

and

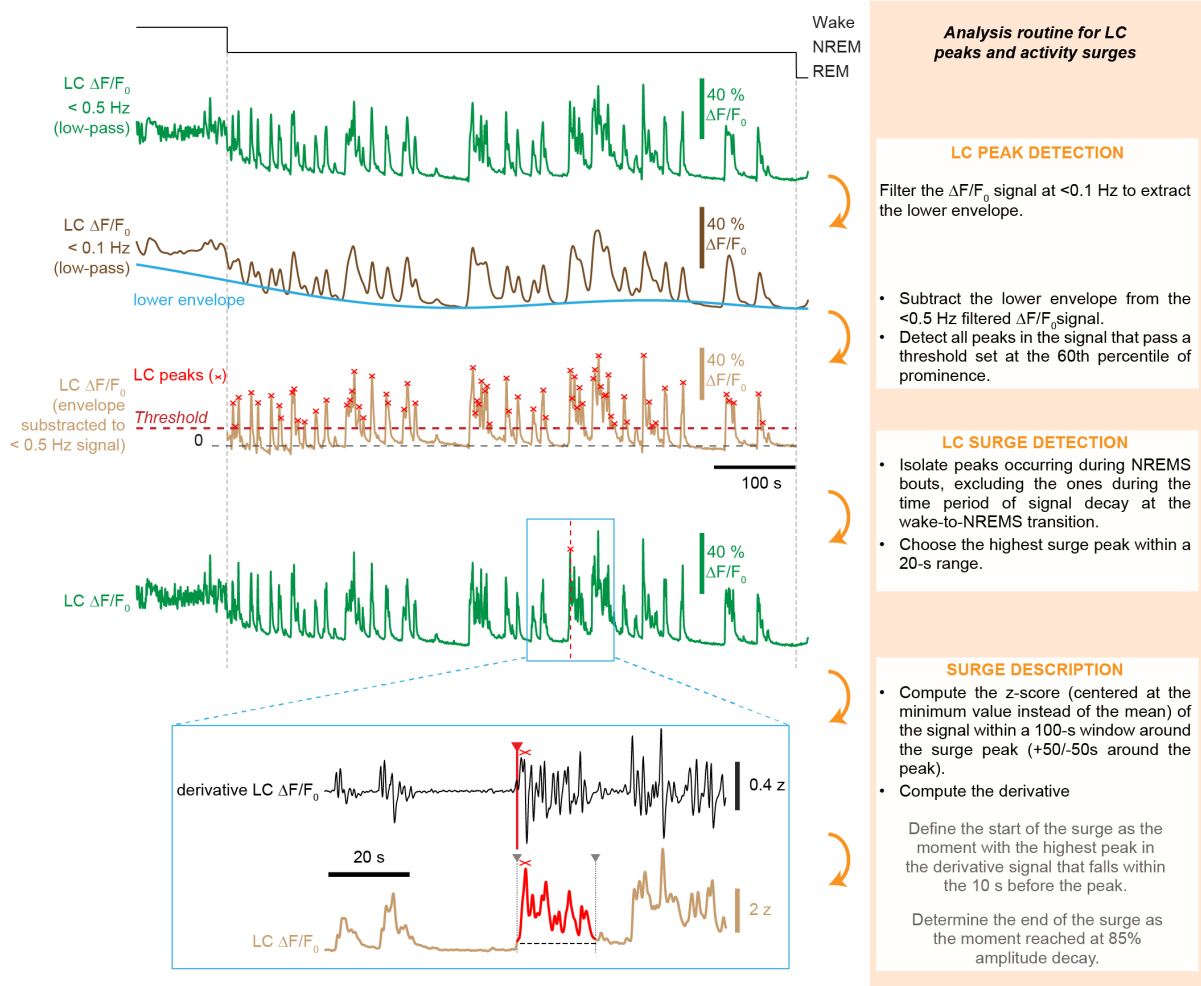
Extended Data Supplementry Tables 1 and 2.



Extended Data Figure 1. Histological verification of viral expression specificity and quantification of LC activity output during NREMS.

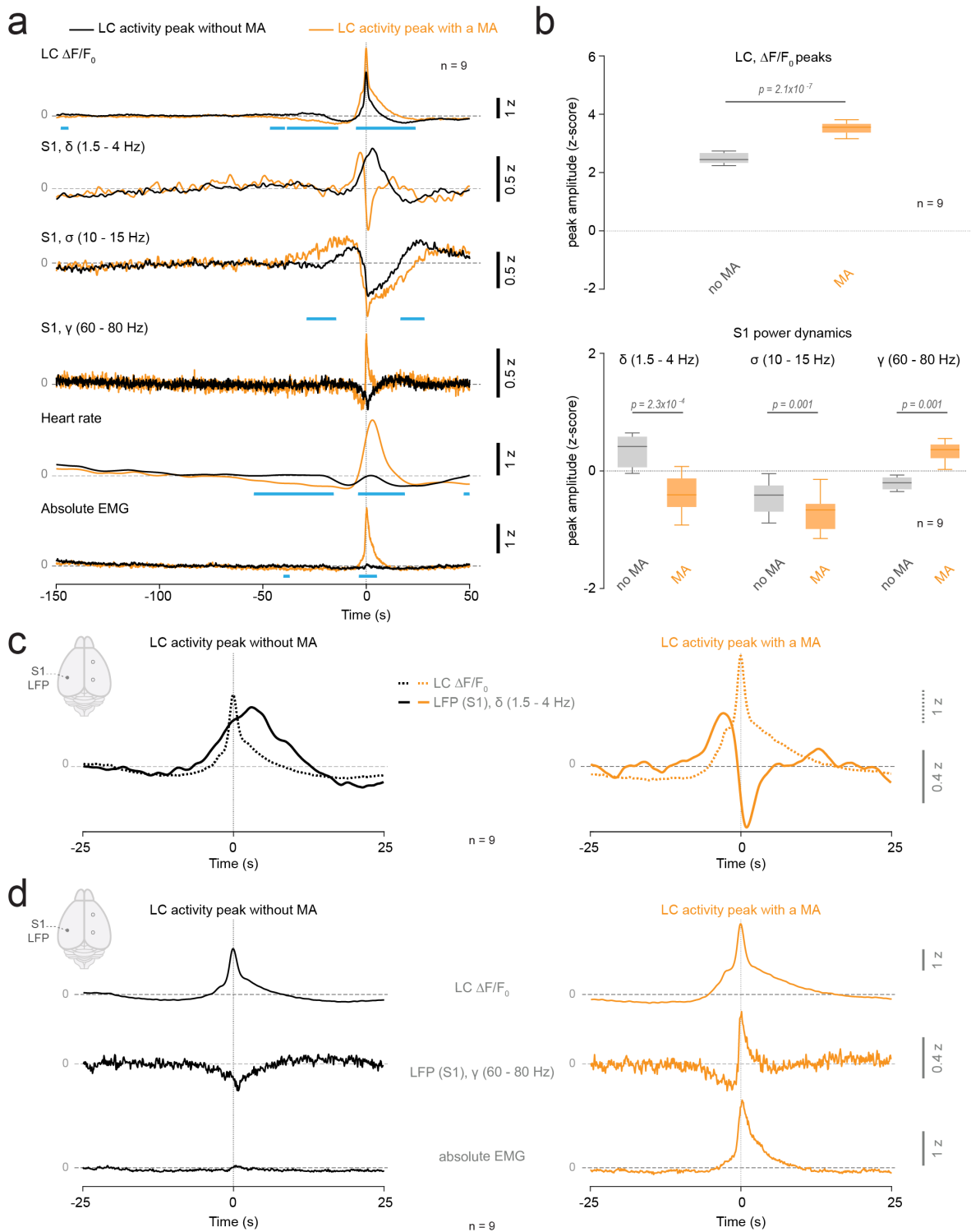
- a) Confocal micrographs taken from a representative DBH-Cre mouse expressing jGCaMP8s (green, same animal as **Figure 1c**) in the LC. Dotted square in the left image indicates the area expanded on the right, with corresponding immunostaining for tyrosine hydroxylase (TH, red) and overlay.

- b) Scatter plot highlighting the relationship between the dynamic range of the LC fluorescence signal (green dots) and the overlap of LC activity levels between Wake and NREMS (blue dots). This overlap was calculated up to a threshold of mean - 2 standard deviations of wake levels for $n = 10$ animals included in **Figure 1**. High dynamic ranges show the lowest overlap, whereas low dynamic ranges provide more variable values of overlap. The mean value of overlap indicated in the main text was calculated by taking the average across the blue datapoints.
- c) Example dual fiber photometric recording from an animal that expresses jGCaMP8s in LC and GRAB_{NE1h} in somatosensory thalamus. From the top, Hypnogram (black), LC-jGCaMP8s and free NA-GRAB_{NE1h} fluorescence, S1 LFP sigma (σ , 10 – 15 Hz) power, CA1 local field potential (LFP) theta/delta (θ/δ) ratio and absolute EMG levels. Portion of trace underlain in grey expanded on the right. Vertical lines highlight the coordination between LC and NA fluorescence signals.
- d) Mean cross-correlation of LC activity with free NA levels for 2 dual fiber photometric recordings in two DBH-Cre animals expressing jGCaMP8s in LC and the NA sensor GRAB_{NE1h} in primary somatosensory thalamus. Data from one such recording are shown in panel c. Cross-correlation coefficients: 0.56 and 0.59 at a positive lag of 2.9 and 3.1 s for the two recordings.
- e) Anticorrelation of LC activity and σ power. e1) Time-frequency plot of S1 LFP in NREMS, aligned with LC activity. Same recording as in Fig. 1c. S1 LFP σ (10 – 15 Hz) power and individual sleep spindles (black dots) shown below. e2) Cross-correlations for LC fluorescence and S1 σ power from ZT0-ZT12 (same animals as e1) and mean cross-correlation across $n = 10$ animals. Signals were anticorrelated with a time lag of 2.1 ± 0.5 s ($n = 10$) and showed side peaks at 48.3 ± 2.2 s, range 38.5 – 58.1 s, measured in $n = 6/10$ animals in which these side peaks were clearly detectable). Vertical dotted lines: side peaks. Insets; zoom-ins with crosscorrelation magnitude and lag values.



Extended Data Figure 2. Illustration of analysis routine to identify LC activity peaks and transients.

Step-by-step visual illustration of the algorithm, starting from the original LC fluorescence signals. From top to bottom, traces shown are: Hypnogram (black), corresponding LC fluorescent signal (green), low-pass-(0.1 Hz) filtered signal (dark brown) with lower envelope (blue), subtracted trace (light brown). On this last signal, peak analysis was carried out using a threshold and peak prominence $>40\%$ (for more details, see Methods). Detected peaks are indicated by red crosses. From these individual peaks, activity surges were identified, of which an example is given in red in the expanded trace portion surrounded by a blue rectangle.

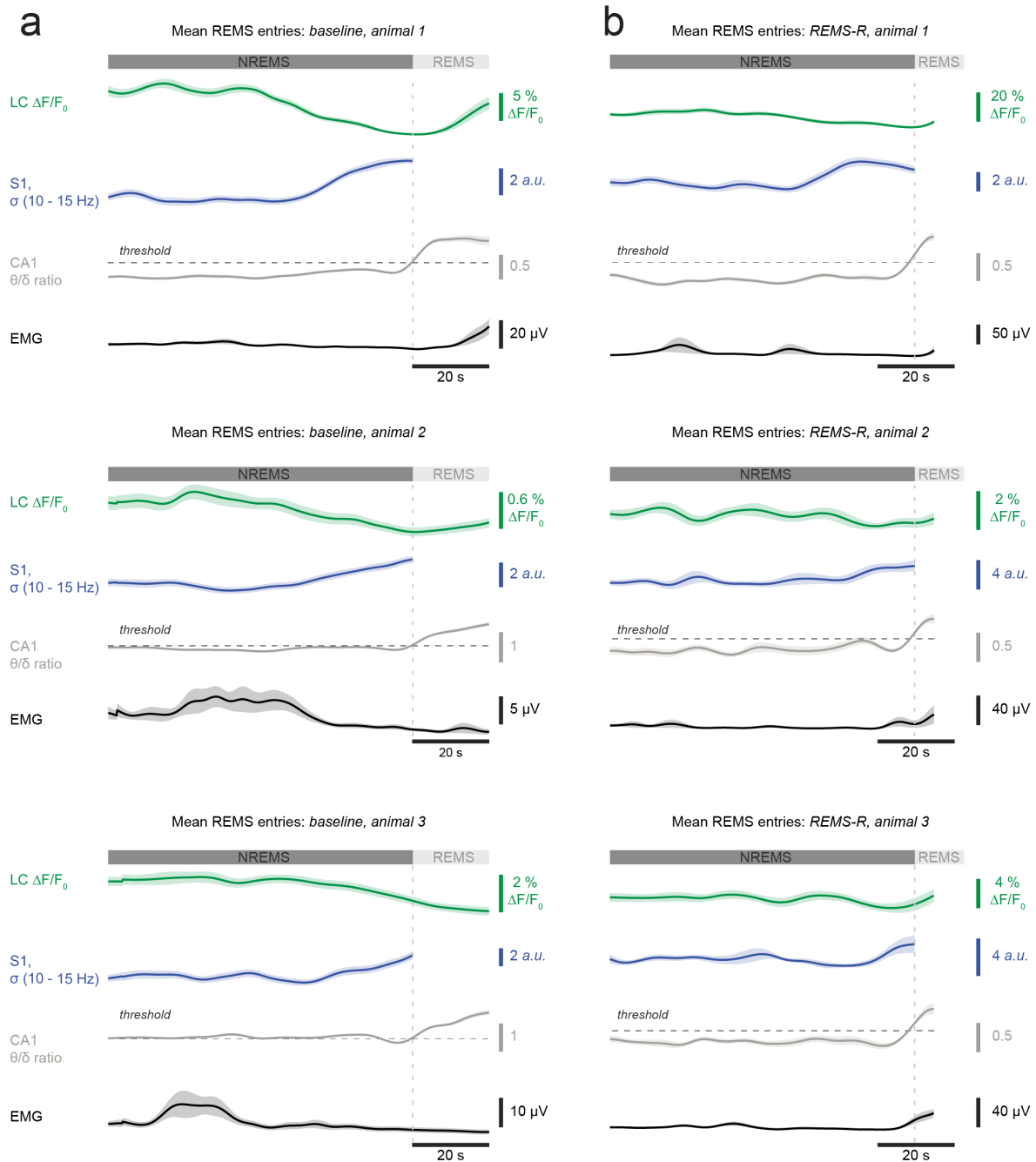


Extended Data Figure 3. Extended spectral analysis of LC activity peaks

- a) Spectral analysis of S1 LFP signals corresponding to LC peaks that were classified based on whether they did not (black traces) or did co-occur with a MA (orange traces). Corresponding power dynamics for the delta (δ), sigma (σ) and gamma (γ) frequency bands are aligned

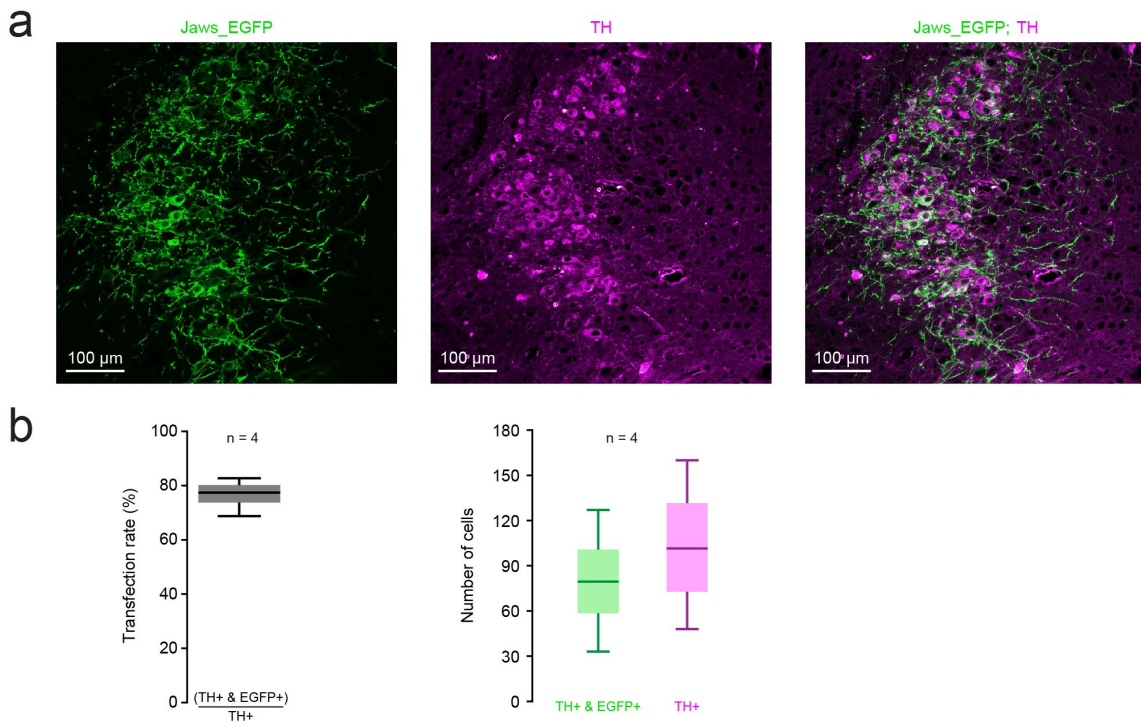
vertically, together with heart rate and absolute EMG. Traces are means across $n = 9$ animals. Blue bars denote significance as calculated by false discovery rates (see Methods, Statistics).

- b) Quantification of mean peak values as in **Figure 1i**.
- c) Overlay of LC signal (dotted line) and δ power (continuous line) on an expanded time scale, with traces taken from panel a, with the same color code. Note the increase in δ power accompanying the onset of the LC activity peak that becomes inverted to reach negative values in the case of a MA-associated LC activity peak (orange trace).
- d) As c, for LC signal and γ power.



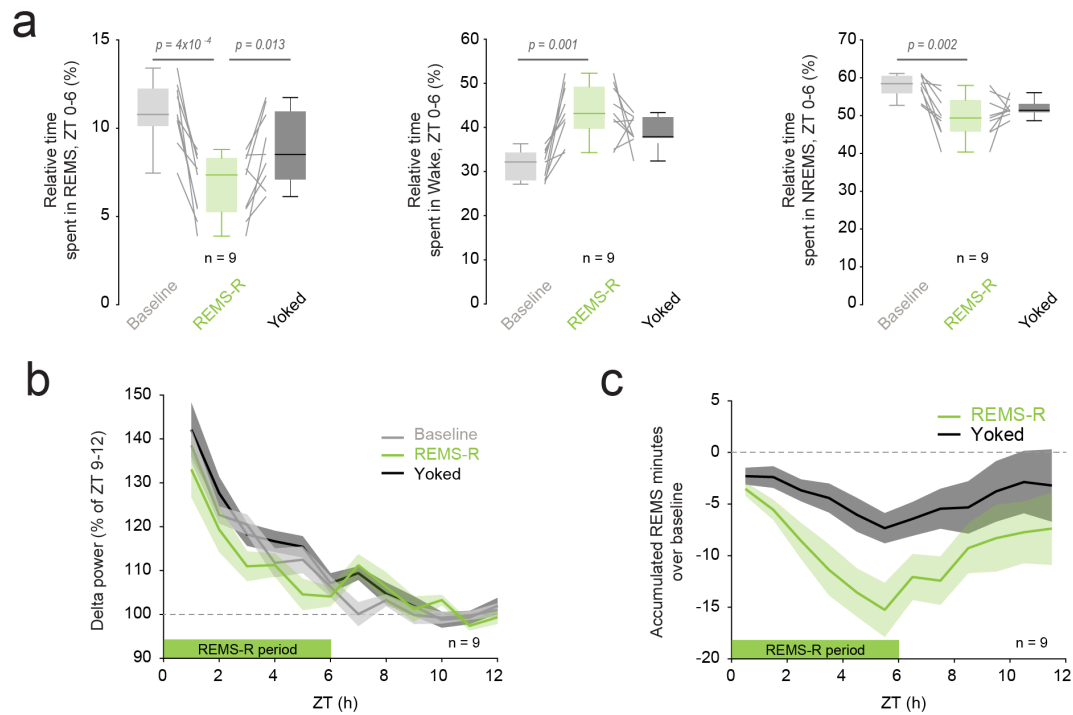
Extended Data Figure 4. Additional examples of LC activity and spectral dynamics at NREMS-to-REMS transitions.

- a) 3 recordings from 3 different mice during baseline recordings, presented as in Fig. 2a (mean of all transitions per mouse from ZT0-ZT2).
- b) 3 recordings from 3 different mice during REMS-R, presented as in Fig. 3c (mean of all transitions per mouse from ZT0-ZT6). The tendency for the EMG to increase during REMS in these mean traces is due to the interruption of REMS that leads to wake-up.



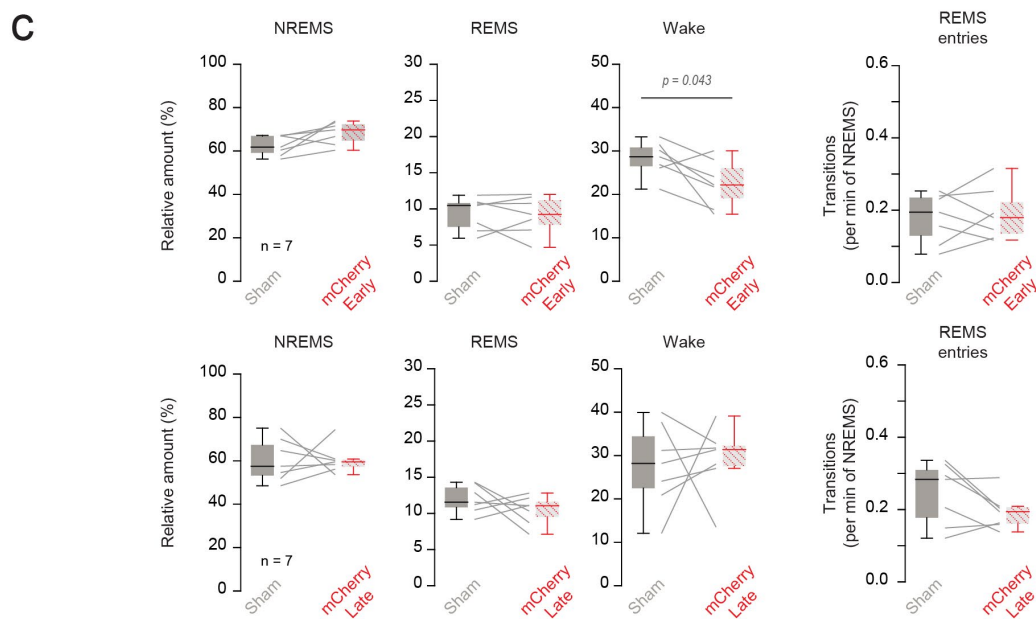
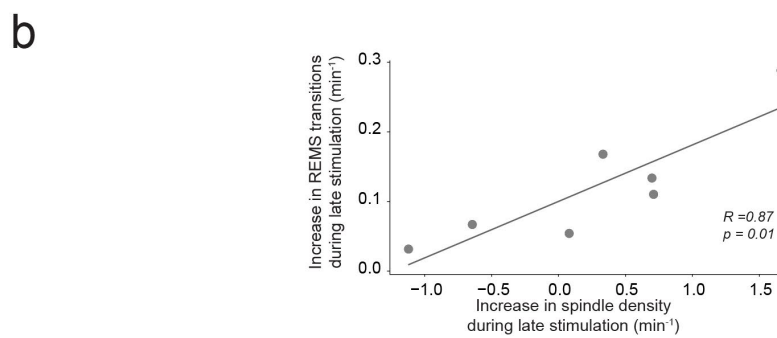
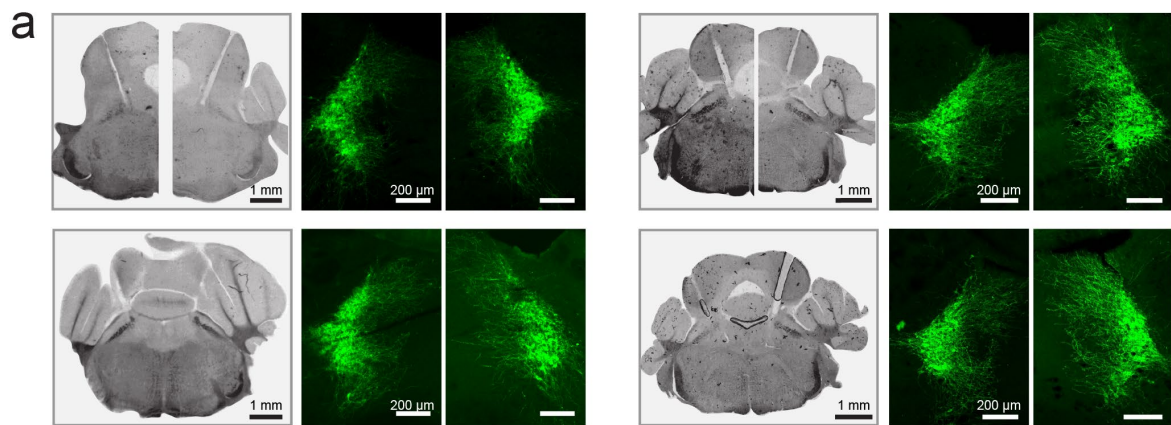
Extended Data Fig. 5. Quantification of viral transfection efficiency.

- a) Representative micrographs showing LC immunofluorescence for Jaws_EGFP (green) and TH (red), with overlay on the right.
- b) Mean transfection rate of viral injection, quantified as the ratio of Jaws_EGFP- and TH-expressing neurons in relation to the total number of TH-expressing neurons (n = 4 animals).
- c) Corresponding mean cell counts.



Extended Data Figure 6. Validation of the efficiency and specificity of the REMS-R technique.

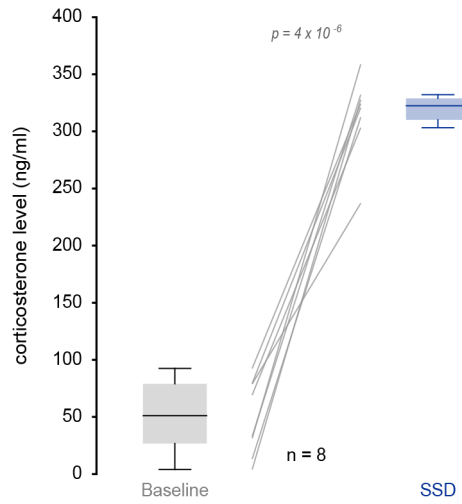
- Box-and-whisker plots of times spent in REMS, wake and NREMS for baseline, REMS-R and yoked conditions. Experiments were done in a paired design, with each animal once used for REMS-R and as yoked control. Paired data are connected with grey lines. Paired *t*-tests with Bonferroni corrected $p = 0.025$.
- The decline in low-frequency δ power (1.5 – 4 Hz) power in the 12-h light phase during which REMS-R was carried out from ZT0-ZT6.
- Cumulated time spent in REMS during the REMS-R and the subsequent recovery period in undisturbed conditions. Note the greater loss of REMS time during REMS-R compared to yoked animals, followed by recovery after the end of the REMS-R.



Extended Data Figure 7. Validating the efficiency of Jaws-mediated inhibition of LC using histological and functional methods.

- a) Representative fluorescent micrographs of 4 mice included in the experiment in **Figure 4c, d** illustrating EGFP fluorescence of Jaws-expressing LC neurons and position of optic fibers on top of LC.

- b) Linear correlation between light-induced sleep spindle density changes and REMS transitions for the experiment involving LC inhibition late in the undisturbed NREMS-REMS cycle (**Figure 4d**).
- c) Summary data of control experiments for the experiments described in **Figure 4c, d** using animals expressing non-light-sensitive (mCherry-expressing) viral constructs (n = 7). Sham corresponds to LED-off conditions. Paired *t*-tests or Wilcoxon signed-rank tests.



Extended Data Figure 8. Plasma corticosterone levels after SSD in comparison to undisturbed conditions at the same time of day.

Box-and-whisker plots, with grey lines connecting paired datasets taken at ZT4, once in baseline undisturbed sleep, once after a 4-h SSD for $n = 8$ animals. Paired t -test.

Extended Data Table S1. Statistical table for Main and Extended Data Figures.

This table describes statistical tests used for each figure/panel in this paper. Per figure panel, the number of animals, the test statistics (F/t values) and the degrees of freedom (Df/df) are indicated. P values are given in a separate column. Bonferroni-corrected p values are given in the legends when appropriate. Effect size is given whenever significance was reached.

Figs and panels	Test used	n numbers (animals unless otherwise indicated)	Test statistics (F, t) & degrees of freedom (Df, df)	P Value	Post hoc tests with multiple comparisons, Test statistics & df	Post-hoc tests, p values	Effect size (Cohen's D)
1d	One-way RM ANOVA with factor 'vigilance state)	10	F= 472.3, Df = 9	$4.36 * 10^{-9}$	For Wake vs NREMS: t = 6.192, df = 9 For NREMS vs REMS: t = 4.641, df = 9	For Wake vs NREMS: p=0.00016 For NREMS vs REMS: p = 0.0012	For Wake vs NREMS: D=3.24 For NREMS vs REMS: D=2.08
1g	Student's paired t-test	10	For duration of activity transients: t = -2.679; Df = 9 For area of activity transient: t = -6.959; Df = 9	For duration of activity transients: p = 0.025 For area of activity transients: p = $6.6 * 10^{-5}$			For duration of activity transient: D = -0.48 For area of activity transient: D = -1.11
1i	Student's paired t-test for measures between non-MA-associated and	10	For $\Delta F/F_0$ signal: t = -15.04, Df = 9 For delta power:	For $\Delta F/F_0$ signal: p = $1.09 * 10^{-7}$ For delta power:			For $\Delta F/F_0$ signal: D = -6.77 For delta power: D = 3.95

	MA-conditions		<p>t = 10.21, Df = 9</p> <p>For sigma power: t = 9.74, Df=9</p> <p>For gamma power: t=-13.09, Df=9</p> <p>For heart rate: t = -9.67, Df=9</p>	<p>p = 3.02×10^{-6}</p> <p>For sigma power: p = 4.4×10^{-6}</p> <p>For gamma power: p = 3.66×10^{-7}</p> <p>For heart rate: p = 4.73×10^{-6}</p>			<p>For sigma power: D = 2.54</p> <p>For gamma power: D = -4.71</p> <p>For heart rate: D = -3.87</p>
2b	Wilcoxon signed-rank for effects of LC stim compared to Sham Stim on % Time spent in Wake, NREMS and REMS and on REMS entries	9	<p>For Wake: V = 28</p> <p>For NREMS: V = 4</p> <p>For REMS: V=44</p> <p>For REMS entries: V=44</p>	<p>For Wake: p = 0.6</p> <p>For NREMS: p = 0.03</p> <p>For REMS: p=0.008</p> <p>For REMS entries: p=0.008</p>			<p>For NREMS: D = -1.28</p> <p>For REMS: D = 1.97</p> <p>For REMS entries: D = 2.28</p>
2c	Wilcoxon signed-rank for effects of LC inhibition compared to Sham Stimulation on % Time spent in Wake, NREMS and REMS	9	<p>For Wake: V = 43</p> <p>For NREMS: V = 22</p> <p>For REMS: V=1</p> <p>For REMS entries: V=0</p>	<p>For Wake: p = 0.13</p> <p>For NREMS: p = 0.63</p> <p>For REMS: p=0.004</p> <p>For REMS entries: p=0.002</p>			<p>For REMS: D = -1.35</p> <p>For REMS entries: D = -1.08</p>

2d	Wilcoxon signed-rank tests	N = 45 events for n = 2 animals	Test statistics for Wilcoxon test: V=269.0	p = 0.0043			
2f	One-way RM ANOVA with factor 'moment in NREMS bout'	10	F = 8.54, Df = 1	p = 0.017	For time points 0.3-0.4 vs 0.8-0.9 of NREMS bout: t = -3.0216, df = 9	p = 0.4936	
3b	Transitions to REMS: Wilcoxon signed-rank	9	Baseline vs REMSD: V = 0 REMSD vs Yoked: V = 45	Baseline vs REMSD: p = 0.0039 REMSD vs Yoked: p = 0.0039			Baseline vs REMSD: D = -2.04 REMSD vs Yoked: D = 1.91
3e1,e2	Inter REMS interval: Paired t-test LC activity before REMS entry: Paired t-test	8	Inter REMS interval: t = 5.86; df = 7 LC activity before REMS entry: t = -0.698; df = 7	Inter REMS interval: p = 0.0006 LC activity before REMS entry: p = 0.514			Inter REMS interval: D = 1.93
3f	Optogenetic LC stim during REMS-R Wilcoxon signed-rank	6	V=0	p = 0.031			D = 3.16
4c	Transitions to REMS: Wilcoxon	7	Transitions to REMS: V = 10.0	Transitions to REMS: p = 0.58			

	<p>signed-rank</p> <p>Time spent in REMS: Paired <i>t</i>-test</p> <p>Time spent in NREMS: Paired <i>t</i>-test</p> <p>Time spent in Wake: Paired <i>t</i>-test</p>		<p>Time spent in REMS: $t = -0.7263$; $df = 6$</p> <p>Time spent in NREMS: $t = 7.3184$; $df = 6$</p> <p>Time spent in Wake: $t = -5.1531$; $df = 6$</p>	<p>Time spent in REMS: $p = 0.4950$</p> <p>Time spent in NREMS: $p = 0.0003$</p> <p>Time spent in Wake: $p = 0.0021$</p>			<p>For time spent in NREMS: $D = 2.28$</p> <p>For time spent in wake: $D = -2.59$</p>
4d	<p>Transitions to REMS: Wilcoxon signed-rank</p> <p>Time spent in REMS: Paired <i>t</i>-test</p> <p>Time spent in NREMS: Paired <i>t</i>-test</p> <p>Time spent in Wake: Paired <i>t</i>-test</p>	7	<p>Transitions to REMS: $V = 0.0$</p> <p>Time spent in REMS: $t = -3.6183$; $df = 6$</p> <p>Time spent in NREMS: $t = 2.8396$; $df = 6$</p> <p>Time spent in Wake: $t = -1.6369$; $df = 6$</p>	<p>Transitions to REMS: $p = 0.0156$</p> <p>Time spent in REMS: $p = 0.0111$</p> <p>Time spent in NREMS: $p = 0.0295$</p> <p>Time spent in Wake: $p = 0.1527$</p>			<p>Transitions to REMS: $D = -1.76$</p> <p>Time spent in REMS: $D = -0.80$</p> <p>Time spent in NREMS: $D = 1.38$</p>

5d	Delta power increase after SD vs SSD Paired t-test	7	t = -0.145753; df = 8	p = 0.8877			
5e	MA density after SD vs SSD Paired t-test	7	t = 6.9188; df = 8	p = 0.000122			D = -2.86
5f	LC peak frequency after SD vs SSD Paired t-test	7	t = 3.84; df = 6	p = 0.008			D = -184
5g	REMS Latency: Wilcoxon signed-rank Transitions to REMS: Paired t-test	9	REMS Latency: V = 1.0 Transitions to REMS: t = 3.2497; df = 8	REMS Latency: p = 0.007 Transitions to REMS: p = 0.011			D = -1.59 D = 1.5833
6a	Student's paired t-test for measures between non-MA-associated and MA-conditions	7	$\Delta F/F_0$ signal: t = -8.2717, df = 6 Delta power: t = 7.1402, df = 6 Sigma power:	$\Delta F/F_0$ signal: p = 0.00017 Delta power: p = 0.00038 Sigma power: p = 0.0026			For $\Delta F/F_0$ signal: D = -3.48 For Delta power: D = 3.31 For Sigma power: D = 2.12

			t = 4.9354, df = 6 Gamma power: t = -8.2717, df = 6	Gamma power: p = 0.00044			For Gamma power: D = -4.49
6c	MA density: Paired t-test REM latency: Paired t-test	9	MA density: t = 2.677; df = 8 REM latency: t = 3.086 df = 8	MA density: p = 0.0280 REM latency: p = 0.0149			For MA density: D = 0.85 For REM latency: D = 1.36
Extended Data Fig 3b	Non-MA vs MA-associated LC peaks and spectral signatures Paired t-test	9	$\Delta F/F_0$ signal: t = -16.251, df = 8 Delta power: t = 6.3263, df = 8 Sigma power: t = 4.972, df = 8 Gamma power: t = -4.8073, df = 8	$\Delta F/F_0$ signal: p = $2.07 \cdot 10^{-7}$ Delta power: p = 0.00023 Sigma power: p = 0.0011 Gamma power: p = 0.0013			For $\Delta F/F_0$ signal: D = -5.17 For Delta power: D = 2.48 For Sigma power: D = 0.88 For Gamma power: D = -2.25
Extended Data Fig 6a	Time spent in REMS: Paired t-test	n = 9	Time spent in REMS: For Baseline vs REMS-R: t = 5.822; df = 8 For REMS-R	Time spent in REMS: For Baseline vs REMS-R: p = 0.0004 For REMS-R vs yoked: p = 0.0132			Time spent in REMS: D = 2.34 D = -1.11

	<p>Time spent in Wake: Paired <i>t</i>-test</p> <p>Time spent in NREMS: Paired <i>t</i>-test</p>		<p>vs yoked: $t = -3.171$; $df = 8$</p> <p>Time spent in Wake: For Baseline vs REMS-R: $t = -4.933$; $df = 8$</p> <p>For REMS-R vs yoked: $t = 1.611$; $df = 8$</p> <p>Time spent in NREMS: For Baseline vs REMS-R: $t = 4.346$; $df = 8$</p> <p>For REMS-R vs yoked: $t = -1.024$; $df = 8$</p>	<p>Time spent in Wake: For Baseline vs REMS-R: $p = 0.0011$</p> <p>For REMS-R vs yoked: $p = 0.1459$</p> <p>Time spent in NREMS: For Baseline vs REMS-R: $p = 0.0025$</p> <p>For REMS-R vs yoked: $p = 0.3357$</p>		<p>Time spent in Wake: $D = -2.41$</p> <p>Time spent in NREMS: $D = 1.78$</p>
<p>Extended Data Fig 7c</p>	<p><u>Early</u></p> <p>Transitions to REMS: Paired <i>t</i>-test</p> <p>Time spent in REMS:</p>	<p>$n = 7$</p>	<p><u>Early</u></p> <p>Transitions to REMS: $t = -0.4087$; $df = 6$</p> <p>Time spent in REMS: $t =$</p>	<p><u>Early</u></p> <p>Transitions to REMS: $p = 0.6968$</p> <p>Time spent in REMS: $p = 0.8514$</p>		

	Paired <i>t</i> -test		0.1955; df = 6				
	Time spent in NREMS: Paired <i>t</i> -test		Time spent in NREMS: t = -2.3997; df = 6	Time spent in NREMS: p = 0.053			
	Time spent in Wake: Paired <i>t</i> -test		Time spent in Wake: t = 2.5490; df = 6	Time spent in Wake: p = 0.0435			
	Late:		Late	Late			
	Transitions to REMS: Paired <i>t</i> -test		Transitions to REMS: t = 1.9133; df = 6	Transitions to REMS: p = 0.1042			
	Time spent in REMS: Paired <i>t</i> -test		Time spent in REMS: t = 1.1423; df = 6	Time spent in REMS: p = 0.2968			
	Time spent in NREMS: Wilcoxon signed-rank		Time spent in NREMS: V = 13; df = 6	Time spent in NREMS: p = 0.9375			
	Time spent in Wake: Paired <i>t</i> -test		Time spent in Wake: t = -0.2941; df = 6	Time spent in Wake: p = 0.8226			

Extended Data Fig. 8	t-test	8	t = -12.8; df = 7	p = 4*10 ⁻⁶			D = -7.65
-----------------------------	--------	---	----------------------	---------------------------	--	--	-----------

Extended Data Table 2.

Full information on sleep-wake times (in % of time) and of REMS transitions (min⁻¹ of NREMS). For calculation of times spent, the time periods of optogenetic manipulations were taken into account. All other times are specified in the Table.

Figure 1							
All the recording (BL)							
Animal	Wake	NREM	REM				
CI03	31,14	57,84	9,62				
CI05	35,89	53,27	10,84				
CI06	40,38	50,94	8,46				
CI07	35,71	53,77	9,19				
CI08	30,85	58,59	10,52				
CI10	25,09	59,31	11,79				
CI13	32,08	56,30	10,45				
CI14	32,00	58,01	9,65				
LCTH01	37,15	52,43	10,33				
LCTH03	20,71	63,51	10,83				
Figure 1							
First 2 hr (BL)							
Animal	Wake	NREM	REM				
CI03	35,50	54,89	9,56				
CI05	42,94	49,08	7,94				
CI06	66,03	29,11	4,69				
CI07	55,97	38,36	5,53				
CI08	28,22	61,67	10,11				
CI10	16,17	67,17	10,42				
CI13	30,28	57,17	11,06				
CI14	50,78	45,39	3,50				
LCTH01	62,47	34,58	2,78				
LCTH03	18,75	70,03	9,25				
Figure 2b							
Animal	Wake		NREM		REM		
	Sham	Stm	Sham	Stm	Sham	Stm	
Os17	26,86	29,11	66,22	69,82	6,92	1,06	
Os18	17,15	21,88	70,41	71,54	12,45	6,58	

Os19	37,68	23,76	52,6	71,33	9,72	4,91		
Os21	13,86	29,92	77,53	65,98	8,61	4,09		
Os22	20,51	15,09	67,8	71,19	11,68	13,72		
Os23	13,38	13,78	69,87	83,7	16,75	2,51		
Os24	25,39	13,59	61,83	80,89	12,78	5,51		
Os25	24,56	21,48	62,54	74,59	12,9	3,93		
Os26	23,6	19,36	62,89	75,53	13,51	5,11		

Figure 2c

Animal	Wake		NREM		REM			
	Sham	Inh	Sham	Inh	Sham	Inh		
Li01	29,77	20,43	56,02	55,68	14,22	23,89		
Li06	30,93	17,19	60,03	67,78	9,05	15,03		
Li08	34,47	16,68	55,83	68,18	9,7	15,14		
Li10	30,99	22,4	59,2	64,22	9,81	13,38		
Li12	19,6	18,81	69,4	68,09	10,99	13,09		
Li14	25,77	15,13	63,44	69,74	10,79	15,12		
Li15	32,1	24,75	57,92	61,03	9,97	14,22		
Li16	30,8	21	58,07	59,3	11,13	19,7		
Li18	17,46	26,18	67,86	53,81	18,3	19,14		
Li17	13,84	27,05	66,62	58,47	15,92	15,35		

Figure 3c

Animal	NREM	REM	Wake	REMS entries				
CI03	52,777 75	7,2222 2	40	1,177985 5				
CI04	45,416 65	8,2777 8	46,305 55	1,76122				
CI05	48,898 1	7,2222 2	43,879 6	1,403972				
CI06	47,796 3	5,0462 95	47,157 4	0,846716 5				
CI07	47,768 5	5,2592 6	46,972 2	1,059294 5				
CI10	47,185 2	7,6481 5	45,166 7	1,83673				
CI13	55,425 9	5,7222 2	38,851 9	0,596392				
CI14	54,907 4	5,2963	39,796 3	0,667791				

Figure 4c

	NREMS		REMS		Wake		REM entries	
Animal	Sham	Light	Sham	Light	Sham	Light	Sham	Light

RT05	68,258 3	55,413 02	9,1536 58	14,15690 82	9,1536584 6	14,156 91	0,1647 28	0,3278 29
RT09	66,859 79	54,344 94	13,839 62	11,52339 5	13,839624 37	11,523 4	0,2779 97	0,2001 36
RT10	71,391 76	65,105 11	7,0307 5	7,081335 71	7,0307501 8	7,0813 36	0,1720 98	0,1268 1
RT11	63,736 25	54,413 99	9,4598 45	11,16957 73	9,4598445 5	11,169 58	0,1630 95	0,2992 57
RT13	69,175 93	64,590 15	8,1185 24	10,58163	8,118524	10,581 63	0,1590 33	0,2275 77
RT15	68,879 57	62,422 54	10,407 39	5,746108	10,407394 17	5,7461 08	0,2051 23	0,1515 29
RT18	71,537 06	61,293 81	6,9007 85	11,45750 1	6,9007852 4	11,457 5	0,1655 15	0,2107 03

Figure 4d

	NREMS		REMS		Wake		REM entries	
Animal	Sham	Light	Sham	Light	Sham	Light	Sham	Light
RT05	53,768 41	52,964 03	9,7868 65	17,03562 8	36,44475	30,000 36	0,1759 25	0,4642 29
RT09	64,821 76	52,951 6	14,776 41	16,48778 57	20,401802 14	30,560 62	0,2580 53	0,3683 65
RT10	63,904 1	61,883 75	9,7887 58	12,17932 83	26,307163 64	25,936 91	0,2237 4	0,2553 58
RT11	64,511 94	43,711 21	13,147 71	16,53928 73	22,340343 53	39,749 5	0,2392 56	0,4072 43
RT13	63,113 12	56,085 66	8,8972 19	10,95404	27,989666 67	32,960 27	0,1672 12	0,2213 49
RT15	54,030 79	52,720 17	4,7992 35	6,693905 8	41,169970 67	40,585 9	0,1796 09	0,2465 99
RT18	68,820 96	57,575 02	10,273 7	11,39041 56	20,905345 45	31,034 57	0,2024 84	0,3361 89

Figure 5, 1st h after SD

Animal	NREM	REM	Wake	REMS entries				
CI03	75,055 55	12,277 8	12,666 67	0,156118				
CI04	82,888 9	12,777 8	4,3333 3	0,140751				
CI05	80,555 55	10,444 45	8,9999 9	0,155116				
CI06	78,833 35	13,277 8	7,8888 9	0,179816 5				
CI07	76,277 75	6	17,722 25	0,077361 1				

CI10	84	8,6666 7	7,3333 3	0,079365 1				
CI13	79,555 6	12,222 2	8,2222 2	0,209497				
CI14	78	12,111 1	9,8888 9	0,106838				

Figure 5, 1st h after SSD

mouse_name	NREM	REM	Wake	REMS entries				
CI03	76,666 7	4,2222 2	19,111 1	0,108696				
CI04	82,111 1	6,6666 7	11,222 2	0,060893 1				
CI05	70,777 8	5,5555 6	23,666 7	0,094191 5				
CI06	57,111 1	0,6666 67	42,222 2	0,029182 9				
CI07	70,444 4	4,2222 2	25,333 3	0,070977 9				
CI10	69,888 9	0,2222 22	29,888 9	0,023847 4				
CI13	73	2,7777 8	24,222 2	0,045662 1				
CI14	71,444 4	6,3333 3	22,222 2	0,069984 5				

Figure 6, for the LC inhibition window after SSD

Animal		NREM	REM	Wake	REMS entries			
NEJaws01	Sham	63,565 9	0,5537 1	35,8804	0,0522648			
	Stim	61,836 3	4,0929 2	34,0708	0,0805009			
RT15	Sham	81,526 6	5,6415 9	12,8319	0,162822			
	Stim	68,327 8	2,9900 3	28,6822	0,0486224			
RT20	Sham	53,266 9	2,4363 2	44,2968	0,0623701			
	Stim	61,572 5	3,5437 4	34,8837	0,0539568			
RT29	Sham	62,610 6	2,1017 7	35,2876	0,0530035			
	Stim	51,106 2	1,7699 1	47,1239	0,0324675			

RT31	Sham	64,712 4	1,2168 1	34,0708	0,025641			
	Stim	47,345 1	0,6637 17	51,9911	0,0350467			
RT35	Sham	56,333 3	4,8333 3	38,8333	0,0591716			
	Stim	65,968 9	6,9547 6	27,0763	0,184237			
RT42	Sham	56,755 3	4,7619	38,4828	0,0878049			
	Stim	62,977 3	6,9175 4	30,1051	0,237258			
RT43	Sham	65,67	4,6511 6	29,6788	0,10118			
	Stim	55,893 7	6,1427 8	37,9635	0,0891089			
RT44	Sham	74,986 2	4,4825 7	20,5313	0,0774908			
	Stim	54,510 2	4,5379 1	40,9519	0,0609137			

Extended Data Figure 7

% time spent in NREMS, REMS wake and REM entries (min-1 of NREMS) for early stimulation								
	NREMS		REMS		Wake		REM entries	
Animal	Sham	Light	Sham	Light	Sham	Light	Sham	Light
RT07	66,976 37	62,874 3	6,9515 09	7,075566 67	26,072122 73	30,050 12	0,1026 76	0,1916 62
RT08	67,184 21	69,738 47	5,9391 43	8,533639 17	26,876634	21,727 89	0,0786 5	0,1231 92
RT14	56,261 69	60,353 79	10,472 04	11,63659 98	33,26625	28,009 59	0,2306 73	0,3153 59
RT22	57,839 3	73,794 41	10,687 1	10,75432 2	31,473605 71	15,451 25	0,1944 87	0,1464 96
RT23	60,415 88	66,687 96	10,934 22	9,227985 56	28,649912 38	24,084 05	0,2532 26	0,1795 72
RT25	66,885 99	71,502 49	11,881 4	12,00039 5	21,208870 71	16,497 11	0,2394 4	0,2524 52
RT27	61,762 71	73,155 59	8,0406 22	4,683341 25	30,171112 31	22,161 09	0,1561 52	0,1174 26
% time spent in NREMS, REMS wake and REM entries (min-1 of NREMS) for late stimulation								
	NREMS		REMS		Wake		REM entries	
Animal ID	Sham	Light	Sham	Light	Sham	Light	Sham	Light
RT07	69,967 65	60,838 29	9,1672 08	11,11868 33	20,86515	28,043 02	0,1206 28	0,1632 52

RT08	64,713 46	60,155 52	11,212 38	12,80748 91	24,074174 55	27,037	0,1489 27	0,1588 84
RT14	48,505 99	56,165 56	11,551 45	11,06279 83	39,94255	32,771 65	0,2832 3	0,2881 83
RT22	51,837 75	74,374 68	10,456 43	12,12421 31	37,705822	13,501 1	0,2942 03	0,2090 16
RT23	57,510 12	58,312 52	14,311 02	10,32463 5	28,178864 62	31,362 84	0,3251 67	0,1938 13
RT25	54,572 33	59,538 24	14,249 23	8,722582 22	31,17844	31,739 18	0,3360 25	0,2034 46
RT27	75,055 81	53,612 98	12,886 13	7,121675	12,058042 5	39,099 8	0,2054 26	0,1381 26



Review

When the Locus Coeruleus Speaks Up in Sleep: Recent Insights, Emerging Perspectives

Alejandro Osorio-Forero , Najma Cherrad , Lila Banterle , Laura M. J. Fernandez and Anita Lüthi *

Department of Fundamental Neurosciences, University of Lausanne, CH-1005 Lausanne, Switzerland; alejandro.osorioforero@unil.ch (A.O.-F.); najma.cherrad@unil.ch (N.C.); lila.banterle@unil.ch (L.B.); laura.fernandez@unil.ch (L.M.J.F.)

* Correspondence: anita.luthi@unil.ch

Abstract: For decades, numerous seminal studies have built our understanding of the *locus coeruleus* (LC), the vertebrate brain's principal noradrenergic system. Containing a numerically small but broadly efferent cell population, the LC provides brain-wide noradrenergic modulation that optimizes network function in the context of attentive and flexible interaction with the sensory environment. This review turns attention to the LC's roles during sleep. We show that these roles go beyond down-scaled versions of the ones in wakefulness. Novel dynamic assessments of noradrenaline signaling and LC activity uncover a rich diversity of activity patterns that establish the LC as an integral portion of sleep regulation and function. The LC could be involved in beneficial functions for the sleeping brain, and even minute alterations in its functionality may prove quintessential in sleep disorders.

Keywords: NREM sleep; REM sleep; monoamine; noradrenaline; arousability; sleep architecture; infraslow time scale; microvasculature; sleep disorder; Alzheimer's disease



Citation: Osorio-Forero, A.; Cherrad, N.; Banterle, L.; Fernandez, L.M.J.; Lüthi, A. When the Locus Coeruleus Speaks Up in Sleep: Recent Insights, Emerging Perspectives. *Int. J. Mol. Sci.* **2022**, *23*, 5028. <https://doi.org/10.3390/ijms23095028>

Academic Editors: Michael Lazarus and Wang Yi-Qun

Received: 28 February 2022

Accepted: 19 April 2022

Published: 30 April 2022

Publisher's Note: MDPI stays neutral with regard to jurisdictional claims in published maps and institutional affiliations.



Copyright: © 2022 by the authors. Licensee MDPI, Basel, Switzerland. This article is an open access article distributed under the terms and conditions of the Creative Commons Attribution (CC BY) license (<https://creativecommons.org/licenses/by/4.0/>).

1. Introduction

Noradrenaline (NA) is a monoamine neurotransmitter that acts in the brain and body to induce and coordinate states of wakefulness, and to facilitate adaptive behaviors in response to environmental novelty. The mammalian brainstem contains a cluster of up to seven NA-synthesizing nuclei (A1–A7) that have been anatomically identified in >80 mammals [1], from rat [2], to cat [3], to human [4]. The tightly appositioned A4 and A6 nuclei stand out as the largest, often densest, and predominant forebrain-projecting nuclei that share a common embryonic origin [5] and in which activity levels correlate with the degree of wakefulness (for review, see [6–9]). In tissue sections, these nuclei appear sky-blue because of their pigmentation with neuromelanin, a by-product of catecholamine metabolism, which gave it the name *locus coeruleus* (LC, Latin for “sky-blue spot”). The LC lies in the pontine brainstem as an anteroposteriorly extended tube with a central ventral extension along the fourth ventricle (for review, see [1,8]) and it is part of the ascending arousal systems, together with other monoaminergic and cholinergic nuclei (for review, see [10,11]). The LC provides brain-wide axonal arborizations and fine meshworks of varicose fibers that arise from a comparatively small number of NA-synthesizing neurons (thousands in rodents [12,13], tens of thousands in humans [14]). The axons from LC cells span the neuraxis from the spinal cord to the cerebellum, midbrain, thalamus, and cortex and are thought to release NA through both synaptic and non-synaptic release mechanisms (for review, see [15,16]) to regulate neurons, glial cells, and fine microvessels (for review, see [17–19]), stimulating wakefulness and attentional orienting (for review, see [8]), sensory processing (for review, see [20]), muscle tone (for review, see [21]), and breathing (for review, see [22]), while inhibiting sleep-promoting brain areas (for review, see [10,23]). The LC also plays prominent roles in pathological forms of arousals, commonly linked to acute stress (for review, see [24]), post-traumatic stress disorder (for review, see [25]), pain

and analgesia [26], motivation and relapse (for review, see [27]), hypercapnia (for review, see [28]), and hypotension (for review, see [29]), many of which are accompanied by sleep disturbances.

Novel anatomical and physiological technologies, together with advanced behavioral measures, are about to bring fundamentally renewed insights into the LC's functions. The LC shows a genetic and/or functional heterogeneity at multiple levels from its embryonic and evolutionary origins (for review, see [1,5]), its synaptic interactions with the pericoerulear area (for review, see [30]), its input–output connectivity (for review, see [31]), to its cellular identities and neurotransmitter release (for review, see [6,30]), neuronal ensemble formation (for review, see [32]), regulation of whole-brain states [33], brain-state-dependent firing patterns (for review, see [7,30]), and behavioral roles (for review, see [34]). The LC emerges as a dynamic and plastic assembly of functionally specialized LC neuronal subgroups that act locally or globally according to recently lived experiences, ongoing demands, and future challenges (for review, see [30,35]).

Time is also ready to complement the prevalent LC-wakefulness association with the appreciation that the LC is important for sleep. The central message of this review is that LC's role in sleep has remained underestimated. Novel real-time monitoring and interferential approaches now start to indicate that LC contributes to sleep in fundamental ways—to its cellular functions, its micro- and macroarchitectural organization and regulation, associated behaviors, and possible roles in disease. These insights are at their very beginnings, yet they indicate that the LC could become an important factor in profiles of perturbed sleep that arise from diverse conditions. In this review, we discuss these exciting developments primarily based on animal experimentation, but we include human studies whenever they help complement available evidence. For a more human sleep-oriented recent review on the LC's role in sleep, we refer to Van Egroo et al. [36].

2. The Activity of the LC in Sleep: Pioneering Studies

This chapter reviews studies from the last decades that provided evidence for a maintained activity of the LC in sleep. Quantitatively, these studies revealed that the LC unit activity was clearly lower compared to wakefulness, yet remained distinctly elevated during non-rapid-eye-movement (NREM) sleep compared to REM sleep. NREM and REM sleep are the two major mammalian sleep states, also referred to as “quiescent” and “active” sleep, respectively. These two states show distinct spectral characteristics and functions for sleep (for review, see [37]). Qualitatively, the studies summarized in this chapter suggest that the noradrenergic system appeared to be involved in the alternation of NREM and REM sleep. For these results, diverse techniques in animals and humans were used that span from electrophysiology and pharmacology to microdialysis and functional imaging. A summary of the traditional view that has emerged from these studies is shown in Figure 1 (left).

2.1. Animal Studies

Rat [38,39], cat [40–42], and monkey [38,43] recordings showed that the action potential discharge rates of LC units during NREM and REM sleep were minor compared to wakefulness. Unit activity was low during NREM sleep, but remained detectable, while it ceased during REM sleep [38,39]. However, researchers also noted that not all putative LC units reduced activity during NREM and/or REM sleep [40,41]. LC activity was also low in quiet—as opposed to active—wakefulness [39,42]. More recent studies indicate that some LC units may even be as active in NREM sleep as in quiet wakefulness and occasionally fire in bursts [44–46]. Furthermore, although activity during sleep states was overall low, it nevertheless was not random. For example, LC unit activity has been related to the organization [39] and termination [46] of sleep spindles, an essential NREM sleep rhythm in the 10–15 Hz frequency range originating from the thalamo-cortical loop [47]. Additionally, LC unit activity during NREM sleep preceded the cortical up-state periods

from another important NREM sleep-associated slow rhythm, the cortical slow oscillation (~1 Hz) [45], and was increased during a post-learning NREM-sleep period [44].

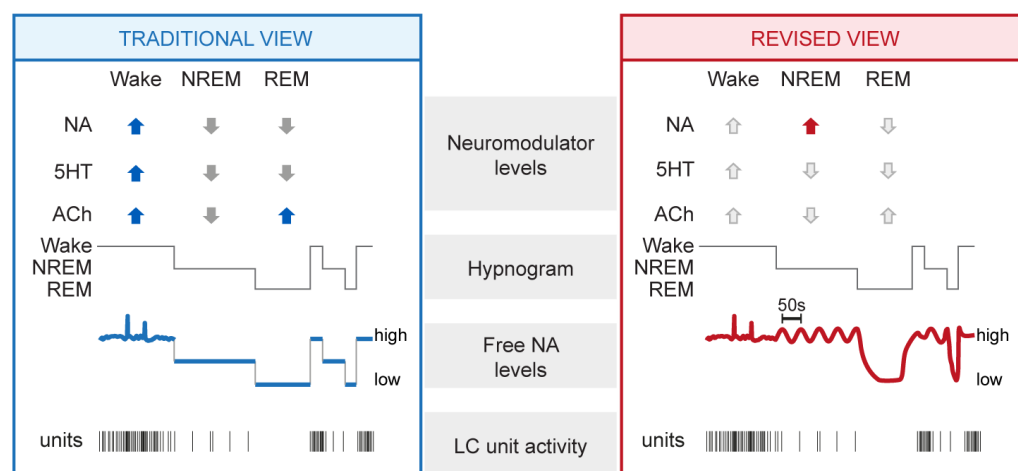


Figure 1. Summary of traditional and revised views on the neuromodulatory profiles of wakefulness and sleep, with a focus on noradrenergic signaling. Traditional (left) and revised (right) views derived from animal experimentation are summarized and complemented with data-derived schematic representations of NA dynamics and LC unit activity. From top to bottom: mean levels of major neuromodulators (blue up and gray down arrows symbolize high and low levels in the traditional view), a representative hypnogram of mouse sleep–wake behavior, free NA levels, and representative discharges of a LC unit. Novel insights central to the revised view are highlighted with the red arrow, whereas unaltered neuromodulatory levels are shown with light grey arrows. NA, noradrenaline; 5HT, serotonin; ACh, acetylcholine; NREM, NREM sleep; REM, REM sleep.

Microdialysis allows sampling of mean concentrations of neurochemicals present in the extracellular fluid surrounding neural tissue. Microdialysis for NA revealed its levels to be lower for states of sleep compared to wakefulness across rodents, cats, and seals, yet values for NREM sleep consistently were intermediate with respect to the ones for wakefulness and REM sleep in various brain areas (for review, see [48]). This suggested that even low LC unit activity leads to detectable NA release. However, no or minor increases in cortical NA levels in response to electrical or chemical stimulation of the LC were observed at low (1–3 Hz) compared to higher (>5 Hz) stimulation frequencies [49–51]. The fast-scan cyclic electrochemical voltammetry technique allows millisecond-resolution assessments of NA levels with nanomolar sensitivity, but it has so far been mostly applied for high-frequency stimulation of the LC [52]. Therefore, the relation between LC unit activity and real-time NA output has remained undefined.

Jouvet’s monoaminergic theory of sleep–wake control [53] prompted examinations of the spontaneous sleep–wake cycle after lesion or pharmacological manipulation of LC and NA signaling, or after constitutive removal of genes encoding proteins involved in NA turnover. These approaches made it clear that noradrenergic activity sustains wakefulness at the expense of sleep (for review, see [7–9,23]). At the same time, they provided the first hints that NA signaling remained relevant for sleep. For example, neurotoxic lesions of noradrenergic LC neurons or genetic elimination of the NA-synthesizing enzyme dopamine-β-hydroxylase (DBH) altered the relative times spent in NREM and REM sleep [54–56]. These approaches lacked the necessary specificity in time and in the site of action to conclude about the LC’s role in regulating the timing of NREM and REM sleep. Furthermore, noradrenergic receptors are expressed both centrally and peripherally, and LC projections target both sympathetic and parasympathetic autonomic pathways (for review, see [29]). Therefore, systemic drug administration may affect sleep–wake states

by acting on the autonomic nervous system. Nevertheless, these studies are part of initial evidence that monoaminergic systems, including NA, could remain active in sleep.

Particularly noteworthy are the effects of pharmacological α 2-adrenergic receptor activation. These receptors are G_i -protein-coupled receptors activated by NA in the central nervous system and periphery. In the brain, they act as both presynaptic negative autoreceptors within the LC and in sleep–wake regulatory centers to suppress NA release and attenuate postsynaptic excitability [57] (for review, see [58]). These receptors are also the target of powerful sedatives used in clinics, such as dexmedetomidine (for review see [58]). The α 2 agonist clonidine suppresses the activity of the LC [59,60] but also targets pre- and postsynaptic receptors in sleep-regulatory areas (for review, see [23]). α 2 agonists such as clonidine or detomidine, when applied locally in cat pontine brainstem [61] or peri-coerulear areas [62], or systemically in rat [63], suppressed REM sleep while increasing the depth of NREM sleep. The use of clonidine in humans was also found to attenuate REM sleep (see Section 2.2). These effects on sleep macroarchitecture are in line with an active LC during sleep.

2.2. Human Studies

The functional activity within dorsal brainstem areas, including the LC, was examined through functional magnetic resonance imaging (fMRI) in sleeping healthy individuals [64]. This imaging technique uses magnetic resonance signals to detect changes in brain activity based on increases in the flow of oxygenated over non-oxygenated blood. Signal increases involving the LC were particularly prominent during NREM sleep-associated slow (<1 Hz) waves. More recently, advances in high-resolution neuroimaging techniques allow for a refined investigation of the human LC, which has raised much attention regarding its role in sleep (for review, see [36,65]). Neuromelanin's paramagnetic properties make MRI-based anatomical measures of the LC possible to determine its location and structural integrity. Positron emission tomography can provide estimates of noradrenergic terminal density. First studies have correlated structural and functional read-outs of the LC to human sleep, finding associations between these and microarchitectural alterations in sleep [66] that are relevant in the context of neurodegenerative disorders (see Section 5.1) (for review, see [36]).

Similar to animal models, pharmacological studies in humans using α 2-receptor-specific agonists provide evidence for the role of noradrenergic signaling in the timing of NREM and REM sleep. The α 2 agonists clonidine or guanfacine produced a reduction of REM sleep [67] and an increase of NREM sleep [68] while the α 2 antagonist idazoxan increased the time spent in wake but also reduced the time in REM sleep [68]. Furthermore, clonidine decreased peripheral NA levels during sleep [69], consistent with a suppression of an active LC during sleep. Administration of the NA reuptake inhibitors reboxetine, maprotiline, or nomifensine, for which there is evidence that they elevate peripheral levels of NA, also suppressed REM sleep [69,70]. These studies indicate that noradrenergic signaling, in part through α 2 receptor activation, is a pathway for sleep control. How this signaling modulates both local LC networks and their synaptic targets to both NREM and REM sleep control centers remained open for further study.

3. The Activity of the LC in Sleep: Novel Insights

The development of genetically encoded sensors for free NA now makes it possible to measure its real-time dynamics with high spatial and temporal resolution [71]. It enables a direct estimation of the relative NA levels released during the natural sleep–wake cycle and how they relate to traditional LC activity measures. These sensors are G-protein-coupled-receptor-activation-based (GRAB) and are constructed from mutated α 2 adrenoceptors coupled to an EGFP moiety. When expressed in vivo through viral vectors, these GRAB sensors become localized on membrane surfaces and emit green fluorescence (\sim 520 nm) upon blue light excitation (\sim 510 nm) once NA released from LC fiber binds. High (GRAB_{NE1h}) and medium (GRAB_{NE1m}) affinity versions of these sensors have been presented, and

renewed versions keep being developed, expanding the range of sensitivity and kinetics with which measures can be taken (see <http://www.yulonglilab.org/faq.html>, accessed on 1 February 2022). Furthermore, a mutant version of the sensor that is not responsive to NA should be used to control for potential non-specific alterations of the fluorescence signal that can limit its interpretation. For example, local alterations in neuronal environments, such as in brain temperature or blood pressure accompany transitions between NREM and REM sleep. These could alter light scattering or biosensor properties in vivo. Two studies in mouse, one published [72], one yet to be peer-reviewed [73], have now used these GRAB_{NE} sensors to describe the real-time dynamics of free NA levels in the medial prefrontal cortex [73] and in the primary sensory thalamus [72] during the natural sleep–wake cycle. These studies report unexpectedly high levels of NA during NREM sleep compared to wakefulness. Furthermore, they observe a dynamically varying signal during states of sleep. This chapter presents the most important findings derived from these two studies. A summary of the resulting revised view on NA signaling in sleep is shown in Figure 1 (right).

3.1. Mean NA Levels Differ across the Sleep–Wake Cycle

The signals provided by the genetic sensor showed characteristic alterations across wakefulness, NREM sleep, and REM sleep. In the prefrontal cortex, mean NA levels during wakefulness were high but variable [73], which is consistent with the large variations in LC activity in wakefulness (see Section 2.1). During NREM sleep, the mean free NA levels became lower but still overlapped with the ones of wakefulness. During REM sleep, the levels of NA were consistently low. In the sensory thalamus, similar measures of NA even revealed that mean levels were significantly higher during NREM sleep when compared specifically to quiet wakefulness (Figure 2) [72]. Again, values were low during REM sleep in this area. These findings provide the first evidence that NA levels remain more elevated in NREM sleep in forebrain areas than what was expected based on unit measures (see Section 2.1). The expected low NA levels during REM sleep appear as a common feature across the recorded areas. The considerable discrepancy between the numerically sparse LC unit activity (see Section 2.1) and high free NA levels generated during NREM sleep shows that much remains to be learned about the mode of operation of LC neuronal ensembles in different states of vigilance.

3.2. NA Levels and LC Activity Fluctuate During NREM Sleep

The next notable observation found in both the thalamus and prefrontal cortex is that NA levels were not steady during NREM sleep (Figure 2A–C). Instead, these fluctuated on an infraslow timescale of tens of seconds, with an average cycle length of 30–50 s [72,73]. These fluctuations in NA levels were linked to phasic bouts of LC neuronal activity over the same intervals, as evident by correlated Ca²⁺ transients in LC somata [73]. This activity pattern points to a periodic synchronization of LC population activity on an infraslow time scale during NREM sleep [74].

The role of these recently identified fluctuations is a current topic of investigation [72,75,76] (for review, see [77]). Optogenetic modulation of noradrenergic LC neuronal activity evoked variations in the appearance of sleep rhythms and heart rate, suggesting that infraslow NA fluctuations are relevant for NREM sleep's physiological correlates. Thus, NA released by the LC lead to a periodic clustering of sleep spindles, such that they appeared at high density when NA levels were low and they were scarce when these levels were high (Figure 2A) [72,73]. Mechanistically, sleep spindle clustering relied on the α 1- and β -adrenergic receptor-mediated modulation of membrane potentials in the thalamic circuits, in which sleep spindles are generated [72]. Sleep spindles are involved in the sleeping brain's elaboration of sensory input (for review, see [78]), which implies the LC in NREM sleep-related sensory processing (see Section 4.1).

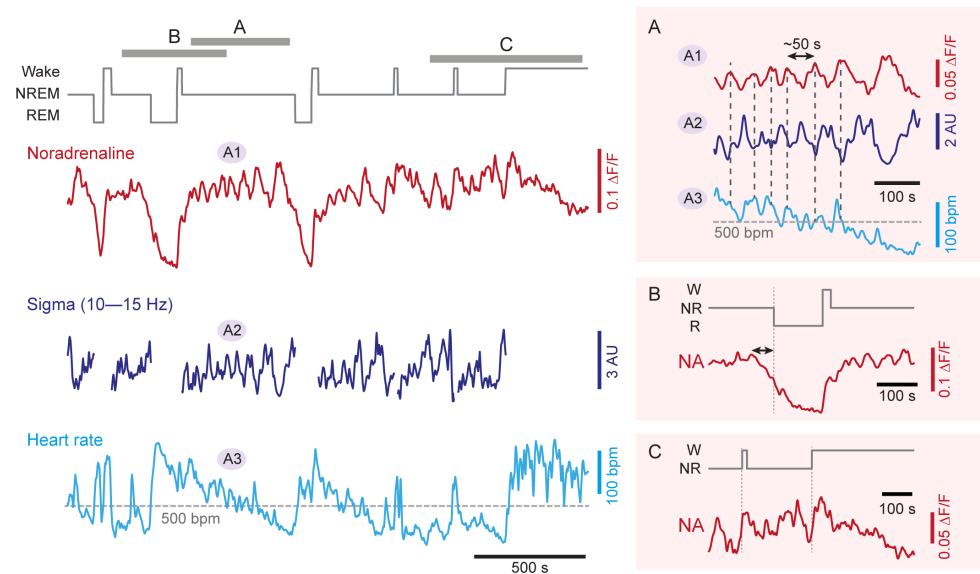


Figure 2. Real-time dynamics of NA levels in somatosensory thalamus, forebrain sleep spindle power, and heart rate during NREM sleep. Representative simultaneous recordings in a freely behaving mouse combining (from top to bottom): hypnogram (gray), free NA levels in somatosensory thalamus obtained through fiberphotometry imaging (red, A1), local field potential sigma power (10–15 Hz) in somatosensory cortex (dark blue, A2) and heart rate (light blue, A3), with labeled portions (A, B, C) shown expanded on the right. The variations in sigma power reflect the clustering of sleep spindle density ([72]). Insets on the right expand portions of the traces highlighted with letters in the hypnogram to show (A) NREM sleep (double-headed arrow marks the 50 s periodicity); (B) NREM-to-REM sleep transitions (double-headed arrow marks the decay time of NA levels prior to REM sleep onset); (C) NREM-to-wake transitions. Portions of two of these traces have been published previously [72]. NA, noradrenaline; W, wakefulness; NR, NREM sleep; R, REM sleep; $\Delta F/F$, relative fluorescence changes; AU, arbitrary unit; bpm, beats per minute.

NA fluctuations also correlated with infraslow variations in heart rate during NREM sleep (Figure 2A). The LC thus acts bidirectionally to coordinate forebrain sleep spindle rhythms with heart rate variations. Indeed, optogenetic activation of LC noradrenergic neurons disrupted the heart rate variations during NREM sleep and their anticorrelation with the spindle clustering [72,76]. Mechanistically, the coupling of LC activity to the heart rate depended on parasympathetic signaling. Likewise, parasympathetic signaling also underlies coordinated infraslow fluctuations between pupil diameter and sigma power during NREM sleep [79].

3.3. NA Levels Decay to Low Levels during REM Sleep

The NA levels declined in both the prefrontal cortex [73] and the thalamus [72] during REM sleep, in line with the quiescence of LC units in this behavioral state (Figure 2B). As a result, NA levels reached a level that lay below that of wakefulness and NREM sleep. This result directly and strikingly supports the proposition that REM sleep periods are relatively NA-free (see Section 5.2). The quantification of the extent and time course of this decline will now allow us to refine this proposition, in particular in terms of the relation to REM sleep bout duration.

3.4. NA Levels Show Characteristic Dynamics at Behavioral State Transitions

The dynamics of NA levels at moments of transition from NREMS to REMS or wakefulness showed characteristic properties. At NREM-to-REM transitions, a decrease in NA levels began ~ 40 s before the onset of REM sleep (Figure 2B). This time period recalls a transitional moment of sleep that has been referred to as “intermediate sleep” in rodents [80], cats [81] and humans [82,83]. Intermediate sleep shows a mixed spectral profile combining

an increase in sigma power and the density of fast spindles, while hippocampal theta rhythms appear (for review, see [78]). On the time scale of intermediate sleep, there is a cessation of LC unit activity [39,73] and the appearance of cholinergic activity in REM sleep-promoting tegmental nuclei [84,85]. The coincidence of declining NA levels with unit and spectral correlates of intermediate sleep suggests that the activity levels of the LC during NREM sleep may determine the timing of NREM-to-REM sleep transitions.

Transition periods from NREM sleep to both sustained wakefulness and to microarousals were both associated with an increase in NA levels in the prefrontal cortex that appeared to start before the transition (~ 10 s) [73]. On the same time scale, there was an increase in Ca^{2+} activity of noradrenergic LC neurons that was higher for transitions to consolidated wakefulness compared to microarousals. This appeared also to be the case for NA levels at NREM sleep-to-wake transitions (Figure 2C). These alterations are in line with unit activity measures around moments of wake-up (see Sections 2.1 and 4.1).

3.5. Emerging Dynamics of Other Monoamines and Wake-Promoting Neurotransmitters

In vivo measures using genetically encoded sensors showed that, in addition to NA, other monoamines and wake-promoting neurotransmitters remain high during NREM sleep. In Ca^{2+} -based fiber photometric measures of spontaneous activity in the dorsal raphe, fluctuations were observed in phase relation to spontaneous brief arousals [86]. Furthermore, measures with a genetically encoded sensor for free serotonin levels revealed slow fluctuations in both the orbital frontal cortex and the bed nucleus of the *stria terminalis* during NREM sleep, and declines during REM sleep [87]. The time course of these fluctuations, and their consistent appearance at two distant brain sites, are reminiscent of the findings with NA described in this chapter. Given the rapid advance in the availability of novel sensors for dopamine [88,89] but also for other neuromodulatory transmitters involved in sleep–wake control (such as acetylcholine, [90] or hypocretin [91]), more details on the spatiotemporal map of neurotransmitter dynamics during states of sleep will soon become available. Intriguingly, transient free dopamine increases in the basolateral amygdala were just discovered as triggers for NREM-to-REM sleep transitions [92].

4. The Role of the LC in the Regulation of Sleep and Sleep Functions

This chapter builds on the newly revealed real-time dynamics of NA levels described in Section 3. It aims to review how these findings advance insight and motivate experimentation in the quest for the functional roles of the LC during sleep.

4.1. LC as Part of Sensory Arousal Circuits during NREM Sleep

Pioneering recordings from LC units found that these respond with a short latency to stimuli from different sensory modalities [38,42,43,93,94]. Increases in LC unit discharge rates also preceded spontaneous, unsolicited awakenings from NREM sleep [38,39,94]. Moreover, activation of LC through electrical, opto-, or chemogenetic stimulation elicited transitions from sleep to wakefulness [46,95,96] and recruited whole-brain networks involved in salience processing [33]. Acute knockdown of DBH specifically in LC neurons disrupted sleep-to-wake transitions elicited by optogenetic LC stimulation, confirming the importance of NA signaling for wake-ups [96]. Given LC's powerful capacity to drive sleep-to-wake transitions, LC activity might be involved in sensory-induced sleep–wake transitions.

Indeed, Hayat et al. [63] showed a causal link between the levels of ongoing LC activity during NREM sleep and the probability of sensory stimulus-evoked awakenings. Mild optogenetic LC stimulation lowered the auditory arousal threshold, whereas inhibiting LC heightened it. In line with this, the natural infraslow fluctuations of LC activity during undisturbed NREM sleep coincided with variations of auditory and somatosensory arousability [75,76]. Furthermore, spontaneous brief arousals from NREM sleep in mice were most frequent at moments of low spindle density, when LC activity is high [72,75].

The exact roles of the LC in the cognitive, motor, and autonomic aspects of arousal remain to be determined. As LC neurons are activated by sensory input (Figure 3A), NA release is promoted by the sensory stimulus itself. It is also noteworthy that even low-frequency LC discharge (1–2 Hz) sharpened sensory responsiveness and receptive fields at the level of the thalamus and cortex [97–99]. Through depolarizing thalamic neurons, the LC also suppresses the appearance of sleep spindles that limit sensory throughput in thalamocortical areas [78]. The LC could hence promote sequential arousal-promoting actions that are graded with its activity levels as the transition from sleep to wakefulness takes place.

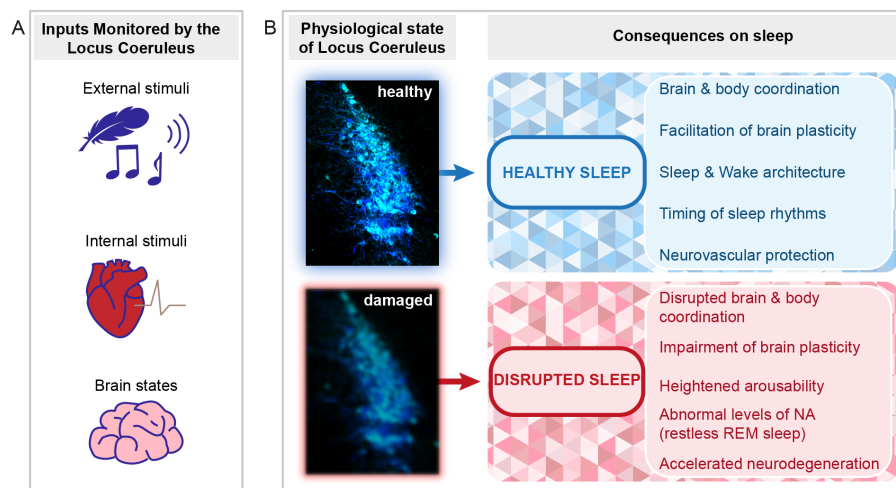


Figure 3. Perspectives for the implication of the LC in healthy and disrupted sleep. Schematic indicating the types of signals monitored by the LC and the implications of LC function and dysfunction for sleep. (A) The LC monitors external stimuli (e.g., sensory stimuli such as touch or sound, symbolized by a feather and a musical note, see Section 4.1), internal stimuli (symbolized by the heart, see Section 4.5), and internal brain states important for the regulation of NREM-to-REM sleep transitions (symbolized by the brain, see Sections 3.4 and 4.3). (B) Depending on the LC status (healthy or damaged), beneficial or adverse consequences on sleep can arise. Several outcomes are listed on the right. The LC micrograph was obtained from an immunohistochemically stained brain section of one of the mice used for the data published in [72]. The color choice of cell labeling was made deliberately to mark it as the sky-blue spot. The blurring of the blue color in the bottom micrograph symbolizes both structural and functional alterations that can lead to LC dysfunction.

4.2. The LC as Part of the Regulatory Mechanisms of NREM Sleep

The real-time dynamics of NA for the first few hours of the light phase, the predominant resting phase of rodents, underscore the importance of the LC in the regulation of sleep architecture [72]. The elucidation of these dynamics across the light–dark cycle and across major sleep–wake control areas will reveal the full impact of NA on sleep’s brain states and associated sleep–wake behaviors. The LC is part of arousal circuits that are under circadian control [100] and it receives afferents from hypothalamic preoptic areas involved in NREM sleep homeostasis [31]. Therefore, beyond its regulation of sleep architecture and spectral composition, the LC could also contribute to circadian and homeostatic regulation of NREM sleep (Figure 3B).

4.3. The LC in REM Sleep Control

In spite of much pioneering work (see Sections 2.1 and 2.2), how LC regulates REM sleep remains an open question (for review, see [101]). Recent research has focused on glutamatergic and GABA-ergic circuits involved in REM sleep regulation, whereas monoaminergic systems were attributed mostly a modulatory role (for review, see [102]). Measures of real-time NA dynamics, together with NREM sleep-specific optogenetic manipulation of

the LC in rodents, instead indicate important changes in LC activity at moments of REM sleep onset. These recent data revive the questions about the LC's role in REM sleep that we outline here in three aspects that could be important in future studies.

First, as described in Section 3, forebrain NA levels remained high during NREM sleep (Figure 2A) and LC neurons continue to be active [73]. This elevated activity in noradrenergic signaling suppresses REM sleep, as suggested by electrical or pharmacological LC stimulation in the rat [103,104] and by NREM sleep-specific optogenetic activation of noradrenergic LC neurons at low frequency [72]. A noradrenergic inhibition of REM sleep-promoting brain areas is a likely underlying mechanism for this suppression [105–107]. Importantly, the spontaneous activity of LC during natural undisturbed sleep seems even sufficient to antagonize NREM-to-REM sleep transitions. This was concluded from NREM sleep-specific optogenetic inhibition of the LC in freely sleeping mice, which increased the time spent in REM sleep [72]. This indicates that the LC is a powerful target to manipulate the balance between NREM and REM sleep in response to various regulatory and experience-dependent processes (see below and Section 5.2).

Second, NA levels declined in both the thalamus and cortex in REM sleep (Figure 2B). This decline took tens of seconds to complete once REM sleep began, raising the question of which are the determinants of this time course. The LC is inhibited by GABAergic mechanisms [108,109], of which several have been tested for their role in REM sleep control. Monosynaptic inhibitory afferents arise from the local and pericoerulear interneurons [110], ventrolateral periaqueductal gray [111], and from *nucleus prepositus hypoglossi* and dorsal paragigantocellular reticular nucleus [107,112,113]. Acetylcholine release from cholinergic REM sleep-promoting areas could also act through GABAergic mechanisms [109]. Cholinergic areas are likely initiating the LC inhibition as their discharge onset precedes REM sleep [84], but auto-inhibitory mechanisms within the LC could also play in at this moment [114]. At least one of the dorsal medullary inhibitory afferents increases activity exactly at REM sleep onset [113], suggesting that NA decline could become strengthened due to additional sources of inhibition. NA uptake mechanisms lagging behind synaptic inhibition of the LC could instead retard the decline of free NA levels. How the strength and the efficiency of synaptic inhibition regulate LC silencing and NA decline and/or interact with other excitatory and/or modulatory synaptic mechanisms of LC inhibition (see e.g., [110]) is currently unexplored. The determinants of NA dynamics at NREM-to-REM sleep transitions are critical to understanding how REM sleep evolves into an NA-free state because of its likely role in the regulation of emotional memory (see Section 5.2).

Third, the fluctuating levels of NA during NREM sleep indicate that chances for a NREM-to-REM sleep transition increase at moments of relatively low NA levels. Interestingly, the probability to enter REM sleep was indeed found to be phase-locked to the infraslow fluctuation of sigma power measured at the level of the EEG [113]. This lends support to the idea that fluctuating LC activity during NREM sleep generates brain states that are permissive for transitions, such as the ones to REM sleep (Figure 3A) [75,76]. The LC activity oscillating between high and low levels might suppress REM sleep on the one hand, but also open moments where transitions are favored. The LC is, therefore, positioned as a brain area capable of autonomously regulating the timing of REM sleep in a bidirectional manner during NREM sleep, yet how it is integrated into REM sleep regulatory mechanisms will require further research.

Alterations in REM sleep propensity, duration, and hippocampal-related theta activity are ubiquitous after stress- and fear-related experiences. These are part of the acute physiological responses to the hormonal and autonomic changes accompanying stress [115], but they also contribute to the consolidation of fear- [116] and extinction-related memories [115]. Increases in REM sleep are part of an adaptive process to mild stress exposure [117]. Given the LC's high reciprocal connectivity with areas implied in fear, such as the amygdala (for review, see [31]), it is a strong candidate for linking stress-related experiences during the day to the timing of REM sleep. Indeed, acute decreases in REM sleep in response to inescapable footshock could be alleviated by optogenetic inhibition of excitatory neurons

in the basolateral amygdala [118] or by dual hypocretin receptor antagonism in the LC or the dorsal raphe [119]. In case of such or even more traumatic experience, states of hyperarousal associated with elevated monoaminergic activity may arise, to which the LC contributes (for review, see [120]) (see Section 5.2).

4.4. The LC in Hippocampus-Dependent and Independent Memory Consolidation

LC activity, in part due to its implication in novelty detection, has been found to actively contribute to online memory consolidation. A series of studies found that activation of the LC favors different types of learning such as spatial learning [121–124], fear learning and reconsolidation [124–126], and perceptual learning [127,128]. Optogenetically activating LC tyrosine hydroxylase-positive neurons shortly after memory encoding of food rewards in a navigation task promoted memory retention in mice, which persisted until the next experimental assessment [121]. Such LC stimulation mimicked the effects of environmental novelty on memory encoding. Intriguingly, local pharmacological inhibition of dopaminergic but not noradrenergic receptors in the hippocampus implied a role of LC fiber-dependent dopamine release in novelty enhancement of hippocampus-dependent memory. Optogenetic stimulation of the LC during a spatial object recognition task lead to similar results [122]. Inhibition of the LC had, on the contrary, a detrimental effect on hippocampal place cell formation in goal-directed spatial learning [123]. The LC's role in cued fear conditioning concerned both, memory acquisition of the pairing between the conditioned and the unconditioned stimulus, and later extinction [126]. Here, a dual role for LC afferent projections to the amygdala and to the medial prefrontal cortex could be identified, with the former implied in the acquisition, and the latter in the extinction of fear memory, demonstrating a modular functionality of LC subgroups depending on their projection targets. Pairing LC activation with stimulus presentation could also accelerate the learning of a new target sound in a perceptual learning paradigm [127] in rats and electrical/optogenetic stimulation of the LC during sound presentation promoted NA-dependent long-term plastic strengthening in auditory tuning curves of primary auditory cortex neurons [128].

The LC's role as a regulator of memory acquisition likely relies on manifold actions of NA on neuronal excitability, in particular in hippocampal circuits, and on enduring changes in synaptic strength (for review, see [129]). One principal action of endogenously released NA, identified through optogenetic stimulation of LC fibers, appears to be a suppression of postsynaptic potassium currents, which enhanced the excitability of CA1 pyramidal neurons in response to Schaffer collateral stimulation [130]. This effect was blocked by β adrenoceptor antagonists, with no apparent implication of dopamine release. It is noteworthy that this action was already present when fibers were stimulated at low frequency (1 Hz), suggesting that such neuromodulation could be effective during NREM sleep, when the LC discharges at low frequencies (see Section 2.1).

In contrast to the strong evidence for the LC's involvement in the memory acquisition phase, evidence that it plays a role during offline processing, including during sleep, is currently scarce. Pioneering pharmacological studies found that rats trained in an olfactory reward association task performed less well when they were injected with adrenergic antagonists intracerebroventricularly [131] or within prefrontal cortex [132] 2 h after training, but not at shorter or longer time intervals. These authors also provided evidence for a transient increase in NA levels during the time window in which these antagonists were effective. This pointed to a delayed re-activation of the LC that facilitated offline processing and memory consolidation. Follow-up studies suggest that such re-activation of the LC may indeed occur during post-learning sleep stages, as LC unit activity transiently doubled within the presumed re-activation window, without apparent alteration in sleep architecture [44]. The activity of LC units was further observed to be time-locked to slow waves in both rat [45] and human [64] and to hippocampal sleep spindles [46], suggesting that enhanced NA release is linked to the sleep rhythms that enable active systems consolidation. Finally, high-frequency stimulation of the LC disrupted the coupling of sleep

spindles with hippocampal ripples that are high-frequency oscillatory patterns critical for memory consolidation [133]. This adds to evidence that the degree of LC activity might be critical in coordinating sleep rhythms relevant for offline processing (for review, see [134]).

4.5. The LC as Mediator of Vagal Afferent Information

Among the innervations that the LC receives, one is of particular interest as a gate for interoceptive signals, the Nucleus Tractus Solitarius [135,136] (for review, see [137]). This brainstem nucleus is part of the dorsal vagal complex (nucleus tractus solitarius, *area postrema* and dorsal motor nucleus of the vagus) which is the first recipient for vagal afferents (for review, see [138]). The vagus nerve is part of the parasympathetic system and it is a mixed nerve containing both motor and sensory fibers. Sensory information arising from the vagus nerve is important for autonomic feedback reflexes, such as the baroreceptor reflex and the Hering–Breuer reflex that serves to control breathing (for review, see [139]), and it reaches the LC via the dorsal vagal complex [140]. Vagus nerve stimulation is well-known for its beneficial role in clinical conditions, as evident from the highly diversified effects of vagus nerve stimulation (VNS). Indeed, this technique has been proposed to facilitate brain plasticity [141] (for review, see [142]) and memory formation (for review, see [143]). Some important domains of clinical application for VNS include drug-resistant epilepsy [144] (for review, see [145,146]), depression [147] (for review, see [148]), eating disorders [149], and neurodegenerative disorders [150].

Several animal studies support the LC as a major target of vagal afferent nerve stimulation. VNS caused an increase in the expression of the immediate-early gene *c-fos* in LC neurons in conscious unanesthetized rabbits [151] and in anesthetized rats [152]. Moreover, lesioning of the LC led to a suppression of the anticonvulsant effects of VNS in epileptic rats, supporting the idea that the LC is involved in this circuitry [153]. This implication of the LC was further supported by directly recording LC unit activity during VNS [154–157]. Using *in vivo* Ca^{2+} imaging in head-fixed awake mice, a recent study showed an increase in the noradrenergic neuromodulatory system in response to VNS [158]. Furthermore, *in vivo* microdialysis showed an increase in NA extracellular levels in the hippocampus and cortex during chronic VNS in anesthetized rats [159,160] and an increase in dopamine in extracellular levels in the prefrontal cortex and nucleus accumbens [161]. Additionally, vagal afferent electrical stimulation has been related to pupil dilation in animals and humans [162–165], consistent with the correlation between pupil diameter and firing of noradrenergic LC cells (for review, see [7]). Together, these results indicate that monoaminergic systems, including the LC, act as monitors of internal stimuli conveyed by vagal afferents (Figure 3A).

Given the role of the LC in the regulation of sleep, stimulation of vagal afferents may contribute to LC-dependent sleep regulatory effects. Animal studies suggest that VNS can promote REM sleep [166,167] and/or increase NREM sleep quantity as well as power in the delta and sigma bands [168] in freely moving cats. Several clinical studies also investigated the effects of VNS on sleep regulation. In epileptic and depressive patients, VNS treatment improved daytime alertness [169], increased the mean sleep latency [170], decreased awake time and stage 2 sleep and increased stage 1 sleep [171], increased delta power during NREM sleep and reduced REM sleep quantity [172,173], increased time spent in NREM sleep and decreased sleep latency and stage 1 sleep [174], and increased wakefulness and decreased light sleep and REM sleep [175]. These differences in the outcome could be related to the variability of the VNS parameters and/or the use of antiepileptic drugs which are known to affect sleep architecture (for review, see [176]).

So far, the contributions of sensory and motor components of VNS to sleep have not been determined. In a first step in this direction, a chemogenetic stimulation of the sensory afferents of the vagus nerve showed an alteration of sleep architecture and spectral composition, and a strong increase in the latency to REM sleep onset [177].

4.6. The Role of the LC in the Regulation of Brain Vascular Activity

DBH-positive LC terminals are tightly apposed on the fine arborizations of the neurovascular tree, notably the intraparenchymal capillaries. There is also evidence that released NA regulates cerebral blood flow, neurovascular coupling, and the maintenance of the blood–brain barrier (for review, see [178]). For example, the localized increase in blood supply to the somatosensory cortex, in response to paw stimulation depended on an intact LC [179,180].

As NA levels remain high in the forebrain during NREM sleep, it is likely that its actions on the microvasculature continue (Figure 3B). The LC innervates several components of the neurovascular unit, including astrocytic endfeet, as well as peri- and endocytes, which control different aspects of glial and capillary function (for review, see [181]) that are regulated differentially between sleep and wake [73]. One of the most important insights in this field was obtained for the brain's glymphatic system that regulates the entry of cerebrospinal fluid along the perivascular space of small capillaries (for review, see [182]). Fluid exchange via the glymphatic system is enhanced during NREM sleep and cleanses the brain from toxic products such as amyloid- β -protein [183]. The fluctuating NA levels during NREM sleep could hence contribute to the pulsatile nature of this exchange process, perhaps through acting on vasomotor activity that is thought to be critical for the paravascular clearance of solutes, in particular when occurring at infraslow frequencies [184]. Interestingly, a recent study indicated a temporal correlation between cerebrospinal fluid exchange and the occurrence of slow and infraslow electrical activity in the EEG [185]. In view of these most exciting developments, we speculate that the LC's dual capability of modulating neural oscillation control and arteriolar vasoconstriction makes it a master regulator of the sleeping brain's functions because it could potentially play a role in coordinating the timing of sleep architecture, sleep electrical rhythms, and brain waste clearance.

An implication of the LC in gross cerebral blood flow arises from functional MRI studies. These have repeatedly reported the presence of spontaneous slow signal fluctuations during rest and sleep, including during N2 sleep in humans. Frequencies involved are in the infraslow range, close to values found for infraslow activity fluctuations of the LC during NREM sleep in rodent [186–188]. Furthermore, chemogenetic activation of the LC in lightly anesthetized mice generates a functional activation pattern [33] that overlaps with some of the areas found in early sleep stages [188]. The infraslow activity of the LC during NREM sleep could conceivably impose a time frame for resting-state network activity, which remains a question for future work.

5. The LC and Sleep Function in Pathology

As the LC has been known primarily as a wake- and attention-promoting brain area, the idea that LC dysfunctions could play a role in sleep (rather than wake) problems has been less considered. Moreover, the idea that a dysfunctional LC could be involved in a decrement of some major neuroprotective roles of sleep is so far underexplored. As the LC's profound implication in sleep architecture and sleep function is increasingly recognized, these possibilities come to center stage and open novel inroads for preventive strategies (Figure 3B).

5.1. Aging and Neurodegenerative Disorders

Many aspects of sleep, from its timing and initiation to its maintenance and depth deteriorate with aging (for review, see [189]), and this process is aggravated in the case of neurodegenerative dementias, of which Alzheimer's disease (AD) is the most common form (for review, see [190]). In healthy aging mice, hypothalamic orexin neurons undergo increases in intrinsic excitability that cause sleep fragmentation [191]. In aging accompanied by neurodegeneration, much interest has recently focused on the LC that appears to be afflicted at early stages of AD [192]. Ample evidence further indicates that disturbed sleep adversely affects the progression of AD pathology (for review, see [193]).

Therefore, addressing whether early LC pathology links to sleep disruptions bears potential to identify early stages of disease. This potential is strengthened by newest evidence that structural measures of LC integrity in vivo can be related to the initial stages of AD-related neurodegeneration and cognitive decline [194].

It is currently open how exactly LC neuronal activity and NA signaling are altered with aging and pathologically aggravated with the progression of AD. Chemogenetically stimulating LC in a rat model of AD recovered spatial learning capacities, but how much and in which brain areas NA signaling was restored remained an open question [195]. As free NA dynamics have become accessible through biosensors (see Ch. 3), it is now possible to determine when and how these are affected by the neurodegenerative processes and to which types of sleep disruptions they might be linked. Amongst the diverse alterations in sleep in patients with neurodegenerative disorders (for review, see [190]), recent focus has been on alterations in sleep's microarchitecture [66,196] and possible links to LC dysfunction, which make altered NA signaling during NREM sleep as a reasonable path to be pursued. On top of this, evidence for the LC's implication in the vascular pathology and decline of glymphatic activity in AD pathogenesis has attracted enormous interest (for review, see [178]). At this stage, deepening the causal links between LC dysfunction and altered NA signaling is a very promising path to the LC's broad implication in sleep disorders linked to neurodegenerative diseases (for review, see [36,182]).

5.2. Stress-Related Disorders

Increased noradrenergic LC activity is a common observation after stressful or traumatic life experiences (for review, see [25]). This increase persists beyond the momentary insult and may continue during sleep. Even comparatively mild stress in rats, such as a simple cage exchange, activates major wake-promoting areas, including the LC, and leads to sleep fragmentation [197]. Both mild and excessive stress, such as the one inflicted by traumatic events, have been related to a maintained hyperactivity of the LC noradrenergic system (for review, see [25]). As stress and various sleep disruptions are tightly linked, it is likely that the NA signaling profile during NREM and REM sleep becomes altered at various levels and adversely affects sleep physiology.

First, elevated LC activity and NA signaling is arousal-promoting through its desynchronizing effect on EEG that favors high- over low-frequency oscillatory activity, as demonstrated by pharmacologic [198], electrical [199], chemogenetic [200], or optogenetic [63] activation of LC neurons. Alteration in the LC noradrenergic system may thus contribute to cortical hyperarousal states during sleep. Interestingly, cortical hyperarousal states are a common trait of sleep disruptions arising from neuropsychiatric conditions, but also from pain (for review, see [201]) and primary insomnia (for review, see [202]).

Second, elevated LC activity promotes arousability to external stimuli (see Section 4.1), facilitating sleep disruptions. It is well accepted that lightened NREM sleep and more frequent awakenings are part of the disease profile in post-traumatic stress disorder (for review, see [25,203]).

Third, elevated LC activity may compromise the decline of NA levels during REM sleep. While this possibility awaits a direct demonstration, the idea that insufficient decline of NA levels during REM sleep has been put forward as a mechanism inhibiting extinction of emotional memory (for review, see [25,202]). Mechanistically, it is thought that the quiescence of LC neurons during REM sleep allows a depotentiation of synaptic strength in anxiety-related networks, including the amygdala. Therefore, during NA-enriched REM sleep, also referred to as "restless REM sleep", behavioral reactions to emotional stress do not decline overnight [204].

More generally, high and fluctuating levels of NA in NREM sleep may support synaptic plasticity while the low levels during REM sleep could promote synaptic depotentiation and downscaling. As a consequence, aberrant noradrenergic activity during REM sleep may contribute to the maladaptive recall of complex experiences in which emotional aspects remain highly salient. The real-time dynamics of NA during NREM and REM sleep

will be essential in refining the proposed picture of the LC as an important coordinator of memory consolidation processes during sleep.

5.3. Sleep and Cardiovascular Regulation

The cardiovascular correlates of NREM and REM sleep arise from the interplay of autonomic reflex arcs and central commands that regulate the balance between sympathetic and parasympathetic activity (for review, see [205]). Both circadian and sleep-driven mechanisms contribute to the central control of the cardiovascular system (for review, see [206]). NREM sleep is dominated by parasympathetic influences, whereas sympathetic ones prevail in REM sleep (for review, see [206,207]). LC efferents target both preganglionic sympathetic and parasympathetic output areas, activating the former while inhibiting the latter. Further cardiovascular impact may arise through the LC's connections with stress- and attention-responsive brain areas (for review, see [29]). However, the LC's role in the central autonomic commands for cardiovascular control in sleep is not clarified, although brainstem mechanisms are particularly prevalent in cardiovascular control during NREM sleep (for review, see [207]). In mice, infraslow variations in heart rate during NREM sleep were mediated by the parasympathetic system [72]. Furthermore, continuous and global optogenetic stimulation of LC noradrenergic neurons during NREM sleep disrupted previously observed anticorrelations between spindle clustering and heart rate, whereas LC stimulation at infraslow frequencies strengthened this anticorrelation [72]. The LC is thus positioned to regulate central and autonomic activity during NREM sleep. Given the numerous sleep-related cardiovascular alterations in neuropsychiatric and neurodegenerative diseases, it will be of great interest to examine the LC's and other monoaminergic's contributions to the pathophysiological manifestations of these conditions [207].

6. Closing Remarks and Future Directions

We outlined novel evidence showing that the noradrenergic LC plays important and previously underestimated roles in sleep. We reviewed and contrasted existing literature with recent findings that unraveled the real-time dynamics of the LC and its NA output during sleep.

A central step forward is the recognition that NA signals span an unexpectedly high dynamic range, from high and comparable levels between wakefulness and NREM sleep to low levels in REM sleep, at least in the two forebrain areas measured so far. This dynamic currently is not congruent with what we know about variations in LC unit activity across sleep and wakefulness. Clearly, much is still unknown about how LC neuronal activity determines NA release, possible target-specific presynaptic release properties, and variations in local uptake mechanisms, all of which shape NA dynamics. It is furthermore going to be important to determine whether these fluctuations arise as part of the LC's spontaneous activity and/or secondarily from its integration into large-scale sleep-regulatory networks within the central and autonomic nervous systems. In this review, we outlined that recognizing NA as a neuromodulator during sleep opens novel mechanistic ideas on how sleep architecture and spectral dynamics are organized to the benefit of sleep functions. Future studies will undoubtedly reveal that fluctuations in other neuromodulators, such as the ones already reported for serotonin [86] and dopamine [92], work conjointly with NA in these processes.

An additional unique observation is the infraslow fluctuations in NA levels that characterize NREM sleep. These dynamics bring, for the first time, a neural *in vivo* foundation to a time scale of brain oscillatory activity that has long revolved in whole-brain measures and behavioral output, but that has not been a systematic part in the check-box list of sleep rhythms that are important for sleep functions [77]. Now, times become ready for speculations about its origins in the coordination of sleep and offline brain functions that are central to brain and bodily health.

As they currently stand, these new observations will have manifold implications for the LC's role in healthy and disordered sleep. Some of these implications have been proposed

but not pursued for years, yet they are now accessible with unprecedented spatiotemporal control. Most intriguingly, we may soon come to realize that the high NA levels are integral to enabling restorative NREM sleep and generating its unique benefits for health. Some other implications, however, are newly emerging. The NA, and perhaps other monoamines, present a profile of sleep as a behavioral state that integrates neuromodulation to monitor environmental, bodily, and brain states to enable adaptive behaviors. We propose that NA could show us the way to the neural foundation of a vigilance system for sleep, based on which novel insights into sleep's benefits and in-roads for therapeutic treatments of sleep disorders arise.

Author Contributions: A.L. and A.O.-F. conceptualized this review; A.O.-F., N.C., L.B., L.M.J.F. and A.L. contributed portions of the main text; L.M.J.F. designed the figure layout. Original data presented in Figure 2 were obtained by A.O.-F. All authors have read and agreed to the published version of the manuscript.

Funding: This article was funded by SNF grant number 310030-184759 to AL and Etat de Vaud. AOF was supported by a LifeSciences PhD Fellowship from the University of Lausanne.

Acknowledgments: The authors are grateful for the critical and constructive reading of earlier versions of the manuscript, in particular S. Astori, M. Bandarabadi, G. Foustoukos, F. Siclari and M. Tafti. We also acknowledge the many inspiring discussions by colleagues within the DNF and at the University of Lausanne.

Conflicts of Interest: The authors declare no conflict of interest.

Abbreviations

The following abbreviations are used in this manuscript:

LC	Locus Coeruleus
NA	Noradrenaline
NREM	Non-Rapid-Eye-Movement
REM	Rapid-Eye-Movement
DBH	Dopamine- β -Hydroxylase
MRI	Magnetic Resonance Imaging
5HT	5-hydroxytryptamine (or serotonin)
ACh	Acetylcholine
GRAB	G-Protein-Coupled-Receptor-Activation-Based
EEG	Electroencephalogram
VNS	Vagus Nerve Stimulation
AD	Alzheimer's Disease

References

1. Manger, P.R.; Eschenko, O. The Mammalian Locus Coeruleus Complex—Consistencies and Variances in Nuclear Organization. *Brain Sci.* **2021**, *11*, 1486. [[CrossRef](#)] [[PubMed](#)]
2. Fuxe, D. Evidence for existence of monoamine-containing neurons in central nervous system. I. Demonstration of monoamines in the cell bodies of brain stem neurons. *Acta Physiol. Scand.* **1964**, *62*, 1–55.
3. Maeda, T.; Pin, C.; Salvert, D.; Ligier, M.; Jouvet, M. Les neurones contenant des catecholamines du tegmentum pontique et leurs voies de projection chez le chat. *Brain Res.* **1973**, *57*, 119–152. [[CrossRef](#)]
4. Bogerts, B. A brainstem atlas of catecholaminergic neurons in man, using melanin as a natural marker. *J. Comp. Neurol.* **1981**, *197*, 63–80. [[CrossRef](#)]
5. Robertson, S.D.; Plummer, N.W.; De Marchena, J.; Jensen, P. Developmental origins of central norepinephrine neuron diversity. *Nat. Neurosci.* **2013**, *16*, 1016–1023. [[CrossRef](#)]
6. Aston-Jones, G. Locus Coeruleus, A5 and A7 Noradrenergic Cell Groups. In *The Rat Nervous System*, 3rd ed.; Elsevier: Amsterdam, The Netherlands, 2004; pp. 259–294. [[CrossRef](#)]
7. Aston-Jones, G.; Cohen, J.D. Adaptive gain and the role of the locus coeruleus–norepinephrine system in optimal performance. *J. Comp. Neurol.* **2005**, *493*, 99–110. [[CrossRef](#)]
8. Sara, S.J.; Bouret, S. Orienting and reorienting: The locus coeruleus mediates cognition through arousal. *Neuron* **2012**, *76*, 130–141. [[CrossRef](#)]

9. Berridge, C.W.; Schmeichel, B.E.; España, R.A. Noradrenergic modulation of wakefulness/arousal. *Sleep Med. Rev.* **2012**, *16*, 187–197. [[CrossRef](#)]
10. Saper, C.B.; Fuller, P.M.; Pedersen, N.P.; Lu, J.; Scammell, T.E. Sleep state switching. *Neuron* **2010**, *68*, 1023–1042. [[CrossRef](#)]
11. Jones, B.E. Arousal systems. *Front. Biosci.* **2003**, *8*, 438–451. [[CrossRef](#)]
12. Touret, M.; Valatx, J.L.; Jouvet, M. The locus coeruleus: A quantitative and genetic study in mice. *Brain Res.* **1982**, *250*, 353–357. [[CrossRef](#)]
13. Sturrock, R.; Rao, K. A quantitative histological study of neuronal loss from the locus coeruleus of ageing mice. *Neuropath. Appl. Neurobiol.* **1985**, *11*, 55–60. [[CrossRef](#)]
14. Mouton, P.R.; Pakkenberg, B.; Gundersen, H.J.G.; Price, D.L. Absolute number and size of pigmented locus coeruleus neurons in young and aged individuals. *J. Chem. Neuroanat.* **1994**, *7*, 185–190. [[CrossRef](#)]
15. Descarries, L.; Mechawar, N. Ultrastructural evidence for diffuse transmission by monoamine and acetylcholine neurons of the central nervous system. *Prog. Brain Res.* **2000**, *125*, 27–47.
16. Fuxe, K.; Agnati, L.F.; Marcoli, M.; Borroto-Escuela, D.O. Volume transmission in central dopamine and noradrenaline neurons and its astroglial targets. *Neurochem. Res.* **2015**, *40*, 2600–2614. [[CrossRef](#)]
17. Cohen, Z.; Molinatti, G.; Hamel, E. Astroglial and vascular interactions of noradrenaline terminals in the rat cerebral cortex. *J. Cereb. Blood Flow Metab.* **1997**, *17*, 894–904. [[CrossRef](#)]
18. McCormick, D.A.; Bal, T. Sleep and arousal: Thalamocortical mechanisms. *Ann. Rev. Neurosci.* **1997**, *20*, 185–215. [[CrossRef](#)]
19. Wahis, J.; Holt, M.G. Astrocytes, Noradrenaline, α 1-Adrenoreceptors, and Neuromodulation: Evidence and Unanswered Questions. *Front. Cell. Neurosci.* **2021**, *15*, 42. [[CrossRef](#)]
20. Waterhouse, B.D.; Navarra, R.L. The locus coeruleus-norepinephrine system and sensory signal processing: A historical review and current perspectives. *Brain Res.* **2019**, *1709*, 1–15. [[CrossRef](#)]
21. Arrigoni, E.; Chen, M.C.; Fuller, P.M. The anatomical, cellular and synaptic basis of motor atonia during rapid eye movement sleep. *J. Physiol.* **2016**, *594*, 5391–5414. [[CrossRef](#)]
22. Guyenet, P.G.; Bayliss, D.A. Neural control of breathing and CO₂ homeostasis. *Neuron* **2015**, *87*, 946–961. [[CrossRef](#)]
23. Yu, X.; Franks, N.P.; Wisden, W. Sleep and sedative states induced by targeting the histamine and noradrenergic systems. *Front. Neural Circuits* **2018**, *12*, 4. [[CrossRef](#)]
24. Valentino, R.J.; Van Bockstaele, E. Convergent regulation of locus coeruleus activity as an adaptive response to stress. *Eur. J. Pharmacol.* **2008**, *583*, 194–203. [[CrossRef](#)]
25. Vanderheyden, W.M.; Poe, G.R.; Liberzon, I. Trauma exposure and sleep: Using a rodent model to understand sleep function in PTSD. *Exp. Brain Res.* **2014**, *232*, 1575–1584. [[CrossRef](#)]
26. Hirschberg, S.; Li, Y.; Randall, A.; Kremer, E.J.; Pickering, A.E. Functional dichotomy in spinal-vs prefrontal-projecting locus coeruleus modules splits descending noradrenergic analgesia from ascending aversion and anxiety in rats. *eLife* **2017**, *6*, e29808. [[CrossRef](#)]
27. España, R.A.; Schmeichel, B.E.; Berridge, C.W. Norepinephrine at the nexus of arousal, motivation and relapse. *Brain Res.* **2016**, *1641*, 207–216. [[CrossRef](#)]
28. Kaur, S.; Saper, C.B. Neural circuitry underlying waking up to hypercapnia. *Front. Neurosci.* **2019**, *13*, 401. [[CrossRef](#)]
29. Wood, S.K.; Valentino, R.J. The brain norepinephrine system, stress and cardiovascular vulnerability. *Neurosci. Biobehav. Rev.* **2017**, *74*, 393–400. [[CrossRef](#)]
30. Breton-Provencher, V.; Drummond, G.T.; Sur, M. Locus coeruleus norepinephrine in learned behavior: Anatomical modularity and spatiotemporal integration in targets. *Front. Neural Circuits* **2021**, *15*, 638007. [[CrossRef](#)]
31. Schwarz, L.A.; Luo, L. Organization of the locus coeruleus-norepinephrine system. *Curr. Biol.* **2015**, *25*, R1051–R1056. [[CrossRef](#)]
32. Totah, N.K.; Logothetis, N.K.; Eschenko, O. Noradrenergic ensemble-based modulation of cognition over multiple timescales. *Brain Res.* **2019**, *1709*, 50–66. [[CrossRef](#)] [[PubMed](#)]
33. Zerbi, V.; Floriou-Servou, A.; Markicevic, M.; Vermeiren, Y.; Sturman, O.; Privitera, M.; von Ziegler, L.; Ferrari, K.D.; Weber, B.; De Deyn, P.P.; et al. Rapid reconfiguration of the functional connectome after chemogenetic locus coeruleus activation. *Neuron* **2019**, *103*, 702–718. [[CrossRef](#)] [[PubMed](#)]
34. Chandler, D.J.; Jensen, P.; McCall, J.G.; Pickering, A.E.; Schwarz, L.A.; Totah, N.K. Redefining noradrenergic neuromodulation of behavior: Impacts of a modular locus coeruleus architecture. *J. Neurosci.* **2019**, *39*, 8239–8249. [[CrossRef](#)] [[PubMed](#)]
35. Poe, G.R.; Foote, S.; Eschenko, O.; Johansen, J.P.; Bouret, S.; Aston-Jones, G.; Harley, C.W.; Manahan-Vaughan, D.; Weinschenker, D.; Valentino, R.; et al. Locus coeruleus: A new look at the blue spot. *Nat. Rev. Neurosci.* **2020**, *21*, 644–659. [[CrossRef](#)]
36. Van Egroo, M.; Koshmanova, E.; Vandewalle, G.; Jacobs, H.I. Importance of the locus coeruleus-norepinephrine system in sleep-wake regulation: Implications for aging and Alzheimer’s disease. *Sleep Med. Rev.* **2022**, *62*, 101592. [[CrossRef](#)]
37. Pace-Schott, E.F.; Hobson, J.A. The neurobiology of sleep: Genetics, cellular physiology and subcortical networks. *Nat. Rev. Neurosci.* **2002**, *3*, 591–605. [[CrossRef](#)]
38. Foote, S.; Aston-Jones, G.; Bloom, F. Impulse activity of locus coeruleus neurons in awake rats and monkeys is a function of sensory stimulation and arousal. *Proc. Natl. Acad. Sci. USA* **1980**, *77*, 3033–3037. [[CrossRef](#)]
39. Aston-Jones, G.; Bloom, F. Activity of norepinephrine-containing locus coeruleus neurons in behaving rats anticipates fluctuations in the sleep-waking cycle. *J. Neurosci.* **1981**, *1*, 876–886. [[CrossRef](#)]

40. Chu, N.S.; Bloom, F.E. Activity patterns of catecholamine-containing pontine neurons in the dorso-lateral tegmentum of unrestrained cats. *J. Neurobiol.* **1974**, *5*, 527–544. [[CrossRef](#)]
41. Hobson, J.A.; McCarley, R.W.; Wyzinski, P.W. Sleep cycle oscillation: Reciprocal discharge by two brainstem neuronal groups. *Science* **1975**, *189*, 55–58. [[CrossRef](#)]
42. Rasmussen, K.; Morilak, D.A.; Jacobs, B.L. Single unit activity of locus coeruleus neurons in the freely moving cat: I. During naturalistic behaviors and in response to simple and complex stimuli. *Brain Res.* **1986**, *371*, 324–334. [[CrossRef](#)]
43. Rajkowski, J.; Kubiak, P.; Aston-Jones, G. Locus coeruleus activity in monkey: Phasic and tonic changes are associated with altered vigilance. *Brain Res. Bull.* **1994**, *35*, 607–616. [[CrossRef](#)]
44. Eschenko, O.; Sara, S.J. Learning-dependent, transient increase of activity in noradrenergic neurons of locus coeruleus during slow wave sleep in the rat: Brain stem–cortex interplay for memory consolidation? *Cereb. Cort.* **2008**, *18*, 2596–2603. [[CrossRef](#)]
45. Eschenko, O.; Magri, C.; Panzeri, S.; Sara, S.J. Noradrenergic neurons of the locus coeruleus are phase locked to cortical up-down states during sleep. *Cereb. Cort.* **2012**, *22*, 426–435. [[CrossRef](#)]
46. Swift, K.M.; Gross, B.A.; Frazer, M.A.; Bauer, D.S.; Clark, K.J.; Vazey, E.M.; Aston-Jones, G.; Li, Y.; Pickering, A.E.; Sara, S.J.; et al. Abnormal locus coeruleus sleep activity alters sleep signatures of memory consolidation and impairs place cell stability and spatial memory. *Curr. Biol.* **2018**, *28*, 3599–3609. [[CrossRef](#)]
47. Fernandez, L.M.; Vantomme, G.; Osorio-Forero, A.; Cardis, R.; Béard, E.; Lüthi, A. Thalamic reticular control of local sleep in mouse sensory cortex. *eLife* **2018**, *7*, e39111. [[CrossRef](#)]
48. Menon, J.M.L.; Nolten, C.; Achterberg, E.J.M.; Joosten, R.N.J.M.A.; Dematteis, M.; Feenstra, M.G.P.; Drinkenburg, W.H.P.; Leenaars, C.H.C. Brain microdialysate monoamines in relation to circadian rhythms, sleep, and sleep deprivation—A systematic review, network meta-analysis, and new primary data. *J. Circ. Rhythms* **2019**, *17*, 1. [[CrossRef](#)]
49. Devoto, P.; Flore, G.; Saba, P.; Fa, M.; Gessa, G.L. Stimulation of the locus coeruleus elicits noradrenaline and dopamine release in the medial prefrontal and parietal cortex. *J. Neurochem.* **2005**, *92*, 368–374. [[CrossRef](#)]
50. Florin-Lechner, S.M.; Druhan, J.P.; Aston-Jones, G.; Valentino, R.J. Enhanced norepinephrine release in prefrontal cortex with burst stimulation of the locus coeruleus. *Brain Res.* **1996**, *742*, 89–97. [[CrossRef](#)]
51. Berridge, C.; Abercrombie, E. Relationship between locus coeruleus discharge rates and rates of norepinephrine release within neocortex as assessed by in vivo microdialysis. *Neuroscience* **1999**, *93*, 1263–1270. [[CrossRef](#)]
52. Dugast, C.; Cespuglio, R.; Suaud-Chagny, M. In vivo monitoring of evoked noradrenaline release in the rat anteroventral thalamic nucleus by continuous amperometry. *J. Neurochem.* **2002**, *82*, 529–537. [[CrossRef](#)] [[PubMed](#)]
53. Jouvet, M. The role of monoamines and acetylcholine-containing neurons in the regulation of the sleep-waking cycle. In *Neurophysiology and Neurochemistry of Sleep and Wakefulness*; Springer: Berlin/Heidelberg, Germany, 1972; pp. 166–307.
54. Monti, J.M.; D’Angelo, L.; Jantos, H.; Barbeito, L.; Abo, V. Effect of DSP-4, a noradrenergic neurotoxin, on sleep and wakefulness and sensitivity to drugs acting on adrenergic receptors in the rat. *Sleep* **1988**, *11*, 370–377. [[CrossRef](#)] [[PubMed](#)]
55. Ouyang, M.; Hellman, K.; Abel, T.; Thomas, S.A. Adrenergic signaling plays a critical role in the maintenance of waking and in the regulation of REM sleep. *J. Neurophysiol.* **2004**, *92*, 2071–2082. [[CrossRef](#)] [[PubMed](#)]
56. Blanco-Centurion, C.; Gerashchenko, D.; Salin-Pascual, R.J.; Shiromani, P.J. Effects of hypocretin2-saporin and antidopamine- β -hydroxylase-saporin neurotoxic lesions of the dorsolateral pons on sleep and muscle tone. *Eur. J. Neurosci.* **2004**, *19*, 2741–2752. [[CrossRef](#)]
57. Manns, I.D.; Lee, M.G.; Modirrousta, M.; Hou, Y.P.; Jones, B.E. Alpha 2 adrenergic receptors on GABAergic, putative sleep-promoting basal forebrain neurons. *Eur. J. Neurosci.* **2003**, *18*, 723–727. [[CrossRef](#)]
58. Langer, S.Z. α 2-Adrenoceptors in the treatment of major neuropsychiatric disorders. *Trends Pharm. Sci.* **2015**, *36*, 196–202. [[CrossRef](#)]
59. Washburn, M.; Moises, H.C. Electrophysiological correlates of presynaptic alpha 2-receptor-mediated inhibition of norepinephrine release at locus coeruleus synapses in dentate gyrus. *J. Neurosci.* **1989**, *9*, 2131–2140. [[CrossRef](#)]
60. Svensson, T.; Bunney, B.; Aghajanian, G. Inhibition of both noradrenergic and serotonergic neurons in brain by the α -adrenergic agonist clonidine. *Brain Res.* **1975**, *92*, 291–306. [[CrossRef](#)]
61. Tononi, G.; Pompeiano, M.; Cirelli, C. Suppression of desynchronized sleep through microinjection of the α 2-adrenergic agonist clonidine in the dorsal pontine tegmentum of the cat. *Pflügers Arch.* **1991**, *418*, 512–518. [[CrossRef](#)]
62. Crochet, S.; Sakai, K. Alpha-2 adrenoceptor mediated paradoxical (REM) sleep inhibition in the cat. *Neuroreport* **1999**, *10*, 2199–2204. [[CrossRef](#)]
63. Hayat, H.; Regev, N.; Matosevich, N.; Sales, A.; Paredes-Rodriguez, E.; Krom, A.J.; Bergman, L.; Li, Y.; Lavigne, M.; Kremer, E.J.; et al. Locus coeruleus norepinephrine activity mediates sensory-evoked awakenings from sleep. *Sci. Adv.* **2020**, *6*, eaaz4232. [[CrossRef](#)]
64. Dang-Vu, T.T.; Schabus, M.; Desseilles, M.; Albouy, G.; Boly, M.; Darsaud, A.; Gais, S.; Rauchs, G.; Sterpenich, V.; Vandewalle, G.; et al. Spontaneous neural activity during human slow wave sleep. *Proc. Natl. Acad. Sci. USA* **2008**, *105*, 15160–15165. [[CrossRef](#)]
65. Kelberman, M.; Keilholz, S.; Weinshenker, D. What’s that (blue) spot on my MRI? Multimodal neuroimaging of the locus coeruleus in neurodegenerative disease. *Front. Neurosci.* **2020**. [[CrossRef](#)]

66. Doppler, C.E.; Smit, J.A.; Hommelsen, M.; Seger, A.; Horsager, J.; Kinnerup, M.B.; Hansen, A.K.; Fedorova, T.D.; Knudsen, K.; Otto, M.; et al. Microsleep disturbances are associated with noradrenergic dysfunction in Parkinson's disease. *Sleep* **2021**, *44*, zsab040. [\[CrossRef\]](#)
67. Spiegel, R.; DeVos, J. Central effects of guanfacine and clonidine during wakefulness and sleep in healthy subjects. *Brit. J. Clin. Pharmacol.* **1980**, *10*, 165S–168S. [\[CrossRef\]](#)
68. Nicholson, A.; Pascoe, P.A. Presynaptic alpha2-adrenoceptor function and sleep in man: Studies with clonidine and idazoxan. *Neuropharmacology* **1991**, *30*, 367–372. [\[CrossRef\]](#)
69. Gais, S.; Rasch, B.; Dahmen, J.C.; Sara, S.; Born, J. The memory function of noradrenergic activity in non-REM sleep. *J. Cogn. Neurosci.* **2011**, *23*, 2582–2592. [\[CrossRef\]](#)
70. Nicholson, A.; Pascoe, P.A. Rapid Eye Movement Sleep and Sleep Continuity Depression and Antidepressants. *Drugs* **1989**, *38*, 4–13. [\[CrossRef\]](#)
71. Feng, J.; Zhang, C.; Lischinsky, J.E.; Jing, M.; Zhou, J.; Wang, H.; Zhang, Y.; Dong, A.; Wu, Z.; Wu, H.; et al. A genetically encoded fluorescent sensor for rapid and specific in vivo detection of norepinephrine. *Neuron* **2019**, *102*, 745–761. [\[CrossRef\]](#)
72. Osorio-Forero, A.; Cardis, R.; Vantomme, G.; Guillaume-Gentil, A.; Katsioudi, G.; Devenoges, C.; Fernandez, L.M.; Lüthi, A. Noradrenergic circuit control of non-REM sleep substates. *Curr. Biol.* **2021**, *31*, 5009–5023. [\[CrossRef\]](#)
73. Kjaerby, C.; Andersen, M.; Hauglund, N.L.; Ding, F.; Wang, W.; Xu, Q.; Deng, S.; Kang, N.; Peng, S.; Sun, Q.; et al. Dynamic fluctuations of the locus coeruleus-norepinephrine system underlie sleep state transitions. *BioRxiv* **2020**, preprint. [\[CrossRef\]](#)
74. Totah, N.K.; Neves, R.M.; Panzeri, S.; Logothetis, N.K.; Eschenko, O. The locus coeruleus is a complex and differentiated neuromodulatory system. *Neuron* **2018**, *99*, 1055–1068. [\[CrossRef\]](#) [\[PubMed\]](#)
75. Cardis, R.; Lecci, S.; Fernandez, L.M.; Osorio-Forero, A.; Chung, P.C.S.; Fulda, S.; Decosterd, I.; Lüthi, A. Cortico-autonomic local arousals and heightened somatosensory arousability during NREMS of mice in neuropathic pain. *eLife* **2021**, *10*, e65835. [\[CrossRef\]](#) [\[PubMed\]](#)
76. Lecci, S.; Fernandez, L.M.; Weber, F.D.; Cardis, R.; Chatton, J.Y.; Born, J.; Lüthi, A. Coordinated infraslow neural and cardiac oscillations mark fragility and offline periods in mammalian sleep. *Sci. Adv.* **2017**, *3*, e1602026. [\[CrossRef\]](#) [\[PubMed\]](#)
77. Watson, B.O. Cognitive and physiologic impacts of the infraslow oscillation. *Front. Syst. Neurosci.* **2018**, *44*. [\[CrossRef\]](#)
78. Fernandez, L.M.; Lüthi, A. Sleep spindles: Mechanisms and functions. *Physiol. Rev.* **2020**, *100*, 805–868. [\[CrossRef\]](#)
79. Yüzgeç, Ö.; Prsa, M.; Zimmermann, R.; Huber, D. Pupil size coupling to cortical states protects the stability of deep sleep via parasympathetic modulation. *Curr. Biol.* **2018**, *28*, 392–400. [\[CrossRef\]](#)
80. Glin, L.; Arnaud, C.; Berracochea, D.; Galey, D.; Jaffard, R.; Gottesmann, C. The intermediate stage of sleep in mice. *Physiol. Behav.* **1991**, *50*, 951–953. [\[CrossRef\]](#)
81. Gottesmann, C.; Gandolfo, G.; Zernicki, B. Intermediate stage of sleep in the cat. *J. Physiol.* **1984**, *79*, 365–372.
82. Aeschbach, D.; Borbély, A.A. All-night dynamics of the human sleep EEG. *J. Sleep Res.* **1993**, *2*, 70–81. [\[CrossRef\]](#)
83. Purcell, S.; Manoach, D.; Demanuele, C.; Cade, B.; Mariani, S.; Cox, R.; Panagiotaropoulou, G.; Saxena, R.; Pan, J.; Smoller, J.; et al. Characterizing sleep spindles in 11,630 individuals from the National Sleep Research Resource. *Nat. Comm.* **2017**, *8*, 15930. [\[CrossRef\]](#)
84. El Mansari, M.; Sakai, K.; Jouvet, M. Unitary characteristics of presumptive cholinergic tegmental neurons during the sleep-waking cycle in freely moving cats. *Exp. Brain Res.* **1989**, *76*, 519–529. [\[CrossRef\]](#)
85. Steriade, M.; Datta, S.; Pare, D.; Oakson, G.; Dossi, R.C. Neuronal activities in brain-stem cholinergic nuclei related to tonic activation processes in thalamocortical systems. *J. Neurosci.* **1990**, *10*, 2541–2559. [\[CrossRef\]](#)
86. Oikonomou, G.; Altermatt, M.; Zhang, R.w.; Coughlin, G.M.; Montz, C.; Gradinaru, V.; Prober, D.A. The serotonergic raphe promote sleep in zebrafish and mice. *Neuron* **2019**, *103*, 686–701. [\[CrossRef\]](#)
87. Wan, J.; Peng, W.; Li, X.; Qian, T.; Song, K.; Zeng, J.; Deng, F.; Hao, S.; Feng, J.; Zhang, P.; et al. A genetically encoded sensor for measuring serotonin dynamics. *Nat. Neurosci.* **2021**, *24*, 746–752. [\[CrossRef\]](#)
88. Sun, F.; Zeng, J.; Jing, M.; Zhou, J.; Feng, J.; Owen, S.F.; Luo, Y.; Li, F.; Wang, H.; Yamaguchi, T.; et al. A genetically encoded fluorescent sensor enables rapid and specific detection of dopamine in flies, fish, and mice. *Cell* **2018**, *174*, 481–496. [\[CrossRef\]](#)
89. Patriarchi, T.; Mohebi, A.; Sun, J.; Marley, A.; Liang, R.; Dong, C.; Puhger, K.; Mizuno, G.O.; Davis, C.M.; Wiltgen, B.; et al. An expanded palette of dopamine sensors for multiplex imaging in vivo. *Nat. Meth.* **2020**, *17*, 1147–1155. [\[CrossRef\]](#)
90. Jing, M.; Li, Y.; Zeng, J.; Huang, P.; Skirzewski, M.; Kljakic, O.; Peng, W.; Qian, T.; Tan, K.; Zou, J.; et al. An optimized acetylcholine sensor for monitoring in vivo cholinergic activity. *Nat. Meth.* **2020**, *17*, 1139–1146. [\[CrossRef\]](#)
91. Duffet, L.; Kosar, S.; Panniello, M.; Viberti, B.; Bracey, E.; Zych, A.D.; Radoux-Mergault, A.; Zhou, X.; Deric, J.; Ravotto, L.; et al. A genetically encoded sensor for in vivo imaging of orexin neuropeptides. *Nat. Meth.* **2022**, *19*, 231–241. [\[CrossRef\]](#)
92. Hasegawa, E.; Miyasaka, A.; Sakurai, K.; Cherasse, Y.; Li, Y.; Sakurai, T. Rapid eye movement sleep is initiated by basolateral amygdala dopamine signaling in mice. *Science* **2022**, *375*, 994–1000. [\[CrossRef\]](#)
93. Aston-Jones, G.; Bloom, F. Nonrepinephrine-containing locus coeruleus neurons in behaving rats exhibit pronounced responses to non-noxious environmental stimuli. *J. Neurosci.* **1981**, *1*, 887–900. [\[CrossRef\]](#)
94. Takahashi, K.; Kayama, Y.; Lin, J.; Sakai, K. Locus coeruleus neuronal activity during the sleep-waking cycle in mice. *Neuroscience* **2010**, *169*, 1115–1126. [\[CrossRef\]](#)
95. Carter, M.E.; Yizhar, O.; Chikahisa, S.; Nguyen, H.; Adamantidis, A.; Nishino, S.; Deisseroth, K.; De Lecea, L. Tuning arousal with optogenetic modulation of locus coeruleus neurons. *Nat. Neurosci.* **2010**, *13*, 1526–1533. [\[CrossRef\]](#)

96. Yamaguchi, H.; Hopf, F.W.; Li, S.B.; de Lecea, L. In vivo cell type-specific CRISPR knockdown of dopamine beta hydroxylase reduces locus coeruleus evoked wakefulness. *Nat. Comm.* **2018**, *9*, 5211. [[CrossRef](#)] [[PubMed](#)]
97. Devilbiss, D.M.; Waterhouse, B.D. The effects of tonic locus ceruleus output on sensory-evoked responses of ventral posterior medial thalamic and barrel field cortical neurons in the awake rat. *J. Neurosci.* **2004**, *24*, 10773–10785. [[CrossRef](#)] [[PubMed](#)]
98. Manella, L.C.; Petersen, N.; Linster, C. Stimulation of the locus ceruleus modulates signal-to-noise ratio in the olfactory bulb. *J. Neurosci.* **2017**, *37*, 11605–11615. [[CrossRef](#)] [[PubMed](#)]
99. Rodenkirch, C.; Liu, Y.; Schriver, B.J.; Wang, Q. Locus coeruleus activation enhances thalamic feature selectivity via norepinephrine regulation of intrathalamic circuit dynamics. *Nat. Neurosci.* **2019**, *22*, 120–133. [[CrossRef](#)]
100. Aston-Jones, G.; Chen, S.; Zhu, Y.; Oshinsky, M.L. A neural circuit for circadian regulation of arousal. *Nat. Neurosci.* **2001**, *4*, 732–738. [[CrossRef](#)]
101. Park, S.H.; Weber, F. Neural and homeostatic regulation of REM sleep. *Front. Psychol.* **2020**, *11*, 1662. [[CrossRef](#)]
102. Luppi, P.H.; Gervasoni, D.; Verret, L.; Goutagny, R.; Peyron, C.; Salvert, D.; Leger, L.; Fort, P. Paradoxical (REM) sleep genesis: the switch from an aminergic–cholinergic to a GABAergic–glutamatergic hypothesis. *J. Physiol. Paris* **2006**, *100*, 271–283. [[CrossRef](#)]
103. Singh, S.; Mallick, B.N. Mild electrical stimulation of pontine tegmentum around locus coeruleus reduces rapid eye movement sleep in rats. *Neurosci. Res.* **1996**, *24*, 227–235. [[CrossRef](#)]
104. Kaur, S.; Saxena, R.; Mallick, B.N. GABA in locus coeruleus regulates spontaneous rapid eye movement sleep by acting on GABAA receptors in freely moving rats. *Neurosci. Lett.* **1997**, *223*, 105–108. [[CrossRef](#)]
105. Crochet, S.; Sakai, K. Effects of microdialysis application of monoamines on the EEG and behavioural states in the cat mesopontine tegmentum. *Eur. J. Neurosci.* **1999**, *11*, 3738–3752. [[CrossRef](#)]
106. Cirelli, C.; Tononi, G.; Pompeiano, M.; Pompeiano, O.; Gennari, A. Modulation of desynchronized sleep through microinjection of α 1-adrenergic agonists and antagonists in the dorsal pontine tegmentum of the cat. *Pflügers Arch.* **1992**, *422*, 273–279. [[CrossRef](#)]
107. Clément, O.; Valencia Garcia, S.; Libourel, P.A.; Arthaud, S.; Fort, P.; Luppi, P.H. The inhibition of the dorsal paragigantocellular reticular nucleus induces waking and the activation of all adrenergic and noradrenergic neurons: A combined pharmacological and functional neuroanatomical study. *PLoS ONE* **2014**, *9*, e96851. [[CrossRef](#)]
108. Nitz, D.; Siegel, J. GABA release in the locus coeruleus as a function of sleep/wake state. *Neuroscience* **1997**, *78*, 795–801. [[CrossRef](#)]
109. Mallick, B.; Kaur, S.; Saxena, R. Interactions between cholinergic and GABAergic neurotransmitters in and around the locus coeruleus for the induction and maintenance of rapid eye movement sleep in rats. *Neuroscience* **2001**, *104*, 467–485. [[CrossRef](#)]
110. Breton-Provencher, V.; Sur, M. Active control of arousal by a locus coeruleus GABAergic circuit. *Nat. Neurosci.* **2019**, *22*, 218–228. [[CrossRef](#)]
111. Weber, F.; Do, J.P.H.; Chung, S.; Beier, K.T.; Bikov, M.; Doost, M.S.; Dan, Y. Regulation of REM and non-REM sleep by periaqueductal GABAergic neurons. *Nat. Comm.* **2018**, *9*, 354. [[CrossRef](#)]
112. Kaur, S.; Saxena, R.; Mallick, B.N. GABAergic neurons in prepositus hypoglossi regulate REM sleep by its action on locus coeruleus in freely moving rats. *Synapse* **2001**, *42*, 141–150. [[CrossRef](#)]
113. Stucynski, J.A.; Schott, A.L.; Baik, J.; Chung, S.; Weber, F. Regulation of REM sleep by inhibitory neurons in the dorsomedial medulla. *Curr. Biol.* **2022**, *32*, 37–50. [[CrossRef](#)]
114. Ennis, M.; Aston-Jones, G. Evidence for self-and neighbor-mediated postactivation inhibition of locus coeruleus neurons. *Brain Res.* **1986**, *374*, 299–305. [[CrossRef](#)]
115. Machida, M.; Sutton, A.M.; Williams, B.L.; Wellman, L.L.; Sanford, L.D. Differential behavioral, stress, and sleep responses in mice with different delays of fear extinction. *Sleep* **2019**, *42*, zsz147. [[CrossRef](#)]
116. Boyce, R.; Glasgow, S.D.; Williams, S.; Adamantidis, A. Causal evidence for the role of REM sleep theta rhythm in contextual memory consolidation. *Science* **2016**, *352*, 812–816. [[CrossRef](#)]
117. Nollet, M.; Hicks, H.; McCarthy, A.P.; Wu, H.; Möller-Levet, C.S.; Laing, E.E.; Malki, K.; Lawless, N.; Wafford, K.A.; Dijk, D.J.; et al. REM sleep's unique associations with corticosterone regulation, apoptotic pathways, and behavior in chronic stress in mice. *Proc. Natl. Acad. Sci. USA* **2019**, *116*, 2733–2742. [[CrossRef](#)]
118. Machida, M.; Wellman, L.L.; Fitzpatrick, B.; Mairén, E.; Hallum, B.; Sutton, B.; Amy, M.; Lonart, G.; Sanford, L.D. Effects of optogenetic inhibition of BLA on sleep brief optogenetic inhibition of the basolateral amygdala in mice alters effects of stressful experiences on rapid eye movement sleep. *Sleep* **2017**, *40*, zsx020. [[CrossRef](#)]
119. Lo, Y.; Yi, P.L.; Hsiao, Y.T.; Chang, F.C. Hypocretin in locus coeruleus and dorsal raphe nucleus mediates inescapable footshock stimulation-induced REM sleep alteration. *Sleep* **2022**, *in press*. [[CrossRef](#)]
120. Borodovitsyna, O.; Joshi, N.; Chandler, D. Persistent stress-induced neuroplastic changes in the locus coeruleus/norepinephrine system. *Neural Plast.* **2018**, *2018*, 1892570. [[CrossRef](#)] [[PubMed](#)]
121. Takeuchi, T.; Duzsikiewicz, A.J.; Sonneborn, A.; Spooner, P.A.; Yamasaki, M.; Watanabe, M.; Smith, C.C.; Fernández, G.; Deisseroth, K.; Greene, R.W.; et al. Locus coeruleus and dopaminergic consolidation of everyday memory. *Nature* **2016**, *537*, 357–362. [[CrossRef](#)] [[PubMed](#)]
122. Kempadoo, K.A.; Mosharov, E.V.; Choi, S.J.; Sulzer, D.; Kandel, E.R. Dopamine release from the locus coeruleus to the dorsal hippocampus promotes spatial learning and memory. *Proc. Natl. Acad. Sci. USA* **2016**, *113*, 14835–14840. [[CrossRef](#)] [[PubMed](#)]
123. Kaufman, A.M.; Geiller, T.; Losonczy, A. A role for the locus coeruleus in hippocampal CA1 place cell reorganization during spatial reward learning. *Neuron* **2020**, *105*, 1018–1026. [[CrossRef](#)]

124. Wagatsuma, A.; Okuyama, T.; Sun, C.; Smith, L.M.; Abe, K.; Tonegawa, S. Locus coeruleus input to hippocampal CA3 drives single-trial learning of a novel context. *Proc. Natl. Acad. Sci. USA* **2018**, *115*, E310–E316. [[CrossRef](#)]
125. Debiec, J.; LeDoux, J.E. Noradrenergic signaling in the amygdala contributes to the reconsolidation of fear memory: Treatment implications for PTSD. *Ann. N. Y. Acad. Sci.* **2006**, *1071*, 521–524. [[CrossRef](#)]
126. Uematsu, A.; Tan, B.Z.; Ycu, E.A.; Cuevas, J.S.; Koivumaa, J.; Junyent, F.; Kremer, E.J.; Witten, I.B.; Deisseroth, K.; Johansen, J.P. Modular organization of the brainstem noradrenergic system coordinates opposing learning states. *Nat. Neurosci.* **2017**, *20*, 1602–1611. [[CrossRef](#)]
127. Glennon, E.; Carcea, I.; Martins, A.R.O.; Multani, J.; Shehu, I.; Svirsky, M.A.; Froemke, R.C. Locus coeruleus activation accelerates perceptual learning. *Brain Res.* **2019**, *1709*, 39–49. [[CrossRef](#)]
128. Martins, A.R.O.; Froemke, R.C. Coordinated forms of noradrenergic plasticity in the locus coeruleus and primary auditory cortex. *Nat. Neurosci.* **2015**, *18*, 1483–1492. [[CrossRef](#)]
129. Palacios-Filardo, J.; Mellor, J.R. Neuromodulation of hippocampal long-term synaptic plasticity. *Curr. Opin. Neurobiol.* **2019**, *54*, 37–43. [[CrossRef](#)]
130. Bacon, T.J.; Pickering, A.E.; Mellor, J.R. Noradrenergic release from locus coeruleus terminals in the hippocampus enhances excitation-spike coupling in ca1 pyramidal neurons via β -adrenoceptors. *Cereb. Cortex* **2020**, *30*, 6135–6151. [[CrossRef](#)]
131. Sara, S.J.; Rouillet, P.; Przybyslawski, J. Consolidation of memory for odor-reward association: β -adrenergic receptor involvement in the late phase. *Learn. Mem.* **1999**, *6*, 88–96. [[CrossRef](#)]
132. Tronel, S.; Feenstra, M.G.; Sara, S.J. Noradrenergic action in prefrontal cortex in the late stage of memory consolidation. *Learn. Mem.* **2004**, *11*, 453–458. [[CrossRef](#)]
133. Novitskaya, Y.; Sara, S.J.; Logothetis, N.K.; Eschenko, O. Ripple-triggered stimulation of the locus coeruleus during post-learning sleep disrupts ripple/spindle coupling and impairs memory consolidation. *Learn. Mem.* **2016**, *23*, 238–248. [[CrossRef](#)] [[PubMed](#)]
134. Sara, S.J. Locus coeruleus in time with the making of memories. *Curr. Opin. Neurobiol.* **2015**, *35*, 87–94. [[CrossRef](#)] [[PubMed](#)]
135. Van Bockstaele, E.J.; Peoples, J.; Telegan, P. Efferent projections of the nucleus of the solitary tract to peri-locus coeruleus dendrites in rat brain: Evidence for a monosynaptic pathway. *J. Comp. Neurol.* **1999**, *412*, 410–428. [[CrossRef](#)]
136. Lopes, L.T.; Patrone, L.G.A.; Li, K.Y.; Imber, A.N.; Graham, C.D.; Gargaglioni, L.H.; Putnam, R.W. Anatomical and functional connections between the locus coeruleus and the nucleus tractus solitarius in neonatal rats. *Neuroscience* **2016**, *324*, 446–468. [[CrossRef](#)]
137. Aston-Jones, G. The locus coeruleus, A5 and A7 noradrenergic cell groups. In *The Rat Nervous System*, 2nd ed.; Academic Press: Cambridge, MA, USA, 1994; Chapter 11, pp. 259–294.
138. Ruggiero, D.A.; Pickel, V.M.; Milner, T.A.; Anwar, M.; Otake, K.; Mtui, E.P.; Park, D. Viscerosensory Processing in Nucleus Tractus Solitarius: Structural and Neurochemical Substrates. In *Nucleus of the Solitary Tract*; CRC Press: Boca Raton, FL, USA, 1994; Chapter 1, pp. 3–34.
139. Berthoud, H.R.; Neuhuber, W.L. Functional and chemical anatomy of the afferent vagal system. *Auton. Neurosci.* **2000**, *85*, 1–17. [[CrossRef](#)]
140. Han, W.; Tellez, L.A.; Perkins, M.H.; Perez, I.O.; Qu, T.; Ferreira, J.; Ferreira, T.L.; Quinn, D.; Liu, Z.W.; Gao, X.B.; et al. A neural circuit for gut-induced reward. *Cell* **2018**, *175*, 665–678. [[CrossRef](#)]
141. Childs, J.E.; Alvarez-Dieppa, A.C.; McIntyre, C.K.; Kroener, S. Vagus nerve stimulation as a tool to induce plasticity in pathways relevant for extinction learning. *J. Vis. Exp.* **2015**, *102*, e53032. [[CrossRef](#)]
142. Hays, S.A.; Rennaker, R.L.; Kilgard, M.P. Targeting plasticity with vagus nerve stimulation to treat neurological disease. *Prog. Brain Res.* **2013**, *207*, 275–299.
143. Broncel, A.; Bocian, R.; Kłos-Wojtczak, P.; Kulbat-Warycha, K.; Konopacki, J. Vagal nerve stimulation as a promising tool in the improvement of cognitive disorders. *Brain Res. Bull.* **2020**, *155*, 37–47. [[CrossRef](#)]
144. Englot, D.J.; Rolston, J.D.; Wright, C.W.; Hassnain, K.H.; Chang, E.F. Rates and predictors of seizure freedom with vagus nerve stimulation for intractable epilepsy. *Neurosurgery* **2016**, *79*, 345–353. [[CrossRef](#)]
145. Schachter, S.C.; Saper, C.B. Vagus nerve stimulation. *Epilepsia* **1998**, *39*, 677–686. [[CrossRef](#)]
146. Berger, A.; Vespa, S.; Dricot, L.; Dumoulin, M.; Iachim, E.; Doguet, P.; Vandewalle, G.; El Tahry, R. How is the norepinephrine system involved in the antiepileptic effects of Vagus Nerve Stimulation (VNS)? *Front. Neurosci.* **2021**. [[CrossRef](#)]
147. Rush, A.J.; George, M.S.; Sackeim, H.A.; Marangell, L.B.; Husain, M.M.; Giller, C.; Nahas, Z.; Haines, S.; Simpson, R.K., Jr.; Goodman, R. Vagus nerve stimulation (VNS) for treatment-resistant depressions: A multicenter study. *Biol. Psych.* **2000**, *47*, 276–286. [[CrossRef](#)]
148. Austelle, C.W.; O’Leary, G.H.; Thompson, S.; Gruber, E.; Kahn, A.; Manett, A.J.; Short, B.; Badran, B.W. A comprehensive review of vagus nerve stimulation for depression. *Neuromodulation Technol. Neural Interface* **2022**, *25*, 309–315. [[CrossRef](#)]
149. Faris, P.L.; Hofbauer, R.D.; Daughters, R.; VandenLangenberg, E.; Iversen, L.; Goodale, R.L.; Maxwell, R.; Eckert, E.D.; Hartman, B.K. De-stabilization of the positive vago-vagal reflex in bulimia nervosa. *Physiol. Behav.* **2008**, *94*, 136–153. [[CrossRef](#)]
150. Sjogren, M.J.; Hellstrom, P.T.; Jonsson, M.A.; Runnerstam, M.; Hans, C.; Ben-Menachem, E. Cognition-enhancing effect of vagus nerve stimulation in patients with Alzheimer’s disease: A pilot study. *J. Clin. Psychiatry* **2002**, *63*, 3113. [[CrossRef](#)]
151. Gieroba, Z.; Blessing, W. Fos-containing neurons in medulla and pons after unilateral stimulation of the afferent abdominal vagus in conscious rabbits. *Neuroscience* **1994**, *59*, 851–858. [[CrossRef](#)]

152. Naritoku, D.K.; Terry, W.J.; Helfert, R.H. Regional induction of fos immunoreactivity in the brain by anticonvulsant stimulation of the vagus nerve. *Epilepsy Res.* **1995**, *22*, 53–62. [[CrossRef](#)]
153. Krahl, S.E.; Clark, K.B.; Smith, D.C.; Browning, R.A. Locus coeruleus lesions suppress the seizure-attenuating effects of vagus nerve stimulation. *Epilepsia* **1998**, *39*, 709–714. [[CrossRef](#)]
154. Takigawa, M.; Mogenson, G. A study of inputs to antidromically identified neurons of the locus coeruleus. *Brain Res.* **1977**, *135*, 217–230. [[CrossRef](#)]
155. Groves, D.A.; Bowman, E.M.; Brown, V.J. Recordings from the rat locus coeruleus during acute vagal nerve stimulation in the anaesthetised rat. *Neurosci. Lett.* **2005**, *379*, 174–179. [[CrossRef](#)]
156. Hulseley, D.R.; Riley, J.R.; Loerwald, K.W.; Rennaker II, R.L.; Kilgard, M.P.; Hays, S.A. Parametric characterization of neural activity in the locus coeruleus in response to vagus nerve stimulation. *Exp. Neurol.* **2017**, *289*, 21–30. [[CrossRef](#)]
157. Dorr, A.E.; Debonnel, G. Effect of vagus nerve stimulation on serotonergic and noradrenergic transmission. *J. Pharmacol. Exp. Ther.* **2006**, *318*, 890–898. [[CrossRef](#)]
158. Collins, L.; Boddington, L.; Steffan, P.J.; McCormick, D. Vagus nerve stimulation induces widespread cortical and behavioral activation. *Curr. Biol.* **2021**, *31*, 2088–2098. [[CrossRef](#)]
159. Roosevelt, R.W.; Smith, D.C.; Clough, R.W.; Jensen, R.A.; Browning, R.A. Increased extracellular concentrations of norepinephrine in cortex and hippocampus following vagus nerve stimulation in the rat. *Brain Res.* **2006**, *1119*, 124–132. [[CrossRef](#)]
160. Manta, S.; Dong, J.; Debonnel, G.; Blier, P. Enhancement of the function of rat serotonin and norepinephrine neurons by sustained vagus nerve stimulation. *J. Psych. Neurosci.* **2009**, *34*, 272.
161. Manta, S.; El Mansari, M.; Debonnel, G.; Blier, P. Electrophysiological and neurochemical effects of long-term vagus nerve stimulation on the rat monoaminergic systems. *Int. J. Neuropsychopharm.* **2013**, *16*, 459–470. [[CrossRef](#)] [[PubMed](#)]
162. Bianca, R.; Komisaruk, B.R. Pupil dilatation in response to vagal afferent electrical stimulation is mediated by inhibition of parasympathetic outflow in the rat. *Brain Res.* **2007**, *1177*, 29–36. [[CrossRef](#)] [[PubMed](#)]
163. Mridha, Z.; de Gee, J.W.; Shi, Y.; Alkashgari, R.; Williams, J.; Suminski, A.; Ward, M.P.; Zhang, W.; McGinley, M.J. Graded recruitment of pupil-linked neuromodulation by parametric stimulation of the vagus nerve. *Nat. Comm.* **2021**, *12*, 1539. [[CrossRef](#)] [[PubMed](#)]
164. Jodoin, V.D.; Lespérance, P.; Nguyen, D.K.; Fournier-Gosselin, M.P.; Richer, F. Effects of vagus nerve stimulation on pupillary function. *Int. J. Psychophys.* **2015**, *98*, 455–459. [[CrossRef](#)]
165. Sharon, O.; Fahoum, F.; Nir, Y. Transcutaneous vagus nerve stimulation in humans induces pupil dilation and attenuates alpha oscillations. *J. Neurosci.* **2021**, *41*, 320–330. [[CrossRef](#)]
166. Fernández-Guardiola, A.; Martínez, A.; Valdés-Cruz, A.; Magdaleno-Madrigal, V.; Martínez, D.; Fernández-Mas, R. Vagus nerve prolonged stimulation in cats: Effects on epileptogenesis (amygdala electrical kindling): Behavioral and electrographic changes. *Epilepsia* **1999**, *40*, 822–829. [[CrossRef](#)]
167. Valdés-Cruz, A.; Magdaleno-Madrigal, V.M.; Martínez-Vargas, D.; Fernández-Mas, R.; Almazán-Alvarado, S.; Martínez, A.; Fernández-Guardiola, A. Chronic stimulation of the cat vagus nerve: Effect on sleep and behavior. *Prog. Neuro-Psychopharm. Biol. Psych.* **2002**, *26*, 113–118. [[CrossRef](#)]
168. Valdés-Cruz, A.; Magdaleno-Madrigal, V.M.; Martínez-Vargas, D.; Fernández-Mas, R.; Almazán-Alvarado, S. Long-term changes in sleep and electroencephalographic activity by chronic vagus nerve stimulation in cats. *Prog. Neuro-Psychopharm. Biol. Psych.* **2008**, *32*, 828–834. [[CrossRef](#)]
169. Malow, B.A.; Edwards, J.; Marzec, M.; Sagher, O.; Ross, D.; Fromes, G. Vagus nerve stimulation reduces daytime sleepiness in epilepsy patients. *Neurology* **2001**, *57*, 879–884. [[CrossRef](#)]
170. Galli, R.; Bonanni, E.; Pizzanelli, C.; Maestri, M.; Lutzemberger, L.; Giorgi, F.S.; Iudice, A.; Murri, L. Daytime vigilance and quality of life in epileptic patients treated with vagus nerve stimulation. *Epilepsia* **2003**, *44*, 185–191. [[CrossRef](#)]
171. Armitage, R.; Husain, M.; Hoffmann, R.; Rush, A.J. The effects of vagus nerve stimulation on sleep EEG in depression: A preliminary report. *J. Psychosom. Res.* **2003**, *54*, 475–482. [[CrossRef](#)]
172. Rizzo, P.; Beelke, M.; De Carli, F.; Canovaro, P.; Nobili, L.; Robert, A.; Tanganelli, P.; Regesta, G.; Ferrillo, F. Chronic vagus nerve stimulation improves alertness and reduces rapid eye movement sleep in patients affected by refractory epilepsy. *Sleep* **2003**, *26*, 607–611. [[CrossRef](#)]
173. Rizzo, P.; Beelke, M.; De Carli, F.; Canovaro, P.; Nobili, L.; Robert, A.; Fornaro, P.; Tanganelli, P.; Regesta, G.; Ferrillo, F. Modifications of sleep EEG induced by chronic vagus nerve stimulation in patients affected by refractory epilepsy. *Clin. Neurophysiol.* **2004**, *115*, 658–664. [[CrossRef](#)]
174. Hallböök, T.; Lundgren, J.; Stjernqvist, K.; Blennow, G.; Strömblad, L.G.; Rosén, I. Vagus nerve stimulation in 15 children with therapy resistant epilepsy; Its impact on cognition, quality of life, behaviour and mood. *Seizure* **2005**, *14*, 504–513. [[CrossRef](#)]
175. Ravan, M.; Begnaud, J. Investigating the effect of short term responsive VNS therapy on sleep quality using automatic sleep staging. *IEEE Trans. Biomed. Eng.* **2019**, *66*, 3301–3309. [[CrossRef](#)]
176. Al-Biltagi, M.A. Childhood epilepsy and sleep. *World J. Clin. Pediatr.* **2014**, *3*, 45. [[CrossRef](#)]
177. Cherrad, N.; Cardis, R.; Osorio-Forero, A.; Arnold, M.; Fernandez, L.M.J.; Lüthi, A. Chemogenetic activation of VGLUT2 neurons in the left nodose ganglion of the vagal nerve suppresses rapid-eye-movement sleep in mouse [Abstract]. *J. Sleep Res.* **2020**, *29*, e13181.

178. Giorgi, F.S.; Galgani, A.; Puglisi-Allegra, S.; Limanaqi, F.; Busceti, C.L.; Fornai, F. Locus Coeruleus and neurovascular unit: From its role in physiology to its potential role in Alzheimer's disease pathogenesis. *J. Neurosci. Res.* **2020**, *98*, 2406–2434. [[CrossRef](#)] [[PubMed](#)]
179. Bekar, L.K.; Wei, H.S.; Nedergaard, M. The locus coeruleus-norepinephrine network optimizes coupling of cerebral blood volume with oxygen demand. *J. Cereb. Blood Flow Metab.* **2012**, *32*, 2135–2145. [[CrossRef](#)] [[PubMed](#)]
180. Toussay, X.; Basu, K.; Lacoste, B.; Hamel, E. Locus coeruleus stimulation recruits a broad cortical neuronal network and increases cortical perfusion. *J. Neurosci.* **2013**, *33*, 3390–3401. [[CrossRef](#)] [[PubMed](#)]
181. O'Donnell, J.; Zeppenfeld, D.; McConnell, E.; Pena, S.; Nedergaard, M. Norepinephrine: A neuromodulator that boosts the function of multiple cell types to optimize CNS performance. *Neurochem. Res.* **2012**, *37*, 2496–2512. [[CrossRef](#)] [[PubMed](#)]
182. Rasmussen, M.K.; Mestre, H.; Nedergaard, M. Fluid transport in the brain. *Physiol. Rev.* **2022**, *102*, 1025–1151. [[CrossRef](#)]
183. Xie, L.; Kang, H.; Xu, Q.; Chen, M.J.; Liao, Y.; Thiyagarajan, M.; O'Donnell, J.; Christensen, D.J.; Nicholson, C.; Iliff, J.J.; et al. Sleep drives metabolite clearance from the adult brain. *Science* **2013**, *342*, 373–377. [[CrossRef](#)]
184. van Veluw, S.J.; Hou, S.S.; Calvo-Rodriguez, M.; Arbel-Ornath, M.; Snyder, A.C.; Frosch, M.P.; Greenberg, S.M.; Bacsikai, B.J. Vasomotion as a driving force for paravascular clearance in the awake mouse brain. *Neuron* **2020**, *105*, 549–561. [[CrossRef](#)]
185. Fultz, N.E.; Bonmassar, G.; Setsompop, K.; Stickgold, R.A.; Rosen, B.R.; Polimeni, J.R.; Lewis, L.D. Coupled electrophysiological, hemodynamic, and cerebrospinal fluid oscillations in human sleep. *Science* **2019**, *366*, 628–631. [[CrossRef](#)]
186. Horovitz, S.G.; Fukunaga, M.; de Zwart, J.A.; van Gelderen, P.; Fulton, S.C.; Balkin, T.J.; Duyn, J.H. Low frequency BOLD fluctuations during resting wakefulness and light sleep: A simultaneous EEG-fMRI study. *Hum. Brain Mapp.* **2008**, *29*, 671–682. [[CrossRef](#)]
187. Fukunaga, M.; Horovitz, S.G.; van Gelderen, P.; de Zwart, J.A.; Jansma, J.M.; Ikonomidou, V.N.; Chu, R.; Deckers, R.H.; Leopold, D.A.; Duyn, J.H. Large-amplitude, spatially correlated fluctuations in BOLD fMRI signals during extended rest and early sleep stages. *Magn. Res. Imag.* **2006**, *24*, 979–992. [[CrossRef](#)]
188. Larson-Prior, L.J.; Zempel, J.M.; Nolan, T.S.; Prior, F.W.; Snyder, A.Z.; Raichle, M.E. Cortical network functional connectivity in the descent to sleep. *Proc. Natl. Acad. Sci. USA* **2009**, *106*, 4489–4494. [[CrossRef](#)]
189. Mander, B.A.; Winer, J.R.; Walker, M.P. Sleep and human aging. *Neuron* **2017**, *94*, 19–36. [[CrossRef](#)]
190. Gagnon, J.F.; Lafrenière, A.; Rauchs, G.; Petit, D.; Carrier, J. Sleep in normal aging, Alzheimer's disease, and mild cognitive impairment. In *Handbook of Behavioral Neuroscience*; Elsevier: Amsterdam, The Netherlands, 2019; Volume 30, pp. 677–692.
191. Li, S.B.; Damonte, V.M.; Chen, C.; Wang, G.X.; Kebschull, J.M.; Yamaguchi, H.; Bian, W.J.; Purmann, C.; Pattni, R.; Urban, A.E.; et al. Hyperexcitable arousal circuits drive sleep instability during aging. *Science* **2022**, *375*, eabh3021. [[CrossRef](#)]
192. Lew, C.H.; Petersen, C.; Neylan, T.C.; Grinberg, L.T. Tau-driven degeneration of sleep-and wake-regulating neurons in Alzheimer's disease. *Sleep Med. Rev.* **2021**, *60*, 101541. [[CrossRef](#)]
193. Wang, C.; Holtzman, D.M. Bidirectional relationship between sleep and Alzheimer's disease: Role of amyloid, tau, and other factors. *Neuropsychopharmacology* **2020**, *45*, 104–120. [[CrossRef](#)]
194. Jacobs, H.I.; Becker, J.A.; Kwong, K.; Engels-Domínguez, N.; Prokopiou, P.C.; Papp, K.V.; Properzi, M.; Hampton, O.L.; d'Oleire Uquillas, F.; Sanchez, J.S.; et al. In vivo and neuropathology data support locus coeruleus integrity as indicator of Alzheimer's disease pathology and cognitive decline. *Sci. Transl. Med.* **2021**, *13*, eabj2511. [[CrossRef](#)]
195. Rorabaugh, J.M.; Chalermpananupap, T.; Botz-Zapp, C.A.; Fu, V.M.; Lembeck, N.A.; Cohen, R.M.; Weinshenker, D. Chemogenetic locus coeruleus activation restores reversal learning in a rat model of Alzheimer's disease. *Brain* **2017**, *140*, 3023–3038. [[CrossRef](#)]
196. Chylinski, D.O.; Van Egroo, M.; Narbutas, J.; Grignard, M.; Koshmanova, E.; Berthomier, C.; Berthomier, P.; Brandewinder, M.; Salmon, E.; Bahri, M.A.; et al. Heterogeneity in the links between sleep arousals, amyloid- β , and cognition. *JCI Insight* **2021**, *6*, e152858. [[CrossRef](#)]
197. Cano, G.; Mochizuki, T.; Saper, C.B. Neural circuitry of stress-induced insomnia in rats. *J. Neurosci.* **2008**, *28*, 10167–10184. [[CrossRef](#)]
198. Berridge, C.W.; Foote, S.L. Effects of locus coeruleus activation on electroencephalographic activity in neocortex and hippocampus. *J. Neurosci.* **1991**, *11*, 3135–3145. [[CrossRef](#)]
199. Marzo, A.; Totah, N.K.; Neves, R.M.; Logothetis, N.K.; Eschenko, O. Unilateral electrical stimulation of rat locus coeruleus elicits bilateral response of norepinephrine neurons and sustained activation of medial prefrontal cortex. *J. Neurophysiol.* **2014**, *111*, 2570–2588. [[CrossRef](#)]
200. Vazey, E.M.; Aston-Jones, G. Designer receptor manipulations reveal a role of the locus coeruleus noradrenergic system in isoflurane general anesthesia. *Proc. Natl. Acad. Sci. USA* **2014**, *111*, 3859–3864. [[CrossRef](#)]
201. Ploner, M.; Sorg, C.; Gross, J. Brain rhythms of pain. *Trends Cogn. Sci.* **2017**, *21*, 100–110. [[CrossRef](#)]
202. Van Someren, E.J. Brain mechanisms of insomnia: New perspectives on causes and consequences. *Physiol. Rev.* **2021**, *101*, 995–1046. [[CrossRef](#)]
203. Kobayashi, I.; Boarts, J.M.; Delahanty, D.L. Polysomnographically measured sleep abnormalities in PTSD: A meta-analytic review. *Psychophysiol.* **2007**, *44*, 660–669. [[CrossRef](#)] [[PubMed](#)]
204. Wassing, R.; Lakbila-Kamal, O.; Ramautar, J.R.; Stoffers, D.; Schalkwijk, F.; Van Someren, E.J. Restless REM sleep impedes overnight amygdala adaptation. *Curr. Biol.* **2019**, *29*, 2351–2358. [[CrossRef](#)] [[PubMed](#)]
205. de Zambotti, M.; Trinder, J.; Silvani, A.; Colrain, I.M.; Baker, F.C. Dynamic coupling between the central and autonomic nervous systems during sleep: A review. *Neurosci. Biobehav. Rev.* **2018**, *90*, 84–103. [[CrossRef](#)] [[PubMed](#)]

-
206. Silvani, A.; Dampney, R.A. Central control of cardiovascular function during sleep. *Am. J. Physiol.-Heart Circ. Physiol.* **2013**, *305*, H1683–H1692. [[CrossRef](#)]
207. Chouchou, F.; Desseilles, M. Heart rate variability: A tool to explore the sleeping brain? *Front. Neurosci.* **2014**, *8*, 402. [[CrossRef](#)]